

UTILIZATION OF CARBON DIOXIDE AND METHANE VIA CATALYTIC
REFORMING REACTIONS

by

Şeyma Özkara Aydınođlu

B. S., Chemical Engineering, Bođaziçi University, 2000

M. S., Chemical Engineering, Bođaziçi University, 2002

Submitted to the Institute for Graduate Studies in
Science and Engineering in partial fulfillment of
the requirements for the degree of
Doctor of Philosophy

Graduate Program in Chemical Engineering

Bođaziçi University

2008

to my family

ACKNOWLEDGEMENT

Firstly, I would like to express my truthful gratitude to my thesis supervisor Prof. Ahmet Erhan Aksoylu for his guidance, encouragement and trust in me. My respect and admiration in his personality as well as his invaluable way of teaching inspired me all the time. It was a privilege for me to work with Prof. Aksoylu during my PhD thesis.

I would like to express my great appreciations for Prof. Ayşe Nilgün Akın, Prof. Mahir Arıkol, Assist. Prof. Ahmet Kerim Avcı and Prof. Zeynep İlsen Önsan, who devoted their valuable time to guiding me, helping me all the time. It was a great opportunity for me to learn from their experiences and knowledge.

I would like to thank Prof. Mehmet Çamurdan and Prof. Öner Hortaçsu for giving me direction and sharing their great knowledge with me.

Very special thanks to Defne Kayrak-Talay, Seda Keskin, Özlem Yılmaz, Sahar J. Vardani, Ahu Sekendiz and Ayşegül Gökyalaz for their everlasting help and encouragement. Their friendships are the biggest assets that I have gained in my life.

I was very lucky to work with the CATREL team, Feyza Gökaliiler, Duygu Başaran, Tuğba Davran, Sadi Tezcanlı, Yasemin Döker, Fatma Soyak Baltacıoğlu, Seda Acun, Berrin Gülyüz, Görkem Oğur, Bayram Ali Göçmen, Ilgaz Soykal and Sabriye Güven for giving me their true friendship and making me feel happy all the time. I also would like to thank to all my friends in Chemical Engineering Department, especially Eralp Bolkent and Murat Şen for their support.

Cordial thanks are for Bilgi Dedeoğlu, Nurettin Bektaş for their technical assistance and friendship during my thesis. Heartfelt thanks are for Melike Gürbüz and Fatma Odak for their friendship and kindness to me. My thanks are also for Yakup Bal for his friendly attitude.

I would like to express my thanks to Bilge Gedik Uluocak for her considerable time and effort in electron microscopy studies conducted at Boğaziçi University Advanced Technologies R&D Center.

Finally; I would like to thank my husband, Temmuz Aydınoğlu, and all my family for their patience, encouragement and moral support throughout my whole education. They believed in me and loved me all the time. This thesis would not have been possible without their everlasting support. I dedicate this work to them.

Financial support provided by Boğaziçi University through the projects DPT-07K120630, DPT-03K120250 and BAP-06A506D is gratefully acknowledged.

ABSTRACT

UTILIZATION OF CARBON DIOXIDE AND METHANE VIA CATALYTIC REFORMING REACTIONS

The overall purpose of this research study was to investigate new catalysts to produce synthesis gas via CO₂ reforming of methane under optimized reaction conditions. The thesis consists of four parts. In the first part of the study; the purpose was to design and develop effective Pt-based bimetallic dry reforming catalysts supported on zirconia. Aiming to have bimetallic catalysts with enhanced performance properties, Ce was used as a promoter in order to increase the oxygen storage capacity of the catalysts via controlling the electronic structure of the metals over the support. The results have shown that introduction of 1 wt.% Ce to the Pt/ZrO₂ catalyst by coimpregnation method led to superior catalytic activities and stabilities due to the to strong and extensive Pt-Ce surface interaction. In the second part of the thesis, Pt-Ni bimetallic catalysts supported on δ -Al₂O₃ were designed and developed for carbon dioxide reforming of methane to determine an effective catalyst with optimum Pt/Ni metal composition assuring both high activity and stability. The different activity levels of the catalysts showed that the catalytic performances of bimetallic Pt-Ni samples strongly depended on the metal loading and Ni/Pt ratio. Among all the catalysts, 0.3Pt-10Ni catalyst with the lowest Ni/Pt ratio exhibited the highest catalytic activity and stability. By changing the Ni/Pt ratios of the catalysts and with the addition of small amounts of either oxygen or water to the feed stream, the catalysts' resistance to coking reactions were also tried to elucidate. Based on the different performance and stability profiles of the Pt-Ni catalysts in part two in response to the changes in their Ni/Pt ratio as well as the reaction conditions, a kinetic study was performed in the third part of the study. In the final part of the research, the effect of addition of metal additives to Co/ZrO₂ on both surface micro-structural properties and catalytic performance was investigated. The results have shown that La-modified catalyst exhibited high stability, but moderate activity. Ce-doped Co/ZrO₂ displayed the highest activity among all the catalysts prepared and had a very limited activity loss.

ÖZET

KARBONDİOKSİT VE METANIN KATALİTİK REFORMLAMA REAKSİYONLARI İLE KULLANILMASI

Bu çalışmanın amacı, optimize edilmiş reaksiyon koşullarında metanın karbondioksitle reformlanması ile sentez gazı üretiminde yeni katalizörleri araştırmaktır. Bu tez dört bölümden oluşmaktadır. Tezin ilk bölümünde amaç etkili zirkonya destekli Pt bazlı iki metalli kuru reformlama katalizörleri tasarlamak ve geliştirmektir. Geliştirilmiş performans özelliklerine sahip iki metalli katalizörler elde etmek amacıyla, destek üzerindeki metallerin elektronik yapılarını kontrol etmek suretiyle katalizörlerin oksijen depolama kapasitelerini artırmak için yardımcı olarak Ce kullanılmıştır. Sonuçlar kütlece %1'lik Ce'nin koimpregnasyon yöntemiyle Pt/ZrO₂ katalizörü üzerine eklenmesinin, güçlü ve yaygın Pt-Ce yüzey etkileşimi sayesinde yüksek katalitik etkinlik ve kararlılık sağladığını göstermiştir. Tezin ikinci kısmında metanın karbondioksit reformlamasında kullanılmak üzere yüksek etkinlik ve kararlılıkta, optimum Pt/Ni metal yapısına sahip etkili bir katalizör tespit etmek için δ -Al₂O₃ destekli Pt-Ni iki metalli katalizörleri tasarlanmış ve geliştirilmiştir. Katalizörlerin farklı etkinlik seviyeleri, iki metalli Pt-Ni örneklerinin katalitik performanslarının metal yükleme ve Ni/Pt oranına yakından bağlı olduğunu göstermiştir. Tüm katalizörler içinde en yüksek katalitik etkinlik ve kararlılığı, en düşük Ni/Pt oranlı 0.3Pt-10Ni katalizörü göstermiştir. Katalizörlerin Ni/Pt oranlarını değiştirerek ve beslenme akımına düşük miktarlarda oksijen veya su ilave ederek katalizörlerin kömürleşme reaksiyonlarına dirençleri de belirlenmeye çalışılmıştır. İkinci bölümdeki Pt-Ni katalizörlerin reaksiyon koşullarındaki ve Ni/Pt oranlarındaki farklılıklara bağlı olarak değişen performans ve kararlılık profillerine dayanarak, tezin üçüncü bölümünde bir kinetik çalışması gerçekleştirilmiştir. Tezin son bölümünde, Co/ZrO₂'ye ilave edilen metallerin yüzey mikro-yapı özellikleri ve katalitik performans üzerine etkileri araştırılmıştır. Sonuçlara göre La ilave edilen katalizör yüksek bir kararlılık, ancak orta dereceli bir etkinlik göstermiştir. Ce ilave edilmiş Co/ZrO₂, hazırlanan tüm katalizörler içinde en yüksek etkinliği göstermiş ve çok az bir etkinlik kaybına uğramıştır.

TABLE OF CONTENTS

ACKNOWLEDGEMENT	iv
ABSTRACT	vi
ÖZET	vii
LIST OF FIGURES	xii
LIST OF TABLES	xx
1. INTRODUCTION	1
2. LITERATURE SURVEY	5
2.1. CO ₂ Reforming of Methane	5
2.2. Catalysts for CO ₂ Reforming of Methane	8
2.2.1. Ni-based Catalysts	8
2.2.2. Co-based Catalysts	16
2.2.3. Noble Metal Catalysts	17
2.3. Combined CO ₂ Reforming and Partial Oxidation of Methane	22
2.4. Combined CO ₂ Reforming and Steam Reforming of Methane	24
2.5. Inhibition of the Catalytic Processes	25
2.5.1. Coke Deposition	26
2.5.2. Poisoning	30
2.5.3. Sintering	31
2.6. Kinetics of CO ₂ Reforming of CH ₄	32
2.6.1. Suggested Mechanisms and Rate Expressions for CO ₂ Reforming of CH ₄	34
2.7. Catalyst Supports	41
2.7.1. Zirconia (ZrO ₂)	43
3. EXPERIMENTAL WORK	45
3.1. Materials	45
3.1.1. Chemicals	45
3.1.2. Gases	46
3.2. Experimental Systems	47
3.2.1. Catalyst Preparation Systems	47

3.2.2. Catalyst Characterization Systems	48
3.2.2.1. Thermal Gravimetric Analysis	48
3.2.2.2. Total Surface Area	50
3.2.2.3. Scanning Electron Microscopy (SEM)	50
3.2.2.4. X-Ray Photoelectron Spectroscopy (XPS)	51
3.2.2.5. X-Ray Diffraction (XRD)	51
3.2.3. Catalytic Reaction System	51
3.2.4. Product Analysis System	54
3.3. Catalyst Preparation and Pretreatment	55
3.3.1. Support Preparation	55
3.3.1.1. Alumina	55
3.3.1.2. Zirconia	55
3.3.2. Preparation of Catalysts	57
3.3.2.1. Ce Promoted Pt/ZrO ₂ Catalysts	57
3.3.2.2. Pt-Ni/ δ -Al ₂ O ₃ Bimetallic Catalysts	58
3.3.2.3. Co/ZrO ₂ Catalysts with Different Promoters	58
3.4. Catalyst Characterization	58
3.4.1. Temperature Programmed Reduction Experiments	58
3.4.2. Total Surface Area Experiments	59
3.4.3. X-Ray Photoelectron Spectroscopy (XPS)	60
3.5. Reaction Tests	60
3.5.1. Blank Tests	60
3.5.2. Carbon Dioxide Reforming of Methane over Ce-promoted Pt/ZrO ₂ Catalysts	61
3.5.3. Combined Methane Reforming Reactions over Pt-Ni/ δ -Al ₂ O ₃ Catalysts	61
3.5.4. Kinetic Experiments over Pt-Ni/ δ -Al ₂ O ₃ Catalysts	62
3.5.5. Carbon Dioxide Reforming of Methane over Co-X/ZrO ₂ Catalysts (X = La, Ce, Mn, Mg, K)	63
4. RESULTS AND DISCUSSION	66
4.1. Carbon Dioxide Reforming of Methane over Ce-promoted Pt/ZrO ₂ Catalysts	66

4.1.1. Characterization Tests	67
4.1.1.1. Temperature Programmed Reduction	67
4.1.1.2. X-Ray Photoelectron Spectroscopy	68
4.1.1.3. Scanning Electron Microscopy	72
4.1.1.4. Temperature Programmed Oxidation	75
4.1.2. Carbon Dioxide Reforming of Methane	76
4.1.2.1. Effect of Reaction Temperature	77
4.1.2.2. Effect of Time-on-Stream (TOS)	81
4.1.2.3. Activation Energies	84
4.1.2.4. Effect of CH ₄ /CO ₂ Ratio in the Feed	85
4.1.3. Summary	87
4.2. Methane Reforming Combined with SR and POX over Pt-Ni/ δ -Al ₂ O ₃	88
4.2.1. Characterization Tests	89
4.2.1.1. X-Ray Photoelectron Spectroscopy	89
4.2.1.2. X-Ray Diffraction	91
4.2.2. Carbon Dioxide Reforming of Methane	92
4.2.3. Combined Partial Oxidation and Dry reforming	95
4.2.4. Combined CO ₂ and Steam Reforming of CH ₄	99
4.2.5. Stability Test	101
4.2.6. Coke Deposition	102
4.2.6.1. TGA/DTA of Spent Catalysts	102
4.2.6.2. SEM/EDX of Spent Catalysts	103
4.2.7. Summary	106
4.3. Kinetic Experiments over Pt-Ni/ δ -Al ₂ O ₃ Catalysts	107
4.3.1. Determination of Temperature Region for Kinetic Tests	107
4.3.2. Kinetic Measurements	109
4.3.2.1. Apparent Activation Energies	110
4.3.2.2. Power-Law Type Kinetics	111
4.3.2.3. Effect of CO on CDRM	116
4.3.2.4. Effect of H ₂ on CDRM	119
4.3.2.5. Langmuir-Hinshelwood Type Surface Reaction Models ..	120
4.3.3. Summary	126

4.4. Carbon Dioxide Reforming of Methane over Co-X/ZrO ₂ Catalysts (X = La, Ce, Mn, Mg, K)	127
4.4.1. Characterization Tests	127
4.4.1.1. Scanning Electron Microscopy	127
4.4.1.2. X-Ray Diffraction	133
4.4.1.3. Temperature Programmed Oxidation	133
4.4.2. CO ₂ Reforming of Methane over Co-X/ZrO ₂ (X=La, K, Mn, Mg, Ce)	134
4.4.3. Effect of Space Velocity on CDRM Activity	139
4.4.4. Summary	141
5. CONCLUSIONS AND RECOMMENDATIONS	142
5.1. Conclusions	142
5.2. Recommendations	145
APPENDIX A: CALIBRATION CURVES OF THE MASS FLOW CONTROLLERS	146
APPENDIX B: CALIBRATION CURVES OF THE GAS CHROMATOGRAPH ..	148
APPENDIX C: CONVERSION VERSUS RESIDENCE TIME GRAPHS	150
REFERENCES	155

LIST OF FIGURES

Figure 2.1.	Schematic diagram of the chemical energy transmission system (CETS)	6
Figure 2.2.	Deactivation mechanisms: A) Coke formation, B) Poisoning, C) Sintering of the active metal particles, and D) Sintering and solid-solid phase transitions of the washcoat and encapsulation of active metal particles	25
Figure 3.1.	Schematic diagram of the impregnation system	48
Figure 3.2.	Schematic diagram of thermogravimetric analysis system	49
Figure 3.3.	Schematic diagram of the BET equipment	50
Figure 3.4.	Schematic diagram of the microreactor flow system	53
Figure 4.1.	Temperature programmed reduction (TPR) profiles of 1%Pt/ZrO ₂ , 1%Pt-1%Ce/ZrO ₂ (coimp.), 1%Pt-5%Ce/ZrO ₂ (coimp.) and 1%Pt-1%Ce/ZrO ₂ (seq. imp.)	68
Figure 4.2.	Ce 3d XPS spectra of 1%Pt-1%Ce/ZrO ₂ prepared by coimpregnation (cat2)	70
Figure 4.3.	Ce 3d XPS spectra of 1%Pt-1%Ce/ZrO ₂ catalyst prepared by sequential impregnation (cat4)	71
Figure 4.4.	1%Pt-1%Ce/ZrO ₂ catalyst prepared by coimpregnation (cat2): A) SEM bright area image, B) Pt + Ce mapping, C) EDX spectrum	73

Figure 4.5.	1%Pt-1%Ce/ZrO ₂ catalyst prepared by seq. impregnation (cat4): A) SEM bright area image, B) Pt + Ce mapping, C) EDX spectrum	74
Figure 4.6.	Temperature programmed oxidation (TPO) profiles of spent catalysts after 4 h of time on stream reaction tests at 973 K with CH ₄ / CO ₂ = 1/1: 1%Pt-1%Ce/ZrO ₂ (coimp.), 1%Pt-5%Ce/ZrO ₂ (coimp.) and 1%Pt-1%Ce/ZrO ₂ (seq. imp.)	75
Figure 4.7.	Temperature programmed oxidation (TPO) profiles of spent catalysts after 4 h of time on stream reaction tests at 973 K with CH ₄ / CO ₂ = 2/1: 1%Pt-1%Ce/ZrO ₂ (coimp.) and 1%Pt-5%Ce/ZrO ₂ (coimp.)	76
Figure 4.8.	CH ₄ conversion for the different catalysts in the CDRM as a function of the reaction temperature. Conversion values measured at the end of 4 h on stream. CH ₄ / CO ₂ = 1/1. Space velocity = 15,600 mL/h.g-cat	77
Figure 4.9.	CO ₂ conversion for the different catalysts in the CDRM as a function of the reaction temperature. Conversion values measured at the end of 4 h on stream. CH ₄ / CO ₂ = 1/1. Space velocity = 15,600 mL/h.g-cat	78
Figure 4.10.	H ₂ /CO molar ratio in the CDRM product stream as a function of the reaction temperature. Conversion values measured at the end of 4 h on stream. CH ₄ /CO ₂ = 1/1. Space velocity = 15,600 mL/h.g-cat	78
Figure 4.11.	CH ₄ conversions for the different catalysts in the dry reforming as a function of reaction time. Reaction Temperature = 973 K. CH ₄ / CO ₂ = 1/1. Space velocity = 15,600 mL/h.g-cat	82
Figure 4.12.	CO ₂ conversions for the different catalysts in the dry reforming as a function of reaction time. Reaction Temperature = 973 K. CH ₄ / CO ₂ = 1/1. Space velocity = 15,600 mL/h.g-cat	82

Figure 4.13.	H ₂ /CO molar ratio values for the different catalysts in the dry reforming as a function of reaction time. Reaction Temperature = 973 K. CH ₄ / CO ₂ = 1/1. Space velocity = 15,600 mL/h.g-cat	83
Figure 4.14.	Arrhenius plots for CO production over temperatures ranging between 773 and 973 K. Catalyst: 1%Pt-1%Ce/ZrO ₂ (coimp.). Reaction conditions: CH ₄ / CO ₂ = 1. Space velocity = 15,600 mL/h.g-cat	84
Figure 4.15.	CH ₄ & CO ₂ conversions for the different catalysts in the dry reforming as a function of reaction time. Reaction Temperature = 973 K. CH ₄ / CO ₂ = 2/1. Space velocity = 15,600 mL/h.g-cat	86
Figure 4.16.	H ₂ /CO molar ratio values for the different catalysts in the dry reforming as a function of reaction time. Reaction Temperature = 973 K. CH ₄ / CO ₂ = 2/1. Space velocity = 15,600 mL/h.g-cat	87
Figure 4.17.	Ni 2p _{3/2} XPS spectra of 0.2Pt-15Ni sample	90
Figure 4.18.	Ni 2p _{3/2} XPS spectra of 0.3Pt-10Ni sample	91
Figure 4.19.	CH ₄ conversions for the different catalysts in CDRM as a function of reaction time. T _{rxn} = 923 K. CH ₄ / CO ₂ = 1/1. Space velocity = 15,600 mL/h.g-cat	93
Figure 4.20.	CO ₂ conversions for the different catalysts in CDRM as a function of reaction time. T _{rxn} = 923 K. CH ₄ / CO ₂ = 1/1. Space velocity = 15,600 mL/h.g-cat	93

Figure 4.21.	H ₂ /CO molar ratio values for the different catalysts in CDRM as a function of reaction time. T _{rxn} = 923 K CH ₄ / CO ₂ = 1/1. Space velocity = 15,600 mL/h.g-cat	94
Figure 4.22.	Effect of O ₂ addition to CDRM at 923 K. Catalyst: 0.3Pt-10Ni	96
Figure 4.23.	CH ₄ conversion during the combined CDRM and POX at 923 K. Catalyst: 0.3Pt-10Ni	96
Figure 4.24.	Effect of O ₂ addition to CDRM at 923 K. Catalyst: 0.2Pt-15Ni	97
Figure 4.25.	CH ₄ conversion during the combined CDRM and POX at 923 K. Catalyst: 0.2Pt-15Ni	97
Figure 4.26.	CH ₄ conversions for the different catalysts in combined CDRM + SR as a function of reaction time. Reaction Temperature = 923 K. CH ₄ / CO ₂ / H ₂ O = 1/1/1	100
Figure 4.27.	Stability test for CO ₂ reforming of methane. T _{rxn} = 923 K. CH ₄ / CO ₂ = 1/1	101
Figure 4.28.	Temperature programmed oxidation (TPO) profiles of used catalysts after CDRM for 4 h TOS at 923 K	103
Figure 4.29.	Morphology of carbon deposit in the 0.2Pt-15Ni catalyst after 4h of CDRM reaction at 923 K	104
Figure 4.30.	Morphology of carbon deposit in the 0.3Pt-10Ni catalyst after 4h of CDRM reaction at 923 K	105
Figure 4.31.	Morphology of carbon deposit after 4h of combined CDRM and POX reaction at 923 K with C/O = 1.20: (A) 0.3Pt-10Ni, (B) 0.2Pt-15Ni ...	106

Figure 4.32.	The variation of the equilibrium conversions with the reaction temperature for the dry reforming (a), CO disproportionation (b), CO/H ₂ reduction (c), CO/H ₂ methanation (d), and CO ₂ /H ₂ methanation (e)	109
Figure 4.33.	Arrhenius plots for CO over temperatures ranging between 853 and 893 K. Catalyst: 0.3Pt-10Ni. Reaction conditions: CH ₄ /CO ₂ = 1/1. Space velocity = 1,200,000 mL/h.g-cat	110
Figure 4.34.	Variation of the reaction rates for the consumption of methane ($-r_{CH_4}$) as a function of the partial pressure of methane (P_{CH_4}). The points are experimental data. The lines are the fitting using Equation 4.10.	115
Figure 4.35.	Variation of the reaction rates for the consumption of methane ($-r_{CH_4}$) as a function of the partial pressure of carbon dioxide (P_{CO_2}). The points are experimental data. The lines are the fitting using Equation 4.10.	115
Figure 4.36.	Variation of the reaction rates for the consumption of methane ($-r_{CH_4}$) as a function of the partial pressure of carbon monoxide (P_{CO}).	117
Figure 4.37.	Variation of the reaction rates for the consumption of methane ($-r_{CH_4}$) as a function of the partial pressure of hydrogen (P_{H_2})	120
Figure 4.38.	5Co2La: A) SEM image, B) La + Zr mapping, C) Co + Zr mapping ..	128
Figure 4.39.	5Co2K: A) SEM image, B) K + Zr mapping, C) Co + Zr mapping	129

Figure 4.40.	5Co2Mg: A) SEM image, B) Mg + Zr mapping, C) Co + Zr mapping	130
Figure 4.41.	5Co2Mn: A) SEM image, B) Mn + Zr mapping, C) Co + Zr mapping	131
Figure 4.42.	5Co2Ce: A) SEM image, B) Ce + Zr mapping, C) Co + Zr mapping	132
Figure 4.43.	Temperature programmed oxidation (TPO) profiles of spent catalysts after 6 h of time on stream reaction tests at 923 K with SV = 60,000 ml/h.g-cat	134
Figure 4.44.	Effect of modifier on CH ₄ conversion as a function of reaction time. Reaction Temperature = 923 K. CH ₄ / CO ₂ = 1/1. Space velocity = 60,000 mL/h.g-cat	135
Figure 4.45.	Effect of modifier on CO ₂ conversion as a function of reaction time. Reaction Temperature = 923 K. CH ₄ / CO ₂ = 1/1. Space velocity = 60,000 mL/h.g-cat	135
Figure 4.46.	Effect of modifier on H ₂ /CO ratio as a function of reaction time. Reaction Temperature = 923 K. CH ₄ / CO ₂ = 1/1. Space velocity = 60,000 mL/h.g-cat	136
Figure 4.47.	Morphology of carbon deposit on the 5Co catalyst after 6h of CDRM reaction	137
Figure 4.48.	Effect of space velocity (SV) on CH ₄ and CO ₂ conversions. Conversion values measured at the end of 6 h on stream Catalyst: 5Co2La Reaction Temperature = 923 K. CH ₄ / CO ₂ = 1/1	140
Figure 4.49.	Effect of space velocity (SV) on CH ₄ and CO ₂ conversions. Conversion values measured at the end of 6 h on stream Catalyst: 5Co2Ce Reaction Temperature = 923 K. CH ₄ / CO ₂ = 1/1	140

Figure A.1.	Calibration curve of the carbon dioxide mass flow controller	146
Figure A.2.	Calibration curve of the oxygen mass flow controller	146
Figure A.3.	Calibration curve of the argon mass flow controller	147
Figure A.4.	Calibration curve of the hydrogen mass flow controller	147
Figure A.5.	Calibration curve of the methane mass flow controller	147
Figure B.1.	Calibration curve of hydrogen	148
Figure B.2.	Calibration curve of carbon monoxide	148
Figure B.3.	Calibration curve of methane	149
Figure B.4.	Calibration curve of carbon dioxide	149
Figure C.1.	Fractional CH ₄ conversion vs. residence time graph of experiments 1-3. Catalyst: 0.2Pt-15Ni	150
Figure C.2.	Fractional CH ₄ conversion vs. residence time graph of experiments 4-6. Catalyst: 0.2Pt-15Ni	150
Figure C.3.	Fractional CH ₄ conversion vs. residence time graph of experiments 7-9. Catalyst: 0.2Pt-15Ni	151
Figure C.4.	Fractional CH ₄ conversion vs. residence time graph of experiments 10-12. Catalyst: 0.2Pt-15Ni	151
Figure C.5.	Fractional CH ₄ conversion vs. residence time graph of experiments 13-15. Catalyst: 0.2Pt-15Ni	151

Figure C.6.	Fractional CH ₄ conversion vs. residence time graph of experiments 16-18. Catalyst: 0.2Pt-15Ni	152
Figure C.7.	Fractional CH ₄ conversion vs. residence time graph of experiments 19-21. Catalyst: 0.2Pt-15Ni	152
Figure C.8.	Fractional CH ₄ conversion vs. residence time graph of experiments 1- 3. Catalyst: 0.3Pt-10Ni	152
Figure C.9.	Fractional CH ₄ conversion vs. residence time graph of experiments 4- 6. Catalyst: 0.3Pt-10Ni	153
Figure C.10.	Fractional CH ₄ conversion vs. residence time graph of experiments 7- 9. Catalyst: 0.3Pt-10Ni	153
Figure C.11.	Fractional CH ₄ conversion vs. residence time graph of experiments 10-12. Catalyst: 0.3Pt-10Ni	153
Figure C.12.	Fractional CH ₄ conversion vs. residence time graph of experiments 13-15. Catalyst: 0.3Pt-10Ni	154
Figure C.13.	Fractional CH ₄ conversion vs. residence time graph of experiments 16-18. Catalyst: 0.3Pt-10Ni	154
Figure C.14.	Fractional CH ₄ conversion vs. residence time graph of experiments 19-21. Catalyst: 0.3Pt-10Ni	154

LIST OF TABLES

Table 2.1.	Apparent activation energies (E_{app}) over Ni, Pt & Co catalysts	33
Table 2.2.	Reaction orders for reaction conditions of $P = 1$ atm, $CH_4/CO_2 = 1$, $T = 723$ K ($r_i = kP_{CH_4}^a P_{CO_2}^b$)	34
Table 2.3.	Proposed rate expressions for CO_2 reforming of CH_4	40
Table 3.1.	Chemicals used in catalyst preparation (all specifications: research grade)	45
Table 3.2.	Specifications and applications of the liquids used	46
Table 3.3.	Specifications and applications of the gases and standards used	46
Table 3.4.	Reactant and product gas analysis conditions	54
Table 3.5.	List of Ce promoted Pt/ZrO ₂ catalysts	56
Table 3.6.	List of Pt-Ni/Al ₂ O ₃ bimetallic catalysts	56
Table 3.7.	List of Co/ZrO ₂ catalysts with different promoters	56
Table 3.8.	List of reaction experiments performed over Pt-Ni/ δ -Al ₂ O ₃ catalysts ..	62
Table 3.9.	List of kinetic experiments performed over Pt-Ni/ δ -Al ₂ O ₃ catalysts	64
Table 3.10.	List of kinetic experiments performed over Pt-Ni/ δ -Al ₂ O ₃ catalysts (Effect of H ₂ and CO partial pressures)	65

Table 4.1.	Catalyst characterization by XPS	69
Table 4.2.	Weight percentages of the metallic species from SEM-EDX data	73
Table 4.3.	Catalyst activity at 973 K and apparent activation energies (E_{app})	85
Table 4.4.	Summary of XPS B.E. reported in the literature for Ni 2p _{3/2}	90
Table 4.5.	Catalyst characterization by XPS	91
Table 4.6.	Particle size determination by XRD	92
Table 4.7.	Effect of varying C/O ratio in the feed on the H ₂ /CO product ratio	98
Table 4.8.	Effect of varying C/O ratio in the feed on the CO ₂ conversion	98
Table 4.9.	Summary of combined CDRM + SR (T=923 K)	100
Table 4.10.	Apparent activation energies (E_{app}) in the current work and in the related literature	111
Table 4.11.	Partial pressures of methane and carbon dioxide and the corresponding residence time and space velocity values	112
Table 4.12.	Initial rates calculated from conversion-residence time data	113
Table 4.13.	Estimated reaction rate parameters	114
Table 4.14.	Effect of CO partial pressure on CDRM rates	116
Table 4.15.	Estimated reaction rate parameters in the presence of CO	118

Table 4.16.	Estimated power rate laws in the presence of CO	118
Table 4.17.	Effect of H ₂ partial pressure on CDRM rates	119
Table 4.18.	Langmuir-Hinshelwood (LH) type rate expressions	123
Table 4.19.	Model parameters obtained for 0.3Pt-10Ni Catalyst	124
Table 4.20.	Model parameters obtained for 0.2Pt-15Ni Catalyst	125
Table 4.21	Weight percentages of the surface metallic species from SEM-EDX data	133
Table 4.22	The effect of modification of cobalt catalyst for CO ₂ reforming of methane	136

1. INTRODUCTION

The known reserves of dominantly used fossil fuel, crude oil, are rapidly depleting. On the other hand, natural gas, the main component of which is methane, is an abundant fossil fuel resource found all over the world and is predicted to outlast oil reserves by a significant margin (Claridge *et al.* 1998). Methane is the major component of natural gas, with a fraction of 70 to 98%, depending on the location where it is obtained (Ross *et al.*, 1996).

Most of the natural gas reserves, however, are situated in areas remote from the centres of highest energy consumption, and the costs of compression, transportation and storage make methane an unattractive proposition as an energy source. To make remote methane reserves economically more viable, a large amount of research into the conversion of methane to liquids or higher molecular weight hydrocarbons has been carried out. There have been studies on direct oxidative conversions of methane into methanol, formaldehyde, propanal, benzene and other aromatics, and direct oxidative coupling of methane to ethane and ethylene. But all these processes either demonstrate low yields or are not economically viable; they do not meet industrial requirements at the existing price of crude oil (Claridge *et al.* 1998). Current industrial processes make use of methane as a primary feedstock for converting it to a mixture of carbon monoxide and hydrogen (synthesis gas or syngas). Almost 60 per cent of the total cost in liquid fuel production from methane comes from syngas production. Hence, reducing the cost of syngas would play a significant role in the economics of the gas-to-liquids process (Ross *et al.*, 1996; Rostrup-Nielsen and Hansen, 1993). The syngas produced serves as the feedstock in a variety of downstream processes, such as methanol synthesis, Fischer-Tropsch synthesis or ammonia synthesis (Iyer, 2001).

Reforming of methane to syngas can be carried out in three different ways: steam reforming, CO₂ reforming (or dry reforming) and partial oxidation.

In recent years, there has been considerable interest in the reduction of emission of greenhouse gases due to the alarming global warming effect. Methane and carbon dioxide

are both greenhouse gases. Therefore, the reduction and use of these gases would be very much appreciated and has been gaining more importance (Wang *et al.*, 1996). Catalytic reforming of methane with carbon dioxide to syngas has been proposed as one of the most promising technologies utilizing these greenhouse gases as carbon-containing materials. Syngas produced by dry reforming has a higher purity as compared to the conventional steam reforming process. Dry reforming also results in a lower H₂/CO ratio, near unity (Bradford and Vannice, 1999). (Typically, steam reforming produces syngas with a H₂/CO ratio of 3 while partial oxidation can yield a ratio close to 2). In the case of certain applications, like Fischer-Tropsch synthesis of long-chain hydrocarbons, hydroformylation, and synthesis of valuable oxygenated chemicals such as oxo-alcohols, a H₂/CO feed ratio close to unity is desired. Furthermore, carbon dioxide is also a significant component of natural gas at many locations, and dry reforming can be especially useful in those remote gas fields where there is an abundance of CO₂. The process can be employed in those remote gas fields where water is not easily available. The higher operating pressures of steam-reforming process should be also mentioned; this might lead to higher operating expenses. Thus, reducing operating pressures by the dry-reforming process would trim down both operating expenses and equipment costs and improves plant safety as well. Ross *et al.* (1996) have shown that dry reforming has the lowest operating costs, about 20 % lower than any other reforming processes. Finally, CH₄ and CO₂ are both inexpensive owing to their natural abundance and therefore their conversion to higher value compounds is of considerable interest.

The major drawback of dry reforming is that high temperatures are required to reach high conversion levels due to the highly endothermic nature of the process. These severe operating conditions result in deactivation by coke deposition and/or sintering of the metallic phase and support.

The most widely used catalysts for catalytic reforming of methane with carbon dioxide or steam for syngas production are alumina-supported Ni catalysts due to their low cost and high conversion. However, nickel also catalyses coke formation on the surface of the active phase, via methane decomposition and Boudart reaction, both of which lead to catalyst deactivation and plugging of the reformer tubes by carbon deposits (Pompeo *et al.*, 2007). One possible solution could be addition of excess oxidants in order to suppress the

coke deposition. However, this increases the CO_2/CO ratio, which defeats the basic purpose of dry reforming. Hence, notable efforts have been concentrated on exploring new catalysts, which are resistant to carbon formation. Sulfur-passivated nickel catalysts and noble-metal catalysts have been shown to exhibit resistance to carbon formation (Rostrup-Nielsen and Hansen, 1993). But the low activity of sulfur-passivated nickel catalysts, and the high costs as well as scarcity of noble metals, have limited their potential applications.

On this basis, important efforts have been given in order to develop new catalysts with high activity and selectivity and good stability in syngas production by methane reforming with CO_2 .

The overall purpose of this research study is to investigate new catalysts to produce syngas via CO_2 reforming of methane under optimized reaction conditions. The thesis consists of four parts. In the first part of the study; the purpose was to design and develop effective Pt-based bimetallic CDRM catalysts supported on zirconia. Aiming to have bimetallic catalysts with enhanced performance properties, Ce was used as a promoter in order to increase the oxygen storage capacity of the catalysts via controlling the electronic structure of the metals over the support. In the second part of the thesis, a set of Pt-Ni bimetallic catalysts supported on $\delta\text{-Al}_2\text{O}_3$ were designed and developed for carbon dioxide reforming of methane as the main reaction in order to determine an effective catalyst with optimum Pt/Ni metal composition assuring both high activity and stability. By changing the Pt/Ni ratios of the catalysts and with the addition of small amounts of either oxygen or water to the feed stream, the catalysts' resistance to coking reactions were tried to elucidate. Based on the different performance and stability profiles of the Pt-Ni catalysts in part two in response to the changes in their Pt:Ni ratio as well as the reaction conditions, a kinetic and mechanistic study was performed in the third part of the study, which aims to investigate the relation between Pt-Ni loading ratio and kinetics of dry reforming reaction. The conclusions and detailed information provided by the characterization results from the previous section were combined with the present results to propose a plausible mechanistic scheme and a kinetic model of the reaction catalysts with different Pt:Ni ratios. In the final part of the research, the effect of addition of metal additives to Co/ZrO_2 on both surface micro-structural properties and catalytic performance was investigated. The most

promising catalysts with desired micro-structural and catalytic characteristics were chosen for further investigation aimed to optimize the reaction conditions and surface properties.

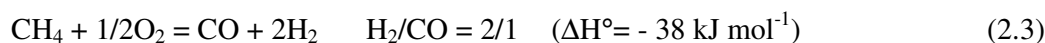
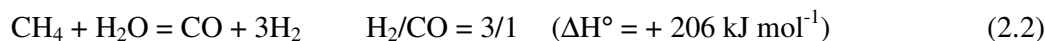
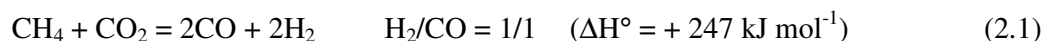
Chapter 2 contains a detailed literature survey on theoretical background of CO₂ reforming of methane, its combination with other reforming reactions and catalyst deactivation mechanism as well as kinetics of CO₂ reforming of methane. Chapter 3 presents the experimental work carried out. The results obtained are presented and discussed in Chapter 4. Chapter 5 consists of the conclusions drawn from the present study and recommendations for future work.

2. LITERATURE SURVEY

2.1. CO₂ Reforming of Methane

The catalytic process of carbon dioxide reforming of methane (CDRM) [Eq. (2.1)] to produce valuable synthesis gas (syngas), a mixture of CO and H₂, which converts two environmentally harmful gases (CH₄ and CO₂) into a useful chemical product, has received considerable attention in recent years (Nandini *et al.*, 2006; Takanahe *et al.*, 2005).

The CDRM process becomes industrially advantageous compared to steam reforming (SR) [Eq. (2.2)] or partial oxidation (POX) [Eq. (2.3)] in syngas production since H₂/CO product ratio is close to 1/1.



This low H₂/CO ratio is suitable for further use in Fischer-Tropsch (F-T) synthesis of long-chain hydrocarbons [Eq. (2.4)], dimethyl ether synthesis [Eq. (2.5)] and methanol production [Eq. (2.6)], all of which require lower H₂/CO ratios than that obtained by conventional SR (Bradford and Vannice, 1998; Souza *et al.*, 2001; Stagg-Williams *et al.*, 2000).



An additional, and perhaps most important, advantage of CDRM is in those cases in which the reactants are simultaneously available at low cost, or even at negative prices. Natural gas reservoirs contain primarily CH_4 , but some reservoirs also have a large fraction of CO_2 . Many of these reservoirs are located in remote regions and have quantities of natural gas that are too small to make the production economical. The capability to convert the natural gas in these reservoirs to higher value products in an efficient manner could increase the cost effectiveness of remotely located reservoirs (Stagg-Williams *et al.*, 2000).

Because of the high endothermicity of the reaction, the process can also be used in energy transfer from solar energy to chemical energy, in energy storage in the form of CO and H_2 and chemical energy transmission systems (CETS). A power source drives the endothermic reforming reaction, and the product gases are transported to consumers at remote areas, where the reverse exothermic methanation reaction can be performed (Figure 2.1).

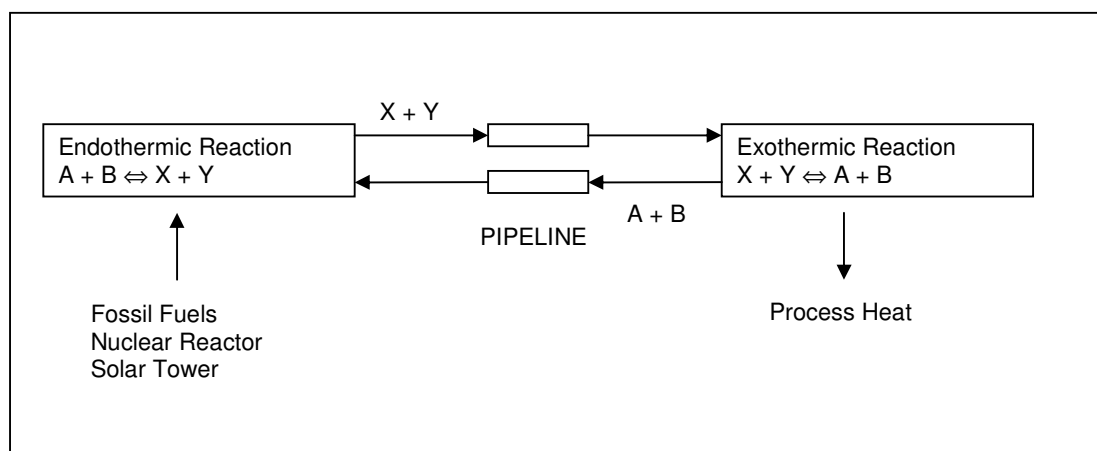
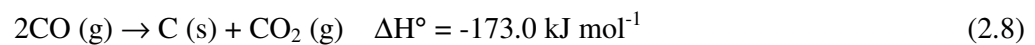
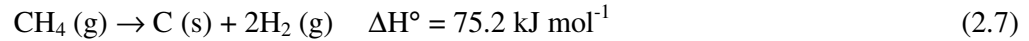


Figure 2.1. Schematic diagram of the chemical energy transmission system (CETS)

The major drawback of dry reforming is that high temperatures are required to reach high conversion levels due to the highly endothermic nature of the process. These severe operating conditions result in deactivation by coke deposition (Ballarini *et al.*, 2005; Djaidja *et al.*, 2006; Nagaoka *et al.*, 2001a) and/or sintering of the metallic phase and support (Guo *et al.*, 2004; Hou *et al.*, 2004a; Ferreira-Aparicio *et al.*, 1998; Montoya *et al.*, 2000). Thus, it is desired to develop (an) effective CDRM catalyst(s) exhibiting high

activity and selectivity as well as good stability in the syngas production. Coke is formed mainly by two reactions, methane decomposition [Eq. (2.7)] and carbon monoxide disproportionation [Eq. (2.8)]. The former is an endothermic reaction and favored at higher temperatures and lower pressures whereas the latter is exothermic and favored at lower temperatures and higher pressures (Nagaoka *et al.*, 2001b).



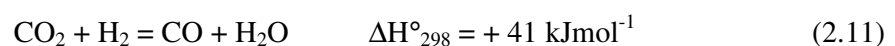
The problem of coke deposition can be resolved either (i) by developing catalysts that minimize the rate of methane decomposition and/or CO disproportion, or (ii) by adding water or oxygen to the feed gas stream (Bradford and Vannice, 1999)

Addition of either H₂O or O₂ to the feed inhibits carbon formation either via gasification [Eq. (2.9)], or oxidation [Eq. (2.10)].



Moreover, addition of H₂O or O₂ to the feed has several practical advantages over CH₄, reforming with CO₂ alone: (i) syngas with a wider range of H₂/CO ratios can be produced via adjustment of the CO₂/H₂O/O₂ feed ratio, and (ii) as CDRM is a highly endothermic process and thus requires a large amount of energy to proceed, its coupling with the exothermic POX would also minimize the energy requirements and have economic advantages.

The reforming of methane with CO₂ is typically influenced by simultaneous occurrence of reverse water-gas shift (RWGS) reaction [Eq. (2.11)], which results in H₂/CO ratios less than unity.



On this basis, important efforts are being done in order to develop new catalysts with high activity and selectivity and good stability in syngas production by using methane reforming with CO₂.

2.2. Catalysts for CO₂ Reforming of Methane

Carbon dioxide reforming of methane was first studied by Fischer and Tropsch over a number of base metal catalysts (Fischer and Tropsch, 1928). The reaction has been extensively studied using catalysts composed of transition metal carbides and sulfides, perovskite-type mixed oxides, unsupported metals, and supported group VIII metals, with the exception of Os. Noble metals, such as ruthenium (Ru) and rhodium (Rh), and the nonnoble metal nickel (Ni) have been studied extensively for this reaction. It has been found that supported Rh, Ru, Pd, Pt, and Ir catalysts can provide stable operations for carbon dioxide reforming of methane with low carbon formation or deposition on the catalysts during the reaction. However, from an industrial standpoint, it is more practical to develop nonnoble metal-based catalysts to avoid the high cost and restricted availability of noble metals. Ni has drawn significant research attention due to its high activity and wide availability. The great challenge for Ni catalysts is that they suffer severe catalyst deactivation due to sintering, metal oxidation, and especially significant carbon formation (Zhang *et al.*, 2007).

2.2.1. Ni-based Catalysts

The most widely used catalysts for catalytic reforming of methane with carbon dioxide or steam for syngas production are alumina-supported Ni catalysts due to their low cost and high conversion. However, nickel also catalyses coke formation on the surface of the active phase, via reactions (2.7) and (2.8), both of which lead to catalyst deactivation and plugging of the reformer tubes by carbon deposits. The Ni metal can dissolve unreactive C residues and generate carbon filaments (whiskers) with the Ni particle on the filament top. During this process, metallic sites remain uncovered despite the deposition of large amounts of carbon, thus resulting in much lower deactivation rates than those expected if metal covering coke deposits occurred. However, whisker formation must absolutely be avoided because it causes a significant expansion of the catalyst bed resulting

in severe operational problems. Besides, as Ni is placed on the filament top, it is difficult to regenerate the catalytic system because the contact between metal and support is lost (Pompeo *et al.*, 2007). This requires using more effective and stable Ni catalysts, resistant to coke formation.

A great effort has been directed to develop Ni-based catalysts with improved performance; lower coke deposition on the metal surface and higher stability against metal sintering. It was reported that coke formation is a structure-sensitive process, and depends on the surface Ni species, particle size and electron density. It has been suggested that the carbon deposition would be enhanced, if the size of Ni metal particle was greater than a critical size. Swaan *et al.* (1994) reported that activity of different Ni-based catalysts appears to depend essentially on the degree of reduction and the dispersion of Ni particles, and not so much on the support. More recently some studies have pointed out that carbon formation is strongly diminished in catalysts with as small as possible Ni particles. A lot of promoters to Ni catalyst, methods of catalyst preparation and many kinds of supports (oxides, combined-oxides, perovskites, zeolites, carbon and SiC) were tried in order to eliminate the coke deposition (Hou and Yashima, 2004b)

Among the reported promoters, alkali and alkaline earth metals (K, Na, Ca and Mg) were helpful for the improvement of the coke resistance ability of Ni and possess the potential to have several kinds of effects on the physicochemical properties of Ni catalysts in reforming reaction: (a) influence on the electronic properties of the Ni clusters as well as their dimensions, (b) modification of the acidity of the support surface and (c) surface enrichment of CO₂ through stabilization of surface carbonate species (Arena *et al.*, 1999; Chang *et al.*, 2000; Hou *et al.*, 2003a; Pompeo *et al.*, 2005).

In published papers, Ca was popularly used as a modification of support materials, but the coke resistance of these modified material-supported Ni catalysts was not good enough (Cheng *et al.*, 1996; Tang *et al.*, 1995). In previous studies on Ca-promoted Ni/ α -Al₂O₃ catalysts, it was found that a small amount of Ca (Ca/Ni<0.1, mole ratio) strengthened the interaction between Ni and support and increased the reforming activity and the stability. However, a greater amount of Ca occupied the limited surface of α -Al₂O₃ and bulk NiO without interaction with the Al₂O₃, which in turn enhanced coke deposition

and accelerated deactivation. This was attributed to the effects of support composition on the morphology and particle size distribution of nickel metal. In the study by Hou et al. (2003), it was found that the influence of Ca on the supported Ni catalysts strongly depended on the properties of supports and the amount of Ca added. Small amounts of Ca increased the activity and stability of Ni/ γ -Al₂O₃. H₂-TPR, XRD and XPS characterizations of different amounts of Ca-promoted Ni/ γ -Al₂O₃ catalyst indicated that Ca improved the dispersion of Ni, strengthened the interaction between Ni and Al₂O₃, and retarded the sintering of Ni. While Ca/Ni = 0.2 is a critical point, above this level an excess amount of Ca would cover the surface of γ -Al₂O₃ and hinder the interaction of Ni with the support. But the negative effect of Ca is that it increased the decomposition of CH₄. Based on the above conclusions, the authors think that the coke deposition on Ni/ γ -Al₂O₃ promoted with higher amounts of Ca would be the main reason for its deactivation, while the poor stability of pure Ni/ γ -Al₂O₃ would be due to the metal sintering.

The addition of K to Ni/Al₂O₃ catalysts resulted in the reduction of not only the coke formation but also the reforming activity. It was found that K could divide the nickel surface into smaller ensembles, while the covering of the surface of the Ni particles with K reduced the reforming activity (Osaki and Mori, 2001). According to the work by Juan-Juan *et al.* (2004) and Nandini *et al.* (2005), the incorporation of K into Ni/Al₂O₃ hinders the accumulation of coke on the catalyst surface. Moreover, Juan-Juan *et al.* (2006) have shown that addition of a low amount of potassium (0.2wt% K₂O) allows obtaining a catalyst with an acceptably high activity (close to thermodynamic equilibrium) and very low coke deposition. Walter *et al.* (1994) have provided evidence that surface OH groups preferentially react with the surface CH_x species rather than surface O, which means that the addition of K would increase the amount of surface OH due to its strong basicity and increase the gasification of the intermediate CH_x fragment.

In the study by Hou and Yashima (2004b), The Ni/Mg/Al catalysts prepared by coprecipitation method possess the meso-porous structure with higher surface area. The higher surface area and the stronger interaction between Ni and Al-Mg improved the dispersion of Ni and retarded the sintering of Ni during the reforming process. The highly dispersed Ni increased the adsorption of CO₂ and increased the decomposition of CH₄; this contributed to a higher reforming activity, lower coke formation and a higher stability.

Several recent publications have demonstrated that solid solution of NiO–MgO enhances catalyst lifetime by decreasing carbon formation. This is related to the small nickel crystallites which are stable toward sintering and carbon formation (Hu and Ruckenstein, 1996; Tomishige *et al.*, 1999).

Choi *et al.* (1998) studied the effect of various modifiers, such as Co, Cu, Zr, Mn, Mo, Ti, Ag, and Sn over Ni/Al₂O₃ catalysts in CO₂ reforming of methane. The major role of these additives was to suppress the deposition of unreactive carbon (“coke”). Relative to unmodified Ni/Al₂O₃, catalysts modified with Co, Cu and Zr showed slightly improved activity, while other promoters reduced the activity of CO₂ reforming.

Mn-promoted catalyst showed a remarkable reduction in coke deposition, while entailing only a small reduction in catalytic activity compared to unmodified catalyst. Detailed studies on Ni/MnO/ γ -Al₂O₃ catalyst revealed that the surface of nickel is partly covered (“decorated”) by patches of MnO_x and that manganese addition also promotes the adsorption of CO₂ by forming a reactive carbonate species. Further study also indicated that the activity and the stability of Mn-containing Ni/Al₂O₃ catalysts were strongly dependent on the preparation method (Seok *et al.*, 2002).

The effects of the Cu addition to Ni/Al₂O₃ catalyst are investigated by Lee *et al.* (2004) to suppress the carbon deposition during CO₂ reforming of methane. The 1 wt. per cent Cu addition to the Ni/Al₂O₃ catalyst enhanced the stability and the activity of the Ni/Al₂O₃ catalyst, but CuNi/Al₂O₃ catalyst added over 5 per cent Cu were deactivate more rapidly than the Ni/Al₂O₃ catalyst without Cu component. Moreover, Chen *et al.* (2004) also studied Cu/Ni catalyst supported on SiO₂ and found that the addition of Cu into Ni catalyst system can fine-tune the catalytic activity so that the CH₄ decomposition and removal of coke by CO₂ is balanced and prevent inactive coke accumulation on Ni particle.

It has also been reported that the addition of cobalt to nickel catalysts reduces the coke formation during reactions such as partial oxidation of methane to synthesis gas (Choudhary *et al.*, 1997), and steam or CO₂ reforming of methane (Choudhary and Mamman, 1998). Nagaoka *et al.* (2004) showed that a partial substitution of nickel for Co/TiO₂ (typically Co/Ni=90/10) enhanced catalytic stability dramatically. It is speculated

that, by accelerating methane decomposition, the nickel provides reductive hydrogen to cobalt via spillover phenomena, thus inhibiting oxidation of cobalt. Moreover, the same authors in 2005 showed that Co-Ni/TiO₂ catalysts with an appropriate Co/Ni ratio showed highly stable activities without carbon deposition.

CeO₂ has also been reported as an effective promoter for Ni catalysts. Addition of CeO₂ into Ni/ γ -Al₂O₃ not only increased the catalytic activity and stability but also suppressed the carbon deposition because CeO₂ enhanced the Ni dispersion and reactivities of carbon deposits (Wang and Lu, 1998). According to the results of Nandini *et al.* (2005), it is suggested that addition of CeO₂ as a promoter to Ni/Al₂O₃ reduces the particle size of nickel, increasing Ni dispersion, thus resulting in stable catalysts for DR of methane. Roh *et al.* (2004) reported enhanced catalytic activity and stability for coprecipitated Ni-Ce-ZrO₂ catalysts, which was attributed to the finely dispersed nano-sized NiO_x crystallite resulting in intimate contact between Ni and support, better Ni dispersion, higher Ni surface area and enhanced oxygen transfer during the reaction. Akpan *et al.* (2006) have recently developed a stable Ni/CeO₂-ZrO₂ catalyst by utilizing the interaction of hydrous oxide of ceria-zirconia with the cationic surfactant under basic condition followed by nickel. The catalyst was found to be stable for DR process for more than 200 h without any appreciable rate of deactivation.

Moreover, the addition of lanthana to Ni based catalysts as a promoter is also studied by several researchers. Slagtern *et al.* (1997) investigated the physical changes of the Ni-La/Al₂O₃ during testing and found that 1.7 per cent La promoted Ni/Al₂O₃ catalyst displayed superior performance compared to unpromoted catalyst, which was explained by higher Ni dispersion. Martinez *et al.* (2004) studied the influence of lanthanum oxide on Ni/Al₂O₃ catalyst by coprecipitation (at variable pH) for DR and the beneficial effect was expressed through better metallic dispersion, slightly higher conversion levels, and a significant decrease in coke formation during reaction. TPR experiments detected a narrower NiO particle size distribution in samples containing lanthanum. After reduction, Ni particles with diameters below 10 nm contributed to catalytic action without coke formation. These samples maintain a greater proportion of Ni particles with diameters below 10 nm than Ni-Al catalysts, thus coke formation is clearly diminished. They also contain La atoms within the Ni lattice after 4 h of reaction, which also leads to a certain

degree of diminution of coke formation. This also indicates a good dispersion of La in the samples.

Zhang and Verykios (1996) also suggested that the interaction between nickel and lanthanum species creates a new type of synergetic active sites at the Ni–La₂O₃ interface, which offer active and stable performance of carbon dioxide reforming of methane to synthesis gas. These results are interesting from the point of view of catalytic stability, because they attribute the higher stability to the lanthanum oxide. Nevertheless, alumina is probably a more suitable support (due to its high mechanical strength, high surface area, and low price) for use in catalysis, especially in the reforming of hydrocarbons. Thus the structural and thermal stability of Ni-B/ γ -Al₂O₃ catalyst, as well as Ni dispersion, was reported to have been improved by La addition (Hou *et al.*, 2004a).

It is well known that bimetallic catalysts may sometimes exhibit superior activity, selectivity and deactivation resistance than the corresponding monometallic catalysts. The modification of Ni-based catalyst by a noble metal can result in a non-expensive bimetallic supported system assuring both high activity of catalyst and its low carbon deposit formation. It has been reported that Ni/ α -Al₂O₃ (Hou and Yashima, 2003b) and Ni/SiO₂ catalyst (Józwiak *et al.*, 2005) doped with a small amount of Rh showed higher activity in the CO₂ reforming of methane than the unpromoted Ni catalysts. The addition of Ru or Pd to Ni/SiO₂ strongly enhanced the activity and stability of the catalyst in the process of CDRM (Crisafulli *et al.*, 1999, 2002). An increased methane conversion in autothermal reforming of methane was observed after introducing small amounts of Pt, Pd and Ir (<0.3 wt. per cent) into Ni/ γ -Al₂O₃ catalysts (15 wt. per cent) (Dias and Assaf, 2004, 2005). Another study showed that introduction of small amount of Pt into Ni/ZSM-5 led to a significant improvement in DR activity and stability, which was attributed to the increased Ni metallic dispersion caused by an intimate contact between Ni and Pt at Ni loading of 6 wt. per cent (Pawelec *et al.*, 2007).

Furthermore, Tomishige *et al.* (2002a, 2003) also studied 0.09 wt. %Pt- 0.9 wt. % Ni bimetallic system supported on alumina, prepared either by coimpregnation or sequential impregnation of the metals, for DR coupled with POX. They carried out the reaction tests for 30 min and they compared the performance of the monometallic Pt and Ni catalysts

with the bimetallic catalysts based on the temperature profile along the catalyst bed at single wall temperature and observed that the addition of little amount of Pt to Ni/Al₂O₃ catalyst resulted in a significant increase of its activity in methane.

One aspect of modifying nickel-based catalysts is to focus on proper choices and improvements of supports. A number of studies on CO₂-CH₄ reforming over supported Ni have indicated that the support may play an important role in the activity and coking resistivity of catalysts. Suitable supports have to be resistant to the high temperature applied and they have to maintain the metal dispersion of the catalyst during operation. Bradford and Vannice (1998) examined Ni- or Pt-based catalysts; their results indicated that carbon deposition could be greatly suppressed when TiO₂ or ZrO₂ was used as a support. Horiuchi *et al.* (1996) suggested that carbon deposition could be suppressed when the metal was supported on a metal oxide of strong Lewis basicity, such as ZrO₂, MgO, CeO₂ and La₂O₃. The increase in Lewis basicity is expected to strengthen the ability of the catalyst to chemisorb CO₂ and, thus, to reduce carbon formation via Boudart reaction (2CO = CO₂ + C) by shifting the equilibrium concentration. Xu *et al.* (1999) reported that Ni supported on nano-sized ZrO₂ (15–25 nm), MgO (10–20 nm) and γ -Al₂O₃ (5–19 nm) were highly active and stable. Hwang *et al.* (2001) reported that meso-porous clay-supported Ni catalysts exhibited high activity and a long lifetime of stability.

It has also been reported that La₂O₃ supported nickel catalyst exhibits high activity and excellent long-term stability. On this Ni/La₂O₃ catalyst, the rate increases during the initial 2–5 h of reaction and then becomes steady with time on stream, displaying very good stability. Studies conducted by Zhang *et al.* (1996) with Ni-Al₂O₃ and Ni-La₂O₃ catalysts in this reaction at 750°C show the stability of the latter. While the former showed a high activity loss after 8 h, the reaction rate with the Ni-La₂O₃ increased during the 3 first hours and remained constant until the end of the experiment (ca. 100 h).

Guo *et al.* (2004) also studied CDRM over Ni catalysts supported on γ -Al₂O₃, MgO-Al₂O₄, and MgAl₂O₄, to seek the activity and deactivation behavior of the catalysts. According to this study, all the catalysts showed high activity towards dry reforming of methane. The MgAl₂O₄ spinel layer that formed over Ni/MgO-Al₂O₃ can effectively suppress the phase transformation to form NiAl₂O₄ spinel phases and can stabilize the tiny

Ni crystallite. While a continuous catalyst deactivation is found over Ni catalyst supported on γ -Al₂O₃, and MgO-Al₂O₃, Ni/MgAl₂O₄ is very effective in CO₂ reforming of methane, 5%Ni/MgAl₂O₄ exhibits stable performance for 55 h on stream without any deactivation, displaying very good stability. The Ni/MgAl₂O₄ showed interactions between Ni and MgAl₂O₄ spinel. XRD results show that no NiO crystalline phase was detected on the fresh Ni/MgAl₂O₄ catalyst with Ni loading lower than 15%. After reduction and reaction, the Ni particle sizes were only 10.4 and 11.8 nm, indicating that little sintering occurred under reaction conditions.

Oxygen-ion conducting oxides, such as Ni-Cr/yttria-doped ceria (YDC) are known to impart metal-support interactions to enhance catalytic performances, due to their easy generation of oxygen vacancies to form interfacial active centers at the metal-support interfaces when used as supports. According to the study of Wang *et al.* (2003), the activity of Ni/YDC for CO₂ reforming of methane is enhanced remarkably compared with Ni/ γ -Al₂O₃, due to the synergistic effect of nickel and surface oxygen vacancies of YDC.

The preparation method of catalysts has significant effect on catalytic activity and coking resistivity for methane conversion to synthesis gas. Chang *et al.* (1994) reported Ni-zeolite catalyst synthesized by two methods: (i) solid-state reaction and (ii) incipient wetness method. The catalyst prepared by incipient wetness method gave much less activity than that prepared by solid-state reaction technique. The latter gave over 90 per cent conversion at 800°C without deactivation by coking. Ruckenstein and Hu (1996) studied the activity of Ni/La₂O₃ catalyst for DR using different precursors and their results showed that Ni precursor employed in the preparation of the catalyst played a significant role. The effect of the preparation procedure on promoted Ni/Al₂O₃ catalysts activity for CDRM was also researched (Cheng *et al.*, 1996). It was found that catalyst by successive impregnation of promoter oxide and nickel oxide was better than those prepared by co-impregnation process. Tang *et al.* (2000) prepared three Ni-based catalysts with same nickel content (10 wt. per cent) by conventional impregnation of commercial Al₂O₃ support, sol-gel made Al₂O₃ and direct sol-gel processing from organometallic compounds, respectively. They found out that three catalysts had almost identical catalytic activity for DR, but substantial different coke resistivity and stability. Ni catalyst supported on sol-gel made Al₂O₃ had excellent coking resistivity with no obvious coke observed after 80 h of reaction on stream.

The outstanding performance was related to the small size of initial Ni particles and the high dispersion of nickel that should be ascribed to the high BET surface area of sol-gel made supports.

2.2.2. Co-based Catalysts

Recently, a few Co-based catalysts, namely Co/MgO (Ruckenstein and Wang, 2000; Wang and Ruckenstein, 2001), Co/Al₂O₃ (Ji *et al.*, 2001; Ruckenstein and Wang, 2002) and Co/CeO₂ (Asami *et al.*, 2003) were developed and tested for CDRM process.

Ruckenstein and Wang (2000) first studied CDRM reaction over Co supported on an alkaline earth metal oxide (MgO, CaO, SrO, or BaO) as well as on γ -Al₂O₃ and on SiO₂. They found that the 12 wt.% Co/MgO catalysts provided a CO yield of 93 per cent and a H₂ yield of 90 per cent at the high space velocity of 60,000 ml g⁻¹ h⁻¹, with very high stability. It was suggested that the suppression of carbon deposition and the resistance to sintering of this catalyst were induced by the formation of a solid solution between CoO and MgO, because both had a NaCl type structure and close lattice parameters and bond distances.

Later, the same authors (Wang and Ruckenstein, 2001) studied the effect of Co loading and calcination temperature on the formation of solid solution between Co and Mg. The results demonstrated that the Co/MgO solid solution catalysts with loadings between 8 and 36 wt. per cent precalcined at 500 and 800°C, provided high and stable activities for the CDRM process. However, it was also observed that a too high calcination temperature (e.g. 900°C) caused a low activity or a long activation period, and a too high Co loading (48 wt. per cent) combined with a calcination temperature 800°C resulted in an unstable activity.

Ruckenstein and Wang (2002) have also investigated the reaction behaviour and carbon deposition during CDRM over Co/Al₂O₃ catalysts as a function of cobalt loading and calcination temperature. It was found that stability was strongly dependent on the Co loading and calcination temperature. For loadings of 6 wt. per cent and 9 wt. per cent, stable activities have been achieved. However, over the catalysts with high Co loadings

(>12 wt. per cent), notable amounts of carbon were accumulated during reforming, and deactivation was observed. Moreover, severe deactivation was also noted over the 2 wt. per cent catalysts.

Ji *et al.* (2001) prepared three Co-based catalysts with same cobalt content (10 wt. per cent) by conventional impregnation of commercial Al_2O_3 support, sol-gel made Al_2O_3 and direct sol-gel processing from organometallic compounds, respectively. At 750°C , all three catalysts had the same catalytic activity. However, the catalyst prepared by direct sol-gel processing showed relatively low catalytic activity at low reaction temperatures ($550\text{--}650^\circ\text{C}$) and high space velocity, due to the formation of CoAl_2O_4 . Compared to other catalysts, possessed smaller metallic Co particles, richer surface OH species and stronger metal-support interaction, all of which benefited the inhibition of coke formation.

Recently, Mondal *et al.* (2007) studied the influence of support on the performance of different Co containing metal oxide catalysts in CO_2 reforming of methane. They found out that the activity, selectivity and coking rate in the CDRM over the cobalt containing catalyst are strongly influenced by both the accompanied metal oxide (MgO , ZrO_2 , CeO_2 , Y_2O_3 or ThO_2) and catalyst support [a commercial low surface-area macro-porous silica-alumina (SA-5205) or zirconia-haffnia (SZ-5564)]. In the absence of the support or the accompanied metal oxide, the CoO_x catalyst showed very poor activity and selectivity and also shows very high coking rate in the CO_2 reforming. The $\text{CoO}_x\text{--MgO/SA-5205}$ and $\text{CoO}_x/\text{MgO/SA-5205}$ were highly active and selective catalysts, having negligibly small coking rate, and hence were highly promising ones for the CDRM.

2.2.3 Noble Metal Catalysts

Noble metal catalysts exhibit better activity and suffer less from carbon deposition as compared to non-noble metal catalysts. Many studies related to the reforming reaction of methane with CO_2 have been conducted over noble metals in order to develop a successful catalyst and to gain an enhanced understanding of the mechanisms of reaction and deactivation. It was reported in literature that the behavior of supported noble metallic catalysts in CDRM depends on several interrelated factors such as the nature of the metal,

the support type, the metallic particle size and the characteristics of metal-support interface. (Zhang *et al.*, 1996; Bitter *et al.*, 1997; Tsipouriari *et al.*, 1994)

The combination of a metal and a support greatly affected the catalytic activity and carbon deposition for this reaction. Rostrup-Nielsen and Hansen (1993) reported that the catalytic CDRM activity of the MgO-supported catalyst decreased in the following order: Ru > Rh > Ir > Pt = Pd. On the other hand, Solymosi *et al.* (1991) reported that the order is Ru > Pd > Rh > Pt > Ir when Al₂O₃ was used as a support.

Zhang *et al.* (1996b) reported the effect of support on the Rh catalyst and concluded that the activity order is YSZ (yttria stabilized zirconia) > Al₂O₃ > TiO₂ > SiO₂ > La₂O₃ > MgO. Later on, Wang and Ruckenstein (2000) studied CDRM over the reduced supported Rh (0.5 wt. per cent) catalysts. They used two kinds of oxides, reducible (CeO₂, Nb₂O₅, Ta₂O₅, TiO₂ and ZrO₂) and irreducible (Al₂O₃, La₂O₃, MgO, SiO₂ and Y₂O₃) as supports. They showed that among the irreducible oxides, Al₂O₃, La₂O₃ and MgO provided stable activities and the activity increased in the sequence: La₂O₃ < MgO ≈ Al₂O₃. SiO₂ and Y₂O₃ were not suitable because the conversions and yields decayed with time on stream. MgO and Al₂O₃ are the most promising supports; they provided high activities and were also stable with time. The reducible oxides were not suitable supports for this reaction as most of them provided relatively low conversions and yields.

With Pd catalyst, the activity order was reported as TiO₂ > Al₂O₃ > SiO₂ > MgO (Erdöhelyi *et al.*, 1994). With supported Ir catalysts, TiO₂ was reported to be the best support by Solymosi *et al.* (1997). Bitter *et al.* (1997) studied the effect of the support (Al₂O₃, ZrO₂, TiO₂ and SiO₂) on Pt-based catalysts and they found that, ZrO₂ was the most effective, resulting in a stable catalyst at 600°C and 1:1 CH₄:CO₂ feed ratio.

It has been shown that certain supports are able to provide oxygen to the metal during the reaction and, by this way, suppress the formation of carbon deposition (Wang and Ruckenstein, 2000; Efstathiou *et al.*, 1996; Ferreira-Aparicio *et al.*, 2000; Slagtern *et al.*, 1997). Thus, oxides with high oxygen exchange capacity and mobility are expected to be good candidates as supports for the CDRM reaction. The use of reducible oxides, like ZrO₂, can result in attractive process benefits when compared to irreducible oxides, such as

Al₂O₃ or SiO₂ (Bradford and Vannice, 1998; Wang and Ruckenstein, 2000; Nagaoka *et al.*, 2000a), due to its complex chemical properties, i.e. redox, and acidic and basic properties, reducibility as well as high thermal stability.

Good activity and stability characteristics of Pt/ZrO₂ catalysts were reported in several papers (Stagg-Williams *et al.*, 2000; Bitter *et al.*, 1997; Nagaoka *et al.*, 2001a). Coke, which may cover the active sites, is hardly formed on Pt/ZrO₂ resulting in stable activity for long periods of time. In earlier studies (Stagg-Williams *et al.*, 2000; Bitter *et al.*, 1997; Stagg *et al.*, 1998), it has been proposed that the reaction involves decomposition of CH₄ on Pt particles leading to the formation of H₂ and partially dehydrogenated species (CH_x), and dissociation of CO₂ into CO and O on the support. The oxygen formed during the dissociation of CO₂ can subsequently oxidize the CH_x species. The balance between the rate of decomposition of CH₄ on metal particles and the rate of its oxidation by the dissociated CO₂ determines the overall stability of the catalyst.

Previous studies (Stagg-Williams *et al.*, 2000; Mattos *et al.*, 2003; Wang *et al.*, 2004) have shown that the addition of promoters to the ZrO₂ support had several promotional effects in CDRM process and that the addition of Ce and La to the ZrO₂ support resulted in significant improvement in the stability, with no decrease in both CH₄ and CO₂ conversions.

Conversely; Stagg *et al.* (1998) also studied the effect of the addition of Sn on ZrO₂ supported Pt catalysts for the dry reforming reaction and showed that co-impregnation of Pt and Sn on ZrO₂ resulted in a decrease in the performance due to segregation of the Pt–Sn alloy, blocking the interaction between the metal particle and the support

Particularly, noble metal catalysts containing ceria as a promoter increase the catalytic reactivity in the oxidation reactions of different hydrocarbons (Monteiro *et al.*, 2001; Sohier *et al.*, 1992; Son and Lane, 2001) and enhance the performance characteristics of three-way catalysts used in elimination of pollutants in automobile exhausts (Farrauto and Heck, 1999; Kašpar *et al.*, 1999; Kozlov *et al.*, 2002). The unique acid-base and redox properties of ceria influence dispersion of the active metals on the support as well as oxidation and reduction cycle of noble metals (Damyanova and Bueno,

2003; Trovarelli, 1996). The oxygen vacancies at the metal–oxide interface of reduced ceria, leading to high oxygen storage capacity, suppresses coke formation (Damyanova and Bueno, 2003; Trovarelli, 1996; Holmgren and Andersson, 1998).

According to the study by Damyanova and Bueno (2003), addition of Ce into Pt/Al₂O₃ results in a bimetallic surface interaction, which affects the surface reducibility. XPS result show that the nature of Pt-Ce interaction varies with CeO₂ loading. Addition of a small amount of CeO₂ (1 wt. per cent) ceria into Pt/Al₂O₃ catalyst prevents the deactivation of the catalyst by acceleration of gasification of coke deposition. The latter is caused by the higher dispersion of Pt on the surface of low-loaded CeO₂ carrier, which leads to a more intimate contact between Ce and Pt and increasing of the surface of metal–support interfacial region. The lower efficiency of ceria on the activity and stability of Pt/CeO₂-Al₂O₃ catalysts with higher CeO₂ loading could be due to the lower surface area of ceria in these systems. The intimate Pt-Ce contact is hindered by the great size of ceria crystallites.

Hashimoto *et al.* (2002) also studied a catalyst consisting of Ru metal and CeO₂ highly dispersed on mordenite and found out that Ru-CeO₂/mordenite was highly active for reforming of CH₄.

Moreover, Menad *et al.* (2003) studied the catalytic properties of a ruthenium-zirconia-ceria system prepared by the microemulsion method. The catalyst originated a high-activity catalytic system with excellent stability at 650°C under a flow rate of 6 L/h with a reactant mixture of CH₄:CO₂ = 1:1. The introduction of cerium as a promoter in the ZrO₂ structure was shown to improve the catalyst performance by increasing the oxygen mobility in the support and consequently reducing deactivation by carbon deposition during reaction.

A ruthenium catalyst supported on activated carbon in the reaction of CH₄ with CO₂ and the promoting effect of the basic oxide MgO is investigated by Schuurman *et al.* (2000). The activated carbon is an inert material under carbon dioxide atmosphere. However, in the presence of ruthenium, gasification of the support takes place indicating the ability of the metal to catalyze carbon dioxide dissociation into CO and surface oxygen,

which is able to spillover to and react with the support. The addition of MgO to the Ru/C catalyst is shown to promote the CO₂ reforming of CH₄ to syngas with (i) an improved selectivity to CO and H₂ and (ii) a higher resistance to deactivation by carbon deposition. The presence of magnesia limits the reverse water-gas shift reaction and gasification of the support. The accumulation/decomposition of CO₂ as magnesium carbonate provides a continuous source of oxygen at the vicinity of the Ru particle which favors the oxidation of carbon arising from CH₄ adsorption and dehydrogenation on the ruthenium particles into CO. Therefore, the Ru surface is maintained clean enough to allow the methane reforming into CO and H₂ to proceed without serious aging. This source of oxygen is however sufficiently limited not to promote the secondary oxidation of adsorbed hydrogen. Hydroxyl groups present at the metal/promoter interface could also contribute to limit the catalyst aging. Thus, the promoted sample may be typical of a bifunctional catalysis for the CO₂ reforming reaction.

Several groups have also focused on TiO₂ and have found that, on TiO₂, Pt reaches much higher conversion than when supported on SiO₂ and Al₂O₃. Bradford and Vannice (1997, 1998) have performed an extensive study of Pt/TiO₂ and model TiO_x/Pt catalysts. The results from the model catalyst studies indicate that the activity of the catalyst increases with increasing TiO_x coverage. They attribute this increase to the formation of new metal–support interfacial sites and propose that these sites promote the dissociation of CH₄, the dissociation and reduction of CO₂, and the decomposition of CH_xO (Bradford and Vannice, 1998). Also, the formation of TiO_x overlayers on the Pt/TiO₂ catalyst was proposed to increase stability due to suppression of carbon deposition via an ensemble effect (Bradford and Vannice, 1997).

Ballarini *et al.* (2005) studied the catalytic performance of alkali metal-doped alumina as a support of noble metals (Pt/Na-Al₂O₃ and Pt/K-Al₂O₃) in methane reforming with CO₂. They found out that Pt/Na-Al₂O₃ catalyst displayed a higher catalytic performance than Pt/K-Al₂O₃ and Pt/ZrO₂ ones.

Souza *et al.* (2001) studied dispersed zirconium oxide on alumina as a support for Pt in CH₄–CO₂ reforming reaction in order to combine the unique chemical properties of ZrO₂ with the high surface area and mechanical stability of alumina. According to the results of

this study, Pt/ZrO₂/Al₂O₃ showed better performance than Pt/Al₂O₃ due to metal support interactions, minimizing carbon deposition.

2.3. Combined CO₂ Reforming and Partial Oxidation of Methane

The primary difficulty associated with the applicability of the CO₂ reforming of methane is the high thermodynamic potential to form coke under the high operating temperatures required to obtain significant conversions. The higher carbon content in the feed stream compared with partial oxidation or steam reforming is thought to be responsible for the higher level of carbon deposition on CO₂ reforming catalysts (Rostrup-Nielsen *et al.*, 1988). Addition of oxygen to the carbon dioxide reforming can reduce the carbon deposition on the catalytic surface and increase methane conversion, although this can also cause the reduction of process selectivity (O'Conner and Ross, 1998). Additionally, as CO₂ reforming is a highly endothermic process and thus requires a large amount of energy to proceed, its coupling with the exothermic partial oxidation would also have economic advantages. The combination of these reactions can improve the reactor temperature control and reduce the formation of hot spots, besides allowing the production of syngas with a wider range of H₂/CO ratios (H₂/CO can be varied between 1 and 2 by manipulating the relative concentrations of O₂ and CO₂ in the feed).

Several studies have been performed on the dry reforming reaction in the presence of oxygen over Pt, Ni and Ir based catalysts (Vernon *et al.*, 1992; Choudhary *et al.*, 1995; Inui *et al.*, 1995; O'Conner and Ross, 1998; Tomishige *et al.*, 2002a; Tomishige *et al.*, 2002b; Tomishige *et al.*, 2003; Souza and Schmal, 2003; Wang *et al.*, 2004;).

Combined POX & CDRM was first studied by Vernon *et al.* (1992). They reported that transition metals supported on inert oxides are active for combined partial oxidation and CO₂ reforming. They obtained high yields of synthesis gas, without carbon deposition, using a 1% Ir/Al₂O₃ catalyst. They were also able to manipulate the CH₄:CO₂:O₂ ratio in order to achieve a thermoneutral reaction

Choudhary *et al.* (1995) have also reported simultaneous catalytic reactions of CH₄ with CO₂ and O₂ over a NiO-CaO catalyst. They found that while coke formation was a

serious problem for CO₂ reforming over this catalyst, little or no coking was found using the coupled process. Conversions above 95% were obtained and the catalyst did not deactivate during 20 h on stream at 850°C for the coupled process. These authors also suggested that it was possible to manipulate the process conditions to achieve a thermoneutral process.

Inui *et al.* (1995) carried out reactions using a feed containing CH₄, CO₂, O₂ and H₂O over a Ni-Ce₂O₃-Pt-Rh catalyst. They found that high rates of H₂ formation could be achieved using high flow rates which could not be achieved by partial oxidation or by reforming using steam and CO₂.

O'Connor and Ross (1998) reported that minimal deactivation occurred for the combined partial oxidation and dry reforming reaction on a 1%Pt/ZrO₂ at low space velocities with a diluted feed. The conversion of methane was found to increase with oxygen content but the selectivity towards H₂ decreased. The decrease in H₂ selectivity was more pronounced at lower temperatures where the formation of CO₂ and H₂O were favored. The reaction mechanism was proposed to proceed through combustion followed by steam and CO₂ reforming.

Tomishige *et al.* (2002a, 2002b, 2003) also studied Pt-Ni bimetallic system supported on alumina, prepared either by coimpregnation or sequential impregnation of the metals, for DR coupled with POX. They observed that the addition of little amount of Pt to Ni/Al₂O₃ catalyst by sequential method resulted in higher performance in methane reforming with CO₂ and O₂ in terms of the catalytic activity and temperature profile of the catalyst bed. They concluded that sequential impregnation method was very effective for locating Pt atoms on the surface as the surface Pt atoms contribute to the enhancement of the catalyst reducibility *via* alloying and/or hydrogen spillover effect.

Combined partial oxidation and CO₂ reforming of methane was also studied by Souza and Schmal (2003), who reported that Pt/ZrO₂/γ-Al₂O₃ was the most active and stable catalyst for CO₂ reforming, partial oxidation of methane and for these two reactions combined, when compared to Pt/γ-Al₂O₃ and Pt/ZrO₂. The addition of O₂ to the feed increased methane conversion and decreased H₂ selectivity. The loss of catalytic activity

with time on stream decreased markedly with the amount of O₂ added to the feed, preventing or reducing coke formation over the catalyst surface.

Wang *et al.* (2004) showed out that Pt/Ce_{0.14}Zr_{0.86}O₂ catalyst was more active, and stable for CO₂ reforming, partial oxidation of methane and for these two reactions combined, than Pt/ZrO₂. The increase in the stability of the Ce-containing catalyst was related to the increased oxygen storage capacity and the ability to facilitate carbon removal from the metal particle.

2.4. Combined CO₂ Reforming and Steam Reforming of Methane

Another strategy to decrease the coke formation is to couple CO₂ reforming with steam reforming (Hegarty *et al.*, 1998; Noronha *et al.*, 2003; Choudhary and Mondal, 2006). Furthermore, the combination of these two reactions allows the control of the H₂/CO ratio through the variation of CO₂/H₂O ratio.

Hegarty *et al.* (1998) conducted CO₂ reforming of methane on a Pt/ZrO₂ catalyst in the presence of different water contents. In that study, it was observed that the water vapor addition caused an increase in both activity and H₂/CO ratio. However, the stability of the catalyst was not studied.

Noronha *et al.* (2003) studied the activity and stability of Pt/ZrO₂ and Pt/Ce-ZrO₂ catalysts on CO₂ reforming coupled with steam reforming. The addition of water strongly decreased the CH₄ and CO₂ conversion during the reaction on the Pt/ZrO₂ catalysts. TPO analysis showed that the addition of water increased the amount of deposited carbon. The lower stability of the Pt/ZrO₂ catalyst was due to the oxidation and decrease of the amount of oxygen vacancies by the water, inhibiting the cleaning mechanism. On the other hand, Pt/Ce-ZrO₂ catalyst was quite stable in the presence of water. This stability was ascribed to the higher amount of oxygen vacancies of the support.

Choudhary and Mondal (2006) showed out that NdCoO₃ perovskite-type mixed metal-oxide was a highly promising catalyst for combined CO₂ reforming and steam

reforming methane to syngas and that the H_2/CO ratio in the simultaneous CO_2 reforming and steam reforming can be controlled by manipulating the CO_2/H_2O ratio in the feed.

2.5. Inhibition of the Catalytic Processes

Deactivation of the catalysts is known to occur via three major routes defined as coke deposition, poisoning and thermal degradation (sintering). In Fig. 2.2, the deactivation mechanisms of catalysts are illustrated. The following sections involve information about the fundamentals of these mechanisms. At this point, it is worth noting that the first two type of deactivation can often be reversed, but sintering is usually irreversible.

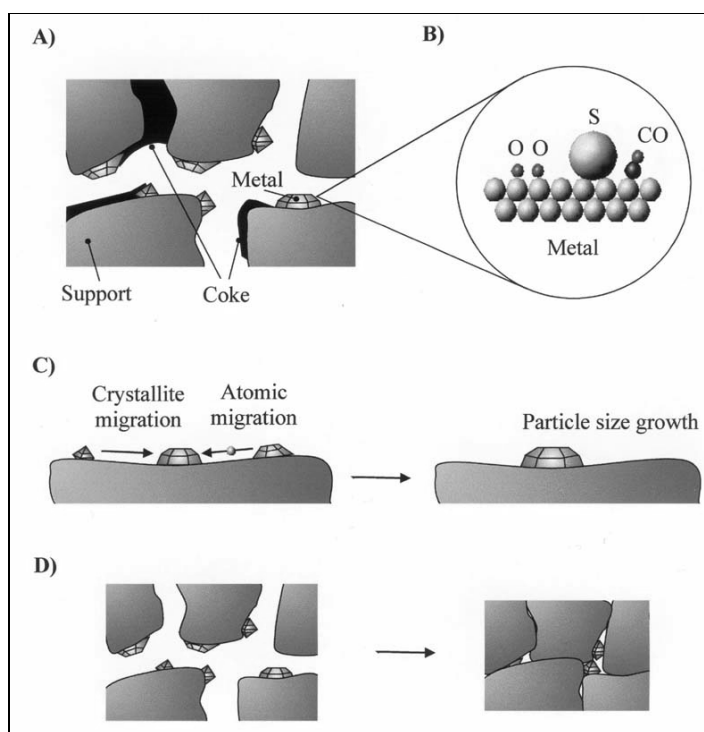


Figure 2.2. Deactivation mechanisms: A) Coke formation, B) Poisoning, C) Sintering of the active metal particles, and D) Sintering and solid-solid phase transitions of the washcoat and encapsulation of active metal particles (Lassi, 2003)

2.5.1. Coke Deposition

The term “coke” is a collective description of various kinds of carbonaceous deposits, since the nature of the deposit can be different. Coking is usually favored under the conditions employed for catalytic steam reforming and CO₂ reforming. It is more pronounced at higher temperatures and at lower quantities of steam. It is formed mainly by two reactions, methane decomposition [Eq. (2.7)] and carbon monoxide disproportionation [Eq. (2.8)]. The former is an endothermic reaction and favored at higher temperatures and lower pressures whereas the latter is exothermic and favored at lower temperatures and higher pressures (Nagaoka *et al.*, 2001a). The reactions are reversible and it is possible to minimize coke formation by adjusting operating conditions. The carbon limit diagrams that present the tendency of carbon formation over nickel catalyst as functions of O/C and H/C were presented by Rostrup-Nielsen (1984).

The formation of carbon over Ni catalysts under conditions of steam reforming reaction has been extensively studied. Three types of carbon have been identified. These are (i) pyrolytic carbon, (ii) whisker-like carbon, (iii) encapsulating carbon (Rostrup-Nielsen, 1984).

Pyrolytic carbon is formed mainly due to the thermal cracking of hydrocarbons which are favored at temperatures higher than ca. 920 K (Rostrup-Nielsen, 1997). The process is further facilitated at lower steam-to-hydrocarbon ratios, at higher pressures and in the case of high surface acidity of the catalysts. This mode of carbon can also be formed as a result of higher residence times and of overheated gas films at the tube walls acting as a source of radicals and coke precursors. Therefore, the nature of the catalyst packing, i.e. void fraction, affects the carbon formation by influencing residence time and the gas film volume. Pyrolytic carbon both deactivates the Ni-based catalyst by encapsulating it and blocks the reactor by accumulation within the voids between the particles (Rostrup-Nielsen, 1984).

The formation of whisker carbon and encapsulated carbon can be explained by the coking mechanism over nickel (Rostrup-Nielsen, 1997). The process is believed to start with the dissociation of hydrocarbons into highly reactive monoatomic carbon (C_α), which

can easily be gasified to form CO. However, if C_α is formed in excessive quantities or gasification is slow, then polymerization to C_β is facilitated. It has been shown that C_β is much less reactive than C_α , and the gasification step is fairly slow (Trimm, 1999). As a result, C_β may either accumulate on the catalyst surface or dissolve in the nickel leading to encapsulated carbon and whisker carbon, respectively. Noble metal catalysts, on the other hand, do not dissolve carbon, i.e. do not favor whisker mechanism, and therefore are resistant against coking (Rostrup-Nielsen, 2000).

As the carbon has dissolved or formed a compound with nickel, diffusion through the metal particle to a grain boundary occurs. As a result, carbon precipitates out and lifts the nickel particle at the tip of a growing whisker. Nickel is still active in this mode of carbon formation, but accumulation of carbon whiskers lead to break-down of the catalyst and blocks the catalyst bed, which increases pressure drop dramatically. In general, the process is favored at temperatures greater than 720 K (Rostrup-Nielsen, 1984).

Some of the coke formed on the catalyst surface remains undissolved and eventually encapsulates nickel. At temperatures lower than ca. 770 K, encapsulation becomes more pronounced with time by polymerization of C_nH_m radicals on the nickel surface, as explained above, and leads to progressive deactivation of the catalyst (Rostrup-Nielsen, 1984).

It was mentioned above that polymerization of C_α species to C_β was an intermediate step in the formation of dissolved or deposited carbon. It is obvious that polymerization is possible by the presence of more than one C_α species, whose formation requires high number of surface sites. Therefore, it has been reported that it is possible to reduce C_α formation by controlling the number of sites in an ensemble, which will minimize coke formation but maintain steam reforming. The process is called ensemble size control (or sulphur passivation) and is achieved by addition of minimal quantities of sulphur in order to facilitate controlled sulphur adsorption on nickel. As a result, the rates of both SR and CDRM are reduced but coke formation is eliminated (Rostrup-Nielsen, 1984; Trimm, 1999).

Zhang *et al.* (1996a) used several surface techniques to study the carbon species formed on 17 wt. per cent Ni/ γ -Al₂O₃ and 17 wt. per cent Ni/La₂O₃ catalysts, and found that surface carbon on spent Ni/ γ -Al₂O₃ catalyst was dominated by graphitic –C–C– species, which eventually blocked the entire Ni surface leading to the total loss of activity. The surface carbon on the working Ni/La₂O₃ catalyst consisted of –C–C– species and a larger amount of oxidized carbon (CO₃⁻ and formate). The interface between Ni and La₂O₃ (in the form of La₂O₂CO₃) offered active and stable performance in CO₂ reforming of methane.

Chen and Ren (1994) reported that filamentous carbon with a hollow inner channel would form on the surface of Ni/ γ -Al₂O₃ catalysts. They did not lose their activity in tests for as long as 120 h.

Gronchi *et al.* (1996) also studied the carbon formation in dry reforming of methane with CO₂ over Ni/La₂O₃ and Ni/SiO₂ catalysts. They found that whisker carbon formed on these catalysts and the deactivation appeared only at very high coverage of the surface.

Wang and Lu (1998) further investigated that on Ni-N catalysts for this reaction, higher nickel loading (>16 wt. per cent) in catalysts would cause severe coking on catalysts, resulting in plugging of the reactor in 5 h. In addition, coking dynamic process in a TGA study indicated that coke on catalyst would generally reach equilibrium in ca. 2-5 h and the amount of carbon deposition would not increase further. All the above investigations seem to suggest that coking rate is larger at the early stage of reaction and the amount of carbon deposition depends on nickel loading. Higher nickel content will result in the formation of larger amounts of coke and, thus, in the total deactivation of catalysts.

Shi *et al.* (1996) also reported that two types of carbon (amorphous carbon and graphite) formed on Ni/ γ -Al₂O₃ in methane dehydrogenation reaction. The morphology of graphitic carbon is that of carbon filaments. The amorphous carbon could be eliminated by CO₂, but the graphite could not be eliminated by CO₂ due to its longer filament and the distance from the nickel particles.

Shi *et al.* (1995) investigated the behavior of carbon by stepwise reaction of methane with CO₂ over Ni/ γ -Al₂O₃ and found that filamentous carbon was the main form of carbon deposit. The elimination of this form of carbon depended on the contact between carbon and nickel crystallite. In the research on deactivation of 4 wt. per cent Ni/SiO₂ catalyst for CO₂ reforming of methane, it has been found that filamentous carbon did not deactivate the catalyst. Deactivation not being related to sintering was due to the proteiform deposits. These two-dimensional structures would encapsulate carbon, thus hindering the diffusion of reactant to the active surface (Kroll *et al.*, 1996).

Matsukata *et al.* (1995, 1996) studied catalytic activities of Ni/SiO₂ for both CH₄ decomposition and CO₂ gasification of deposited carbon and observed that the carbon, having a moss-like morphology, was hardly gasified and caused deactivation of the catalyst. Such type of carbon became dominant at higher amounts of Ni loading on catalyst. In contrast, filamentous carbon with a graphitic structure could be gasified with CO₂ and became dominant with decreasing amount of Ni loaded.

In summary, two types of carbon can be formed on catalysts in CO₂ reforming of methane and their reactivities differ. Graphitic and amorphous carbon can both show activity of gasification. Several researchers have found that the reactivity of carbon depends on its location on the catalyst. The carbon situated on the metal particles or in their close vicinity will exhibit higher gasification activity. Hence, it can be proposed that catalyst deactivation caused by carbon deposition depends on the amount, type and location of the carbon formed. When there is a great amount of carbon formed, almost covering the entire surface active sites, the catalyst will deactivate rapidly. This is often the case for high Ni loadings. With less carbon deposited on catalysts the carbon can have better contact with Ni particles thus exhibiting high activity of gasification and leading to slow deactivation or better catalyst stability (Wang and Lu, 1998).

The addition of various promoters and use of different supports are already reviewed in Section 2.2.1. Techniques developed for preventing carbide formation, which is an intermediate step in coke formation, have been presented by Trimm (1999).

2.5.2. Poisoning

The fundamental reason for catalyst poisoning is the interaction between a component existing within the feed or product and the active sites of the catalyst. The most common type of poisoning is known to be due to sulphur but also heavy metals or their ions can poison metallic catalysts, and organic bases may poison acidic catalysts. Three types of catalyst poisons have been identified, which are (i) Group 5A and 6A elements, including N, P, As, and Sb (5A) and O, S, Se and Te (6A), (ii) toxic heavy metals such as Pb, Hg, Cd and Cu, and (iii) specific molecules that interact with catalyst surfaces (Bartholomew, 2001).

In the first type of poisons, the elements poison metal catalysts by interaction through their 's' and 'p' orbitals. Hence, the number of bonding electrons can be changed by oxidation or reduction, and the degree of poisoning can be modified. The poisoning effect of sulphur increases in the order of $\text{SO}_4^{2-} < \text{SO}_2 < \text{H}_2\text{S}$. It was reported that H_2S present at parts per billion levels is sufficient to result in significant surface coverage (Trimm, 2001).

Oxidation at high temperatures is proposed to regenerate catalysts poisoned by sulphur, since the sulphates, which can react with support such as alumina, break up to give SO_x that can be removed from the system in the gas phase. The sulphur compounds can also be removed before they reach the reactor. This process is known as hydrodesulphurization and involves the conversion of sulphur compounds to H_2S at temperatures between 623 K and 673 K over alumina supported cobalt and molybdenum oxides. The resulting H_2S can then be removed by adsorption on ZnO catalyst (Bartholomew, 2001).

The removal of the second type of poisons is more complex, and involves processes known as abrasion or leaching, which were extensively reviewed by Trimm (2001).

2.5.3. Sintering

High surface area is a feature which is desired in catalysis, but it is not thermodynamically favored. Therefore, at high temperatures and in the presence or absence of a suitable chemical environment, the catalysts will transform into thermodynamically favored lower surface agglomerates. The process is known as sintering. This mechanism of deactivation is more pronounced in high temperature applications in which catalytic combustion is involved (Thevenin *et al.*, 2001).

Sintering, as illustrated in Figures 2.2 C and 2.2 D, is the loss of catalyst's active surface due to crystal growth of either the bulk material or the active phase. In the case of supported metal catalysts, reduction of the active surface area is provoked via agglomeration and coalescence of small metal crystallites into larger ones. Two different models have been proposed for sintering i.e., the atomic migration and the crystallite migration models. As such, sintering occurs either due to metal atoms migrating from one crystallite to another via the surface or gas phase by diminishing small crystallites in size and increasing the larger ones (atomic migration model). Or sintering can occur via migration of the crystallites along the surface, followed by collision and coalescence of two crystallites (crystallite migration model). Figure 2.2 C presents a schematic representation of atomic migration and crystallite migration models (Lassi, 2003).

Sintering on supported metal catalysts involves complex physical and chemical phenomena that make the understanding of the mechanistic aspects of sintering difficult. Experimental observations have shown that sintering is strongly temperature-dependent (Bartholomew, 2001), but is also affected by the surrounding gas atmosphere (Forzatti & Lietti 1999). The rate of sintering increases exponentially with temperature and, for example, the sintering of precious metals becomes significant above 600°C. The underlying mechanism of sintering of small metal particles is the surface diffusion, or at higher temperatures, the mobility of larger agglomerates (Lassi, 2003).

Supported metal catalysts sinter relatively rapidly under an oxidizing atmosphere, however the process is more slow under reducing and inert atmospheres. Sintering is also generally accelerated, e.g. in the presence of water vapor. In addition to temperature,

atmosphere and time, the sintering rate is also dependent on several other factors, such as precious metal loading and washcoat composition. The presence of specific additives is also known to reduce the sintering of a catalyst (Lassi, 2003).

Solid-solid phase transitions, as presented in Fig. 2.2 D, can be viewed as an extreme form of sintering occurring at very high temperatures and leading to the transformation of one crystalline phase into another. Phase transformations typically occur in the bulk washcoat, e.g. aluminium oxide has many phases from the porous γ -Al₂O₃ to non-porous α -Al₂O₃, which is the most stable phase of alumina. The phase transformations of Al₂O₃ become significant at high temperatures and remarkably decrease the surface area of the catalysts. The improvement of the thermal stability of alumina has been investigated by Arai and Machida (1996). They found that addition of oxides like BaO, La₂O₃, SiO₂, Li₂O and K₂O to alumina inhibited sintering, since these stabilizers filled vacancies in the lattice. Among these additives, SiO₂ introduced additional resistance against moist atmospheres. The change in the preparation method of alumina, which would have affected the rate of sintering due to the modified particle morphology and grain structure, was proposed as another method to improve thermal resistance.

2.6 Kinetics of CO₂ Reforming of CH₄

As shown in Section 2.2, the reforming of CH₄ with CO₂ has been extensively studied using catalysts composed of transition metal carbides and sulfides, unsupported metals, and supported group VIII metals, with the exception of Os. However, the fraction of these papers providing any fundamental kinetic parameters is not large.

A wide range of activation energies (E_{app}) has been reported and values for CH₄ disappearance vary from 10 to 29 kcal/mol (Table 2.1). In practice, a heterogeneous catalyst may have a distribution of catalytic active sites with different intrinsic activation barriers for the chemical reaction of interest. An analysis of the reported values allows the following observations. It is remarkable that the activation barrier for CH₄ consumption is higher than that for CO₂ consumption. The activation energy for H₂ is greater than the activation energy of CO. In addition, CO₂ inhibits H₂ formation. These observations

suggest that the apparent E values for CO and H₂ are strongly influenced by the reaction of CO₂ with H₂, presumably via the RWGS reaction (Bradford and Vannice, 1999).

The dependencies of the rates of H₂ and CO formation, as well as CH₄ and CO₂ consumption, on the partial pressures of CH₄ and CO₂ in the feed at 723 K are tabulated in Table 2.2. Since under differential conditions the gas phase concentrations of H₂ and CO are negligible, it was reasonable to exclude their partial pressures from power rate laws. It is observed that the reaction orders vary in a wide range depending on both the active metal and carrier. This indicates that the reaction mechanism differs according to the type of the catalysts used. In addition, the negative b values for H₂ production indicate consumption of H₂, via the RWGS, as discussed previously.

Table 2.1. Apparent activation energies (E_{app}) over Ni, Pt & Co catalysts

Catalyst	E_{app} (kcal/mol)				Reference
	CH ₄	CO ₂	CO	H ₂	
Pt/ZrO ₂	18.4	15.0	15.0	16.8	Souza <i>et al.</i> , 2001
Pt/Al ₂ O ₃	22.5	20.2	18.5	19.3	Souza <i>et al.</i> , 2001
Pt/ZrO ₂	24.0	20.0	21.6	34.0	Bradford and Vannice, 1996
Pt/TiO ₂	23.0	19.0	20.5	32.0	Bradford and Vannice, 1996
Pt/Cr ₂ O ₃	16.0	15.0	16.0	19.0	Bradford and Vannice, 1996
Ni/C	20.0	22.0	24.0	32.0	Bradford and Vannice, 1996
Ni/SiO ₂	23.0	19.0	20.0	27.0	Bradford and Vannice, 1996
Ni/MgO	22.0	21.0	21.0	35.0	Bradford and Vannice, 1996
Ni/TiO ₂	26.0	21.0	23.0	32.0	Bradford and Vannice, 1996
Ni/Al ₂ O ₃	16.9	16.5	17.7	23.5	Ferreira-Aparicio <i>et al.</i> , 1998
Ni/SiO ₂	14.9	16.7	16.5	22.4	Ferreira-Aparicio <i>et al.</i> , 1998
Ni/CaO-Al ₂ O ₃	25.5	23.6	24.6	35.2	Lemonidou and Vasalos, 2002
Ni-K/ CeO ₂ -Al ₂ O ₃	11.0	11.0	11.3	12.9	Nandini <i>et al.</i> , 2006
Co/C	11.0	9.0	9.0	11.0	Guerrero-Ruiz <i>et al.</i> , 1994
Co/SiO ₂	10.0	8.0	9.0	11.0	Guerrero-Ruiz <i>et al.</i> , 1994
Co/MgO/ SiO ₂	12.0	9.0	10.0	13.0	Guerrero-Ruiz <i>et al.</i> , 1994

2.6.1. Suggested Mechanisms and Rate Expressions for CO₂ Reforming of CH₄

In order to develop a high-performance catalyst and to improve the reforming performance, it is essential to identify the reaction mechanism and the rate-determining steps. Kinetic and mechanistic studies have been performed over noble metal and Ni-based catalysts.

van Keulen *et al.* (1997) observed that both methane and carbon dioxide dissociate independently of one another over Pt/ZrO₂. The dissociation of carbon dioxide acts as an oxygen supplier while the decomposition products of methane scavenge the oxygen from the catalyst surface. Bitter *et al.* (1997) also studied the CO₂ reforming of CH₄ over the same catalyst and concluded that catalytic activity is determined by the accessibility of Pt on the Pt-ZrO₂ perimeter. The perimeter concentration can be altered by calcination.

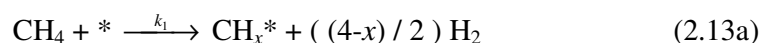
Table 2.2. Reaction orders for reaction conditions of P = 1 atm, CH₄/CO₂ = 1, T = 723 K

$$(r_i = kP_{CH_4}^a P_{CO_2}^b)$$

Catalyst	a				b				Ref.
	CH ₄	CO ₂	CO	H ₂	CH ₄	CO ₂	CO	H ₂	
Pt/TiO ₂	0.28	0.31	0.30	0.59	0.17	0.28	0.24	-0.42	Bradford and Vannice, 1998
Pt/ZrO ₂	0.30	0.30	0.30	0.50	0.21	0.21	0.20	-0.37	Bradford and Vannice, 1998
Ni/SiO ₂	0.44	0.27	0.18	0.49	0.15	0.64	0.44	0.11	Bradford and Vannice, 1996
Ni/MgO	0.72	0.60	0.64	1.22	0.01	0.27	0.15	-0.54	Bradford and Vannice, 1996
Ni/TiO ₂	0.40	0.43	0.44	0.90	0.18	0.41	0.30	-0.15	Bradford and Vannice, 1996

The kinetics of CO₂ reforming of methane over Pt supported on TiO₂, ZrO₂, Cr₂O₃ and SiO₂ as well as over Ni-based catalysts was studied by Bradford and Vannice (1998). The mechanistic model proposed by these authors for CH₄/CO₂ reforming comprises the following steps:

- reversible dissociation of CH₄ to yield CH_x species and H₂;



- non-dissociative adsorption of CO₂ on the support, H-promoted CO₂ dissociation in the metal-support interfacial region;



- reaction of CH_x species with OH (or O) species to yield CH_xO species; and



- CH_xO decomposition in the metal-support interfacial region to yield H₂ and CO.



This mechanism considers that all the elementary steps happen in the metal-support interfacial region. However, Cheng *et al.* (2001) found out that this mechanism could not

account for their observation that the reduction degree of the nickel species has almost no effect on the reforming activity of the catalyst, because the area of the interfacial region was proportional to the reduction degree of the nickel species and the area of the interfacial region strongly affected the activity.

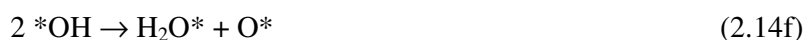
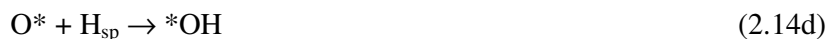
Hence, based on their experimental results, the mechanism proposed by Bradford and Vannice was modified as follows:

- Reversible dissociation of CH_4 to yield CH_x species and H on Ni^0 with a large portion of H spilt over onto the support.



where H_{sp} denotes the spilt over hydrogen.

- H-promoted CO_2 dissociation mainly on the support.

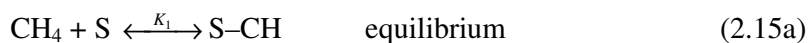


where * represents the oxygen vacancy.

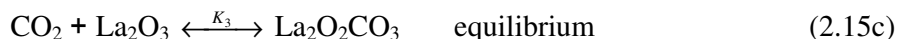
- Reaction of CH_x species with H_2O to yield CH_xO species and H_2 , and CH_xO decomposition in the metal-support interfacial region to yield H_2 and CO . The H_2O mainly comes from the support and migrates to the metal-support interfacial region.

Tsipouriari and Verykios (2001), studying the Ni/La₂O₃ system, detected the presence of La₂O₂CO₃ in the used catalysts and assigned a precise role to this compound in the reaction mechanism. They developed a kinetic equation for the dry reforming of methane over Ni/Al₂O₃ and reported a fractional order dependency of the rate of reactant disappearance for both CH₄ and CO₂.

- Reversible adsorption of methane on the surface of Ni which leads to cracking of methane and production of carbon deposits and hydrogen. Methane cracking is a slow step while methane adsorption is at equilibrium:



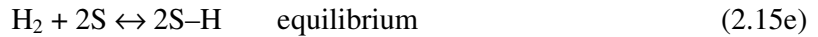
- A strong interaction exists between CO₂ and La₂O₃ which leads to the formation of La₂O₂CO₃ species. This is a fast step, considered to be at equilibrium.



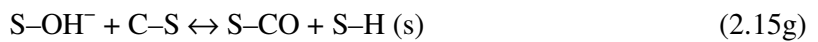
- La₂O₂CO₃ species react with carbon deposited onto Ni particles at the interface between Ni and La₂O₂CO₃. In this way the methane cracking activity of Ni (at the periphery of the La₂O₂CO₃ particles) is restored and the catalyst exhibits good stability. Therefore, the active portion of the catalyst is the interfacial area between Ni and oxycarbonate particles. The remaining surface of Ni is covered by carbon deposits. This step is also considered to be a slow step in the sequence.



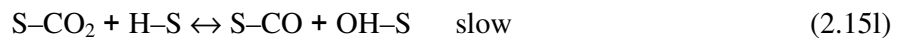
- Adsorbed hydrogen, at very low surface coverage, may also exist and interact with other surface species. This adsorbed hydrogen originates from the sequential cracking of the methane molecule and it is assumed to be at equilibrium with gas phase hydrogen.



- The following steps are assumed to be fast steps in comparison with slow steps (2.15b) and (2.15d) above:



- Simultaneously, the inverse water-gas shift reaction takes place, which may be described by the following sequence of reaction steps:



Although much effort has been spent on the investigation of the reforming mechanisms over the Ni-based catalysts (Wang and Au, 1992; Slagtern *et al.*, 1997; Osaki *et al.*, 1998; Schuurman *et al.*, 1998; Wang *et al.*, 1999; Yan *et al.*, 2003; Cheng *et al.*, 2001; Solh *et al.*, 2003), there are still some debates about the accurate mechanism details. Generally, it is argued that the dry reforming reaction has one single RDS or two RDS.

For the single RDS, the opinions are also different. Wei and Iglesia (2004) reported that CH_4 decomposition as the RDS in the reforming reaction. Luo *et al.* (2000) concluded

that, although the cleavage of C-H bonds was a slow step, the decomposition of CH_xO ($x = 1-2$) into CO gas and adsorbed H species on the catalyst was the RDS in the reforming reaction. Osaki and Mori (2001) also supported the opinion that CH_xO dissociation was the RDS for the reforming reaction over $\text{KNi}/\text{Al}_2\text{O}_3$ catalyst. The reaction between the carbon species originated from CH_4 dissociation and the oxygen atoms resulting from CO_2 decomposition to produce CO gas was also considered as the RDS in the kinetic isotope study of the dry reforming reaction over $\text{Ni}/\text{Al}_2\text{O}_3$ (Schuurman *et al.*, 1998) and Ni/SiO_2 (Kroll *et al.*, 1996b) catalysts. Chang *et al.* (2000) regarded the reaction of oxygen species with carbon species to produce CO gas as the RDS in the reforming reaction over KNiCa catalyst at 600 °C.

The other opinion is that two RDS are involved in the reforming reaction. Bradford and Vannice (1996) and Nandini *et al.* (2006) suggested that both CH_4 dissociation and CH_xO decomposition were the RDS's in the reforming reaction over the supported Ni catalysts. Aparicio (1997) found that further dissociation of CH_4 and desorption of CO had higher activation energy (E_a) compared to other elementary steps in the transient isotope study of the reforming reaction over $\text{Ni}/\text{MgO}-\text{MgAl}_2\text{O}_4$. And the two steps were considered as the RDS's in the reforming reaction. Tsipouriaris and Verykios (2001) concluded that CH_4 dissociation and the reaction of surface carbon species with $\text{La}_2\text{O}_2\text{CO}_3$ were RDSs in the reforming reaction over $\text{Ni}/\text{La}_2\text{O}_3$ catalyst.

Therefore, the RDS in the dry reforming may involve CH_4 dissociation, CH_xO decomposition, formation or desorption of CO and reaction between carbon species and oxygen species on catalyst surface. Cui *et al.* (2007) think that the reasons for the differences in the reported reforming mechanism can be attributed to two facts: (i) the different supports and promoters employed in the reforming reaction may result in the variation of the reforming mechanism, and (ii) the mechanism investigation was conducted at different temperatures, which may remarkably affect the reforming mechanism and the RDS.

Table 2.3. Proposed rate expressions for CO₂ reforming of CH₄

Model	Catalyst	Reference
$r_{CH_4} = \frac{k_{1L}P_{CH_4}}{\left[\frac{k_{1L}P_{CH_4}P_{CO}}{k_{7L}K_aP_{CO_2}} + (K_bP_{CO_2}P_{H_2}^{1/2}/P_{CO}) + (k_{1L}P_{CH_4}/k_{7L}) + 1 \right]}$	Ni-K/CeO ₂ -Al ₂ O ₃	Nandini <i>et al.</i> (2006)
$r_{CH_4} = \frac{k_1P_{CH_4}P_{CO_2}}{(1 + K_1P_{CH_4})(1 + K_2P_{CO_2})}$	Ni/La/Al ₂ O ₃	Olsbye <i>et al.</i> (1996)
$r_{CH_4} = \frac{K_1k_2K_3k_4P_{CH_4}P_{CO_2}}{K_1k_2K_3P_{CH_4}P_{CO_2} + K_1k_2P_{CH_4} + K_3k_4P_{CO}}$	Ni/La ₂ O ₃	Tsipouriari & Verykios (2001)
$r_{CH_4} = \frac{K_1k_2K_3k_4P_{CH_4}P_{CO_2}}{K_1K_3k_4P_{CH_4}P_{CO_2} + K_1k_2P_{CH_4} + K_3k_4P_{CO}}$	Rh/ La ₂ O ₃	Munera <i>et al.</i> (2007)
$r_{CH_4} = \frac{kK_{CO_2}k_{CH_4}P_{CH_4}P_{CO_2}}{kK_{CO_2}P_{CO_2} + (1 + K_{CO_2}P_{CO_2})(k_{CH_4}P_{CH_4} + k_{CH_4}^{-1}P_{H_2}^{4-x/2})}$	Pt/ZrO ₂ /Al ₂ O ₃	Souza <i>et al.</i> (2001)
$r = \frac{k\sqrt{K_1K_2P_{CO_2}P_{CH_4}}}{(1 + \sqrt{K_1P_{CO_2}} + \sqrt{K_2P_{CH_4}})^2}$	Ni/Al ₂ O ₃ Ni/CaO-Al ₂ O ₃ Ni/SiO ₂	Osaki <i>et al.</i> (1997) Horiuchi <i>et al.</i> (1996)
$r = \frac{aP_{CH_4}P_{CO_2}^2}{(P_{CO_2} + bP_{CO_2}^2 + cP_{CH_4})^2}$	Ni/Al ₂ O ₃ Ni/CaO-Al ₂ O ₃	Zhang & Verykios (1994)

Hence, Cui *et al.* (2007) studied the dry reforming reaction over typical Ni/ α -Al₂O₃ catalyst with uniform Ni active in a temperature range of 550 to 750°C in order to investigate the effect of temperature on reforming mechanism and RDS. After elimination of the effects of side reactions, the reforming reaction was controlled by kinetics. The activation energies of the reforming reaction and the reaction orders of CH₄, CO₂, H₂, and CO showed that the reforming reaction could be divided into three regions: 550–575 °C, 575–650 °C, and 650–750 °C. The CH₄ dissociation is the RDS and CO desorption also restrained the dry reforming in 550–575 °C. The reaction between CH_x and CO₂ became the RDS in 650–750 °C. And the restraining steps were switched from the former two steps to the latter step in 575–650 °C. The reaction temperature remarkably influences the reforming mechanism through altering the reaction steps.

2.7. Catalyst Supports

A support can be described as an inert substance that provides a means of spreading out an expensive catalyst ingredient such as platinum for its most effective use, or a means of improving the mechanical strength of an inherently weak (metal/active phase) catalyst.

However, the carrier may actually contribute to catalytic activity, depending upon the reaction type and conditions, and it may react to some extent with other catalyst ingredients during the manufacturing process (Satterfield, 1991). The selection of a support is based on whether it has the desirable characteristics.

The support chosen for a catalyst has a critical impact on catalyst activity, selectivity and ease of catalyst recycling. The support can impart an acidic or basic environment for the active catalyst component. Each support chemistry has different tendencies towards impurities (which can poison the desired reaction or enhance a competing reaction). In addition, each support chemistry has unique range of available pore size distributions and stability to thermal, hydrothermal or acidic conditions. The selection of a support is based on its desirable characteristics such as the following (Satterfield, 1991):

- A support must have desirable mechanical properties, including attrition resistance, hardness, and comparative strength.
- It should be stable under reaction and regeneration conditions.
- It should provide surface area enough to guarantee targeted dispersion of active phases. High surface area is usually, but not always, desirable.
- The support must supply porosity, including average pore size and pore-size distribution. High area implies fine pores, but relatively small pores may become plugged in catalyst preparation, especially if high loadings are sought.
- It should have low cost.
- It should be inert or provide active sites for activity or strong metal/support interaction depending on the reaction.

A supported catalyst facilitates the flow of gases through the reactor and the diffusion of reactants through the pores to the active phase, improving the dissipation of reaction heat, retarding the sintering of the active phase or increasing the poison resistance (Rodrigues-Reinoso, 1998). Some supports that are widely used in industry are as follows:

- Alumina: They have a wide range of surface areas and pore volumes. $\gamma\text{-Al}_2\text{O}_3$ is a commonly used catalyst support, but starts to lose its high surface area (ca. $250\text{ m}^2\text{g}^{-1}$) at temperatures greater than 873 K. As the temperature is increased, γ phase transforms into δ and θ phases, respectively. The final transformation occurs at ca. 1373 K to a highly stable phase (α) which has a surface area as low as ca. $5\text{ m}^2\text{g}^{-1}$.
- Silica: They are designed to have the broadest range of surface areas and pore volumes. Silica can be surface-treated to minimize additional catalytic effects. These materials can be used over a wide range of pH conditions.

- Zeolite: They are designed for reactions that can take advantage of the shape selectivity or size exclusion of the zeolite pores.

2.7.1. Zirconia (ZrO₂)

When used as supports, zirconia is known to impart metal-support interactions to enhance catalytic performances, due to the oxygen-storage/transport characteristics of the support or to the generation of active centres at the interface between metal and support (Damyanova *et al.*, 2008).

ZrO₂ has a high thermal stability as a catalyst support and its tetragonal phase, (t-ZrO₂), has both acid and basic properties. In addition, it has been found that the t-ZrO₂ is the most active phase for some reactions, therefore it is important to reduce at maximum the transition to the monoclinic phase, avoiding also the possible sintering of the support. However, the t-ZrO₂ is considered to be a metastable phase and the transformation to monoclinic phase is complete at around 650–700°C. This change causes a drastic decrease of the surface area. The tetragonal or cubic phases can be stabilized by adding yttria, calcia, or ceria, thus maintaining small crystallite sizes due to their lower surface tension, and avoiding the transition to monoclinic form (Montoya *et al.*, 2000).

Previous studies have shown that the addition of promoters to the ZrO₂ support results in increased activity and stability for the reforming reaction. It is well established that the addition of Y or La oxides enhances the surface area and the thermal stability of ZrO₂ and other supports. Similarly, doping cerium oxide with Zr⁺⁴ results in a material with an enhanced thermal resistance. For example, after calcination at 1073 K, the doped material had more than six times the surface area of the unpromoted CeO₂ catalyst. Furthermore, it is well known that these materials, as well as ceria-doped zirconia, exhibit good oxygen storage capacities and high thermal stability. Several studies have been performed on the redox properties of the CeO₂-doped catalysts and have shown that the redox properties of a Ce_{0.5}Zr_{0.5}O₂ mixed oxide support could be improved by repetitive oxidation/reduction cycles. The high reducibility and high thermal stability of the promoted ZrO₂ materials make them very attractive supports for the reforming reaction (Stagg-Williams *et al.*, 2000).

The mixed $\text{Ce}_x\text{Zr}_{1-x}\text{O}_2$ oxides, as a new generation of oxygen storage capacity systems, have recently been reported in many studies. The distortion of the O^{2-} sublattices in the mixed oxides permits a higher mobility of lattice oxygen, and the reduction occurs not only on the surface but also extends deep into the bulk. Ceria stabilized zirconia has attracted attention in recent years due not only to its good mechanical and electrical properties, but also to its application as catalysts, given their good stability and redox properties. However, the properties of these materials largely depend on the preparation method, the nature of the present phases and their content. It has been shown that phase segregation of binary oxides could be suppressed by doping with proper elements. The substitution of zirconium atoms by iron ones can generate oxygen vacancies in the tetragonal network of $\text{ZrO}_2\text{-CeO}_2$ system prepared by the solid-state route, or phase segregation could be inhibited by doping the mixed oxide with rare earth elements. An important feature associated with binary $\text{CeO}_2\text{-ZrO}_2$ systems is to improve their low-temperature reducibility at moderate temperatures or their oxygen storage/release capacity. It is well known that the reducibility of the carrier of supported metal catalysts is a very important issue regarding its ability to generate oxygen vacancies and transfer the oxygen onto the metal particles. This refers to redox behaviour that is relevant to catalysis and considers all the characteristics of the reduction and oxidation processes (Damyanova *et al.*, 2008).

3. EXPERIMENTAL WORK

3.1. Materials

3.1.1. Chemicals

The chemicals used for catalyst preparation are listed in Table 3.1.

Table 3.1. Chemicals used in catalyst preparation (all specifications: research grade)

Chemicals	Formula	Source	Molecular Weight (g/mole)
Cerium(III) nitrate hexahydrate	$\text{Ce}(\text{NO}_3)_3 \cdot 6\text{H}_2\text{O}$	Merck	434.23
Nickel (II) nitrate hexahydrate	$\text{Ni}(\text{NO}_3)_2 \cdot 6\text{H}_2\text{O}$	Merck	290.81
Lanthanum nitrate hexahydrate	$\text{La}(\text{NO}_3)_3 \cdot 6\text{H}_2\text{O}$	Merck	433.02
Manganese (II) nitrate tetrahydrate	$\text{Mn}(\text{NO}_3)_2 \cdot 4\text{H}_2\text{O}$	Merck	251.01
Magnesium nitrate hexahydrate	$\text{Mg}(\text{NO}_3)_2 \cdot 6\text{H}_2\text{O}$	Merck	256.41
Tetraammineplatinum (II) nitrate	$\text{Pt}(\text{NH}_3)_4(\text{NO}_3)_2$	Aldrich	387.22
Cobalt (II) nitrate hexahydrate	$\text{Co}(\text{NO}_3)_2 \cdot 6\text{H}_2\text{O}$	BDH	290.93
Potassium nitrate	KNO_3	Riedel-de Haën	101.10
Gamma alumina	$\gamma\text{-Al}_2\text{O}_3$	Alcoa	101.96
Zirconium oxide	ZrO_2	Alfa Aesar	123.22

3.1.2. Gases

All of the gases used in this research were supplied by Birleşik Oksijen Sanayi (BOS) and HABAŞ Companies, Istanbul, Turkey. Table 3.2. and Table 3.3 list the specifications and applications of the liquids and gases employed in this research.

Table 3.2. Specifications and applications of the liquids used

Liquid	Specification	Application
Nitrogen	HABAŞ	BET cold trap
Water	Distilled	Aqueous solution, Reactant

Table 3.3. Specifications and applications of the gases and standards used

Gas/Standard	Specification	Application
Methane	99.5 % BOS	GC calibration, Reactant
Carbon dioxide	99.995 % BOS	GC calibration, Reactant
Carbon monoxide	99.999 % BOS	GC calibration
Hydrogen	99.99% BOS	GC calibration, Reduction
Argon	99.998% BOS	Inert, GC Carrier Gas, TGA protective gas
Oxygen	99.998 % BOS	GC calibration, Reactant
Dry air	99.998 % BOS	Calcination, GC 6-way pneumatic valve
Nitrogen	99.998 % BOS	BET
Helium	99.999 % HABAŞ	BET
30% v/v oxygen in helium	BOS	Oxidizing agent in TGA
4% v/v hydrogen in argon	BOS	Reducing agent in TGA

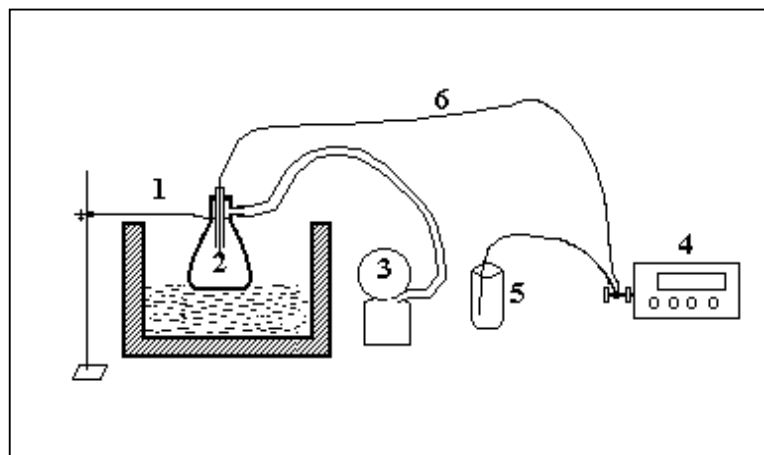
3.2. Experimental Systems

The experimental systems used can be described in four groups:

- **Catalyst Preparation Systems:** The set-up used for preparing catalysts by incipient-to-wetness impregnation technique represents this group of experimental systems.
- **Catalyst Characterization Systems:** This group of systems involves five different analytical and spectroscopic techniques used to characterize the physical, microstructural and electronic properties of the catalyst samples prepared and to examine any carbonaceous deposits produced during the reactions.
- **Catalytic Reaction System:** This continuous flow microreactor system includes gas and liquid flow control, temperature controlled line heating, gas/liquid mixing, and reaction chamber, feed and product sampling sections. This system is used for assessing catalytic activity, selectivity and stability, and for measuring reaction kinetics.
- **Product Analysis System:** The quantitative determination of the composition of the species both in the reactor effluent and feed stream is conducted by a gas chromatograph connected on-line to the microreactor flow system.

3.2.1. Catalyst Preparation Systems

The system used for preparing catalysts by incipient-to-wetness impregnation technique (Figure 3.1) includes a Retsch UR1 ultrasonic mixer, a vacuum pump, a Buchner flask and a MasterFlex computerized-drive peristaltic pump.



1. Ultrasonic mixer, 2. Buchner erlen, 3. Vacuum pump, 4. Peristaltic pump, 5. Reactant storage tank, 6. Silicone tubing

Figure 3.1. Schematic diagram of the impregnation system (Akin, 1996)

3.2.2. Catalyst Characterization Systems

3.2.2.1. Thermal Gravimetric Analysis. All catalyst samples and the support were characterized by temperature- programmed reduction (TPR) tests for their reduction properties. The amount of deposited coke on used catalysts was determined by temperature-programmed oxidation (TPO) tests. Both TPO and TPR tests were performed on a Mettler Toledo TGA/DTA851 apparatus.

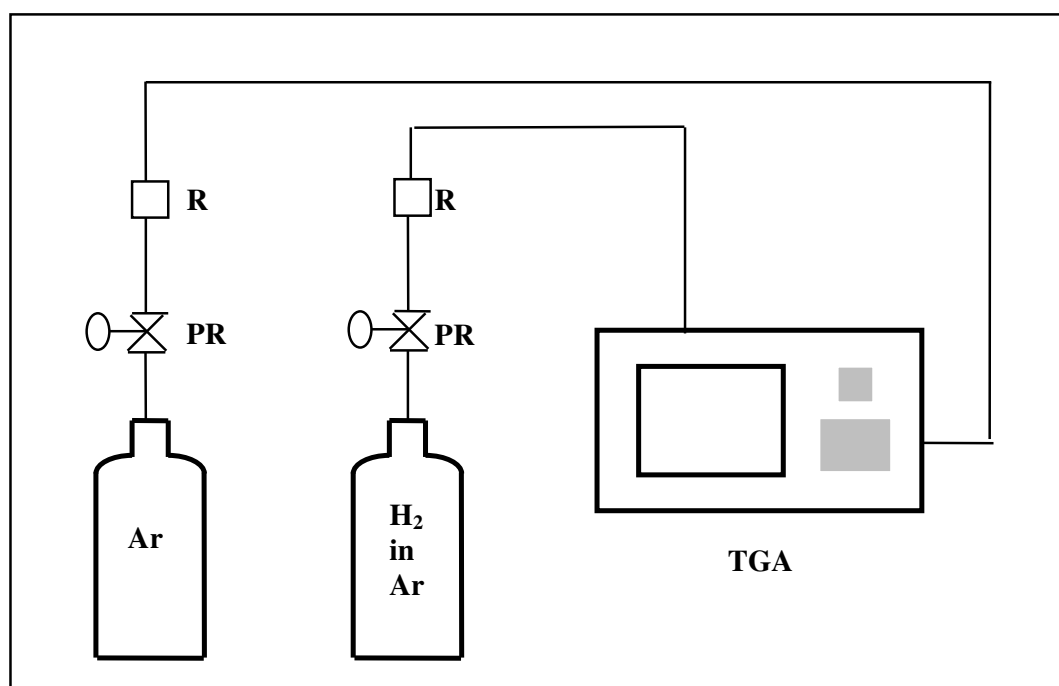
The TGA/DTA apparatus shown in Figure 3.2 consists of two sections:

- gas flow rate control section
- reduction section

In the gas flow rate control section, 1/4" and 1/8" copper tubings, fittings and silicon hoses were used. The flow rates of the gases were controlled by calibrated Aalborg and KDG Mobrey 1100 rotameters for the Ar and the H₂-Ar gas mixture, respectively.

All gases are allowed to flow through the reduction section. This section consists of a Mettler Toledo Star^e System. For the installation of Star^eSW V4.0, the Solaris 2.5.1/×86 operating system is required. The Star^e System consists of the Star^e Software and the

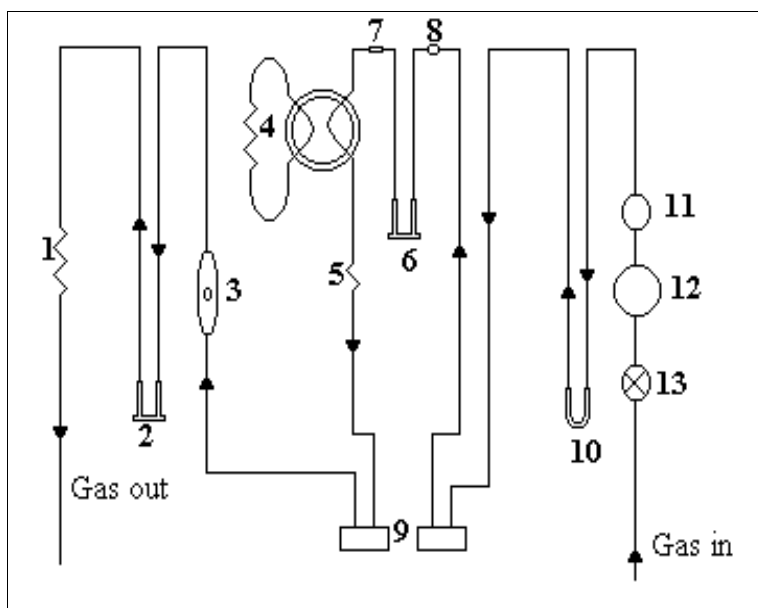
module, which is the Thermogravimetric and Single Differential Thermal Analyzer, TGA/SDTA851^o. The catalyst sample of 35-50 mg is placed in an alumina crucible during experiments. The maximum sample weight used for balance in the instrument is one gram, and the balance has a detection limit of one microgram. The balance housing is also thermostatted for ensuring good reproducibility of the weight signal. Hydrogen in argon gas mixture and oxygen in helium gas mixtures are used as purge gas depending on the characteristic of the test (reduction or oxidation), and argon is used as protective gas passing through the instrument at a fixed flow rate all the time since chemical reactions of the sample can produce reactive gases that may damage the balance. The furnace is located horizontally in the instrument. Unavoidable disturbing influences (gas flow perturbations and thermal buoyancy) through flow phenomena are therefore minimized. The furnace can reach 1373 K as the maximum temperature. The temperatures of the sample and the furnace are measured by platinum and platinum plus 13 per cent rhodium thermocouples (R-type).



Ar: Argon cylinder; H₂ in Ar: Hydrogen in argon cylinder; PR: Pressure regulator; R: rotameter;
TGA: Thermogravimetric analyzer

Figure 3.2. Schematic diagram of thermogravimetric analysis system

3.2.2.2. Total Surface Area. The total surface area of the supports were measured on a Micromeritics Flowsorb II 2300 constant pressure dynamic apparatus (Figure 3.3) by N_2 adsorption from N_2 -He mixtures at liquid nitrogen temperature using a multi-point technique and the BET equation.



1. Back diffusion restrictor, 2. Degas, 3. Flowmeter, 4. Long Path, 5. Short Path, 6. Test Sample, 7. Filter, 8. Septum, 9. Matched Thermal conductivity cells, 10. Cold trap, 11. Flow adjustment valve, 12. Differential flow controller, 13. On-off valve

Figure 3.3. Schematic diagram of the BET equipment (Akın, 1996)

3.2.2.3. Scanning Electron Microscopy (SEM). Micrographs of the used samples after reaction ($Pt-Ni/Al_2O_3$ and $Co-X/ZrO_2$ catalyst samples) were taken, in a scanning electronic microscopy (SEM), to observe the morphology of the carbon deposited. SEM and Energy Dispersive X-Ray (EDX) tests were also conducted on freshly reduced $Co-X/ZrO_2$ catalyst samples in order to elucidate their micro-structural properties. The tests were conducted in a Philips XL 30 ESEM-FEG system, having a maximum resolution of 2 nm. The experiments were performed at the Advanced Technologies Research and Development Center of Boğaziçi University.

In order to obtain information on the dispersion of metals on the catalyst surface, SEM and Energy Dispersive X-Ray (EDX) tests were conducted on fresh bimetallic Pt-Ce

catalysts supported on ZrO_2 . These tests were conducted in a Karl Zeiss EVO40 environmental SEM. The experiments were performed at the Bilkent University by Dr. Emrah Özensoy.

3.2.2.4. X-Ray Photoelectron Spectroscopy (XPS). The extent of electronic interaction between metal components of the freshly reduced catalyst samples was investigated through determination the amounts of metallic phases by X-ray photoelectron spectroscopy (XPS). The tests were performed at the Middle East Technical University Central Laboratory using SPECS spectrometer equipped with a hemispherical electron analyzer and Al- K_{α} 282 W dual X-ray source.

3.2.2.5. X-Ray Diffraction (XRD). The crystalline phases of the catalyst samples and their particle sizes were identified by using a Rigaku D/MAX-Ultima+/PC X-Ray diffraction equipment having an X-ray generator with Cu. The experiments were performed at the Advanced Technologies Research and Development Center of Boğaziçi University.

3.2.3. Catalytic Reaction System

The catalytic reaction system was designed and constructed in the Chemical Engineering Department of Boğaziçi University and involves three characteristic sections:

- Feed section
- Reaction section
- Product analysis section

The feed section was composed of mass flow control systems, 1/4", 1/8" and 1/16" stainless steel tubes and fittings for feeding liquid water and gaseous species, i.e. methane, carbon dioxide, dry air, oxygen, argon and hydrogen (see Table 3.3 for specifications) at desired quantities accurately. The gases that were present in pressurized cylinders were passed through the gas flow regulators (items 1 in Figure 3.4) and the calibrated Brooks Instrument mass flow controllers (items 2 in Figure 3.4), the set values of which were adjusted by the main control unit. An Aalborg GFC171S series standalone controller was

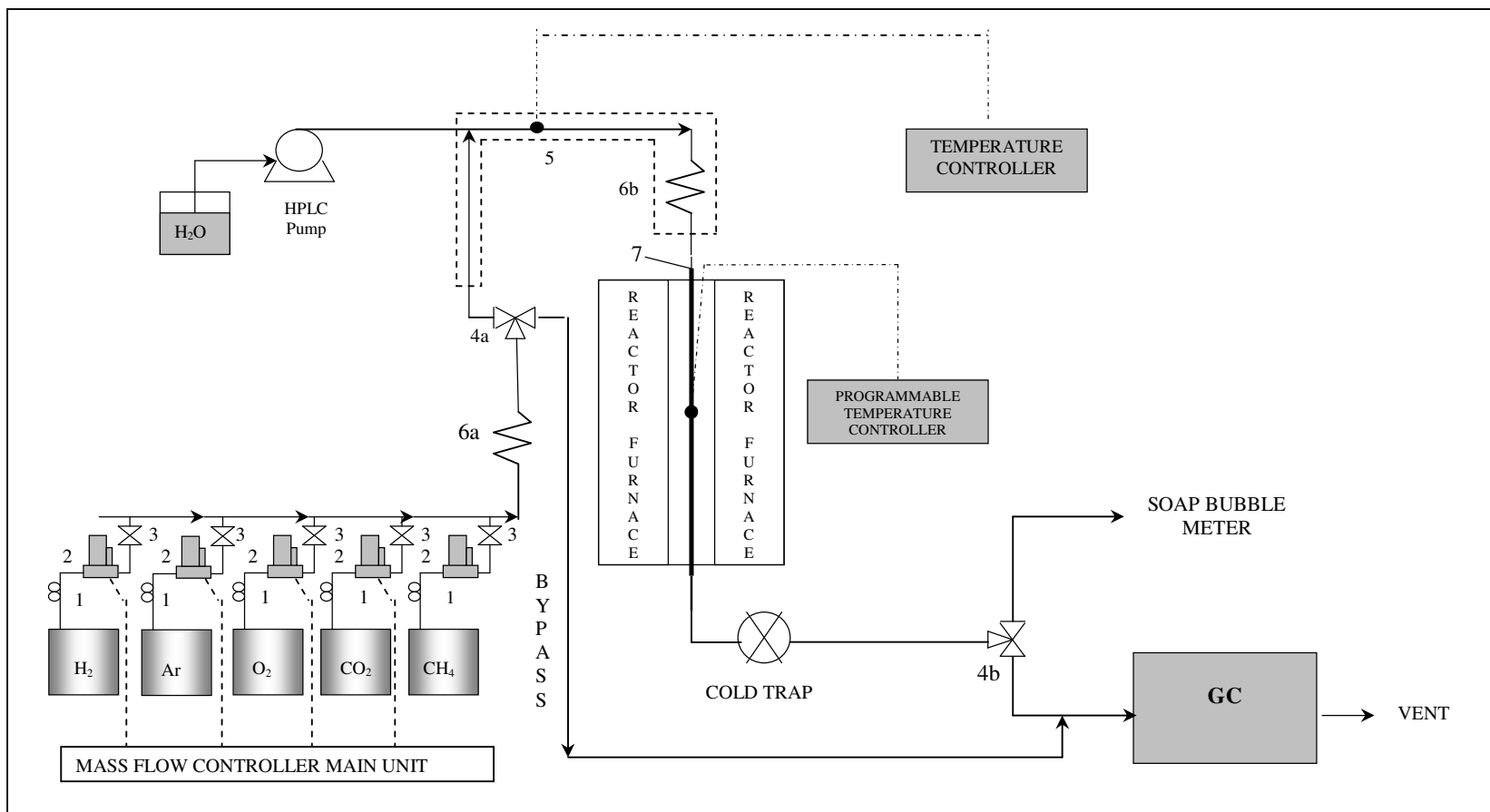
used to regulate methane flow. The calibration curves of the mass flow controllers are presented in Appendix A. On-off valves (items 3 in Figure 3.4) were placed in front of the mass flow controllers to protect them from possible back-pressure fluctuations. Each gas was fed from its independent line, so that it was possible to meter the flow of individual species and adjust desired feed ratios. The gases were then passed through a primary mixing zone (zone 6a in Figure 3.4) to ensure the flow of a homogeneous reactant gas mixture into the reactor.

In the case of combined steam reforming and dry reforming experiments, the liquid water was introduced into the reaction system at constant flow rates using an Autoclave Engineers HPLC pump. The 1/16" tube, through which water was allowed to flow, and the line going to reactor after the primary mixing zone, was kept at 393 ± 3 K using a 1.4 m heating tape and Love Controls temperature controller to feed water in the form of steam (line 5 in Figure 3.4). 16-gauge wire K type sheathed thermocouple was placed at the middle point of heated zone to measure and control the temperatures. The heating tape was covered with ceramic wool insulation to prevent heat losses. Then, steam and homogeneous gas mixture were mixed in a secondary mixing zone (zone 6b in Figure 3.4) to introduce a homogeneous mixture of all the reactants into the reactor.

It was possible to divert the flow direction of feed gases before entering the reactor through the direction of bypass line by using a three way valve 4a, so that the feed composition could be assessed using gas chromatograph.

The reactants, metered and mixed in the feed section, were allowed to flow through the reaction section. This section was composed of a 40 cm \times 2.4 cm ID tube furnace controlled by ± 0.1 K by a Shimaden FP-21 programmable temperature controller and a 6 mm ID quartz microreactor. The reactor length was selected to be 46 cm so that it was longer than the furnace which was also constructed in the Department.

The reaction temperature was determined by a K-type sheathed thermocouple which was placed in the center of the furnace adjacent to the microreactor. The position of the catalyst bed was adjusted to remain within the constant-temperature zone (10 cm) of tube furnace.



1. Gas regulator, 2. Mass flow controller, 3. On-off valve, 4. Three-way valve, 5. Heated zone, 6. Mixing zone, 7. Differential Reactor

Figure 3.4. Schematic diagram of the microreactor flow system

Sintered quartz disc, which was welded to the center of the quartz microreactor, was used to hold the catalyst bed in a fixed position. Ceramic glass wool insulations were placed in top and bottom ends of the reactor furnace to prevent heat loss from the furnace and to provide a good temperature profile.

The product stream leaving the reactor involves steam. Steam existing in the product stream was removed by placing ice cold traps held in flasks at 273 K before GC inlet.

3.2.4. Product Analysis System

Hewlett Packard HP5890, temperature-controlled and programmable gas chromatograph equipped with a Thermal Conductivity Detector (TCD) and a HayeSep D column was used for detecting the feed and the remaining reactant gases after the reaction. Analysis conditions are given in Table 3.4 below.

Table 3.4. Reactant and product gas analysis conditions

GC Parameter	GC-Hewlett Packard HP5890
Detector type	TCD
Column temperature, K	323
Injector Temperature	343
Detector Temperature	373
TCD temperature	373
Carrier Gas	Argon
Carrier Gas flow rate, mL/min	25
Column packing material	HayeSep D
Column tubing material	Stainless steel
Column length & ID	3 m × 3 mm
Sample loop	280 μ L kept at 298 K

Before proceeding with the experiments, the gas chromatograph was calibrated by injecting known values of the species to be analyzed from the injection ports to the column under the conditions given in Table 3.4 and by reading the area under the peak calculated by the integrator. Using this procedure, volume versus peak area curves were constructed for each gas and the corresponding calibration factors were determined by linear regression. The calibration curves are presented in Appendix B.

3.3. Catalyst Preparation and Pretreatment

In this thesis, three sets of catalysts were prepared:

- Ce promoted Pt/ZrO₂ catalysts
- Pt-Ni/Al₂O₃ bimetallic catalysts
- Co/ZrO₂ catalysts with different promoters

The lists of the catalysts are given in Tables 3.5, 3.6 and 3.7.

3.3.1. Support Preparation

Reforming methane with carbon dioxide is known to be a high temperature reaction. Therefore, the catalyst supports should not only have high surface areas but also possess high thermal stabilities.

3.3.1.1. Alumina. The thermally stable δ -Al₂O₃ support was obtained by drying γ -Al₂O₃ at 423 K for 2 h and then calcining it at 1173 K for 4 h. Although this heat treatment caused a reduction in the BET surface area, from 279 m²/g to 81.6 m²/g after calcination, thermal stability of the support was improved.

3.3.1.2. Zirconia. The support was calcined at 1073 K for 4 h in muffle furnace prior to the addition of the metals. Although this heat treatment caused a reduction in the BET surface area, from 93 m²/g to 16 m²/g after calcination, thermal stability of the support was improved.

Table 3.5. List of Ce promoted Pt/ZrO₂ catalysts

Denotation	Pt wt%	Ce wt%	Preparation procedure
cat1	1	0	impregnation
cat2	1	1	coimpregnation
cat3	1	5	coimpregnation
cat4	1	1	sequential impregnation

Table 3.6. List of Pt-Ni/Al₂O₃ bimetallic catalysts

Denotation	Pt wt. %	Ni wt. %	Ni/Pt ratio (molar)
0.3Pt-10Ni	0.3	10	110
0.3Pt-15Ni	0.3	15	165
0.2Pt-10Ni	0.2	10	165
0.2Pt-15Ni	0.2	15	250

Table 3.7. List of Co/ZrO₂ catalysts with different promoters

Denotation	Co wt. %	Promoter	Promoter wt. %
5Co	5	-	-
5Co2La	5	La	2
5Co2K	5	K	2
5Co2Mn	5	Mn	2
5Co2Mg	5	Mg	2
5Co2Ce	5	Ce	2

3.3.2. Preparation of Catalysts

The experimental set-up shown in Figure 3.1 was used for catalyst preparation by the incipient to wetness impregnation. Incipient wetness impregnation method that was used in this study consists of three parts:

- Evacuating the support,
- Contacting the support with the precursor solution, and
- Drying.

For incipient wetness impregnation, five grams of support was placed in the Buchner erlen and kept under vacuum both before and during the addition of precursor solutions. Since trapped air in the pores of the support could prevent penetration of the solutions, vacuum pump was used to remove the trapped air and to give a uniform distribution of the active component. Before impregnating the solution, the support material was mixed with ultrasonic mixer for 25 min.

A Masterflex computerized-drive peristaltic pump was used to feed the precursor solution to the vacuum flask at a rate of 5 mL/min via silicone tubing. The slurry was mixed by an ultrasound mixer during the impregnation in order to maintain uniform distribution of the precursor solutions. After the precursor solution was added, the slurry was ultrasonically mixed for additional 90 min. The thick slurry obtained was dried at 388 K overnight.

3.3.2.1. Ce Promoted Pt/ZrO₂ Catalysts. Monometallic 1 wt. per cent Pt/ZrO₂ was prepared by pore volume impregnation of aqueous tetraammineplatinum nitrate solution. Bimetallic Pt-Ce catalysts were prepared either by coimpregnation, in which aqueous precursor solutions of Pt (tetraammineplatinum nitrate) and Ce (cerium nitrate) were impregnated together onto ZrO₂ with defined concentrations in order to obtain the fixed Pt load of 1 wt. per cent and Ce loads of 1 and 5 wt. per cent, or by sequential impregnation, in which impregnation of aqueous cerium nitrate solution was followed by heat treatment at 773 K for 4 h in muffle furnace and then by impregnation of aqueous tetraammineplatinum nitrate solution. Each impregnation step was conducted under

vacuum. In all monometallic and bimetallic catalysts, the precursor solutions (ca. 0.5 ml/g support) with calculated concentrations were added via a peristaltic pump. After the impregnation step, the samples were dried overnight at 388 K.

3.3.2.2. Pt-Ni/ δ -Al₂O₃ Bimetallic Catalysts. The bimetallic Pt-Ni/ δ -Al₂O₃ catalysts having a Pt loading levels of 0.2 and 0.3 wt. per cent and a Ni loading levels of 10 and 15 wt. per cent were prepared by sequential impregnation, in which impregnation of aqueous nickel nitrate (Ni(NO₃)₂·6H₂O) solution was followed by heat treatment at 873 K for 4 h in muffle furnace and then by impregnation of aqueous tetraammineplatinum nitrate (Pt(NH₃)₄(NO₃)₂) solution. The resulting slurries were dried overnight at 388 K and finally calcined at 773 K for 4 h. Each impregnation step was conducted under vacuum. In all monometallic and bimetallic catalysts, the precursor solutions (ca. 1.0 ml/g support) with calculated concentrations were added via a peristaltic pump.

3.3.2.3. Co/ZrO₂ catalysts with different promoters. Monometallic 5 wt. per cent Co/ZrO₂ was prepared by pore volume impregnation of aqueous cobalt (II) nitrate hexahydrate solution. Doped- Co/ZrO₂ catalysts were prepared by sequential impregnation, in which impregnation of aqueous precursor solutions of the dopants (potassium nitrate, cerium (III) nitrate hexahydrate, lanthanum nitrate hexahydrate, manganese (II) nitrate tetrahydrate and magnesium nitrate hexahydrate) was followed by heat treatment at 773 K for 4 h in muffle furnace and then by impregnation of aqueous cobalt (II) nitrate hexahydrate solution. Each impregnation step was conducted under vacuum. In all monometallic and bimetallic catalysts, the precursor solutions (ca. 0.5 ml/g support) with calculated concentrations were added via a peristaltic pump. After the impregnation step, the samples were dried overnight at 388 K.

3.4. Catalyst Characterization

3.4.1. Temperature Programmed Reduction Experiments

Some of the catalyst samples and the support were characterized by temperature-programmed reduction (TPR) tests for their reduction properties. The amount of deposited

coke on used catalysts was determined by temperature-programmed oxidation (TPO) tests. Both TPO and TPR tests were performed on a Mettler Toledo TGA/DTA851 apparatus.

TPR measurements were carried out by using a H₂ (4% v/v)-He reductive mixture with a heating rate of 5 K/min. The temperature was increased from room temperature up to 1073 K. Prior to the TPR experiments, samples were calcined in flowing air at 773 K for 4 h. In a typical TPO experiment, the catalyst sample, after 4 hours of reaction, was cooled to room temperature, then placed into the system and heated up to 1173 K at a rate of 10 K/min in O₂ (30% v/v)-He mixture with a flowrate of 50 mL/min

3.4.2. Total Surface Area Experiments

Total surface area measurements were performed using the multi-point BET method. The equations used in the total surface area calculations are given as follows:

$$\frac{P}{V(P_o - P)} = \frac{1}{cV_m} + \left[\frac{(c-1)}{cV_m} \right] \frac{P}{P_o} \quad (3.1)$$

$$S = \frac{AV_m A_g}{M} \quad (3.2)$$

In Equations (3.1) and (3.2), A is the Avogadro's number (6.02×10^{23}), A_g is the area of an individually adsorbed molecule, which is 16.2×10^{-20} m² for nitrogen, M is the molar volume of the gas, and V_m is the monolayer volume. A straight line results for P/P_o values from about 0.05 to 0.25 when experimental data are plotted as P/V(P_o-P) on the ordinate against P/P_o on the abscissa. Relative pressures within the prescribed range are typically obtained with gas compositions between about 5 per cent and 25 per cent nitrogen with the inert being helium.

The sample was first dried and degassed under nitrogen flow for two and a half hours at 523 K and then cooled to room temperature. The Flowsorb 2300 unit was calibrated by injecting one milliliter of nitrogen at ambient conditions, calculating the corresponding volume of gas at standard conditions and setting the instrument to indicate thereafter

adsorbed and desorbed gas volumes at standard conditions. Then a flow of the measuring gas (five per cent to 25 per cent nitrogen-helium mixture) was allowed to pass over the sample at liquid nitrogen temperature of 77.4 K and equilibrate. After the adsorption equilibrium was established as indicated by the threshold indicator, the temperature of the sample was raised to ambient temperature and the amount of nitrogen desorbed was measured by the thermal conductivity detector. This nitrogen adsorption-desorption procedure was repeated at least four times with different nitrogen-helium gas concentrations. The total surface area was calculated from In Equations (3.1) and (3.2) by using a software supplied by Micromeritics Inc. together with the Flowsorb 2300 unit.

3.4.3. X-Ray Photoelectron Spectroscopy (XPS)

X-ray photoelectron spectroscopy (XPS) analyses were conducted on (i) Ce promoted Pt/ZrO₂ catalysts and (ii) Pt-Ni/Al₂O₃ bimetallic catalysts. The tests were performed on freshly calcined and reduced samples at the Middle East Technical University Central Laboratory using SPECS spectrometer equipped with a hemispherical electron analyzer and Al-K_α (h= 1486.56 eV; 1 eV = 1.6302 × 10⁻¹⁹ J) 282 W dual X-ray source. The vacuum in analysis chamber was always < 1 × 10⁻⁹ mbar. The spectra were collected at pass energy of 48 eV. The XPS data analysis was performed with the XPSPeak 4.1 program. The intensities were estimated by calculating the integral of each peak, after subtraction of the S-shaped background, and by fitting the curve to a combination of Lorentzian (30%) and Gaussian (70%) lines. All binding energies were referenced to the C 1s line at 284.6 eV, which provided binding energy values with an accuracy of ± 0.2 eV.

3.5. Reaction Tests

3.5.1. Blank Tests

Blank tests were conducted to ensure that the material of construction, quartz disc and the reactor did not interfere with the reaction test outputs. The results indicated that quartz disc and the reactor were inert under the conditions used in the reaction experiments.

3.5.2. Carbon Dioxide Reforming of Methane over Ce-promoted Pt/ZrO₂ Catalysts

The CO₂ reforming of methane has been studied over Pt/ZrO₂ catalysts promoted with Ce at different temperatures and feed compositions. The influence of the impregnation strategy and the cerium amount on the activity and stability of the catalysts were investigated. Prior to reaction tests, the catalysts were calcined *in situ* in dry air (30 mL/min) for 4 h at 773 K and subsequently reduced *in situ* in H₂ (50 mL/min) for 2 h at the same temperature. The reactions were performed in the temperature range of 773-973 K and CH₄: CO₂ ratios of 1:1 & 2:1. The total volumetric flow rate was held constant at 26 mL/min, resulting in space velocity of 15,600 mL/h.g-cat.

3.5.3. Combined Methane Reforming Reactions over Pt-Ni/ δ -Al₂O₃ Catalysts

The purpose of this part of the study was to design and develop Pt-Ni bimetallic catalysts supported on δ -Al₂O₃ for CDRM as the main reaction. An effective catalyst with optimum Pt/Ni metal composition assuring high activity and stability was searched through a parametric study. Small amount of H₂O or O₂ was also added to the feed to inhibit the rate of coke formation through CDRM coupled with SR or POX, respectively. The performance of reforming reactions based on activity, stability and selectivity (ie.H₂/CO ratios) were observed during DR as well as DR-POX and DR-SR.

Prior to reaction tests, the catalyst samples were reduced *in situ* in H₂ (50 mL/min) for 2 h at 773 K. The reaction tests were performed in the temperature range of 773-973 K for 4h time-on-stream (TOS) with a space velocity of 15,600 mL/h.g-cat. The various gas feed compositions used are listed in Table 3.8. No diluents were used in the tests. Stability test was performed at 923 K for 14 h.

Table 3.8. List of reaction experiments performed over Pt-Ni/ δ -Al₂O₃ Catalysts

Catalyst	Feed Composition				C/O ratio in the feed
	CH ₄	CO ₂	H ₂ O	O ₂	
0.3Pt-10Ni	1	1	-	-	1.00
0.3Pt-10Ni	1	1	1	-	0.67
0.3Pt-10Ni	2	1	1	-	1.00
0.3Pt-10Ni	2	1	-	0.25	1.20
0.3Pt-10Ni	1	1	-	0.50	0.67
0.2Pt-10Ni	1	1	-	-	1.00
0.2Pt-10Ni	1	1	1	-	0.67
0.3Pt-15Ni	1	1	-	-	1.00
0.3Pt-15Ni	1	1	1	-	0.67
0.2Pt-15Ni	1	1	-	-	1.00
0.2Pt-15Ni	1	1	1	-	0.67
0.2Pt-15Ni	2	1	1	-	1.00
0.2Pt-15Ni	2	1	-	0.25	1.20
0.2Pt-15Ni	1	1	-	0.50	0.67

3.5.4. Kinetic Experiments over Pt-Ni/ δ -Al₂O₃ Catalysts

The kinetic behavior of the 0.2Pt-15Ni and 0.3Pt-10Ni catalysts in the reforming reaction of methane with carbon dioxide was investigated as a function of temperature and partial pressures of CH₄ and CO₂.

Kinetic experiments were performed under differential conditions at atmospheric pressure at 873 K using 5 mg of catalyst. The total feed flow rate was manipulated between 100-150 mL/min to obtain significantly lower conversions in the range of 5-25 per cent, which were far away from the corresponding thermodynamic equilibrium. Therefore; the study of the CDRM reaction can disclose the intrinsic kinetic information.

To determine the apparent activation energies, the reforming reaction was carried out with a feed composition of $\text{CH}_4:\text{CO}_2 = 1:1$ over a temperature range of 853–893 K.

The partial pressure dependencies were determined at 873 K by maintaining a constant partial pressure of 0.08 atm of one reactant and varying the pressure of the other reactant between 0.02 and 0.08 bar. A balance of argon was adjusted to maintain the pressure close to atmospheric and the total flow constant. The various gas feed compositions used are listed in Table 3.9.

The effect of H_2 and CO addition was studied at 873 K using 5 mg of catalyst and a total flow of 100 mL/min with constant partial pressures of the two reactants 0.08 atm, while the inlet partial pressures of H_2 or CO were changed from 0 to 0.075 atm. The various gas feed compositions used are listed in Table 3.10.

3.5.5. Carbon dioxide reforming of methane over Co-X/ZrO₂ catalysts (X = La, Ce, Mn, Mg, K).

The CO_2 reforming of methane has been studied over Co/ZrO₂ catalysts promoted with cerium, lanthanum, potassium, manganese and magnesium. The influence of the promoters on the activity and stability of the catalysts were investigated. Prior to reaction tests, the catalysts were calcined *in situ* in dry air (30 mL/min) for 4 h at 773 K and subsequently reduced *in situ* in H_2 (50 mL/min) for 2 h at the same temperature. The reactions were performed at a temperature of 923 K with a $\text{CH}_4:\text{CO}_2$ ratios of 1:1. The total volumetric flow rate was held constant at 50 mL/min, resulting in space velocity of 60,000 mL/h.g-cat. Selected samples were also tested at two different space velocities of 30,000 and 15,600 mL/h.g-cat.

Table 3.9. List of kinetic experiments performed over Pt-Ni/ δ -Al₂O₃ Catalysts

Exp. No	CH ₄ /CO ₂	Total Flow (mL/min)	Weight of Catalyst (mg)	Partial Pressures (atm)	
				CH ₄	CO ₂
1	0.25	100	5	0.02	0.08
2	0.25	120	5	0.02	0.08
3	0.25	150	5	0.02	0.08
4	0.50	100	5	0.04	0.08
5	0.50	120	5	0.04	0.08
6	0.50	150	5	0.04	0.08
7	0.75	100	5	0.06	0.08
8	0.75	120	5	0.06	0.08
9	0.75	150	5	0.06	0.08
10	1.00	100	5	0.08	0.08
11	1.00	120	5	0.08	0.08
12	1.00	150	5	0.08	0.08
13	1.33	100	5	0.08	0.06
14	1.33	120	5	0.08	0.06
15	1.33	150	5	0.08	0.06
16	2.00	100	5	0.08	0.04
17	2.00	120	5	0.08	0.04
18	2.00	150	5	0.08	0.04
19	4.00	100	5	0.08	0.02
20	4.00	120	5	0.08	0.02
21	4.00	150	5	0.08	0.02

Table 3.10. List of kinetic experiments performed over Pt-Ni/ δ -Al₂O₃ Catalysts
(Effect of H₂ and CO partial pressures)

Exp. No	Total Flow (mL/min)	Weight of Catalyst (mg)	Partial Pressures (atm)			
			CH ₄	CO ₂	CO	H ₂
22	100	5.00	0.08	0.08	0.015	-
23	100	5.00	0.08	0.08	0.030	-
24	100	5.00	0.08	0.08	0.045	-
25	100	5.00	0.08	0.08	0.060	-
26	100	5.00	0.08	0.08	-	0.015
27	100	5.00	0.08	0.08	-	0.030
28	100	5.00	0.08	0.08	-	0.045
29	100	5.00	0.08	0.08	-	0.060
30	100	5.00	0.08	0.08	-	0.075

4. RESULTS AND DISCUSSION

The results and discussion of this thesis consists of four subparts:

- Carbon dioxide reforming of methane over Ce-promoted Pt/ZrO₂ catalysts,
- Combined methane reforming reactions over Pt-Ni/ δ -Al₂O₃ catalysts,
- Kinetic experiments over Pt-Ni/ δ -Al₂O₃ catalysts, and
- Carbon dioxide reforming of methane over Co-X/ZrO₂ catalysts (X = La, Ce, Mn, Mg, K).

The characterization and performance tests of the catalysts were done considering the “activity, selectivity and stability” as the primary criteria in deciding the direction of experimental tests. The micro-characterization and catalytic performance data obtained were utilized in order to unveil the reasons behind the activity and selectivity characteristics of the catalysts.

4.1. Carbon Dioxide Reforming of Methane over Ce-promoted Pt/ZrO₂ Catalysts

The purpose of this part of the work was to design and develop an effective Pt-based bimetallic CDRM catalyst supported on zirconia. Aiming to have bimetallic catalysts with enhanced performance properties, Ce was used as a promoter, which was added through conventional impregnation method. The main intention was to have high dispersion of the cerium on the surface of the support rather than to have it incorporated in the skeletal structure of the catalyst, like for samples prepared by coprecipitation in literature (Mattos *et al.*, 2003). To determine optimal combination of reaction conditions and catalyst composition leading to superior productivity and selectivity; impregnation strategy, cerium amount, reaction temperature and CH₄/CO₂ ratio were used as the parameters. The reduction characteristics of freshly calcined samples and the amount of coke deposited on the used catalysts were determined by thermogravimetric and differential thermal analyses (TGA/DTA). The extent of interaction between metal components during preparation procedures was investigated by X-ray photoelectron spectroscopy (XPS) analysis through

which the amounts of metallic phases of Pt and Ce were determined. SEM and EDX tests were performed in order to obtain information on the dispersion of metals on the catalyst surface. The catalysts characterized and tested in this part of the work are given in Table 3.5 in Experimental Section.

4.1.1. Characterization Tests

4.1.1.1 Temperature Programmed Reduction. Temperature-programmed reduction (TPR) studies were performed on the support and catalyst samples by using thermogravimetric and differential thermal analysis (TGA-DTA) equipment. The TPR profiles of the catalysts and the support are shown in Figure 4.1. TPR profiles demonstrate that there is no significant weight loss up to 1073 K under hydrogen flow indicating no reduction of support (not shown in the figure). Bozo *et al.* (2000) and Passos *et al.* (2005) obtained similar results in TPR experiments for zirconia. 1 wt. % Pt/ZrO₂ showed a steep bend around at 453 K, which is assigned to the reduction of PtO₂ phase (Passos *et al.*, 2005; Querino *et al.*, 2005). At around 723 K, one can note a gentle decrease in the curvature, most probably related to the reversible adsorption of hydrogen by the support (Querino *et al.*, 2005; Jung and Bell, 2000). All Pt-Ce/ZrO₂ catalysts showed a weight loss at 523-573 K that may be attributed to both the reduction of ceria in close contact with platinum, as well as to the reduction of platinum (i.e. breakdown of Pt-O-CeO₂ species created on calcinations step). The second mild curvatures at about 650-700 K, are related to the surface reduction of CeO₂ not in close contact with the platinum. This is assigned to the ability of the noble metal to promote the reduction of Ce⁺⁴ via spilling of hydrogen species over the support (Passos *et al.*, 2005; Querino *et al.*, 2005; Jung and Bell, 2000).

The weight loss for 1 wt.% Pt-5 wt.% Ce /ZrO₂ catalyst prepared by coimpregnation method (cat3) is the highest when compared with the other 1 wt.% Pt-1 wt.% Ce /ZrO₂ catalysts prepared by either coimpregnation or sequential impregnation method, indicating that the increase in the Ce loading on Pt/ZrO₂ did improve the reducibility of the catalyst. Figure 4.1 and its differential form (not given) also show that the reduction temperatures shift to lower temperatures as the cerium content increases, i.e 523 K for cat3 whereas 548 K for cat2 and 576 K for cat4. This result seems to be related to the increased oxygen mobility favored by the higher amount of Ce species that can be reduced.

In conclusion, it seems clear from the results that in Pt-Ce catalysts, the reduction treatment at 773 K is sufficient to produce ceria at its zero valent state (Ce^{+4}) and/or the creation of oxygen vacancies and presence of Ce^{+3} ions; $\text{Ce}^{+4}/\text{Ce}^{+3}$ ratio on the samples depends on the preparation procedure of the sample prior to reduction (see also section 4.1.1.2). These results are parallel to the results presented in literature (Passos *et al.*, 2005; Querino *et al.*, 2005; Jung and Bell, 2000; Serrano-Ruiz *et al.*, 2006).

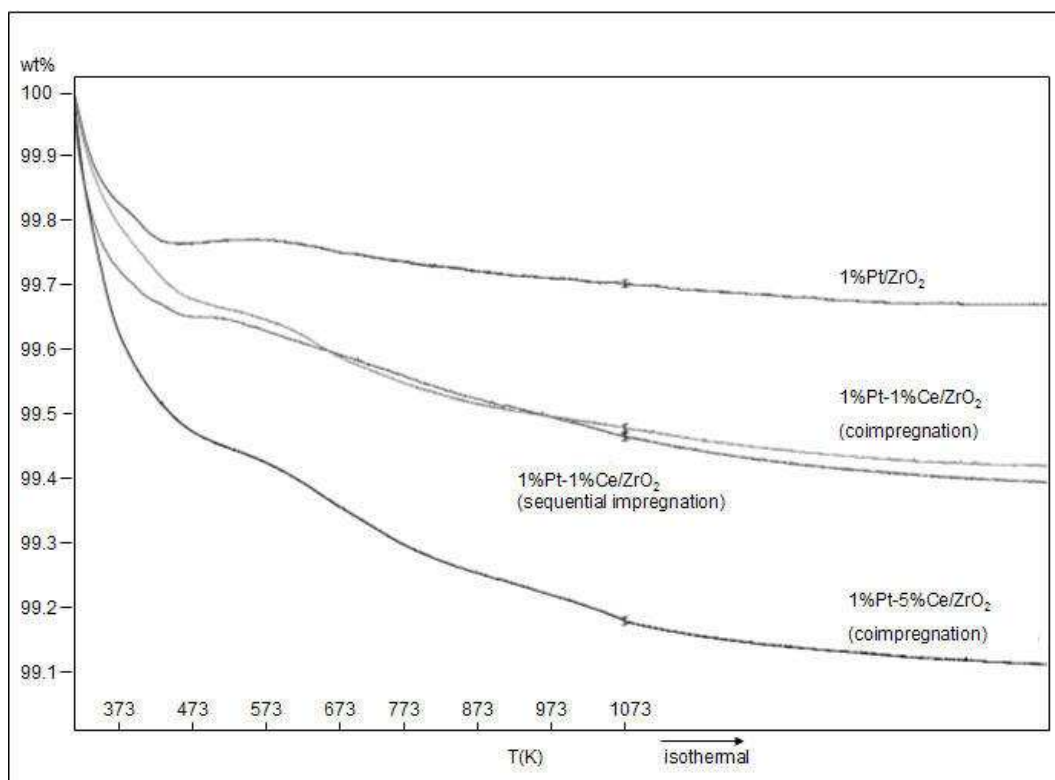


Figure 4.1. Temperature programmed reduction (TPR) profiles of 1%Pt/ZrO₂, 1%Pt-1%Ce/ZrO₂ (coimp.), 1%Pt-5%Ce/ZrO₂ (coimp.) and 1%Pt-1%Ce/ZrO₂ (seq. imp.)

4.1.1.2. X-Ray Photoelectron Spectroscopy. The extent of interaction between Pt and Ce metallic species for the catalysts having same loads but had been prepared by different *impregnation* procedures were determined through analyzing the data obtained from XPS tests. For that purpose, the metallic phases of Pt and Ce present on 1 wt.% Pt-1 wt.% Ce /ZrO₂ catalyst prepared by coimpregnation and sequential impregnation method, cat2 and cat4, respectively, were analyzed by XPS. It can be seen from Table 4.1 that the Zr 3d_{5/2} binding energy remains unchanged, within the precision limits of the measurement, at

around 182.3 eV, which is the typical binding energy for Zr^{+4} , for both catalysts (Serrano-Ruiz *et al.*, 2006).

The main experimental Pt $4f_{7/2}$ peak has been deconvoluted into two components. Their binding energies and their relevant contribution to the main peak are reported in Table 4.1. Table 4.1 also includes the binding energy values of Pt $4f_{7/2}$ core levels of Pt^0 , Pt^{+2} and Pt^{+4} , which were reported in the related literature as reference basis (Shyu and Otto, 1988; Serre *et al.*, 1993). In the XPS profiles of cat4, the peak at 71.9 eV indicates the presence of Pt^{+2} species, and the one centered at 70.7 eV corresponds to Pt^0 species. For cat2, there appeared to be a small electropositive shift in Pt $4f_{7/2}$ peak binding energies measured relative to cat 4 suggesting that Pt may have been slightly more oxidized in this sample. Serre *et al.* (1993) mentioned that a slight increase in Pt oxidation state may reflect charge transfer from metal to ceria, indicating that Ce is slightly reduced. This shift corresponds to a net electron transfer from Pt to Ce due to the existence of strong and extensive Pt-Ce interaction between both Pt and Ce precursors during coimpregnation on the ZrO_2 surface and between Pt and Ce species during subsequent high temperature thermal treatments, i.e. calcination and reduction, at 773 K.

Table 4.1. Catalyst characterization by XPS

Sample	B.E. Zr $3d_{5/2}$ (eV)	B.E. Pt $4f_{7/2}$ (eV) [%]	B.E. Ce u''' (eV)	Ce $^{+3}$ (%)
cat2	182.4	70.8 [39] 72.1 [61]	916.8	25
cat4	182.3	70.7 [62] 71.9 [(38)]	917.8	11
Pt^0 (Shyu and Otto, 1988)	-	71.1 ± 0.2	-	-
Pt^{+2} (Shyu and Otto, 1988)	-	72.2 ± 0.2	-	-
Pt^{+4} (Serre <i>et al.</i> , 1993)	-	74.2 ± 0.2	-	-

Figures 4.2 and 4.3 show the Ce 3d XP spectra obtained with 1 wt.% Pt-1 wt.% Ce /ZrO₂ catalysts prepared by both coimpregnation and sequential impregnation method (cat2 and cat4), respectively, upon reduction at 773 K. The electronic structure of CeO₂ has been a matter of controversy. The first really well-resolved spectra were published by Burroughs *et al.* (1976). The complexity of Ce spectra is caused by strong hybridization between the Ce 4f levels and the O 2p states (Romeo *et al.*, 1993). According to the literature (Romeo *et al.*, 1993; Laachir *et al.*, 1991; Silvestre-Albero *et al.*, 2002), the complex spectrum of Ce 3d can be resolved into 10 components, which can be obtained curve-fitting analysis (v 's represent the Ce 3d_{5/2} contribution and u 's represent the Ce 3d_{3/2} contribution) as shown in Figures 4.2 & 4.3. The peaks labeled v , v'' and v''' can be attributed to Ce⁺⁴; v and v'' are due to a mixture of Ce 3d⁹ 4f² O 2p⁴ and Ce 3d⁹ 4f¹ O 2p⁵ configurations while v''' corresponds to a pure Ce 3d⁹ 4f⁰ O 2p⁶ final state. On the other hand, v_0 and v' are assigned to the Ce 3d⁹ 4f² O 2p⁵ and Ce 3d⁹ 4f¹ O 2p⁶ configurations of Ce⁺³; u structures, due to the Ce 3d_{3/2}, can be explained in the same way.

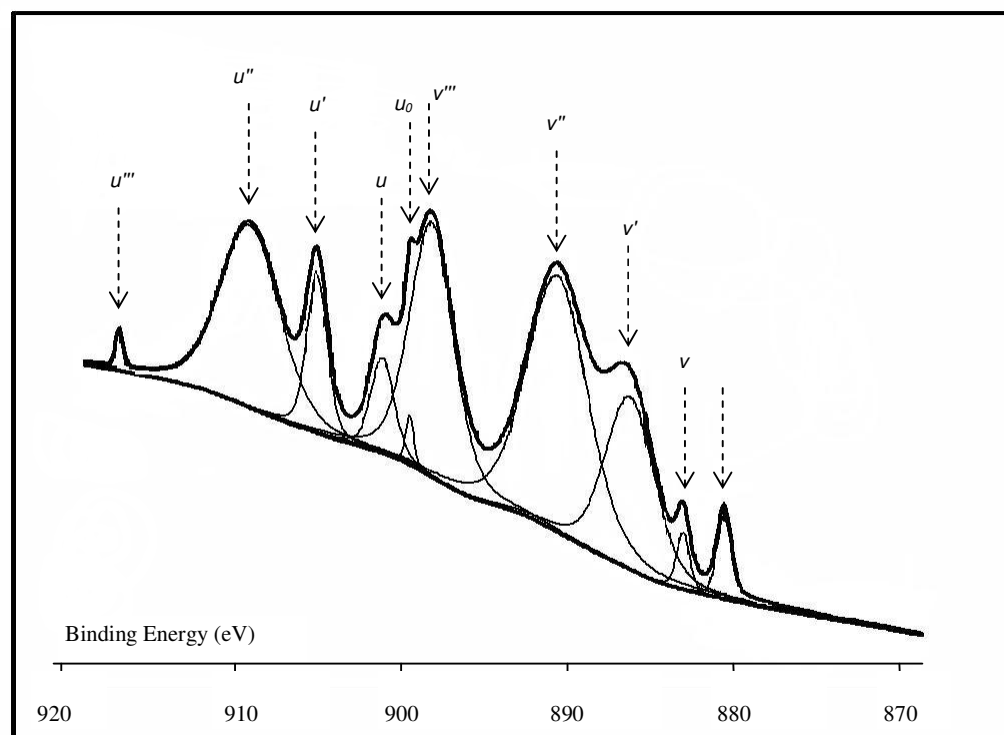


Figure 4.2. Ce 3d XPS spectra of 1%Pt-1%Ce/ZrO₂ prepared by coimpregnation (cat2)

In literature, two different approaches have been followed to evaluate the degree of ceria reduction from XPS. Some authors have used percentage of area of the u''' peak in total Ce 3d region to describe the total amount of Ce^{+4} in the sample (Shyu *et al.*, 1988; Noronha *et al.*, 2001). However, it has been reported that this approach leads to erroneous quantitative results. The second approach considers the relative intensity of the $u_0(v_0)$ and $u'(v')$ peaks as representatives of Ce^{+3} , in total Ce 3d band (Laachir *et al.*, 1991; Silvestre-Albero *et al.*, 2002; Ernst *et al.*, 1999). In this way, after deconvolution of the experimental spectra, the degree of Ce reduction can be calculated from the ratio between the sum of the intensities of u_0, u', v_0 and v' peaks and the sum of the intensities of all the peaks (Equation 4.1).

$$Ce^{+3}(\%) = \frac{100 \cdot [S(u_0) + S(u') + S(v_0) + S(v')]}{\sum [S(u) + S(v)]} \quad (4.1)$$

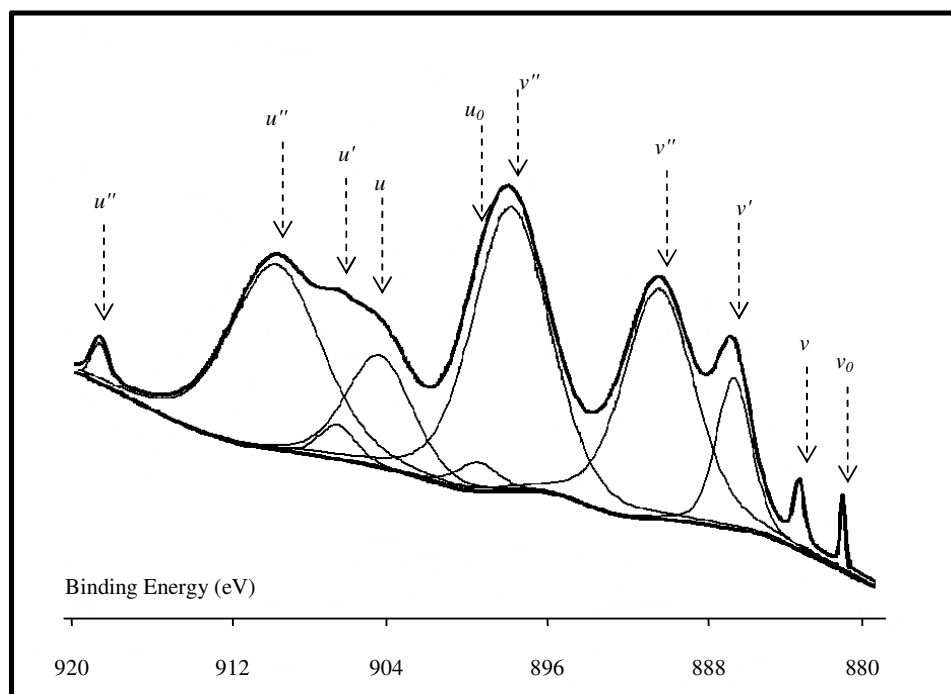


Figure 4.3. Ce 3d XPS spectra of 1%Pt-1%Ce/ZrO₂ catalyst prepared by sequential impregnation (cat4)

Data in Table 4.1 show that the amount of Ce^{+3} estimated from the above equation was 25% for cat2, whereas 11% for cat2. Coimpregnation of Pt and Ce onto ZrO_2 support and subsequent thermal treatments has resulted in an increase in the amount of Ce^{+3} states. It must also be recalled that, as initially reported by Paparazzo (1990), CeO_2 can suffer spontaneous reduction at room temperature during XPS measurements by action of the X-ray irradiation combined with the ultra-high-vacuum environment. Considering that the same support has been used for the preparation of both bimetallic Pt-Ce catalysts, and that the XPS analysis has been carried out under the same conditions for both samples; thus, it can be safely assumed that Ce^{+4} photo reduction by X-ray irradiation is similar for both catalysts, and the differences in reducibility are caused by the impregnation strategy used in their preparation. Additionally, the binding energies of the Ce u''' peak are also reported in Table 4.1. The value is 916.8 eV for cat2 whereas 917.8 eV for cat 4, indicating and validating that cat4, 1wt.%Pt-1 wt.% Ce/ ZrO_2 catalyst prepared by sequential impregnation, has Ce in higher oxidized states.

XPS data indicate that the increase in Pt oxidation state and the higher amount of reduced Ce in cat 2 is a result of net electron transfer from Pt to Ce due to the existence of strong and extensive Pt-Ce interaction during coimpregnation of Pt and Ce precursors on ZrO_2 and during subsequent high temperature thermal treatments (calcination and reduction at 773 K).

4.1.1.3. Scanning Electron Microscopy. Freshly reduced Pt-Ce catalysts prepared by coimpregnation and sequential impregnation (cat2 and cat4) were tested using SEM-EDX to obtain information on their microstructural and metal dispersion properties. Metal mapping studies were used to understand the dispersion of metals and their agglomeration behaviours on the support surface; the Pt + Ce metal mappings obtained for different samples are given in Figures 4.4 and 4.5. For each sample, a representative set including a bright area image, the EDX profile, and Pt + Ce mapping are given. Additionally, the weight percentages of the metallic species on the surface are tabulated in Table 4.2 for all samples.

Table 4.2. Weight percentages of the surface metallic species from SEM-EDX data

Catalyst #	Ce wt. %	Pt wt.%
cat2	2.32	5.08
cat4	1.37	6.86

In particular; Pt is observed to be well and homogeneously dispersed over the surface of 1 wt. % Pt-1 wt. % Ce /ZrO₂ catalyst prepared by coimpregnation (cat2). The low signal of Pt from the EDX spectrum can be attributed to the high dispersion and small particle size of Pt metal on the surface.

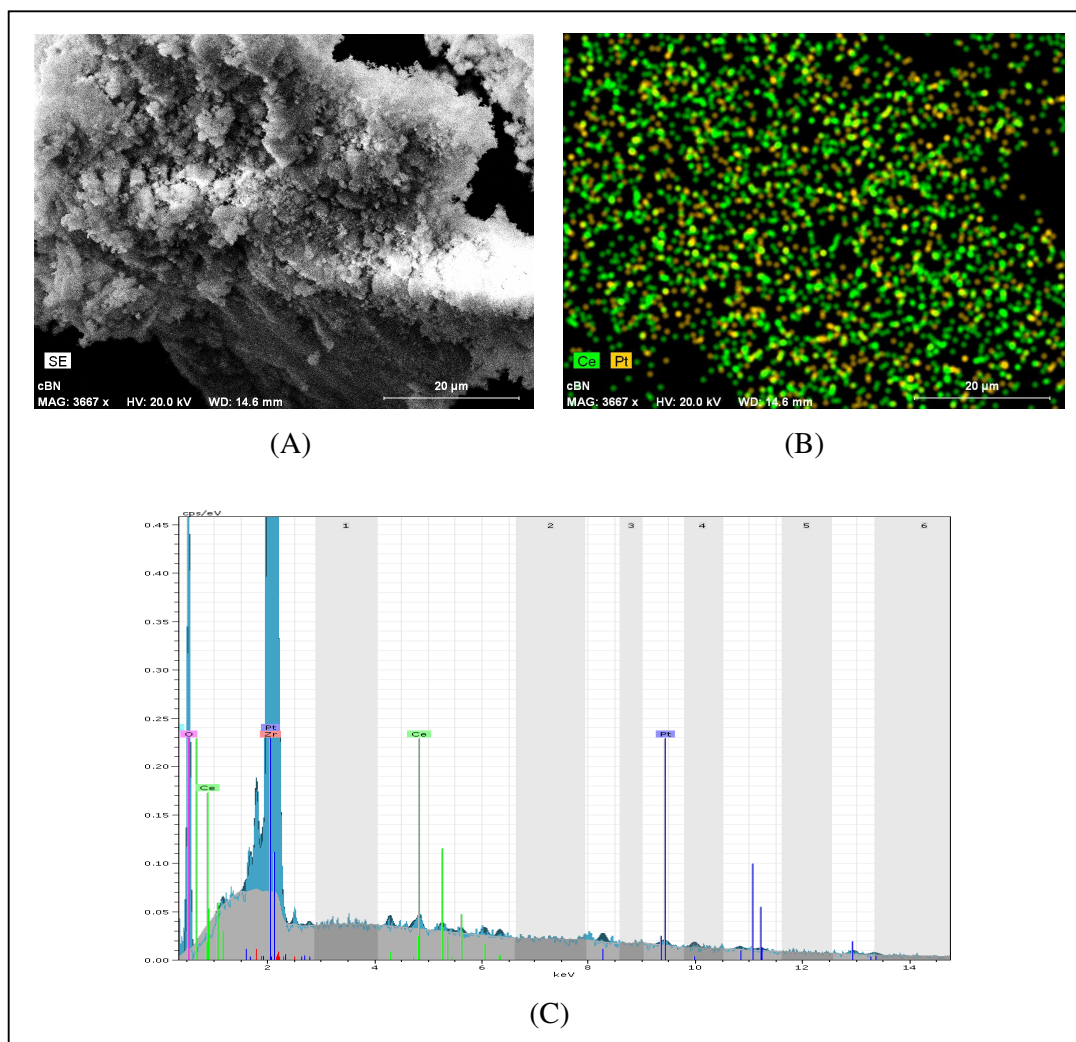


Figure 4.4. 1%Pt-1%Ce/ZrO₂ catalyst prepared by coimpregnation (cat2): A) SEM bright area image, B) Pt + Ce mapping, C) EDX spectrum

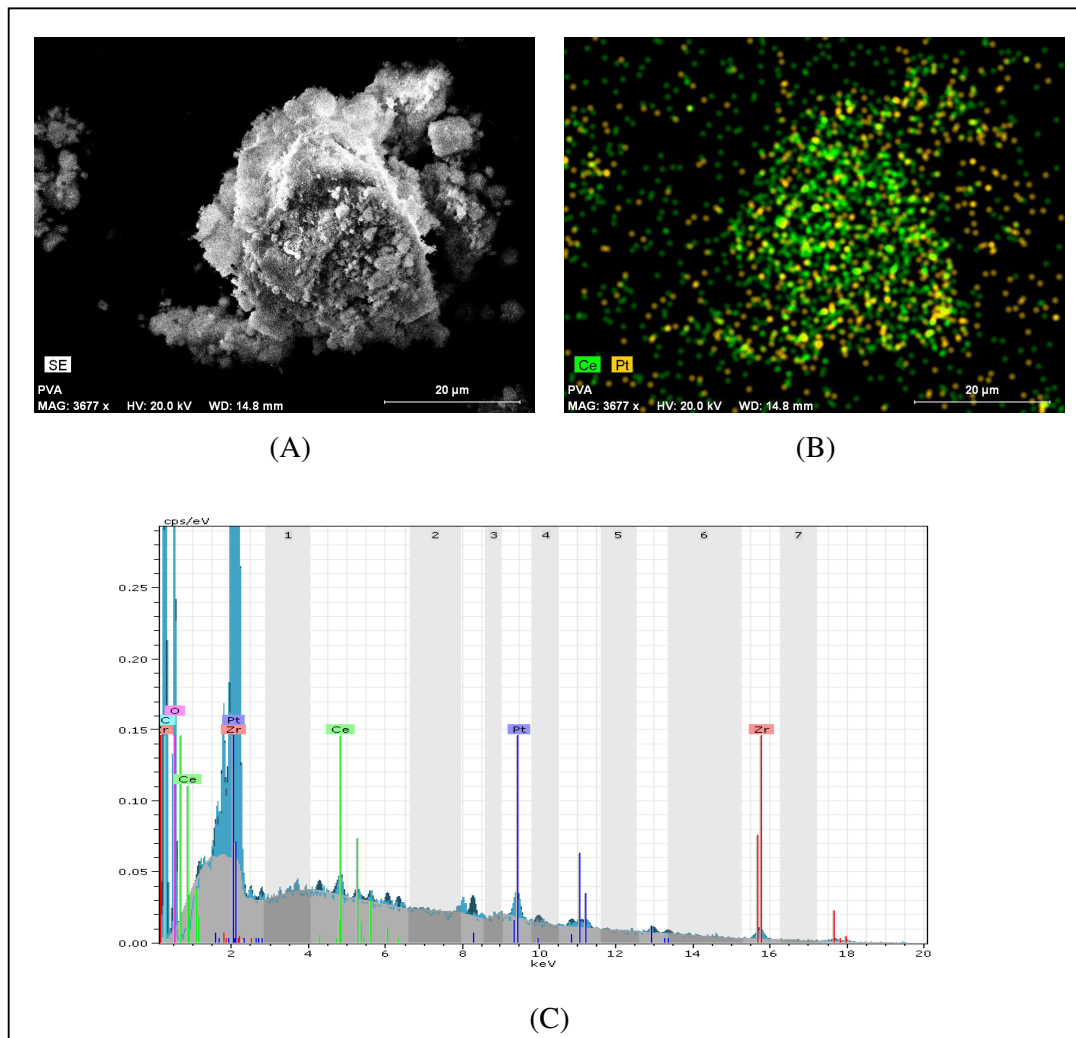


Figure 4.5. 1%Pt-1%Ce/ZrO₂ catalyst prepared by seq. impregnation (cat4): A) SEM bright area image, B) Pt + Ce mapping, C) EDX spectrum

However; over the surface of 1 wt. % Pt-1 wt. % Ce /ZrO₂ catalyst prepared by sequential impregnation (cat 4), there is a significant Pt signal present in EDX spectrum. This shows us that Pt dispersion is low compared to the sample prepared by coimpregnation method and Pt is in the form of agglomerates, which is confirmed by the SEM images.

4.1.1.4. Temperature Programmed Oxidation. Figure 4.6 shows the TGA curves of the used catalysts, namely, cat2, cat3 and cat4, which were used to determine the amount of carbon formation after 4 h of time on stream reaction tests at 973 K for the reaction with the feed having CH₄: CO₂ ratio of 1:1. During the TPO, the weights of 1 wt.% Pt-1 wt.% Ce /ZrO₂ and 1 wt.% Pt-5 wt.% Ce /ZrO₂ catalysts prepared by coimpregnation method (cat2 and cat3) showed very small change with the temperature increase, which is the indication of little coke formation during the reaction. On the other hand, TGA tests showed a weight loss of 7 % on treating the 1 wt.% Pt-1 wt.% Ce /ZrO₂ catalyst prepared by sequential impregnation method (cat4), indicating a significant amount of carbon deposition on that sample during the course of 4 h on-stream reaction. The overall weight loss would correspond to the sum of change due to oxidation of carbonaceous species and oxidation of reduced cerium and platinum (Damyanova and Bueno, 2003).

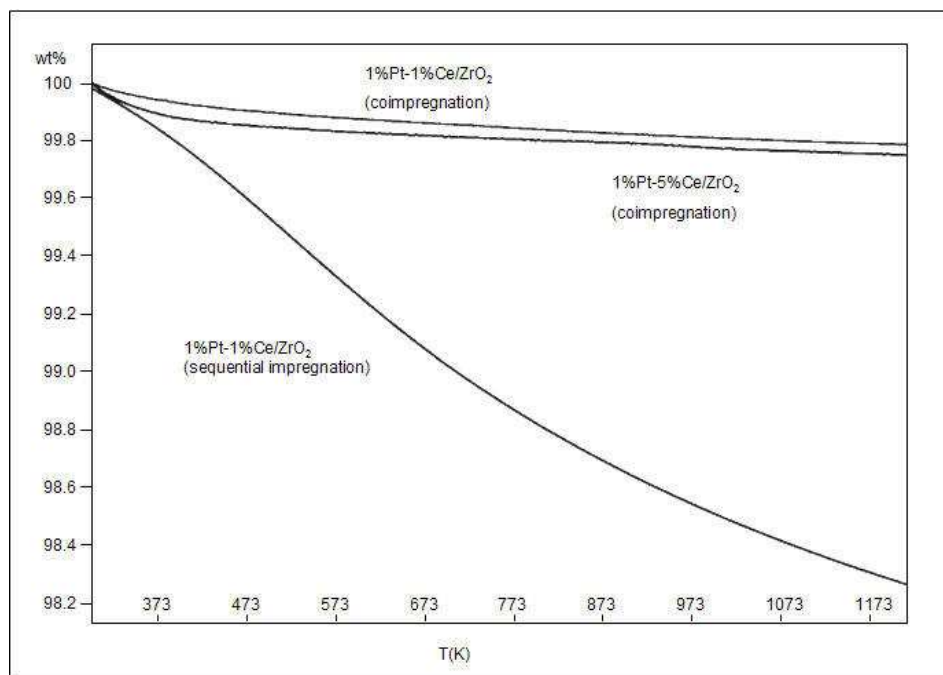


Figure 4.6. Temperature programmed oxidation (TPO) profiles of spent catalysts after 4 h of time on stream reaction tests at 973 K with CH₄/ CO₂ = 1/1: 1%Pt-1%Ce/ZrO₂ (coimp.), 1%Pt-5%Ce/ZrO₂ (coimp.) and 1%Pt-1%Ce/ZrO₂ (seq. imp.)

The TGA tests were also conducted on the catalysts used in the reaction tests with a higher $\text{CH}_4:\text{CO}_2$ ratio. Figure 4.7 shows the TGA curves of the spent catalysts, namely, cat2 & cat3, which were used to determine the amount of carbon formation after 4 h of reaction at 973 K and $\text{CH}_4:\text{CO}_2$ ratio of 2:1. The profiles indicate that carbon formation is not significant even under severe conditions. Additionally, higher Ce load limits carbon deposition.

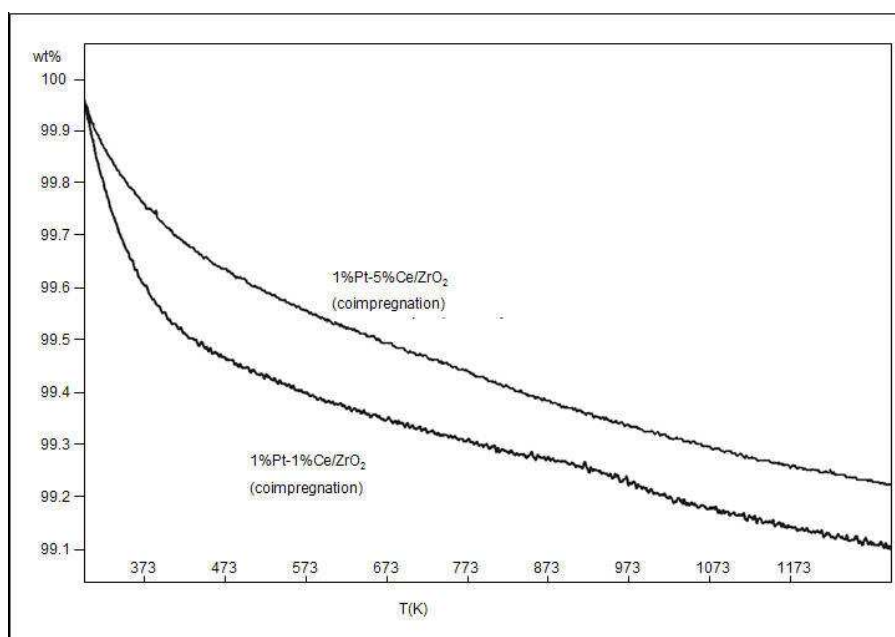


Figure 4.7. Temperature programmed oxidation (TPO) profiles of spent catalysts after 4 h of time on stream reaction tests at 973 K with $\text{CH}_4/\text{CO}_2 = 2/1$: 1%Pt-1%Ce/ZrO₂ (coimp.) and 1%Pt-5%Ce/ZrO₂ (coimp.)

4.1.2. Carbon Dioxide Reforming of Methane

In the current work, a parametric study on Pt-Ce/ZrO₂ system for dry reforming reaction, which considers the effects of reaction temperature, feed composition (i.e. CH_4/CO_2 ratio in the feed), reaction time and catalyst preparation method as the parameters, was conducted.

4.1.2.1. Effect of Reaction Temperature. The catalysts were tested in CO₂ reforming of methane at 773-973 K range with CH₄: CO₂ feed ratio as 1:1. Figures 4.8 - 4.10 show the CH₄ conversion, CO₂ conversion and H₂/CO molar ratio, respectively, as a function of reaction temperature. Activity trends reveal that CH₄ and CO₂ conversions increase with reaction temperature for each catalyst. The different activity levels of the catalysts clearly show the effects of impregnation strategy and Ce loading. CH₄ conversions over 1wt.% Pt-1wt.% Ce /ZrO₂ (cat2) and 1wt.% Pt-5wt.% Ce /ZrO₂ (cat3) prepared by coimpregnation method are close at lower temperatures, whereas at higher temperatures, the catalyst with 5 wt.% Ce loading shows an inferior activity profile. High CH₄ conversions, almost equal to the thermodynamic level, were obtained on 1wt.% Pt-1wt.% Ce /ZrO₂ catalyst prepared by coimpregnation method (cat2) over the whole temperature range investigated: the CH₄ conversion ranged from 20.1% 773 K to 83.6% at 973 K, which correspond to 95.7 % and 96.1% of the thermodynamically maximum attainable conversion levels, respectively.

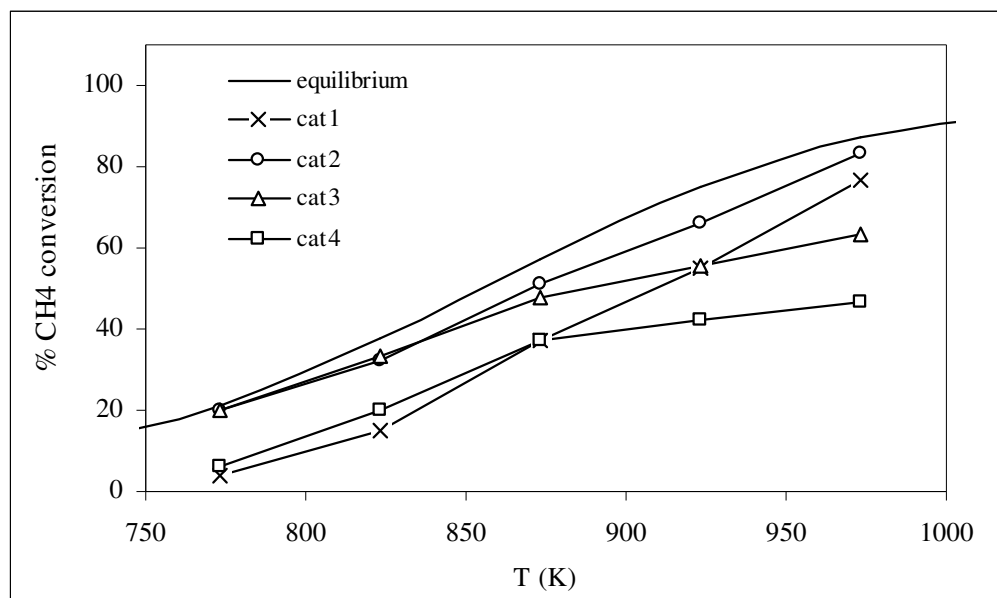


Figure 4.8 CH₄ conversion for the different catalysts in the CDRM as a function of the reaction temperature. Conversion values measured at the end of 4 h on stream.

CH₄ / CO₂ = 1/1. Space velocity = 15,600 mL/h.g-cat

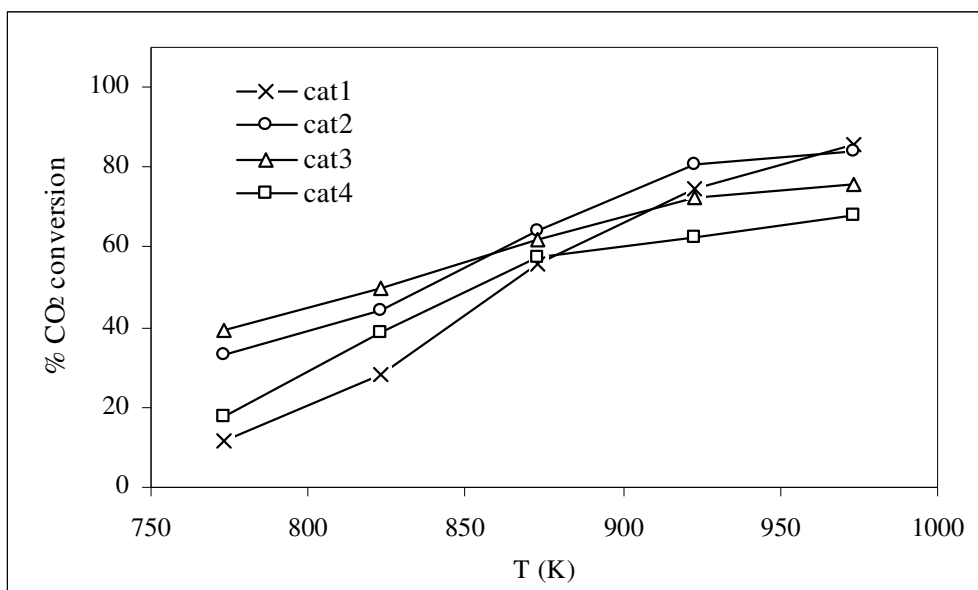


Figure 4.9. CO₂ conversion for the different catalysts in the CDRM as a function of the reaction temperature. Conversion values measured at the end of 4 h on stream.

CH₄ / CO₂ = 1/1. Space velocity = 15,600 mL/h.g-cat

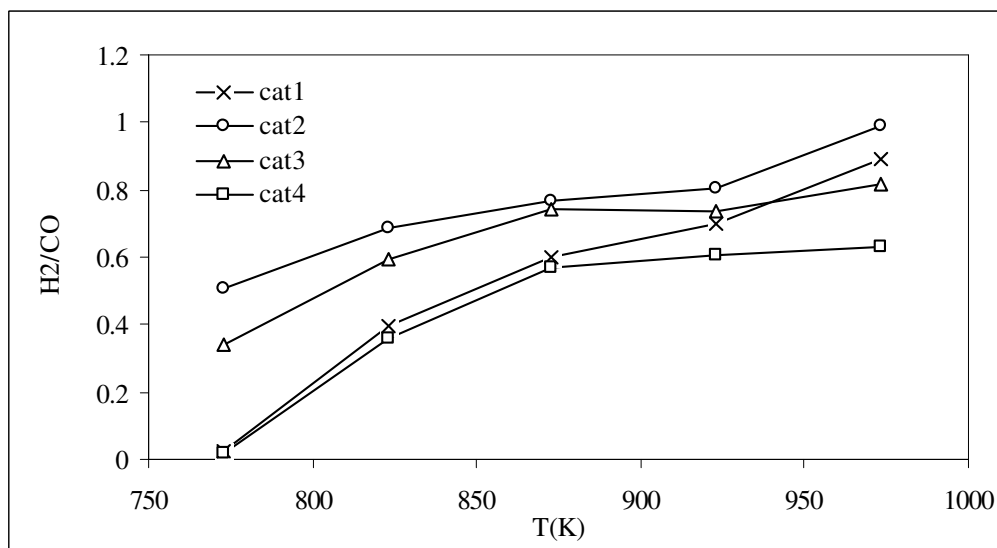


Figure 4.10. H₂/CO molar ratio in the CDRM product stream as a function of the reaction temperature. Conversion values measured at the end of 4 h on stream.

CH₄/CO₂ = 1/1. Space velocity = 15,600 mL/h.g-cat

It is clear that the introduction of small amount of cerium (1 wt%) to Pt/ZrO₂ via coimpregnation method led to an increase in the activity, which may be related both to the increased dispersion of the Pt in low-loaded Ce samples (Tiernan and Finlayon, 1998) and coke gasification by ceria, since such addition of ceria results in an increase in the oxygen transfer ability of the support (Damyanova and Bueno, 2003; Holmgren and Andersson, 1998). As mentioned in the literature (Stagg-Williams *et al.*, 2000; Slagtern *et al.*, 1997; Zhang *et al.*, 1996; Bitter *et al.*, 1997), during CDRM on monometallic Pt/ZrO₂, (i) CH₄ decomposes on Pt forming carbon and hydrogen, (ii) hydrogen partially reduce the support in the metal periphery, (iii) CO₂ dissociates on ZrO₂ support near the metal particle forming CO and oxygen, (iv) oxygen formed on support is transferred to Pt and cleans it from coke and (v) the dissociated oxygen reoxidize the support. As can be easily understood, if oxygen transfer rate from the support to the metal is less than carbon formation rate on Pt, catalyst deactivates. In our case, in addition to O supplied to Pt from ZrO₂, the presence of Ce⁺³ on the surface creates an additional storage capacity for oxygen coming from ZrO₂ support; CeO_x goes through continuous reduction/oxidation cycle during the reaction producing mobile surface oxygen, and enhance the oxygen transfer to Pt, which makes the metal and catalysts more resistant to carbon deposition.

It is noteworthy from Figures 4.8-4.10 that addition of 1 wt. % Ce to the Pt/ZrO₂ catalyst via coimpregnation method led to a superior catalytic performance, while the 1 wt. % Pt-1 wt. % Ce /ZrO₂ catalyst prepared by sequential impregnation (cat4) displays the lowest CH₄ and CO₂ conversions as well as the lowest H₂/CO molar ratios over the whole temperature range. Throughout sequential impregnation process, impregnation of Ce precursor onto the support was followed by high temperature heat treatment in a muffle furnace at 773 K, which resulted in formation of fixed Ce sites on the support and then the Pt precursor was added. Probably, this has caused decreased metal-metal interaction during preparation, which may be an explanation for lower activity levels for the whole temperature range. On the other hand, coimpregnation of Pt and Ce precursors together onto the ZrO₂ surface and subsequent high temperature thermal treatment (calcination and reduction at 773 K) led to strong and extensive Pt-Ce surface interaction, which produced the formation of Ce⁺³ sites. Increased number of oxygen vacancies, which act as oxygen buffer when going through Ce⁺⁴/Ce⁺³ redox cycle, led to cleaning of surface from deposited carbon, produced on Pt by C-H bond breakage during reaction. The XPS

analysis clearly showed that the intensive interaction between Pt and Ce for coimpregnated sample, starting from their precursor states till the metallic states during calcination and reduction, led to a higher amount of Ce^{+3} while suppressing the amount of Pt^0 . As previously mentioned, higher amount of oxidized Pt and simultaneously reduced Ce in cat 2 indicates net electron transfer from Pt to Ce due to the existence of strong and extensive Pt-Ce interaction during coimpregnation of Pt and Ce precursors during high temperature thermal treatments, calcination and reduction at 773 K. This results in higher CDRM activity of coimpregnated sample, which stems from enhanced oxygen transfer from Ce to Pt. Thus, Pt sites of coimpregnated sample has higher rate of oxygen transfer from Ce compared to carbon formation rate on them during the reaction, and have a higher DR activity.

This phenomenon could be also strengthened by the higher dispersion of Pt on the surface of the catalyst, which leads to an increase in the metal-support interface area, favoring the removal of carbon from metal and the increase in catalytic activity. Tiernan and Finlayson (1998) have reported that the presence of Ce^{+3} sites enhance the dispersion of Pt. The results of SEM-EDX studies imply that 1 wt. % Ce to the Pt/ ZrO_2 catalyst via coimpregnation method (cat2) has higher dispersion and small particle sizes of Pt compared to 1 wt. % Pt-1 wt. % Ce / ZrO_2 catalyst prepared by sequential impregnation (cat4). To sum up, we can conclude that coimpregnation of Pt and Ce together onto ZrO_2 surface and subsequent high temperature thermal treatment (calcination and reduction at 773 K) have led to strong and extensive Pt-Ce surface interaction, which resulted in the formation of Ce^{+3} sites and that the presence of Ce^{+3} sites enhanced the dispersion of Pt.

On the other hand; increasing the loading of Ce from 1 to 5 wt. % resulted in a decrease in the activity of the catalyst at high temperatures, which may be explained by decreased Pt dispersion. According to the work of Tiernan and Finlayson (1998), the addition of cerium, particularly at higher levels, results in decreased Pt dispersion. Another reason for the deteriorated activities may be the sintering and encapsulation of Pt particles by high amounts of bulk cerium particles, which lead to the decrease of chemisorption sites on the metal surface and interfacial areas.

Additionally, although CH_4 and CO_2 were present in the feed in a 1:1 ratio, CO_2 conversion levels have always been found to be higher than the CH_4 conversions, which is due to the reverse water-gas shift (RWGS) reaction [Eq. (2.11)] occurring simultaneously with CDRM. This reaction consumes part of the H_2 produced by dry reforming. This also clarifies the observation that the attained H_2/CO ratio values lower than unity, but tend to 1 at higher temperatures due to dominated DR activity, as shown in Figure 4.10. The comparison of CO_2 and CH_4 conversion levels of catalyst clearly shows that the RWGS reaction activity was suppressed when 1 wt. % Pt-1 wt. % Ce / ZrO_2 coimpregnated catalyst (cat2) was used.

4.1.2.2. Effect of Time-on-Stream (TOS). TOS activity tests were performed at 973 K at fixed space velocity with CH_4 : CO_2 ratio of 1:1 in the feed (where the highest conversions were obtained) for all four samples for 4 h of TOS. Figures 4.11-4.13 show the CH_4 and CO_2 conversions and the H_2/CO molar ratio in the product stream as a function of the reaction time, respectively. At the end of 4th hour of TOS, the unpromoted Pt/ ZrO_2 catalyst lost 5.5 % of its initial CH_4 activity whereas both the Ce- promoted catalysts prepared by coimpregnation method (cat2 and cat3) only lost 4% of their CH_4 activity. This shows the beneficial effect of Ce addition on the overall stability. Addition of cerium improved the amount of surface oxygen through reduction/oxidation cycle of CeO_x and the reducibility of the oxide support; this combined effect enhances the long-term activity and stability of the catalyst. As explained in previous section, coimpregnated sample has higher oxygen transfer from CeO_x sites and thus, they do not suffer from activity loss due to carbon deposition. The oxygen vacancies at the metal–oxide interface of reduced ceria, leading to high oxygen storage capacity, suppresses coke formation. The higher amount of mobile surface oxygen results in an enhanced capability to clean the carbon that would normally accumulate on the metal during the decomposition of CH_4 . This cleaning ability was also reflected on the total amount of carbon deposits observed by TPO. Moreover, a higher degree of reduction resulted in an increase in the number of oxygen vacancies formed near the metal particle and a subsequent increase in the ability to dissociate CO_2 . For the 1 wt.%Ce-doped Pt/ ZrO_2 , the increase in the dissociation ability and subsequent cleaning capacity resulted in a catalyst with enhanced activity and stability for the CO_2 reforming reaction. However, increasing the loading of Ce from 1 wt.% to 5 wt.% did not have a significant improvement on the stability for the DR reaction.

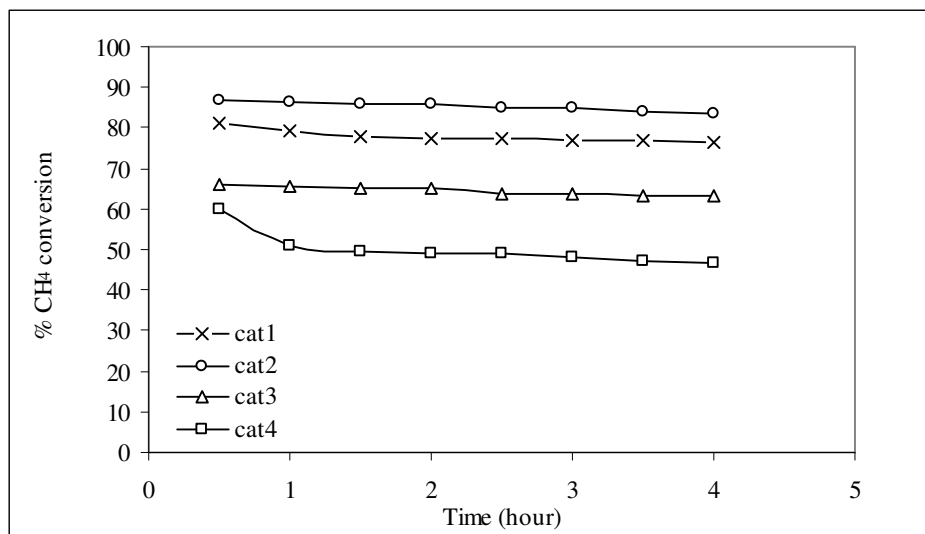


Figure 4.11. CH_4 conversions for the different catalysts in the dry reforming as a function of reaction time. Reaction Temperature = 973 K. $\text{CH}_4 / \text{CO}_2 = 1/1$.
Space velocity = 15,600 mL/h.g-cat

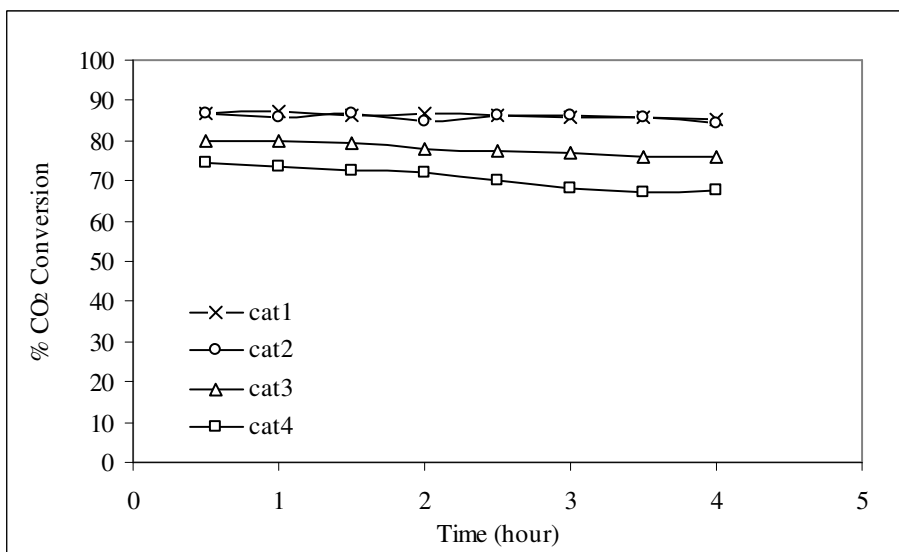


Figure 4.12. CO_2 conversions for the different catalysts in the dry reforming as a function of reaction time. Reaction Temperature = 973 K. $\text{CH}_4 / \text{CO}_2 = 1/1$.
Space velocity = 15,600 mL/h.g-cat

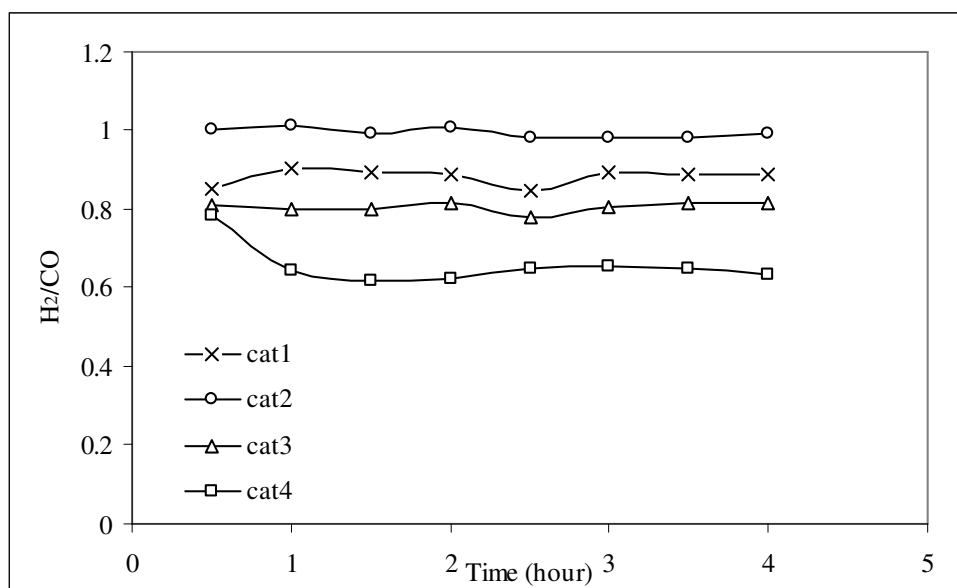


Figure 4.13. H₂/CO molar ratio values for the different catalysts in the dry reforming as a function of reaction time. Reaction Temperature = 973 K. CH₄ / CO₂ = 1/1.

Space velocity = 15,600 mL/h.g-cat

The 1 wt.% Pt-1 wt.% Ce /ZrO₂ catalyst prepared by sequential impregnation (cat4) showed lower activity compared to other samples and exhibited highly linear deactivation during the first 30 min on-stream, due to the fast deposition of the inactive carbon, as observed in TPO experiments. The CH₄ activity leveled off to stable values with ca. 22 % loss at the end of 4 hours. In addition, cat4 was the only catalyst that the conversion of CO₂ conversion decreased continuously by almost 9% during the reaction period whereas for all other catalysts CO₂ conversion was constant about 85 % over the 4 h of reaction. Moreover, 1wt.%Pt-1wt.%Ce/ZrO₂ catalyst prepared by coimpregnation method exhibited tremendous stability, indicating the advantageous effect of the coimpregnation method on the stability of the catalysts.

In our case, the deactivation of the 1 wt.% Pt-1 wt.% Ce /ZrO₂ catalyst prepared by sequential impregnation (cat4) would be related to the limited interaction between Pt-Ce precursors during sequential impregnation, which have created insufficient number of oxygen vacant Ce⁺³ sites, as explained in the above sections. Probably, surface oxygen species produced during the CO₂ activation process on the support- or on the metal-support

boundary- were not enough to oxidize all carbonaceous species formed on the metal sites; thus, due to coke deposition led by insufficient rate of cleaning inhibited the reaction. Parallel to our explanation, many groups have mentioned that the balance between the rate of decomposition and the rate of cleaning determines the overall stability of the catalyst (Stagg-Williams *et al.*, 2000; Slagtern *et al.*, 1997; Zhang *et al.*, 1996; Bitter *et al.*, 1997).

4.1.2.3. Activation Energies. Apparent activation energies were also calculated based on the consumption rates of CH₄ and CO₂ as well as for the production of CO and H₂ (Table 4.3), obtained from Arrhenius plots such as those in Figure 4.14, for CO production. It is remarkable that the activation barrier for CH₄ consumption, 22.0-8.6 kcal/mol, is higher than that for CO₂ consumption, 15.2-5.1 kcal/mol, in agreement with reported values in literature (Souza *et al.*, 2001; Bradford and Vannice, 1999). Also, the apparent activation energies for H₂ production, 22.1-12.5 kcal/mol, are greater than those calculated for the CO formation, 17.7-6.5 kcal/mol, which is probably led by the occurrence of RWGS consuming H₂ to produce additional CO.

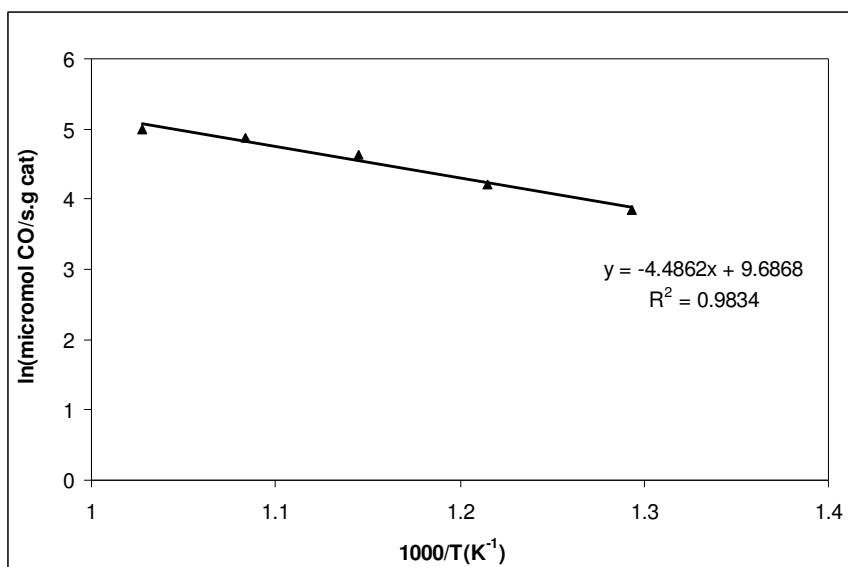


Figure 4.14. Arrhenius plots for CO production over temperatures ranging between 773 and 973 K. Catalyst: 1%Pt-1%Ce/ZrO₂ (coimp.). Reaction conditions: CH₄ / CO₂ = 1.

Space velocity = 15,600 mL/h.g-cat

Table 4.3. Catalyst activity at 973 K and apparent activation energies (E_{app})

Catalyst	Conversion (%)		Activity ($\mu\text{mol/s.g cat}$)		E_{app} (kcal/mol)			
	CH ₄	CO ₂	CO	H ₂	CH ₄	CO ₂	CO	H ₂
cat1	76.5	85.5	143.7	127.7	22.0	15.2	17.7	22.1
cat2	83.6	84.3	148.9	147.6	10.8	7.5	8.9	13.4
cat3	63.3	76.0	123.4	100.8	8.6	5.1	6.5	12.5
cat4	46.7	67.7	101.5	64.2	14.8	9.6	11.4	12.6

4.1.2.4. Effect of CH₄ /CO₂ Ratio in the Feed. A high CH₄/CO₂ feed ratio (>1.0) is considered as a severe condition for CO₂ reforming of methane. The stoichiometry of CDRM reaction is 1 to 1 for CO₂ and CH₄. When the ratio is greater than 1.0, methane becomes excess and the carbon formed upon its decomposition on Pt may not find enough mobile oxygen to be cleaned out; the produced carbon, via the methane decomposition reaction [Eq. (4)], will deposit on the surface of the catalyst, and result in deactivation of the catalyst (Yang and Papp, 2006)

Aiming to understand the performance characteristics, i.e. activity and selectivity, of the catalysts at higher CH₄/CO₂ feed ratios, CH₄:CO₂ ratio was increased to 2:1 at 973 K (Figures 4.15 and 4.16). Under these severe conditions, both reactants for each catalyst demonstrated activity rates in different extents throughout the whole time-on stream test. At the very beginning of the reaction (t = 30 min), the conversion of CH₄ and CO₂ for 1 wt.% Pt-1 wt.% Ce /ZrO₂ catalyst prepared by coimpregnation method (cat2) was 59 % and 100 %, respectively, whereas at the end of the 4h, the conversions decreased to 40 % and 68 %, correspondingly. However, it is seen that the activities of the samples with 5 % Ce loading (cat3) leveled off to stable values, which is about 40 % CH₄ conversion, with approximately 10 % loss of CH₄ activity at the end of 4 h of reaction. Unlike the results at CH₄/CO₂ = 1.0, it is observed that 1 wt.% Pt-5 wt.% Ce /ZrO₂ catalyst prepared by coimpregnation method (cat3) displayed the most favorable stability profile due to its relatively low conversion level at the beginning of the reaction. Addition of higher amount of ceria resulted in an increase in the oxygen storage capacity of the support, as has been

shown for different CeO₂-containing systems (Damyanova and Bueno, 2003). The cleaning of coke formed becomes more important than the original CDRM activity for cat3 when the reaction condition is severe, like CH₄: CO₂ = 2:1 case. Probably, (i) the support near the metal particles in 1 wt.% Pt-5 wt.% Ce /ZrO₂ catalyst (cat3), is sufficiently reduced, which has generated increased of the number of oxygen vacancies and resulting in the dissociation of CO₂, that provide the oxygen for cleaning of Pt from coke, (ii) the cerium on the surface goes to a reduction/oxidation cycle during the reaction producing surface oxygen, which can create mobile oxygen and enhance the oxygen transfer to Pt. This result is also supported with the lower activation energy of 1 wt.% Pt-5 wt.% Ce /ZrO₂ catalyst prepared by coimpregnation method (cat3) for CO₂ consumption, which may explain the high ability of cat3 to dissociatively adsorb CO₂. Likewise, insignificant amount of coke deposition detected as an outcome of TPO tests after the reaction also validate the relatively stable behavior of cat3 under high CH₄/CO₂ feed ratio.

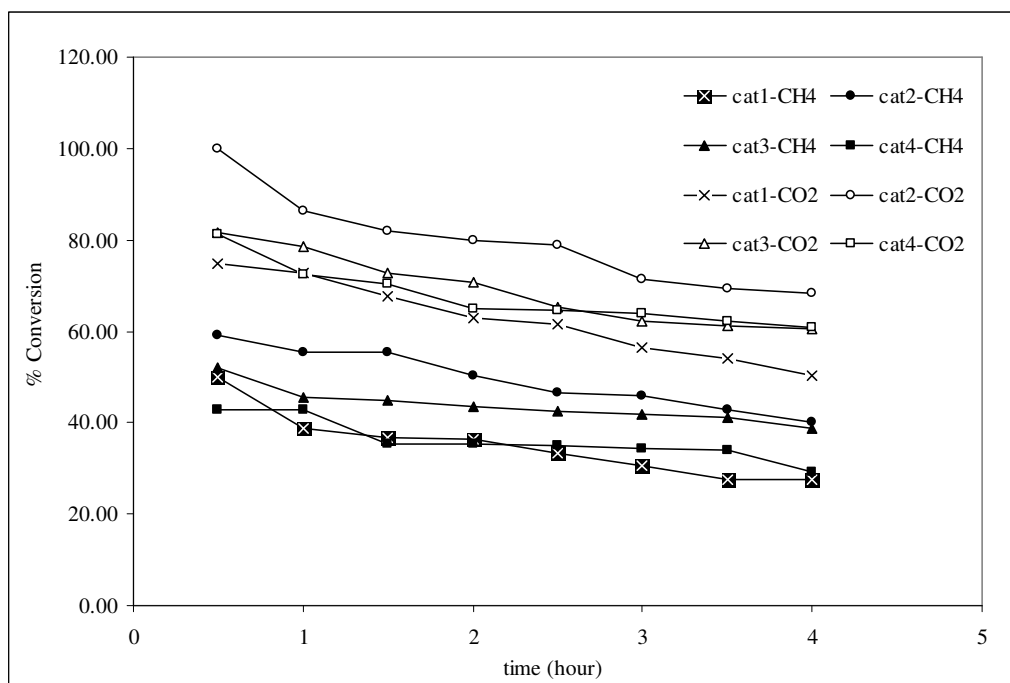


Figure 4.15. CH₄ & CO₂ conversions for the different catalysts in the dry reforming as a function of reaction time. Reaction Temperature = 973 K. CH₄ / CO₂ = 2/1.

Space velocity = 15,600 mL/h.g-cat

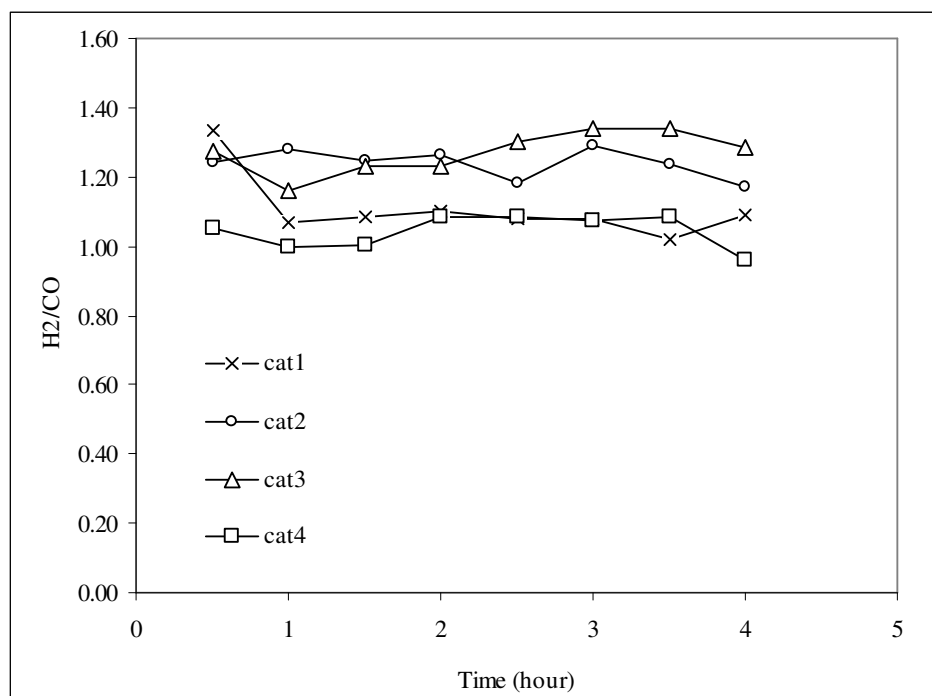


Figure 4.16. H₂/CO molar ratio values for the different catalysts in the dry reforming as a function of reaction time. Reaction Temperature = 973 K. CH₄ / CO₂ = 2/1.

Space velocity = 15,600 mL/h.g-cat

Moreover, for each catalyst, H₂/CO ratio ranged between 1.00-1.35, higher than the stoichiometric ratio of 1.0 and, which may have resulted from the decomposition of CH₄. The higher amount of supplied CH₄ increased the concentration of deposited carbonaceous species, formed by CH₄ decomposition [Eq. (2.7)].

4.1.3. Summary

Dry reforming of methane has been studied over Pt/ZrO₂ catalysts promoted with Ce using different impregnation strategies and cerium amounts. The following conclusions can be drawn from data obtained under atmospheric pressure at various temperatures, times on stream and feed ratios.

- Use of cerium was found to be potentially beneficial for CO₂ reforming of methane activity of Pt/ZrO₂. The effects of the Ce on catalyst activity depended on the cerium loading used and impregnation strategy.
- Introduction of 1 wt.% Ce to the Pt/ZrO₂ catalyst via coimpregnation method led to superior catalytic activities and stabilities. The catalyst displayed a significant improvement in the H₂/CO ratio, ie. H₂/CO ratio tends to unity at high temperatures.
- Coimpregnation of Pt and Ce together onto ZrO₂ surface and subsequent high temperature thermal treatment (calcination and reduction at 773 K) have led to strong and extensive Pt-Ce surface interaction, which produced the formation of Ce⁺³ sites and that the presence of Ce⁺³ sites enhanced the dispersion of Pt.
- Increasing the loading of Ce from 1 wt.% to 5 wt.% resulted in a decrease in the catalytic activity of catalysts at high temperature.
- Under severe reaction conditions, like CH₄: CO₂ = 2:1 case, it is observed that 1 wt.% Pt-5 wt.% Ce /ZrO₂ catalyst prepared by coimpregnation method (cat3) displayed the most favorable stability profile.

4.2. Methane Reforming Combined with SR and POX over Pt-Ni/ δ -Al₂O₃ Catalysts

In a previous study that had been carried out in our laboratory, oxidative steam reforming of propane was tested over different Pt-Ni/ δ -Al₂O₃ bimetallic catalysts and it was found out that the performance of these catalysts strongly depended on the metal loadings and Ni/Pt ratios. As the performance of Pt-Ni bimetallic system supported over alumina for CDRM reaction has not been studied in detail in literature, we have decided to investigate the behavior of these catalysts under CDRM conditions.

A set of Pt-Ni bimetallic catalysts supported on δ -Al₂O₃ were designed and developed for carbon dioxide reforming of methane as the main reaction in order to determine an effective catalyst with optimum Pt/Ni metal composition assuring both high activity and stability. The catalyst samples have two levels of Pt, 0.2 wt. % and 0.3 wt. %,

and two levels of Ni, 10 wt.% and 15 wt.%, loadings. 0.3 wt.% Pt and 10 wt.% Ni monometallic samples were also prepared and tested in order to obtain reference basis for comparison of the performances of bimetallic and monometallic catalysts. Small amount of H₂O or O₂ was also added to the feed for having CDRM coupled with SR and POX in order to inhibit the rate of coke formation. The performances of reforming catalysts are evaluated based on activity, stability and selectivity (ie.H₂/CO ratios). All those criteria were observed during CDRM as well as combined CDRM-POX and CDRM-SR. The details of the experimental sets are given in Table 3.7. The amount of deposited carbon on the surface of the catalysts and the kind of carbonaceous deposits were determined by TGA/DTA and SEM measurements of used Pt-Ni/alumina catalysts. XPS analyses were also conducted on freshly reduced samples in order to see the effect of Pt/Ni ratio on the oxidation states of the metals as well as the support. X-ray diffraction (XRD) tests were conducted in order to determine the particle size of active metal component Ni.

4.2.1. Characterization Tests

The detailed micro-structural characterization of Pt-Ni system had been made before in previous studies from our laboratory (Çağlayan *et al.*, 2005). As the BET surface area of the δ -alumina support is ca. 80 m²/g, the support surface was almost fully covered by Ni layer, which was introduced first in the sequential impregnation procedure. The micro-characterization studies on the 15 wt% Ni loaded sample clearly showed Pt islands formed mostly on Ni layer and rarely on Al₂O₃ support; it is actually an expected result for Ni loadings higher than ca. 10 wt%. The characterization revealed that there is no alloy formation between Pt and Ni.

4.2.1.1. X-Ray Photoelectron Spectroscopy. Freshly reduced 0.2Pt-15Ni and 0.3Pt-10Ni samples were analyzed by XPS to determine whether Ni exists as metal or as in the form of oxide. Table 4.4 and Table 4.5 summarize binding energies (B.E.) and some other spectral characteristics, both from the literature and from the present work, for the Ni species. As the amount of Pt impregnated on our catalysts was very small, its phase could not be detected by XPS.

Table 4.4. Summary of XPS B.E. reported in the literature for Ni 2p_{3/2}

Sample	B.E. Ni 2p _{3/2} (eV)			References
	Main peak	Shoulder	Satellite	
Ni ⁰	852.3–853.1	-	858.8	Qin <i>et al.</i> (2007)
Ni ⁺²	853.9–854.9	855.8–856.8	861.7–862.1	Qin <i>et al.</i> (2007)

Figures 4.17 and 4.18 show the Ni 2p_{3/2} X-ray photoelectron spectra with shoulder and satellite peaks for 0.2Pt-15Ni and 0.3Pt-10Ni samples, respectively. In the XPS profile of 0.3Pt-10Ni sample, the main peak at 853.8 eV indicates the presence of Ni⁺² species, and the one centered at 851.3 eV corresponds to Ni⁰ species. For 0.2Pt-15Ni, there appeared to be a small electropositive shift in Ni 2p_{3/2} peak binding energies measured relative to 0.3Pt-10Ni suggesting that Ni may have been slightly more oxidized in this sample. Data in Table 4.5 also show that the relative intensity of Ni⁺² was 78 % for 0.2Pt-15Ni, whereas it was 60 % for 0.3Pt-10Ni. This is an indication that catalyst with the lowest Ni/Pt ratio molar (ca. 110), 0.3Pt-10Ni, led to relatively easy reduction of nickel oxide species.

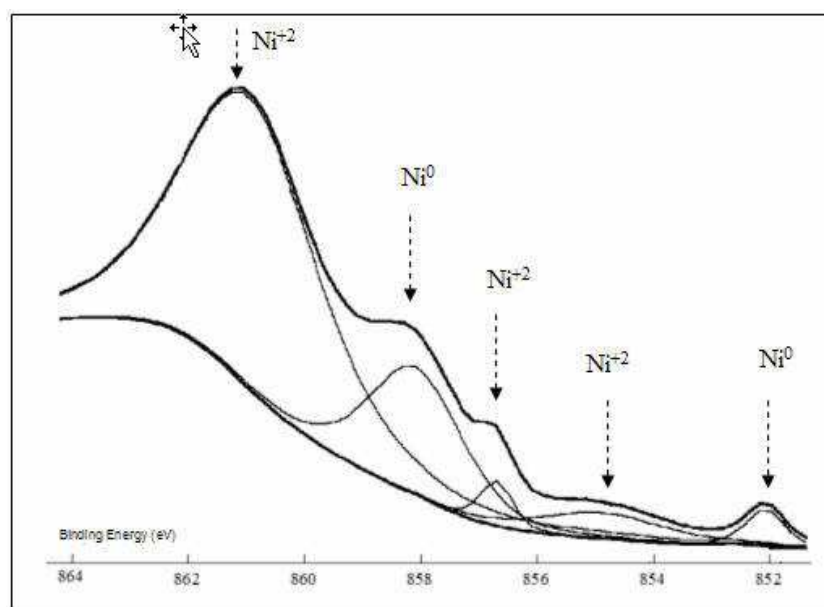
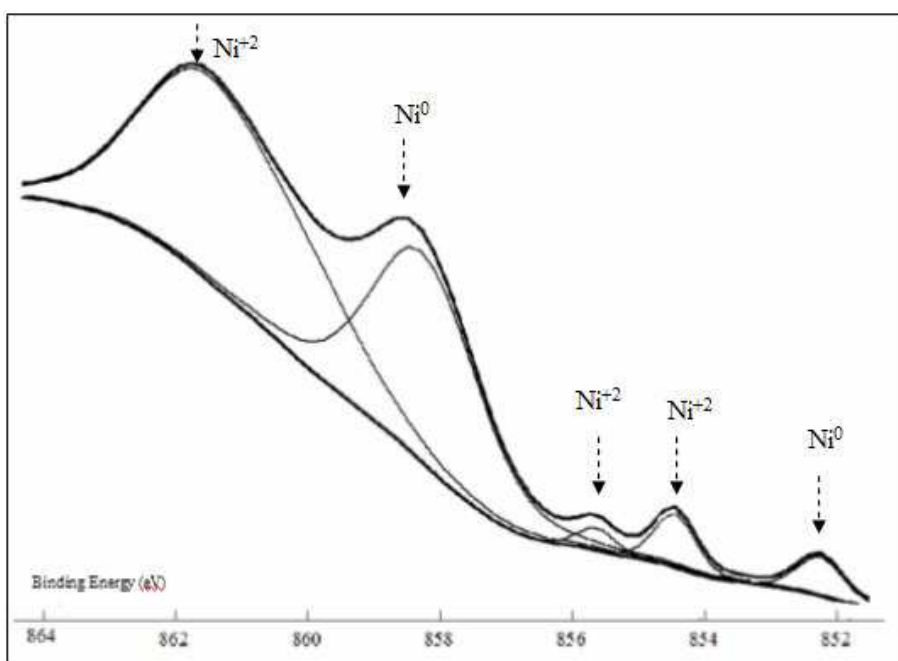
Figure 4.17. Ni 2p_{3/2} XPS spectra of 0.2Pt-15Ni sample

Table 4.5. Catalyst characterization by XPS

Catalyst	Species	B.E. Ni 2p _{3/2} (eV) (Main peak)	Relative Intensity (%)
0.2Pt-15Ni	Ni ⁰	852.1	22
	Ni ⁺²	854.9	78
0.3Pt-10Ni	Ni ⁰	851.3	40
	Ni ⁺²	853.8	60

Figure 4.18. Ni 2p_{3/2} XPS spectra of 0.3Pt-10Ni sample

4.2.1.2. X-Ray Diffraction. From XRD patterns, the particle size of Ni was determined by Scherrer equation and the results are shown in Table 4.6. It can be concluded that the size of nickel particles is a direct function of the Ni loading; the particle size increases with increasing Ni/Pt ratio. The size of Ni increases from 12.6 nm to 19.8 nm for samples with Ni/Pt ratio of 110 and 250, respectively. The higher amount of Pt in PtNi samples provokes

a decrease of the Ni size. This indicates that lower Ni/Pt ratio results in a higher dispersion of the active nickel component and in slightly smaller nano-sized nickel particles.

Moreover, in order to determine whether sintering of Ni particles occurred during reaction at elevated temperatures, the Ni particle size on the used samples after 4 h of CDRM reaction at 923 K was also calculated by XRD analysis. In Table 4.6, it is observed that particle size of metallic Ni did not change after reaction, which indicates that no sintering took place under the present conditions.

Table 4.6. Particle size determination by XRD

Sample	Pt wt. %	Ni wt. %	Ni/Pt ratio (molar)	D _{XRD} , Ni (nm)	D _{XRD} , Ni (nm) after reaction
0.3Pt-10Ni	0.3	10	110	12.6	12.8
0.2Pt-15Ni	0.2	15	250	19.8	20.1

4.2.2. Carbon Dioxide Reforming of Methane

The monometallic and bimetallic PtNi catalysts with different metal loadings were tested in CO₂ reforming of methane at 923 K with CH₄: CO₂ ratio of 1:1 for 4h of times-on-stream (TOS). Figures 4.19-4.21 show the CH₄ and CO₂ conversions and the H₂/CO molar ratio in the product stream as a function of the reaction time, respectively, for all Pt-Ni samples and monometallic Pt/Al₂O₃ and Ni/Al₂O₃ samples as well.

The different activity levels of the catalysts clearly show that the catalytic performances of bimetallic Pt-Ni samples strongly depended on the metal loading and Ni/Pt ratio. The conversions of both CH₄ and CO₂ increased with decreasing Ni/Pt ratio. Among all the catalysts, 0.3Pt-10Ni catalyst with the lowest Ni/Pt ratio (ca. 110) exhibited the highest catalytic activity and stability over the whole TOS data. Between the catalysts with the same Ni/Pt molar ratio of 165 (i.e. 0.3Pt-15Ni & 0.2Pt-10Ni), the one with the higher Pt loading, 0.3Pt-15Ni, displayed a better performance, pointing out the enhancing effect of addition of the noble metal. The monometallic Pt catalyst did not show activity at

all. CH₄ conversion over monometallic Ni and bimetallic 0.2Pt-15Ni with the highest Ni/Pt ratio (ca. 250) catalysts dramatically declined after 2 hours of reaction.

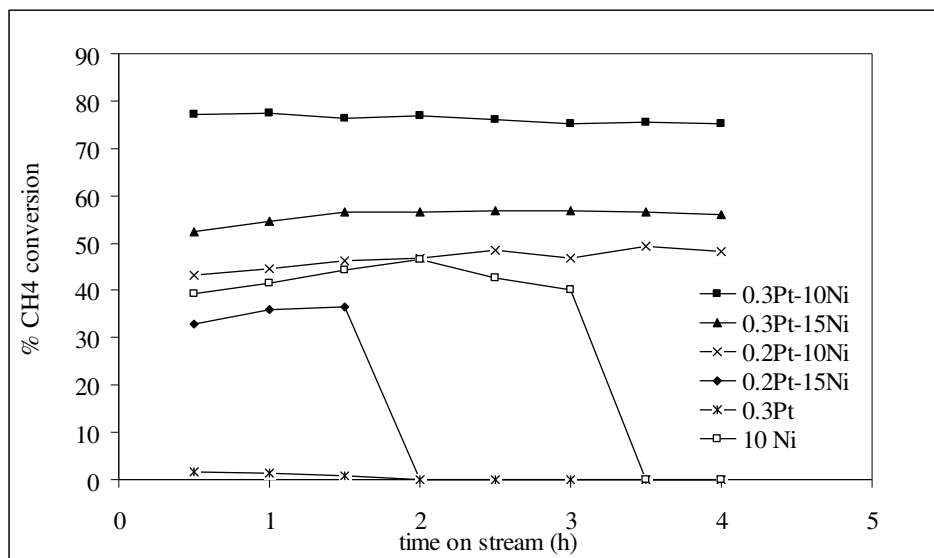


Figure 4.19. CH₄ conversions for the different catalysts in CDRM as a function of reaction time. $T_{\text{rxn}} = 923 \text{ K}$. $\text{CH}_4 / \text{CO}_2 = 1/1$. Space velocity = 15,600 mL/h.g-cat

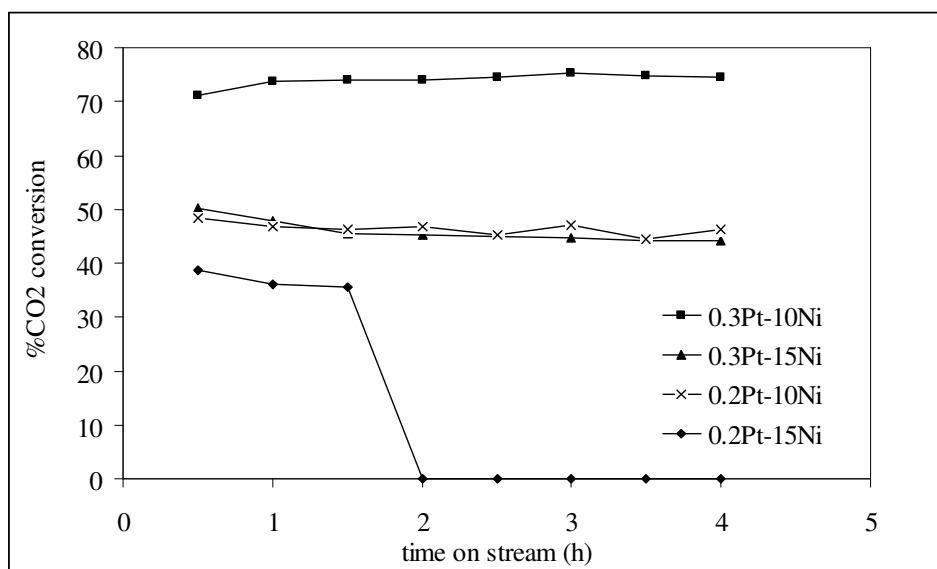


Figure 4.20. CO₂ conversions for the different catalysts in CDRM as a function of reaction time. $T_{\text{rxn}} = 923 \text{ K}$. $\text{CH}_4 / \text{CO}_2 = 1/1$. Space velocity = 15,600 mL/h.g-cat

There may be two main reasons for the rapid deactivation of Ni-based catalysts in DR reaction: (i) blocking of active sites by carbon deposits; (ii) gradual aggregation and sintering of Ni on the surface which may further lead to blockage of pores. There was no indication of catalyst sintering under the present conditions, which was supported by the fact that the particle size of metallic Ni on fresh and spent catalyst calculated from XRD did not change. Hence, deactivation was due to the coke formation problem. No further reaction could be carried out over monometallic Ni and bimetallic 0.2Pt-15Ni catalysts due to the accumulation of carbon whiskers making the catalyst surface inaccessible for reactants and blocking the catalyst bed, which increased pressure drop dramatically.

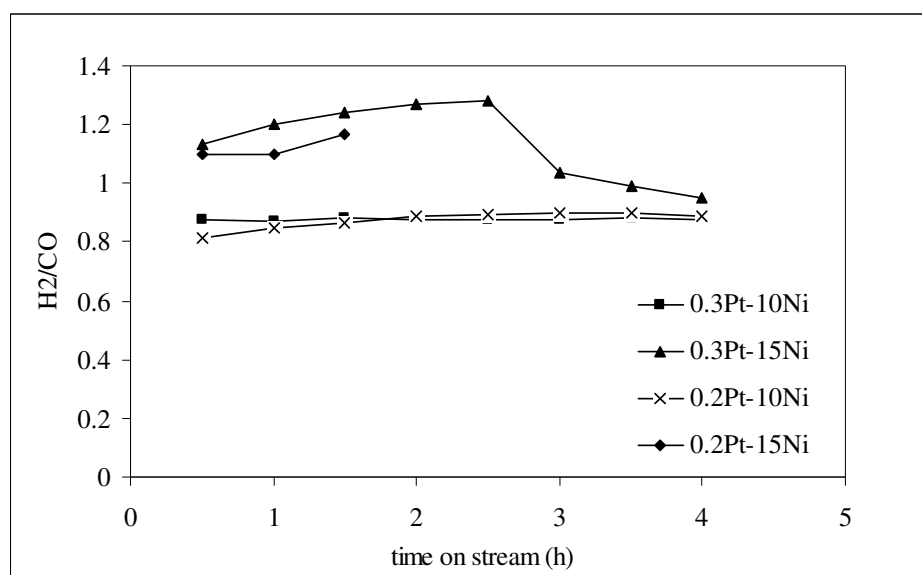


Figure 4.21. H₂/CO molar ratio values for the different catalysts in CDRM as a function of reaction time. T_{rxn} = 923 K CH₄ / CO₂ = 1/1. Space velocity = 15,600 mL/h.g-cat

On the basis of structural and surface characterization data, the improvement of catalytic activity and the stability of the 0.3Pt-10Ni catalyst can be contributed to the higher dispersion of the active nickel component and slightly smaller nano-sized nickel particles (Table 4.6). The stability of this sample can be related with the existence of small Ni metal particles on the surface caused by the “dilution” effect of Pt. Pawelec *et al.* (2007), who studied CDRM reaction over Pt-Ni bimetallic catalysts supported on ZSM-5, reported that the higher dispersion of nickel metal particles was due to the addition of small amount of Pt. The homogeneous surface distribution of nickel particles in the close

vicinity of Pt led to higher activity and stability for the bimetallic catalysts. According to recently published papers (Crisafulli *et al.*, 2002; Irusta *et al.*, 2002; Hou *et al.*, 2006), high coke resistance ability of Ni catalysts promoted with small amount of noble metal was attributed to the formation of noble metal–Ni particles or clusters with the surface mainly covered by Ni, which leads to increasing the dispersion of Ni and favors the formation of more reactive intermediate carbonaceous species. Moreover; 0.3Pt-10Ni sample led to relatively easy reduction of nickel oxide species (Table 4.5) and this also resulted in enhanced activity and stability profiles obtained from the sample.

4.2.3. Combined Partial Oxidation and Dry reforming

To investigate the effects of O₂ addition to the feed stream during CDRM reaction, studies were also performed on the combined CDRM and POX reactions with varying amounts of CO₂ and O₂ in the feed. These tests were conducted over 0.3Pt-10Ni sample (lowest Ni/Pt ratio), which displayed the best CDRM activity profile and over 0.2Pt-15Ni sample (highest Ni/Pt ratio), which exhibited the most inferior activity. The reactions were carried at 923 K and atmospheric pressure. The CH₄:CO₂:O₂ ratios studied were 2:1:0.25 and 1:1:0.5, corresponding to C:O ratios of 1.20 and 0.67, respectively. The results of CDRM tests, conducted without O₂ in the feed, was taken as a reference and compared with the CH₄:CO₂:O₂ = 1:1:0.5 combined CDRM and POX case. Figures 4.22, 4.23, 4.24 and 4.25 show the CH₄ conversion at 0.5, 2 and 4 h of time-on-stream tests for both 0.3Pt-10Ni & 0.2Pt-15Ni catalysts, respectively.

For 0.3Pt-10Ni sample, it was observed that CH₄ conversion is increasing with decreasing C/O ratio over the whole TOS data. Deactivation was observed in small extent at the highest C/O ratio of 1.20, with the conversion level decreased from 65.2% to 58.6 % after 4 h. For sole CDRM and CH₄:CO₂:O₂ = 1:1:0.5 cases, no deactivation was observed at all at the end of 4 h TOS.

However; deactivation was observed over 0.2Pt-15Ni sample, with the highest Ni/Pt ratio (ca. 250), during CDRM reaction; the CH₄ conversion decreased from approximately 33 to 0% after 2 h. But, with the addition of oxygen, the CH₄ and CO₂ conversion levels as

well as H_2/CO ratio remained unchanged. Moreover, addition of O_2 resulted in an increase in both CO_2 and CH_4 conversions for 0.2Pt-15Ni.

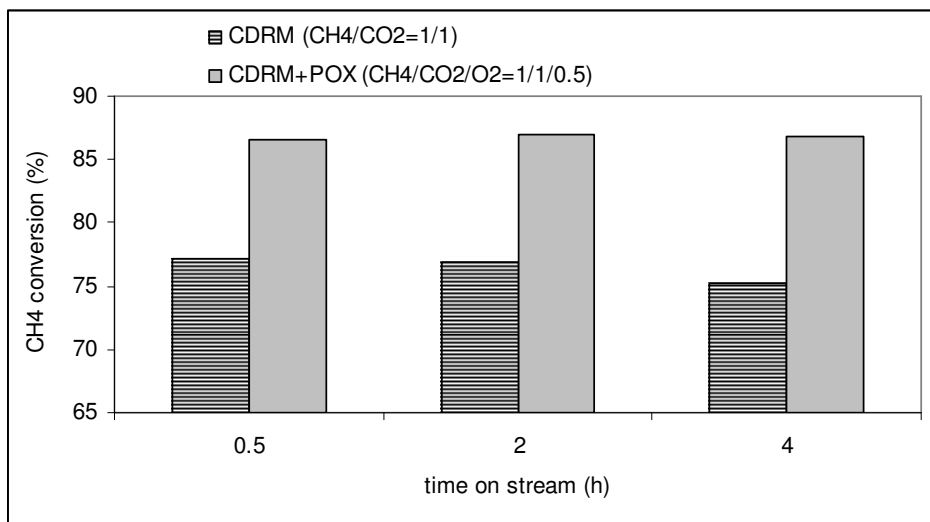


Figure 4.22. Effect of O_2 addition to CDRM at 923 K. Catalyst: 0.3Pt-10Ni

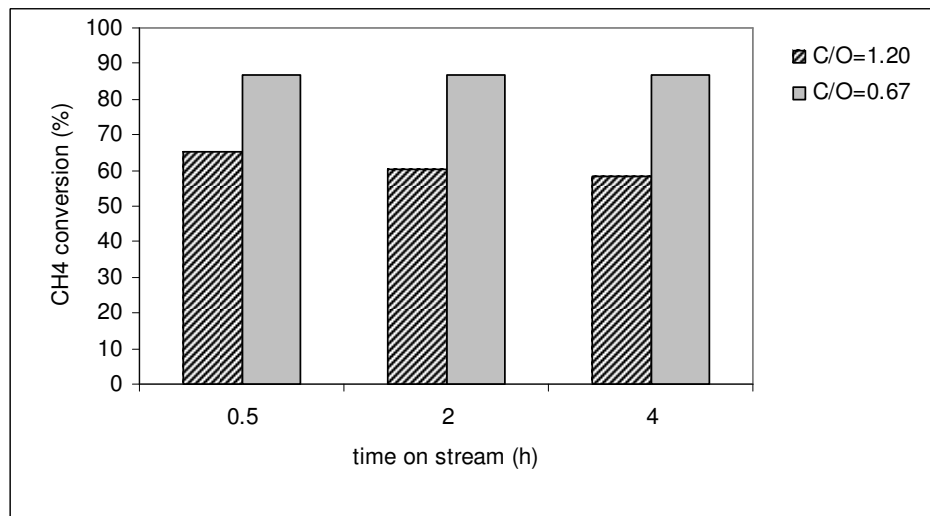


Figure 4.23. CH₄ conversion during the combined CDRM and POX at 923 K.
Catalyst: 0.3Pt-10Ni

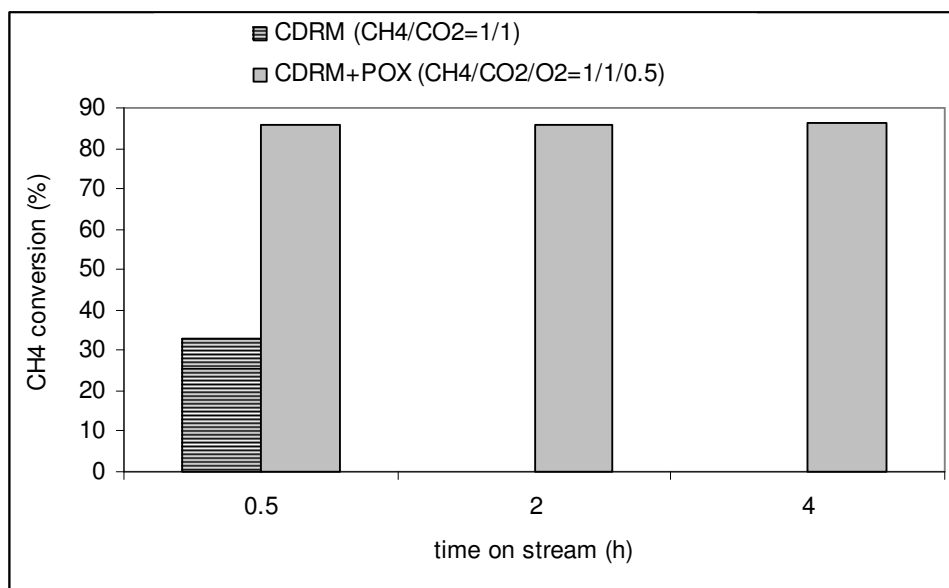


Figure 4.24. Effect of O₂ addition to CDRM at 923 K. Catalyst: 0.2Pt-15Ni

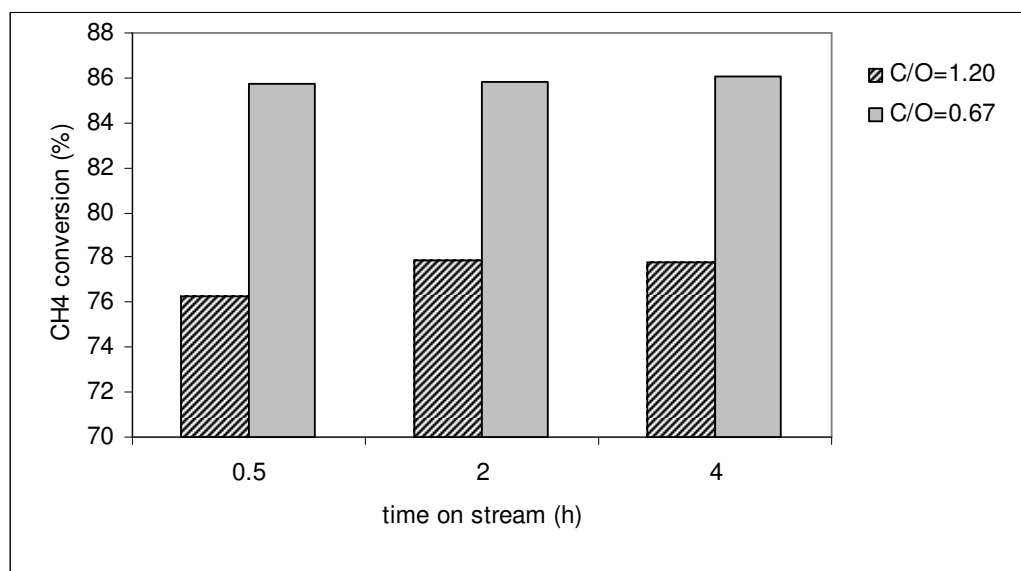


Figure 4.25. CH₄ conversion during the combined CDRM and POX at 923 K.
Catalyst: 0.2Pt-15Ni

Table 4.7 and 4.8 contain the corresponding H₂:CO product ratio and the CO₂ conversion, respectively, for the same experiments over both catalysts. The presence of oxygen in the feed resulted in a significant increase in the H₂:CO product ratio compared to CDRM, which is in accordance with the theoretical equilibrium values. The comparison of CO₂ conversion data obtained from reaction tests over 0.3Pt-10Ni catalyst for CDRM+POX with severe condition (C:O=1.20) and CDRM (C:O=1.0) cases show that its CO₂ use was limited when there is oxygen added to the feed. This is a clear indication that the catalyst utilizes oxygen coming from the oxygen present in the feed for CDRM-POX case; on the other hand, when oxygen is not present in the feed, it utilizes oxygen coming from CO₂. Most probably, high Pt content of the catalyst ease the utilization of oxygen coming from the feed. On the other hand, high level of CO₂ utilization for 0.2Pt-15Ni catalyst especially for severe conditions, C/O=1.2 case, pointed out to a rather limited use of oxygen coming from oxygen present in the feed. The results strongly hint the change in surfac mechanism in response to change in Pt load and Ni:Pt ratio of the catalysts.

Table 4.7. Effect of varying C/O ratio in the feed on the H₂/CO product ratio

Reaction	CH ₄ /CO ₂ /O ₂	C/O	H ₂ /CO (0.3Pt-10Ni)			H ₂ /CO (0.2Pt-15Ni)		
			0.5 h	2 h	4 h	0.5 h	2 h	4 h
CDRM+POX	2/1/0.25	1.20	1.33	1.33	1.35	1.32	1.31	1.30
CDRM	1/1/0	1.00	0.87	0.87	0.88	1.1	-	-
CDRM+POX	1/1/0.5	0.67	1.22	1.21	1.20	1.22	1.21	1.20

Table 4.8. Effect of varying C/O ratio in the feed on the CO₂ conversion

Reaction	CH ₄ /CO ₂ /O ₂	C/O	%CO ₂ conversion (0.3Pt-10Ni)			%CO ₂ conversion (0.2Pt-15Ni)		
			0.5 h	2 h	4 h	0.5 h	2 h	4 h
CDRM+POX	2/1/0.25	1.20	47	51	49	74	71	71.3
CDRM	1/1/0	1.00	71	74	75	38	-	-
CDRM+POX	1/1/0.5	0.67	54	50	49	49	48	45

4.2.4. Combined CO₂ and Steam Reforming of CH₄

Combined CO₂ and steam reforming of CH₄ were performed over all catalysts at 923 K with varying amounts of CO₂ and steam in the feed. The CH₄:CO₂:H₂O ratios studied were 1:1:1, and 2:1:1, corresponding to steam to carbon ratios (S/C) of 0.5 and 0.33, respectively.

Fig. 4.26 shows the effect of the addition of steam to the CO₂ reforming reaction mixture on the CH₄ conversion over all catalysts with S/C of 0.5. It was observed that steam addition caused an increase in CH₄ conversion to 80-90 per cent band for all four samples. The results showed that (i) steam addition eliminates the coke deposition problem, which was severe for especially CDRM over 0.2Pt-15Ni sample; (ii) combined CDRM-SR enhanced the activity for all catalyst samples, (iii) the enhancement of activity is more pronounced for the catalysts having low Pt loading level and those suffer from coke deposition due to their limited coke oxidation ability.

The product composition over the catalysts also varied with varying feed composition. The H₂:CO ratio found for CO₂ reforming at 923 K varied between 0.8-1.2 depending on the catalyst used (Figure 4.21) while that in the presence of steam it was around ca. 1.8 (Table 4.9). This effect on product composition was observed over all samples. It can therefore be concluded that it is possible to tailor the product composition (H₂/CO ratio) by varying the CO₂/H₂O ratio in the feed. The increase in the H₂/CO ratio is not surprising since SR reaction enhanced the H₂ production, and, additionally, the presence of steam eliminates the RWGS, which decreases H₂ production in CDRM case.

Table 4.9 summarizes the results of combined SR + CDRM with varying S/C ratio in terms of methane activity and H₂/CO ratio. Decreasing the S/C ratio to lower values by changing the amount of CH₄ in the feed resulted in severe coke deposition problem on 0.2Pt-15Ni sample due to accumulation of carbon whiskers leading to blocking the catalyst bed in a very short time. However, no activity loss was observed for 0.3Pt-10Ni sample at the end of four hours for any feed conditions employed. This again shows us the important effect of Ni/Pt ratio on the activity and stability of the catalyst in reforming reactions.

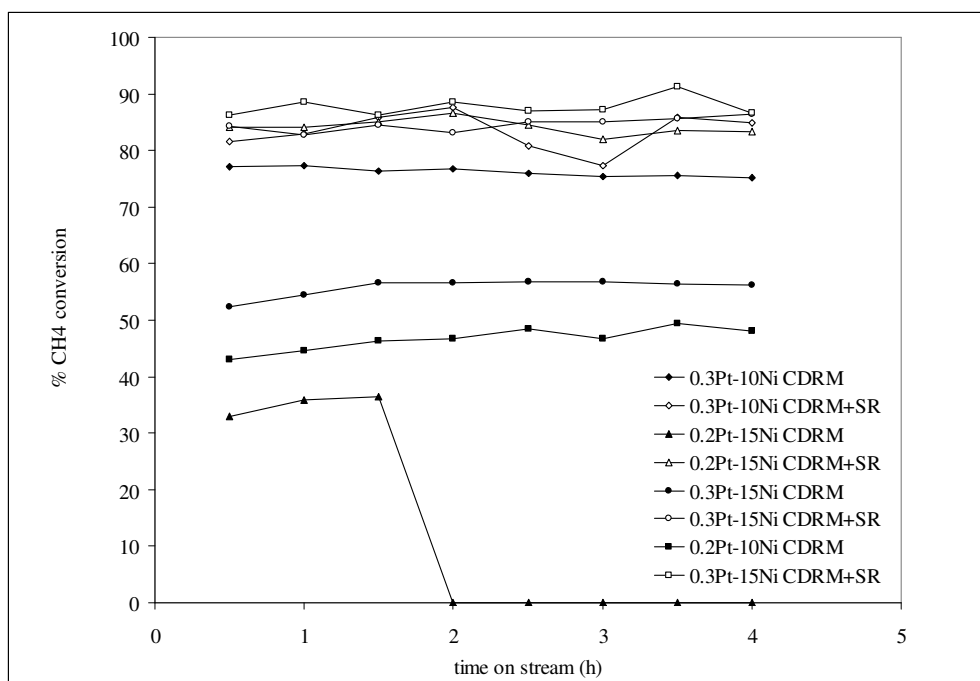


Fig. 4.26. CH₄ conversions for the different catalysts in combined CDRM + SR as a function of reaction time. Reaction Temperature = 923 K. CH₄ / CO₂ / H₂O = 1/1/1.

Table 4.9. Summary of combined CDRM + SR (T=923 K)

Catalyst	S/C	CH ₄ Reaction Rate ($\mu\text{mol/g.s}$)		H ₂ /CO	
		0.5 h	4 h	0.5 h	4 h
0.3Pt-10Ni	0.5	75.5	73.6	1.75	1.42
0.3Pt-10Ni	0.33	126.0	127.6	1.76	1.83
0.2Pt-15Ni	0.5	74.5	73.8	1.87	1.66
0.2Pt-15Ni	0.33	117.4	0	1.86	-
0.2Pt-10Ni	0.5	76.4	76.9	1.87	1.66
0.3Pt-15Ni	0.5	73.4	76.6	1.82	2.09

The results presented in Figures 4.22, 4.23 and 4.26, Tables 4.7 and 4.9 demonstrate that 0.3Pt-10Ni catalyst is capable of operating under a variety of feed conditions without significant deactivation. More importantly, the ability of the catalysts to generate synthesis gas ratios ranging from 0.87 to 1.83 provides flexibility in syngas generation and Fischer-Tropsch reactor. Depending on the downstream application and catalyst being employed, the H_2/CO ratio could be easily modified by varying the CO_2 , O_2 and H_2O content in the feed without significantly impacting catalyst stability. These results suggest that 0.3Pt-10Ni catalyst is very promising for synthesis gas production to be used in GTL technology.

4.2.5. Stability Test

Stability test for CDRM reaction was performed over 0.3Pt-10Ni sample at 923 K for 14 h with a feed ratio of $CH_4/CO_2 = 1/1$ (Figure 4.27). The most remarkable point about these data is that no deactivation has been observed during this long reaction period although coke deposition in filamentous form was observed in the SEM image (see Section 4.2.6.2).

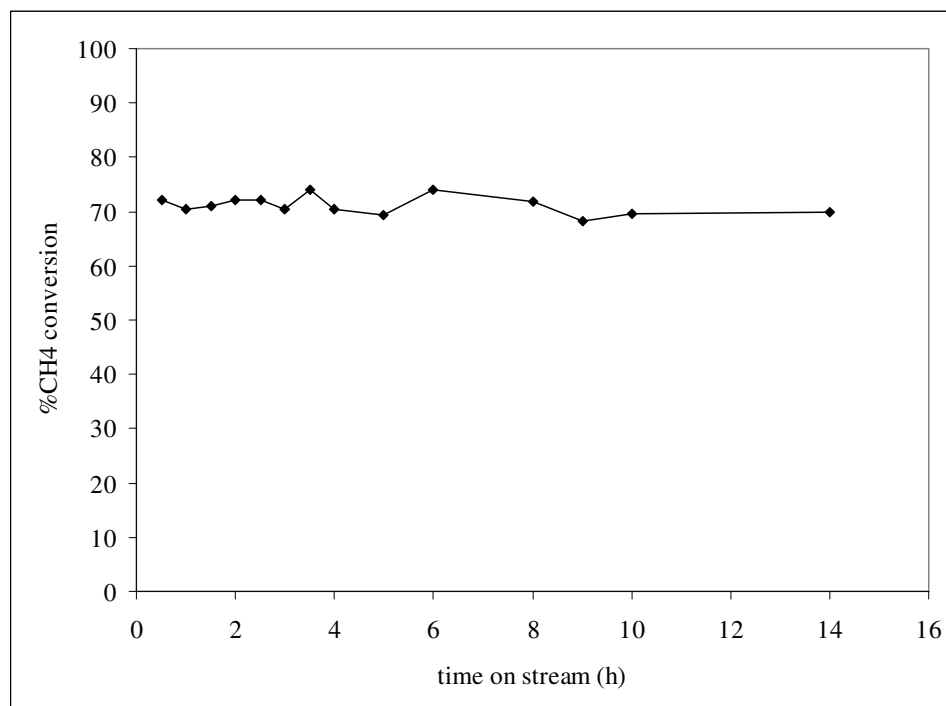


Fig. 4.27. Stability test for CO_2 reforming of methane. $T_{rxn} = 923$ K. $CH_4 / CO_2 = 1/1$.

The reason of this result is explained detail in the following sections through micro-structural and morphological characterization of deposited carbon. It should be mentioned that in a previous study (Wang and Lu, 1998), dynamics of coking process analysis indicated that coke on catalyst would generally reach equilibrium in ca. 2-5 h and the amount of carbon deposition would not increase further. Hence, this would explain the stable activity profile of 0.3Pt-20Ni for very long reaction periods.

4.2.6. Coke Deposition

There are two possible reasons for deactivation of Ni-based catalysts during CDRM: (i) Ni particles gradually aggregate and sinter on the surface of the support and/or in the alumina channels during CDRM process and (ii) deposited carbon blocks the active sites.

In the current study, the former possibility was eliminated based on the XRD results. According to the reported carbon deposition mechanism, the origin of inactive carbon during CDRM originates from methane decomposition [Eq. (2.7)] and from Boudard reaction [Eq. (2.8)], which are favorable under the conditions of CDRM. The amount of deposited carbon on the surface of the Pt-Ni catalysts as well as the type of carbonaceous deposits was studied by TGA/DTA and SEM/EDX.

4.2.6.1. TGA/DTA of Spent Catalysts. The amount of carbon deposition on selected PtNi catalysts used in CDRM reaction conducted at 923 K was investigated by means of TGA and DTA in an oxidative atmosphere, as shown in Figure 4.28. The percentage of the weight loss of the samples increases in the following order: 0.3Pt-10Ni < 0.2Pt-15Ni. It is clear that the largest weight loss takes place for the catalyst with the highest Ni/Pt ratio. These observations are also consistent with the results of TOS data in Figure 4.19.

It is evident that the weight loss shown by TG curves of the used catalysts is due to the burning of deposited carbon present on the catalyst. The contribution from metal oxidation is negligible during temperature-programmed oxidation. Therefore, the TGA/DTA results clearly show that a considerable amount of coke was deposited on the surface of the used catalysts, with the exception of the 0.3Pt-10Ni catalyst having the lowest Ni /Pt ratio. Most probably, the high resistance of this catalyst against carbon

deposition comes from the very high oxygen utilization activity and its very well dispersed Pt sites present all over the Ni-covered surface. On the other hand; as Ni/Pt ratio increases, coke deposition during reaction, which was led by their limited oxygen utilization ability for carbon removal, severely affects the catalyst activity and stability.

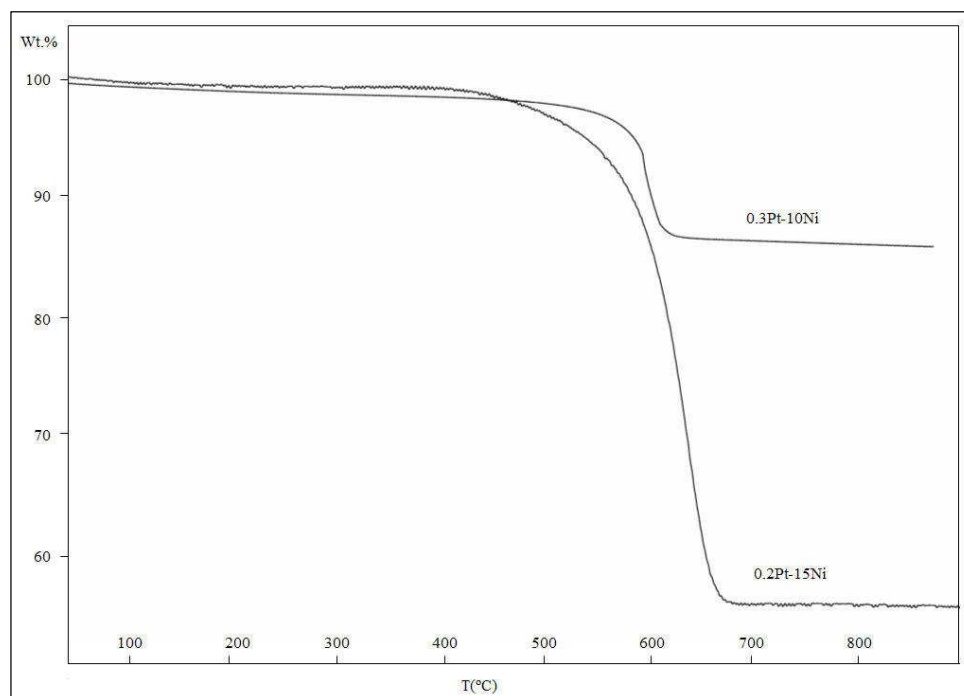


Figure 4.28. Temperature programmed oxidation (TPO) profiles of used catalysts after CDRM for 4 h TOS at 923 K

4.2.6.2. SEM/EDX of Spent Catalysts. It is very well known that the type and amount of carbon deposit are crucial factors that affect activity and performance stability of the catalysts. In order to get a deeper insight on the morphology and structure of the carbon deposits formed on the surface of used catalysts, 0.3Pt-10Ni and 0.2Pt-15Ni samples after CDRM for 4 h time on stream at 923 K were investigated by electron microscopy. Figures 4.29 and 4.30 clearly show filamentous carbon whiskers formed during reaction. It can be observed that the formed carbon nanofibers seem almost identical, which leads to the conclusion that the Ni/Pt ratio does not effect the morphology of the deposited carbon very much. Such morphology is typical of supported nickel catalysts, in which nickel crystallites serve as catalysts for the growth of carbon filaments. The growth of carbon filaments occurs on a metal surface where the active metal is carried on the top of the

carbon filament and, as a consequence, the catalytic activity can be kept with reaction time because the active metal is still exposed to the reactants. The deactivation appears only at very high coverage of the surface (Józwiak *et al.*, 2005; Wang and Lu, 1998; Pawelec *et al.*, 2007).

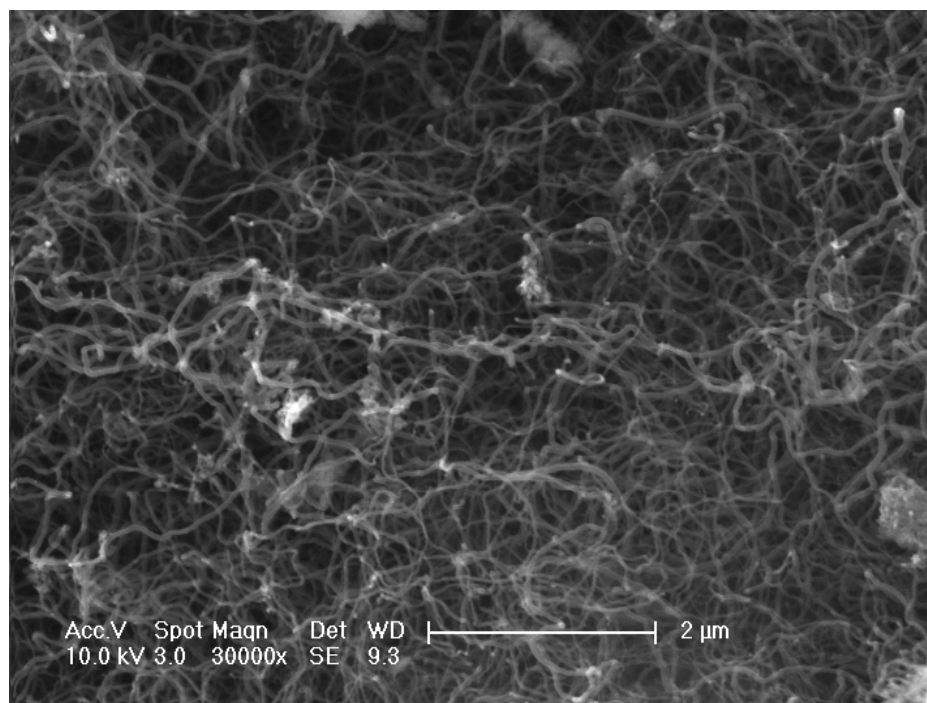


Figure 4.29. Morphology of carbon deposit in the 0.2Pt-15Ni catalyst after 4h of CDRM reaction at 923 K

EDX analysis was also performed in order to quantitatively determine the amount of carbon deposited on the catalyst surfaces. For all of the EDX quantification studies, at least four different clusters of the same catalyst sample, with similar cluster sizes, were chosen for comparison. Quantification values corresponding to the different clusters for a given catalyst type were typically found to be in good correlation with each other. According to the EDX analysis, the amount of coke formed on 0.2Pt-15Ni was around 85 % whereas it was around 50% on 0.3Pt-10Ni. Considering the similar types and amounts of filamentous carbon formed and drastically the higher EDX signal for 0.2Pt-15Ni sample, one can speculate that there is also formation of layered carbon clusters covering the surface as well. The result explains the quick deactivation of the 0.2Pt-15Ni sample. The activity test results as well as SEM/EDX tests together with the TGA/DTA analysis indicate that

almost all active sites of the 0.2Pt-15Ni catalyst are covered with carbon filaments which do not allow the transfer of reactants to the active sites.

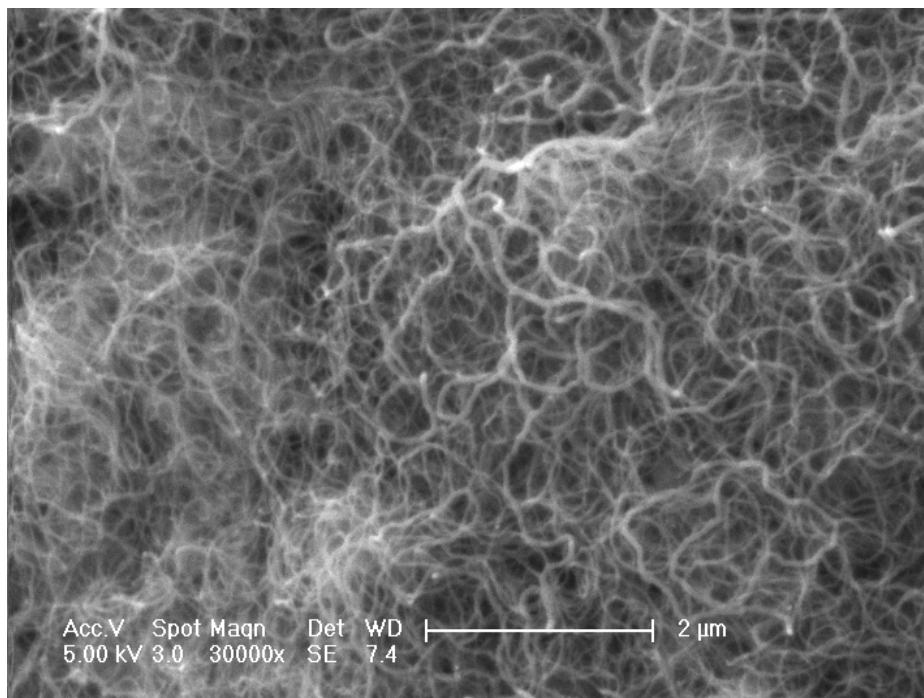


Figure 4.30. Morphology of carbon deposit in the 0.3Pt-10Ni catalyst after 4h of CDRM reaction at 923 K

SEM micrographs were also taken for samples after 4 h of combined POX and CDRM at 923 K with a feed containing C/O ratio of 1.20. The SEM micrographs (Figure 4.31) show that intermediate amount of filamentous carbon has deposited on the 0.3Pt-10Ni catalyst surface during reaction whereas the amount of carbon deposited on 0.2Pt-15Ni is considerably low even with this high and severe C/O ratio, which favors the formation of coke deposition. This finding explains the drastic increase in CH₄ conversion for 0.2Pt-15Ni sample when the reaction changes from CDRM, for which the activity leveled off to zero due to coke deposition, to combined CDRM-POX, for which the activity rose up to ca. 80 per cent.

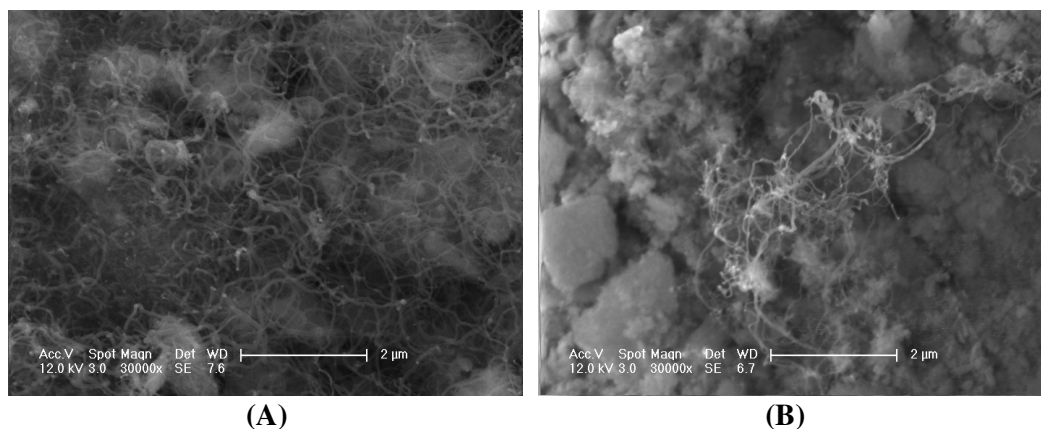


Figure 4.31. Morphology of carbon deposit after 4h of combined CDRM and POX reaction at 923 K with C/O = 1.20: (A) 0.3Pt-10Ni, (B) 0.2Pt-15Ni

4.2.7. Summary

The following conclusions can be drawn on the basis of the characterization and catalytic activity data:

- The different activity levels of the catalysts clearly show that the catalytic performances of bimetallic Pt-Ni samples strongly depended on the metal loading and Ni/Pt ratio. Among all the catalysts, 0.3Pt-10Ni catalyst with the lowest Ni/Pt ratio (ca. 110) exhibited the highest catalytic activity and stability over the whole TOS tests in CDRM reaction.
- The carbon formation on the surface of the catalysts depends on the size of nickel metal particles; the higher coke resistance is observed on smaller nickel particles due to the “dilution” effect of Pt that leads to a higher nickel dispersion.
- Easy reduction of nickel oxide species and a better dispersion of nickel metal particles favor the formation of a more reactive intermediate carbonaceous species, thus limiting the deactivation rate.

- The results from combined CDRM-POX strongly hint the change in surface mechanism in response to change in Pt load and Ni:Pt ratio of the catalysts.
- Combined CDRM-SR enhanced the activity for all catalyst samples. The enhancement of activity is more pronounced for the catalysts having low Pt loading level and those suffer from coke deposition due to their limited coke oxidation ability.
- 0.3Pt-10Ni catalyst is capable of operating under a variety of feed conditions without significant deactivation and this suggests that 0.3Pt-10Ni catalyst is very promising for synthesis gas production for GTL technology.

4.3. Kinetic Experiments over Pt-Ni/ δ -Al₂O₃ Catalysts

The performance (i.e. activity and stability profiles) differences of 0.2Pt-15Ni and 0.3Pt-10Ni catalysts in CDRM as well as their responses to the changes in reactant stream composition during CDRM, CDRM + POX and CDRM + SR tests indicate the mechanistic differences of the surface reaction over those catalysts. In the present part of the work, the kinetic behavior of the 0.2Pt-15Ni and 0.3Pt-10Ni catalysts in CDRM was investigated as a function of temperature and partial pressures of CH₄ and CO₂. The aim was to investigate the performance of these two catalysts further by means of kinetic measurements. The conclusions and detailed information provided by the characterization results from the previous section are combined with the present kinetic results to derive a plausible mechanistic scheme and a kinetic model of the reaction for each catalyst.

4.3.1. Determination of Temperature Region for Kinetic Tests

The dry reforming is generally accompanied by several side reactions, including CO disproportionation reaction, CO/H₂ reduction reaction, CO₂/H₂ methanation reaction and CO/H₂ methanation reaction as well as RWGS (Cui *et al.*, 2007):

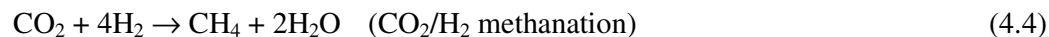
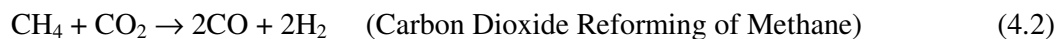


Figure 4.32 shows the variation of the thermodynamic equilibrium conversions with the temperature for the dry reforming reaction, CO disproportionation, CO/H₂ reduction, CO₂/H₂ methanation, and CO/H₂ methanation (Cui *et al.*, 2007). When the temperature is higher than 450°C, the CO/H₂ methanation becomes thermodynamically forbidden (curve d). CO disproportionation and CO/H₂ reduction also become thermodynamically forbidden above 550°C (curves b and c). The thermodynamic equilibrium conversions of CO₂ for the CO₂/H₂ methanation are lower than 2.6% above 550°C (curve e). However, the equilibrium conversions of CH₄ in the dry reforming are higher than 58% above 550°C (curve a). Therefore, when the reaction temperature is higher than 550°C, the influence of the four side reactions on the kinetic study of the dry reforming can be basically neglected (Cui *et al.*, 2007). The temperature of the kinetic study was kept at 600 °C in order to guarantee that dry reforming kinetics do not interfere with those of the side reactions.

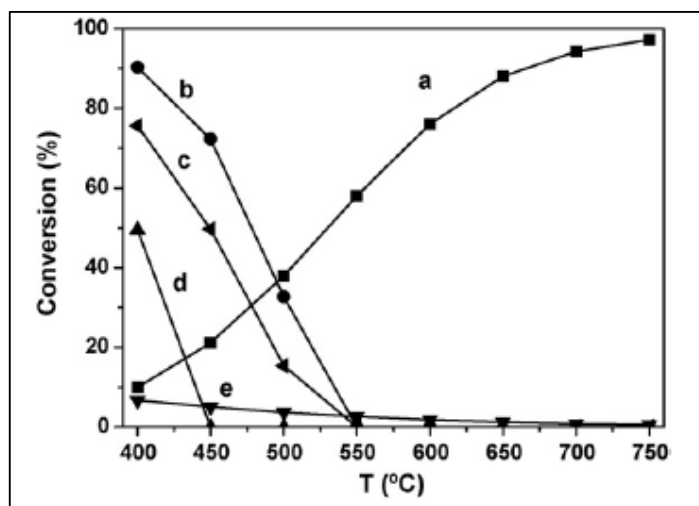


Figure 4.32. The variation of the equilibrium conversions with the reaction temperature for the dry reforming (a), CO disproportionation (b), CO/H₂ reduction (c), CO/H₂ methanation (d), and CO₂/H₂ methanation (e). (Cui *et al.*, 2007)

4.3.2. Kinetic Measurements

Kinetic experiments were performed under differential conditions at atmospheric pressure using 5 mg of catalyst. The reaction temperature was kept fixed at 873 K if not specified otherwise. The total feed flow rate was changed between 100-150 mL/min in order to obtain significantly lower conversion levels in the range of 5-25 per cent, which were far away from the corresponding thermodynamic equilibrium under those reaction conditions and guaranteeing that the CDRM reaction was controlled merely by kinetics.

The catalyst mass-based reaction rates in the kinetic measurements, $(-r_{CH_4})$, can be calculated from the conversion versus residence time (W_{cat} / F_{CH_4}) data as follows:

$$-r_{CH_4} = \frac{x_{CH_4} F_{CH_4}}{W_{cat}} \quad (4.9)$$

where x_{CH_4} is CH₄ conversion, F_{CH_4} is CH₄ flow rate in the feed in mL.min⁻¹ converted to mmol.s⁻¹, W_{cat} is catalyst weight in g and $(-r_{CH_4})$ is the reaction rate in mmol.g⁻¹.s⁻¹.

CH₄ consumption rates were obtained from intrinsic kinetic data in the initial rate region by using differential method of data analysis. The use of differential method of data analysis to determine reaction orders and specific reaction rates is one of the most established methods; in this method, a wide range of conversions can be obtained by varying the ratio of W/F_{CH_4} . In the kinetic tests, a series of experiments were carried out at different initial reactant concentrations and the initial rates were calculated by differentiating the data and extrapolating it to zero times.

4.3.2.1. Apparent Activation Energies. The apparent activation energies were calculated over a temperature range of 853–893 K, based on the consumption rates of CH₄ and CO₂ as well as on the production rates of CO and H₂. The experimental data were taken after 90 min. TOS to ensure stable performance of the catalyst. The Arrhenius plots, through which E_{app} are calculated, are given in Figure 4.33. The activation energies calculated from the slopes of these plots are shown in Table 4.10 and compared with similar data reported in the literature.

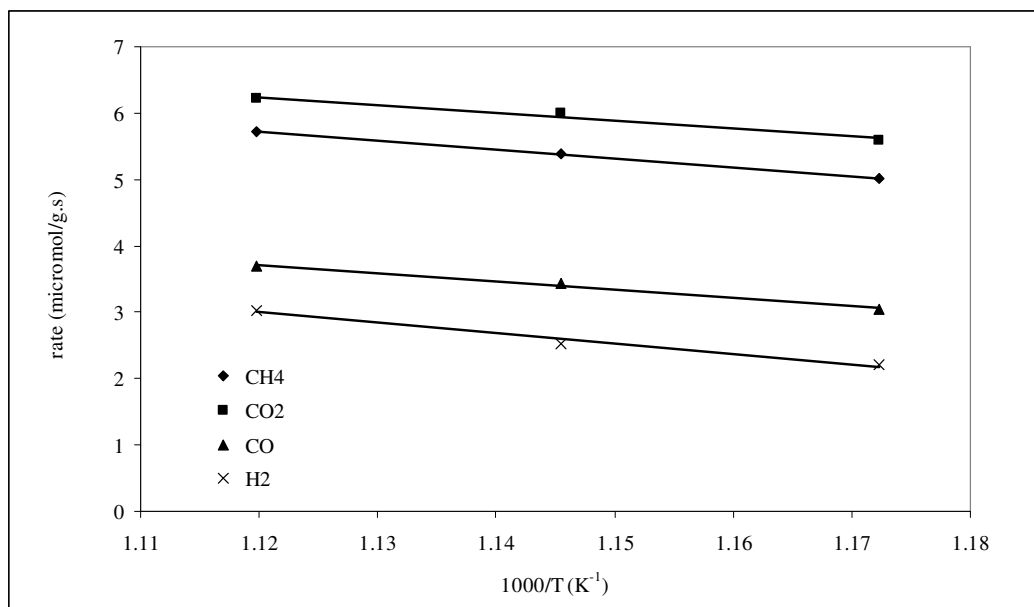


Figure 4.33. Arrhenius plots for CO over temperatures ranging between 853 and 893 K.

Catalyst: 0.3Pt-10Ni. Reaction conditions: CH₄/CO₂ = 1/1.

Space velocity = 1,200,000 mL/h.g-cat

It is remarkable that the activation barrier for CH₄ consumption is higher than that for CO₂ consumption, which is in agreement with reported values in literature. The apparent activation energies for H₂ production are greater than those corresponding to the CO formation, which is probably due to the occurrence of RWGS consuming H₂ to produce additional CO. The differences in the activation energies of the two catalysts, 0.3Pt-10Ni and 0.2Pt-15Ni most probably stem from the Ni/Pt loading ratio of those catalysts. The activation energies of Ni/CaO-Al₂O₃ catalyst obtained by Lemonidou and Vasalos (2002) are in reasonable agreement with the activation energies calculated for 0.3Pt-10Ni in this study.

Table 4.10. Apparent activation energies (E_{app}) in the current work and in the related literature

Catalyst	E_{app} (kcal/mol)				Reference
	CH ₄	CO ₂	CO	H ₂	
0.3Pt-10Ni	26.9	23.6	24.9	35.8	This work
0.2Pt-15Ni	26.6	16.9	21.0	35.2	This work
Ni/SiO ₂	23.0	19.0	20.0	27.0	Bradford and Vannice, 1996
Ni/MgO	22.0	21.0	21.0	35.0	Bradford and Vannice, 1996
Ni/TiO ₂	26.0	21.0	23.0	32.0	Bradford and Vannice, 1996
Ni/Al ₂ O ₃	16.9	16.5	17.7	23.5	Ferreira-Aparicio <i>et al.</i> , 1998
Ni/SiO ₂	14.9	16.7	16.5	22.4	Ferreira-Aparicio <i>et al.</i> , 1998
Ni/CaO-Al ₂ O ₃	25.5	23.6	24.6	35.2	Lemonidou and Vasalos, 2002
Ni-K/ CeO ₂ -Al ₂ O ₃	11.0	11.0	11.3	12.9	Nandini <i>et al.</i> , 2006

4.3.2.2. Power-Law Type Kinetics. The partial pressure dependencies were determined at 873 K by maintaining a constant partial pressure of 0.08 atm of one reactant and varying the pressure of the other reactant between 0.02 and 0.08 atm. A balance of argon was adjusted to maintain the pressure close to atmospheric and the total flow rate constant. The space velocity was varied between 1,200,000-1,800,000 mL/h.gcat in order to perform the reaction in kinetic region. The further details of the experimental conditions are given in Table 3.9 and 4.11.

The power-law type rate expression applied to the CDRM reaction is given below:

$$(-r_{CH_4}) = k(P_{CH_4})^\alpha (P_{CO_2})^\beta \quad (4.10)$$

Table 4.11. Partial pressures of methane and carbon dioxide and the corresponding residence time and space velocity values

Exp. No	Partial Pressures (atm)		CH ₄ /CO ₂	W _{cat} /F _{CH₄} (g.s.mmol ⁻¹)	Space Velocity (mL/h.gcat)
	CH ₄	CO ₂			
1	0.02	0.08	0.25	3.6654	1,200,000
2	0.02	0.08	0.25	3.0545	1,440,000
3	0.02	0.08	0.25	2.4436	1,800,000
4	0.04	0.08	0.50	1.8327	1,200,000
5	0.04	0.08	0.50	1.5273	1,440,000
6	0.04	0.08	0.50	1.2218	1,800,000
7	0.06	0.08	0.75	1.2218	1,200,000
8	0.06	0.08	0.75	1.0182	1,440,000
9	0.06	0.08	0.75	0.8145	1,800,000
10	0.08	0.08	1.00	0.9164	1,200,000
11	0.08	0.08	1.00	0.7636	1,800,000
12	0.08	0.08	1.00	0.6109	1,440,000
13	0.08	0.06	1.33	0.9164	1,200,000
14	0.08	0.06	1.33	0.7636	1,440,000
15	0.08	0.06	1.33	0.6109	1,800,000
16	0.08	0.04	2.00	0.9164	1,200,000
17	0.08	0.04	2.00	0.7636	1,440,000
18	0.08	0.04	2.00	0.6109	1,800,000
19	0.08	0.02	4.00	0.9164	1,200,000
20	0.08	0.02	4.00	0.7636	1,440,000
21	0.08	0.02	4.00	0.6109	1,800,000

Evaluation of the parameters, i.e. orders of reaction with respect to methane and carbon dioxide - α and β , respectively - and the rate constant, k , requires calculation of initial reaction rates. The reaction rates were calculated from slopes of the conversion versus residence time plots given in Appendix C section and are given in Table 4.12 for both 0.3Pt-10Ni and 0.2Pt-15Ni catalysts. The concentrations, given in mole per cent, can be converted into partial pressures very easily, since the total pressure was equal to ca. 1 atm. The resulting rate versus partial pressure data obtained at 873 K were used to estimate the reaction orders shown in Equation (4.10) via utilizing non-linear regression analysis. The results of the regression analysis are given in Table 4.13.

In the non-linear optimization scheme, the Levenberg-Marquardt algorithm provided in the computer software POLYMATH 5.1 was used. The Levenberg-Marquardt algorithm is an iterative technique that locates the minimum of a function that is expressed as the sum of squares of nonlinear functions. The sum of the squared differences of the measured reaction rates, $(-r)_m$, and the calculated reaction rates, $(-r)_c$, for N experiments ($=21$) and p parameter values ($=3$) is defined as variance of experimental error given by the following equation:

$$\sigma^2 = \sum_{i=1}^n \frac{[(r)_{im} - (-r)_{ic}]^2}{(N - p)} \rightarrow \text{minimum} \quad (4.11)$$

Table 4.12. Initial rates calculated from conversion-residence time data

Experiment No.	0.3Pt-10Ni		0.2Pt-15Ni	
	Reaction rate (mmol.g ⁻¹ .s ⁻¹)	Conversion Range	Reaction rate (mmol.g ⁻¹ .s ⁻¹)	Conversion Range
1-3	0.0551	0.12-0.21	0.0917	0.22-0.32
4-6	0.1108	0.14-0.19	0.1941	0.22-0.35
7-9	0.1668	0.13-0.21	0.3074	0.27-0.36
10-12	0.2230	0.13-0.21	0.4183	0.28-0.36
13-15	0.1735	0.10-0.16	0.2821	0.17-0.25
16-18	0.1217	0.06-0.12	0.1581	0.08-0.15
19-21	0.0675	0.04-0.06	0.0613	0.04-0.06

The values of reaction rate parameters, k , α and β of Equation 4.10, are given in Table 4.13 for each catalyst. It is observed that the reaction order for CH_4 was close to first-order for both catalysts. The reaction order for CO_2 was 0.87 for 0.3Pt-10Ni sample, which is lower than the order for CH_4 and typical for CDRM reaction. The orders with respect to CH_4 and CO_2 suggest that CO_2 adsorbs more strongly than CH_4 and that methane surface coverage is relatively lower for 0.3Pt-10Ni sample. However, the order for CO_2 was 1.40 for 0.2Pt-15Ni sample and this suggests us that the reaction rate is more sensitive to CO_2 partial pressure, than to CH_4 partial pressure. It is also observed that higher rate values obtained over 0.2Pt-15Ni sample led to a drastically higher k value compared to that obtained from 0.3Pt-10Ni.

The results indicate that the performance of the 0.2Pt-15Ni sample strongly depends on the CO_2 partial pressures; most probably, the catalyst utilizes oxygen coming from CO_2 to clean up its surface from deposited carbon. Due to its relatively higher amount of Pt in 0.3Pt-10Ni, the CO_2 dependence is rather limited; the reaction rate is a stronger function of methane concentration in the reactant feed.

Table 4.13. Estimated reaction rate parameters

Catalyst	Reaction Orders		k	σ^2 ($\text{mmol.g}^{-1}.\text{s}^{-1}$) ²
	α	B		
0.3Pt-10Ni	1.00	0.87	25.4 ($\text{mmol.g}^{-1}.\text{s}^{-1}.\text{atm}^{-1.87}$)	2.7×10^{-7}
0.2Pt-15Ni	1.09	1.40	230.0 ($\text{mmol.g}^{-1}.\text{s}^{-1}.\text{atm}^{-2.49}$)	2.1×10^{-6}

The reaction rates for the consumption of methane as a function of methane and carbon dioxide are shown in Figures 4.34 and 4.35, respectively. The points in these figures correspond to the experimental results and the lines are the fittings using the power rate-law (Equation 4.10.) It is observed that experimental results and the proposed power rate laws for both catalysts are in good agreement.

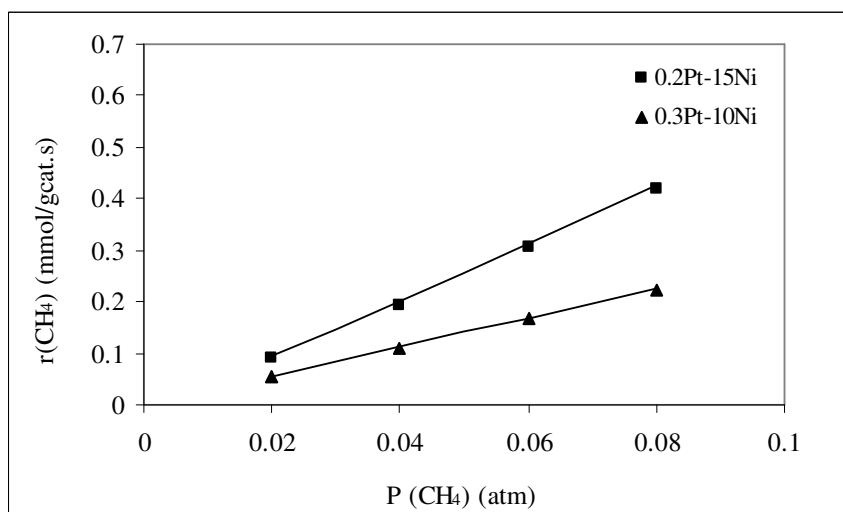


Figure 4.34. Variation of the reaction rates for the consumption of methane ($-r_{\text{CH}_4}$) as a function of the partial pressure of methane (P_{CH_4}). The points are experimental data. The lines are the fitting using Equation 4.10.

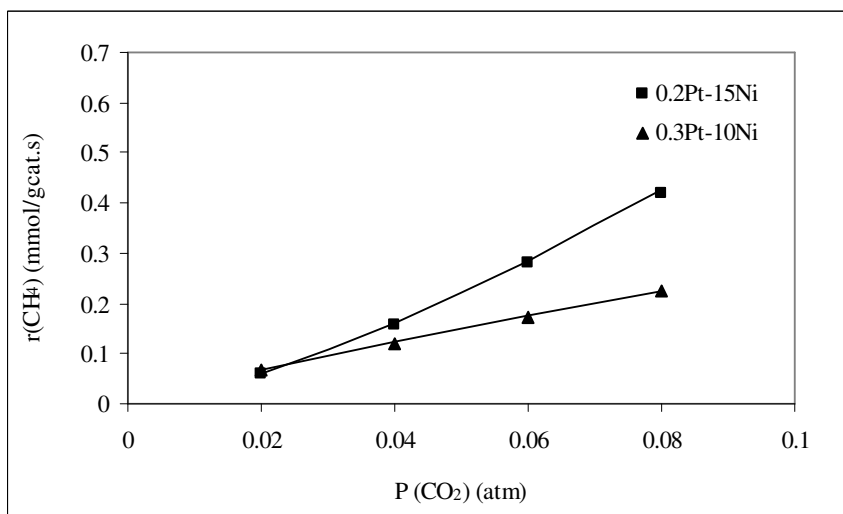


Figure 4.35. Variation of the reaction rates for the consumption of methane ($-r_{\text{CH}_4}$) as a function of the partial pressure of carbon dioxide (P_{CO_2}). The points are experimental data. The lines are the fitting using Equation 4.10.

4.3.2.3. Effect of CO on CDRM. The consumption of methane is also affected by the increased partial pressures of CO in the feed stream. Carbon monoxide with inlet partial pressure varying from 0.015 up to 0.0760 atm was added to the feed stream with constant partial pressures of the two reactants as 0.08 atm at 873 K (Table 4.14).

Table 4.14. Effect of CO partial pressure on CDRM rates

Exp. No	Partial Pressures (atm)			W_{cat}/F_{CH_4} (g.s.mmol ⁻¹)	$(-r_{CH_4})$ (mmol.g ⁻¹ .s ⁻¹)	
	CH ₄	CO ₂	CO		0.3Pt-10Ni	0.2Pt-15Ni
22	0.08	0.08	0.015	0.9164	0.2183	0.2619
23	0.08	0.08	0.030	0.9164	0.1856	0.2158
24	0.08	0.08	0.045	0.9164	0.1638	0.1705
25	0.08	0.08	0.060	0.9164	0.1517	0.1419

The rate values obtained show that the incorporation of CO into the methane dry reforming rate expression is necessary and it has an inhibitory effect. It should be noted that the orders with respect to CH₄ and CO₂ were assumed same as CDRM without CO case and the effect of CO was lumped in the order with respect to CO and in the value of k. The same methodology was also employed in the kinetic study by Gulyuz (2007). Thus, the power-function rate expression for dry reforming reaction becomes:

$$(-r_{CH_4}) = k(P_{CH_4})^\alpha (P_{CO_2})^\beta (P_{CO})^\delta \quad (4.12)$$

Partial pressures of CH₄, CO₂ and CO in the feed and calculated initial reaction rate data used for evaluation of CO reaction order are presented in Table 4.14. CH₄ consumption rates in the presence of CO were also plotted as a function of partial pressure of carbon monoxide in Figure 4.36.

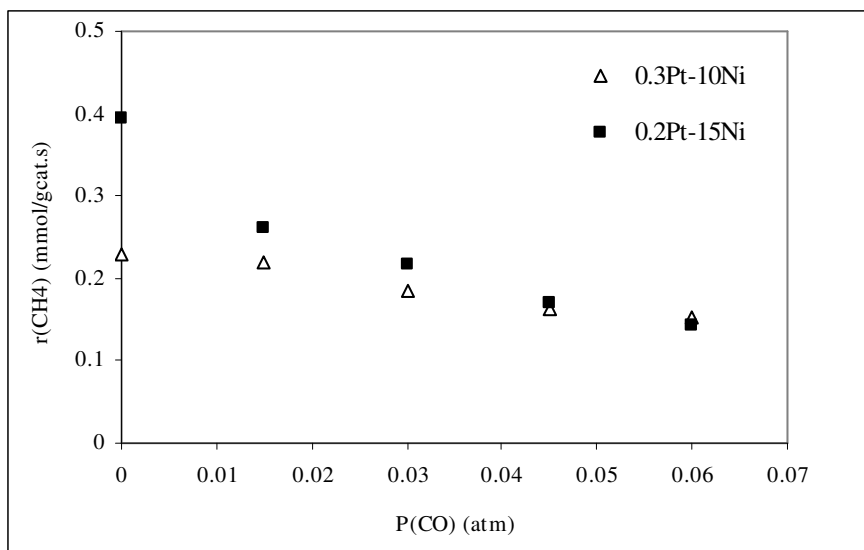


Figure 4.36. Variation of the reaction rates for the consumption of methane ($-r_{CH_4}$) as a function of the partial pressure of carbon monoxide (P_{CO}).

The reaction orders that were obtained in the absence of CO for CH₄ and CO₂ were kept fixed and the analysis was performed to find order with respect to CO. The same computer program provided in POLYMATH (see Section 4.2.1.1) was used for the determination of rate expressions in the presence of CO. The reaction rate parameters, k and δ of Equation 4.12 are determined by POLYMATH software using nonlinear regression technique and their values are given in Table 4.15 for each catalyst.

It is observed that the presence of CO for both catalysts have negative effect on the consumption of methane in CDRM. However; the rate of consumption of reaction on the basis of methane consumption for 0.2Pt-15Ni sample was found more sensitive to the increase in partial pressure of CO as the reaction order with respect to CO for this sample is 1.6 times the value of that of the 0.3Pt-10Ni catalyst.

Table 4.15. Estimated reaction rate parameters in the presence of CO

Catalyst	Reaction order of CO (δ)	k	σ^2 (mmol.g ⁻¹ .s ⁻¹) ²
0.3Pt-10Ni	-0.26	8.2 mmol. g ⁻¹ .s ⁻¹ .atm ^{-1.61}	4.6×10 ⁻⁶
0.2Pt-15Ni	-0.41	25.7 mmol. g ⁻¹ .s ⁻¹ .atm ^{-2.08}	1.7×10 ⁻⁴

Table 4.16. Estimated power rate laws in the presence of CO

Catalyst	Power rate law
0.3Pt-10Ni	$(-r_{CH_4}) = k(P_{CH_4}) (P_{CO_2})^{0.87} (P_{CO})^{-0.26}$
0.2Pt-15Ni	$(-r_{CH_4}) = k(P_{CH_4})^{1.09} (P_{CO_2})^{1.40} (P_{CO})^{-0.41}$

The inhibiting effect of CO on reaction rate is explained by the adsorption of CO on active site where it dissociates to activated carbon and O. This type of activated carbon formed from CO reacts more slowly compared to that of C (or CH) species formed by activation of CH₄ (Lemonidou and Vasalos, 2002). This explanation can also clarify the rapid deactivation of the 0.2Pt-15Ni catalyst as it is more sensitive to the presence of CO than the 0.3Pt-10Ni sample. Olsbye *et al.* (1997) and Cui *et al.* (2007) also observed inhibiting effect of CO in dry reforming of CH₄ using Ni/La-Al₂O₃ and Ni/ α -Al₂O₃ catalysts, respectively.

It has been reported that CH₄ was dissociated on Ni active sites and CO was also adsorbed over Ni active sites (Cui *et al.*, 2007). Some kinetic models suggested that most of the species adsorbed on the Ni active sites were CO and CH species (Watwe *et al.*, 2000; Cui *et al.*, 2007; Goodman *et al.*, 1980). Parallel to the literature, the inhibition effect of CO increases from -0.26 to -0.41 as the Ni content increases from 10 wt. % for 0.3Pt-10Ni catalyst to 15 wt.% for 0.2Pt-15Ni sample. The adsorption of CO on the Ni active sites inhibited the adsorption and dissociation of CH₄, which further restrained the

reforming reaction. However, the present experimental results can still not disclose whether the desorption of CO is a rate determining step in the reforming reaction 873 K.

4.3.2.4. Effect of H₂ on CDRM. The effect of H₂ partial pressure on the rate of methane disappearance was studied at 873 K using 5 mg of catalyst. The total flow was kept fixed at 100 mL/min with constant partial pressures of the two reactants 0.08 atm, while the inlet partial pressures of H₂ was changed from 0 to 0.075 atm (Table 4.17).

Table 4.17. Effect of H₂ partial pressure on CDRM rates

Exp. No	Partial Pressures (atm)			W _{cat} /F _{CH₄} (g.s.mmol ⁻¹)	(-r _{CH₄}) (mmol.g ⁻¹ .s ⁻¹)	
	CH ₄	CO ₂	H ₂		0.3Pt-10Ni	0.2Pt-15Ni
26	0.08	0.08	0.015	0.9164	0.2867	0.2731
27	0.08	0.08	0.03	0.9164	0.2910	0.2826
28	0.08	0.08	0.045	0.9164	0.2955	0.2800
29	0.08	0.08	0.06	0.9164	0.2961	0.2729
30	0.08	0.08	0.075	0.9164	0.2942	0.2806

CH₄ consumption rates in the presence of H₂ were plotted as a function of partial pressure of hydrogen in Figure 4.37. Upon the addition of hydrogen to the feed, the rate of conversion of methane is initially declined for 0.2Pt-15Ni sample whereas it is slightly promoted for 0.3Pt-10Ni sample. However; increasing H₂ partial pressure further had essentially no effect on the CH₄ reforming activity of the both Ni catalysts, as evidenced by the invariance of the rate of methane consumption with increasing H₂ partial pressure (Figure 4.33 and Table 4.15). This result is also consistent with other Ni-based catalysts in literature (Cui *et al.*, 2007; Tsipouriari *et al.*, 2001). We can conclude that Ni-H can be produced on the nickel catalysts and it can reach equilibrium state with the product hydrogen in the dry reforming (Cui *et al.*, 2006, 2007). Therefore, the reaction steps involving the hydrogen species on the catalyst surface were the rapid or equilibrium steps.

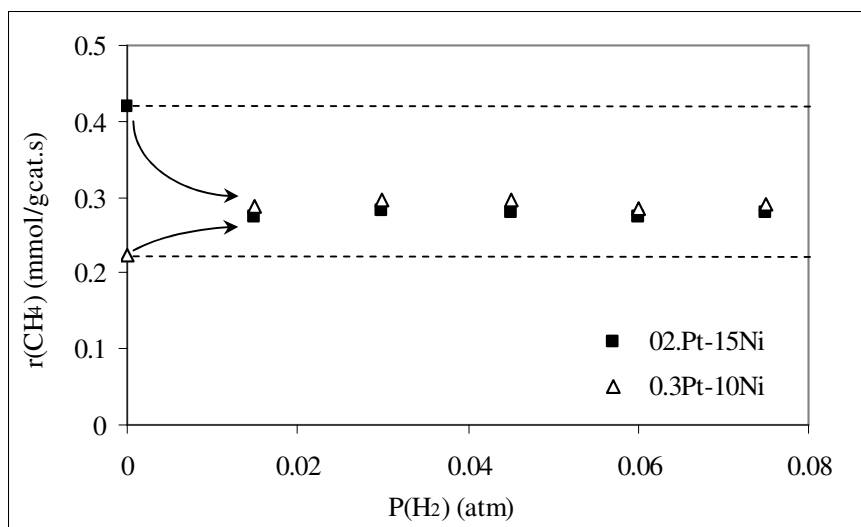


Figure 4.37. Variation of the reaction rates for the consumption of methane ($-r_{CH_4}$) as a function of the partial pressure of hydrogen (P_{H_2}).

4.3.2.5. Langmuir-Hinshelwood Type Surface Reaction Models. There have been various reports where the kinetics of methane dry reforming with carbon dioxide has been expressed as a simple power-law model due to its simplicity in application. However, over a wide range of partial-pressure data, these models are inadequate. Hence, it becomes necessary to understand the mechanistic aspects of the reforming reaction, based on which some researchers have proposed Langmuir-Hinshelwood, Eley-Rideal and Hougen-Watson type of reaction models (Iyer, 2001).

Some of the groups who performed kinetic studies on the CO₂-reforming reaction have also proposed a Langmuir-Hinshelwood-type mechanism with an undefined number of H atoms in the intermediate CH_x species and with dissociative adsorption of CO₂ (Wang and Lu, 1999; Osaki *et al.*, 1994). Zhang and Verykios (1994) have derived a rate expression in a Langmuirian model assuming that methane dissociation was the rate determining step. The results reported by Olsbye *et al.* (1997) showed that the experimental data were consistent with Langmuir-Hinshelwood mechanism, in which the surface reaction is the rate-determining step, or an Eley-Rideal-type mechanism, in which the reaction between CH_x and CO_{2,g} is rate-limiting at low pressures of carbon dioxide.

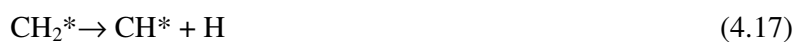
In this study, Langmuir-Hinshelwood rate expressions were also used to fit the dry reforming data obtained. No single rate expression can effectively describe the CDRM reaction data over the entire range of CH₄ and CO₂ concentrations. Experimental CH₄ rate data were analyzed using nonlinear regression analysis with Levenberg-Marquardt algorithm provided in the computer software POLYMATH 5.1 for estimating parameters in the various kinetic models.

A model with smaller variance (Equation 4.11) is likely to represent the data more accurately than a model with larger variance values of this indicator. Models giving either poor correlation coefficients or negative parameter values were ruled out. In some models, the 95% confidence interval was greater than the parameters itself, yielding negative values of the parameters, which is physically impossible. These models were also excluded. The proposed Langmuir-Hinshelwood type rate expressions are given in Table 4.14 for 0.3Pt-10Ni sample.

The equation that best fits the experimental data can be determined by comparing the variance of the experimental error (σ^2) for each model and selecting the equation with a smaller variance.

The Langmuir-Hinshelwood-Hougen-Watson type rate expressions that has been tested for both Pt-Ni catalysts are presented in Table 4.18. In the models, the K_i values stand for the adsorption coefficients for each species. Model 1 was proposed by Mark *et al.* (1997), who investigated the kinetics of CO₂/CH₄ reforming with Ir/Al₂O₃. The model based on the Eley-Rideal (ER) type of heterogeneous model assumes that CO₂ is adsorbed on the catalyst surface in adsorption equilibrium. The slow and the rate-determining step is the reaction of adsorbed CO₂ with CH₄ from the gas phase leading directly to products. While determining the power rate laws, we have found out that CH₄ is weakly adsorbed and the surface coverage of methane is relatively low for 0.3Pt-10Ni sample at the pressures studied. Hence, this model is a good one to describe the behavior 0.3Pt-10Ni sample.

Model 2 was proposed by Wang *et al.* (1999) for Ni/Al₂O₃ catalyst. The rate-determining step was determined as the CO formation step (Equation 4.19). On the basis of their investigation, the mechanism was simplified as:



Zhang and Verykios (1994) proposed a rate expression (Model 3) derived from a Langmuir-type model, assuming methane dissociation is the rate-determining step. Although the model fits the observed data well, Zhang and Verykios did not provide any values for the adsorption and kinetic parameters.

Mark *et al.* (1997) also proposed LH model type rate expression (Model 4), which assumes that both reactants are adsorbed and the rate determining step is the surface

reaction of the adsorbed reactants to form products H₂ and CO. The resulting equation was also proposed by Richardson and Paripatyadar (1990).

Table 4.18. Langmuir-Hinshelwood (LH) type rate expressions

Model No	Proposed Rate Equations
1	$(-r_{CH_4}) = \frac{kK_{CO_2} P_{CH_4} P_{CO_2}}{(1 + K_{CO_2} P_{CO_2})}$
2	$r_{CH_4} = \frac{k_1 P_{CH_4} P_{CO_2}}{(1 + K_1 P_{CH_4})(1 + K_2 P_{CO_2})}$
3	$r = \frac{a P_{CH_4} P_{CO_2}^2}{(P_{CO_2} + b P_{CO_2}^2 + c P_{CH_4})^2}$
4	$(-r_{CH_4}) = \frac{kK_{CO_2} K_{CH_4} P_{CH_4} P_{CO_2}}{(1 + K_{CO_2} P_{CO_2} + K_{CH_4} P_{CH_4})^2}$
5	$(-r_{CH_4}) = \frac{kP_{CH_4} P_{CO_2}}{(1 + K_1 P_{CH_4} + K_2 P_{CO_2})(1 + K_3 P_{CO_2})}$
6	$(-r_{CH_4}) = \frac{kK_{CO_2} P_{CH_4} P_{CO_2}}{(1 + K_{CO_2} P_{CO_2} + K_{CO} P_{CO})}$
7	$(-r_{CH_4}) = \frac{kK_{CH_4} P_{CH_4} P_{CO_2}^m}{(1 + K_{CH_4} P_{CH_4})}$
8	$(-r_{CH_4}) = \frac{kP_{CH_4}^m P_{CO_2}^n}{(1 + K_{CO_2} P_{CO_2} + K_{CO} P_{CO} + K_{CH_4} P_{CH_4})}$

Olsbye *et al.* (1997) have reported the kinetic studies of CO₂/CH₄ reforming over a highly active Ni/La/Al₂O₃ catalyst in a micro-catalytic fixed-bed reactor. The proposed Langmuir-Hinshelwood type rate expression is given by Model 5 (Table 4.18). The observed kinetic data were found to be in fairly good agreement with the predicted rate model. The model was validated with a laboratory scale fluidized-bed reactor. However, Olsbye *et al.* did not present the reaction mechanism from which the model was proposed.

The observed inhibiting effect of CO is not included within the rate expressions proposed up to now. But, the negative influence of CO addition on CH₄ consumption rate should also be represented in the model equations. Hence; model 6 was derived from model 1 simply by adding the inhibiting effect of CO in the denominator.

The discrimination of kinetic models as illustrated in Table 4.19 indicates the Langmuir-Hinshelwood mechanism, as depicted in model no 1, to give the best result among the model equations fitted to the data in this work.

Table 4.19. Model parameters obtained for 0.3Pt-10Ni Catalyst

Model No	Rate Parameters	σ^2 (mmol.g ⁻¹ .s ⁻¹) ²
1	$k = 14.34 \text{ mmol.g}^{-1}.\text{s}^{-1}.\text{atm}^{-1}$ $K_{CO_2} = 2.99 \text{ atm}^{-1}$	2.29×10^{-6}
2	$k_I = 68.18 \text{ mmol.g}^{-1}.\text{s}^{-1}.\text{atm}^{-2}$ $K_I = 1.55 \text{ atm}^{-1}, K_2 = 10.57 \text{ atm}^{-1}$	2.86×10^{-6}
3	$a = 6.2 \text{ mmol.g}^{-1}.\text{s}^{-1}.\text{atm}^{-3}$ $b = 1.7 \text{ atm}^{-2}, c = 0.45 \text{ atm}^{-1}$	4.75×10^{-4}
4	$k = 49.9 \text{ mmol.g}^{-1}.\text{s}^{-1}$ $K_{CO_2} = 1.74 \text{ atm}^{-1},$ $K_{CH_4} = 0.55 \text{ atm}^{-1}$	9.98×10^{-6}
5	$k = 84.6 \text{ mmol.g}^{-1}.\text{s}^{-1}.\text{atm}^{-2}$ $K_I = 1.71 \text{ atm}^{-1}, K_2 = 6.00 \text{ atm}^{-1}$ $K_3 = 15.88 \text{ atm}^{-1}$	2.95×10^{-4}
6	$k = 18.6 \text{ mmol.g}^{-1}.\text{s}^{-1}.\text{atm}^{-1}$ $K_{CO_2} = 2.25 \text{ atm}^{-1}$ $K_{CO} = 9.03 \text{ atm}^{-1}$	3.98×10^{-5}

As the orders for CO₂ and CH₄ were 1.40 and 1.09 for 0.2Pt-15Ni sample, respectively, it was not possible to suit a Langmuir-Hinshelwood type rate expression that had been proposed before by other researchers except the model (Model 5) suggested by Olsbye *et al.* (1997).

Considering that the orders for the reactants are greater than unity, the exponents of the components occurring in the numerator of the LH type rate expressions are left as variables. Model 7 assumes an Eley-Rideal (ER) type of heterogeneous model in which the reaction between CH_x and CO_{2,g} is rate-limiting at low pressures of carbon dioxide. CH₄ is adsorbed on the catalyst surface and dissociates to CH_x and H. The slow and the rate-determining step is the reaction of adsorbed CH_x with CH₄ from the gas phase. This type of model has been previously reported by Olsbye *et al.* (1997) and Mark *et al.* (1997).

However; the inhibiting effect of CO in this sample is very strong and it should also be included in the model equation. Model 8 also takes into account the effect of CO on the reaction rates and gives the best result with the smallest variance among the three rate expressions in Table 4.20.

Table 4.20. Model parameters obtained for 0.2Pt-15Ni Catalyst

Model No	Rate Parameters	σ^2 (mmol.g ⁻¹ .s ⁻¹) ²
5	$k = 71.0 \text{ mmol.g}^{-1}.\text{s}^{-1}.\text{atm}^{-2}$ $K_1 = 1.00 \text{ atm}^{-1}, K_2 = 30.0 \text{ atm}^{-1}$ $K_3 = 1.20 \text{ atm}^{-1}$	7.73×10^{-4}
7	$k = 2020 \text{ mmol.g}^{-1}.\text{s}^{-1}$ $K_{CH_4} = 0.078 \text{ atm}^{-1}, m = 1.36 \text{ atm}^{-1}$	8.88×10^{-5}
8	$k = 428 \text{ mmol.g}^{-1}.\text{s}^{-1}.\text{atm}^{-2}$ $K_{CH_4} = 1.49 \text{ atm}^{-1}, K_{CO_2} = 2.49 \text{ atm}^{-1}$ $K_{CO} = 43.7 \text{ atm}^{-1}, m = 1.14, n = 1.49$	6.76×10^{-5}

4.3.3. Summary

In the present part of the work, the kinetic behavior of the 0.2Pt-15Ni and 0.3Pt-10Ni catalysts in the reforming reaction of methane with carbon dioxide was investigated as a function of temperature and partial pressures of CH₄ and CO₂ in order to elucidate the mechanistic differences of the surface reaction over those catalysts. The following conclusions are given as follows:

- The kinetics of CO₂ reforming of methane within the parameter range investigated over 0.3Pt-10Ni and 0.2Pt-15Ni can be expressed by a simple power-law rate equation, with reaction orders of 1 and 1.09 for CH₄ and 0.87 and 1.40 for CO₂, respectively.
- CH₄ consumption rates were found to decrease with increasing CO content. The reaction order with respect to CO in the power-function rate expression is calculated as -0.26 and -0.41 for 0.3Pt-10Ni and 0.2Pt-15Ni samples, respectively.
- The rate of consumption of methane for 0.2Pt-15Ni sample was found more sensitive to the increase in partial pressure of CO as the reaction order with respect to CO for this sample is 1.6 times the value of that of the 0.3Pt-10Ni catalyst.
- Upon the addition of hydrogen to the feed, the rate of conversion of methane is initially declined for 0.2Pt-15Ni sample whereas it is slightly promoted for 0.3Pt-10Ni sample. However; increasing H₂ partial pressure further had essentially no effect on the CH₄ reforming activity of the both Ni catalysts, as evidenced by the invariance of the rate of methane consumption with increasing H₂ partial pressure.

4.4. Carbon Dioxide Reforming of Methane over Co-X/ZrO₂ Catalysts (X = La, Ce, Mn, Mg, K)

Replacing the noble metals with less costly metals, like Fe, Ni, Co, in catalysis is of crucial importance. The purpose of this part of the work is to design and develop stable and effective Co-based CDRM catalysts supported on zirconia. Aiming to improve the performance of the Co-based catalysts, the effect of addition of metal additives, namely lanthanum, cerium, manganese, potassium and magnesium, was studied. The main intention was to increase the resistance of cobalt based catalysts to coking. SEM and EDX tests were performed in order to obtain information on the dispersion of metals on the catalyst surface. X-ray diffraction (XRD) analyses were performed aiming to detect the formation of different Co-X/ZrO₂ crystalline phases led by various modifiers. The amount of deposited carbon on the surface of the used Co/ZrO₂ catalysts and the kind of carbonaceous deposits were determined by TGA/DTA and SEM measurements. Note that the catalysts characterized and tested in this part of the work are given in Table 3.7 in Experimental Section.

4.4.1. Characterization Tests

4.4.1.1. Scanning Electron Microscopy. Freshly calcined and reduced Co-X/ZrO₂ catalysts were tested using SEM-EDX to obtain information on their microstructural properties and metal dispersion. Metal mapping studies were used to understand the dispersion of metals and their agglomeration behaviors on the support surface. In each EDX elemental mapping and quantification studies, at least three different clusters of the same catalyst sample, having similar cluster sizes, were chosen and tested for comparison. Quantification values corresponding to the different clusters for each catalyst type were typically found to be in good correlation with each other. The metal mappings obtained for different samples are given in Figures 4.38-4.42. For each sample, a representative set including an SEM bright area image, and Co + Zr and promoter + Zr mappings are given. Additionally, the weight percentages of the surface metallic species are tabulated in Table 4.21 for all samples.

It is very well observed from the SEM images and metal mapping studies that both particle size and metal dispersion properties of the catalysts are affected by the presence and type of the promoter used.

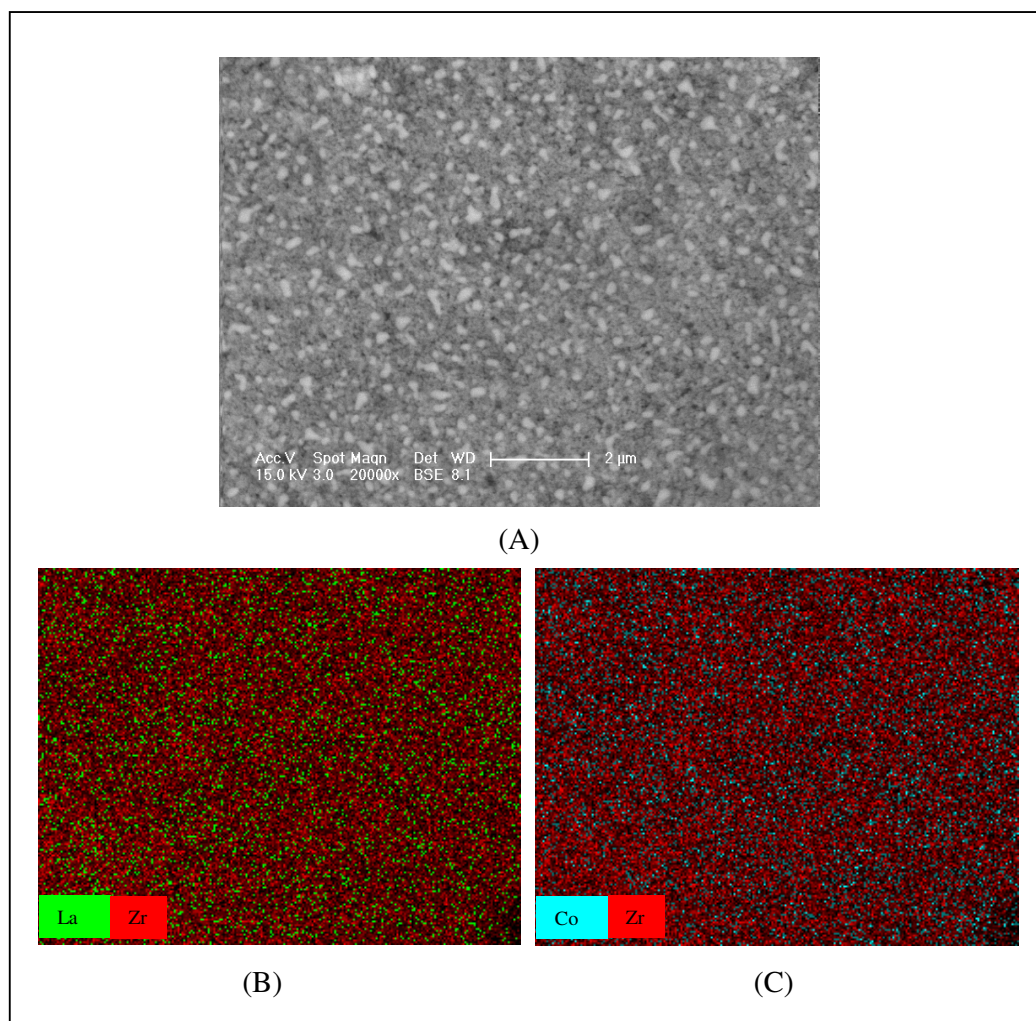


Figure 4.38. 5Co2La: A) SEM image, B) La + Zr mapping, C) Co + Zr mapping

According to the SEM image and metal mappings (Figure 4.38), Co and La are well and homogeneously dispersed over the surface of La promoted Co/ZrO₂ sample (5Co2La). The addition of lanthanum on the ZrO₂ support prior to the impregnation of Co precursor results in smaller particle size of Co metal and enhances the dispersion properties of the catalyst.

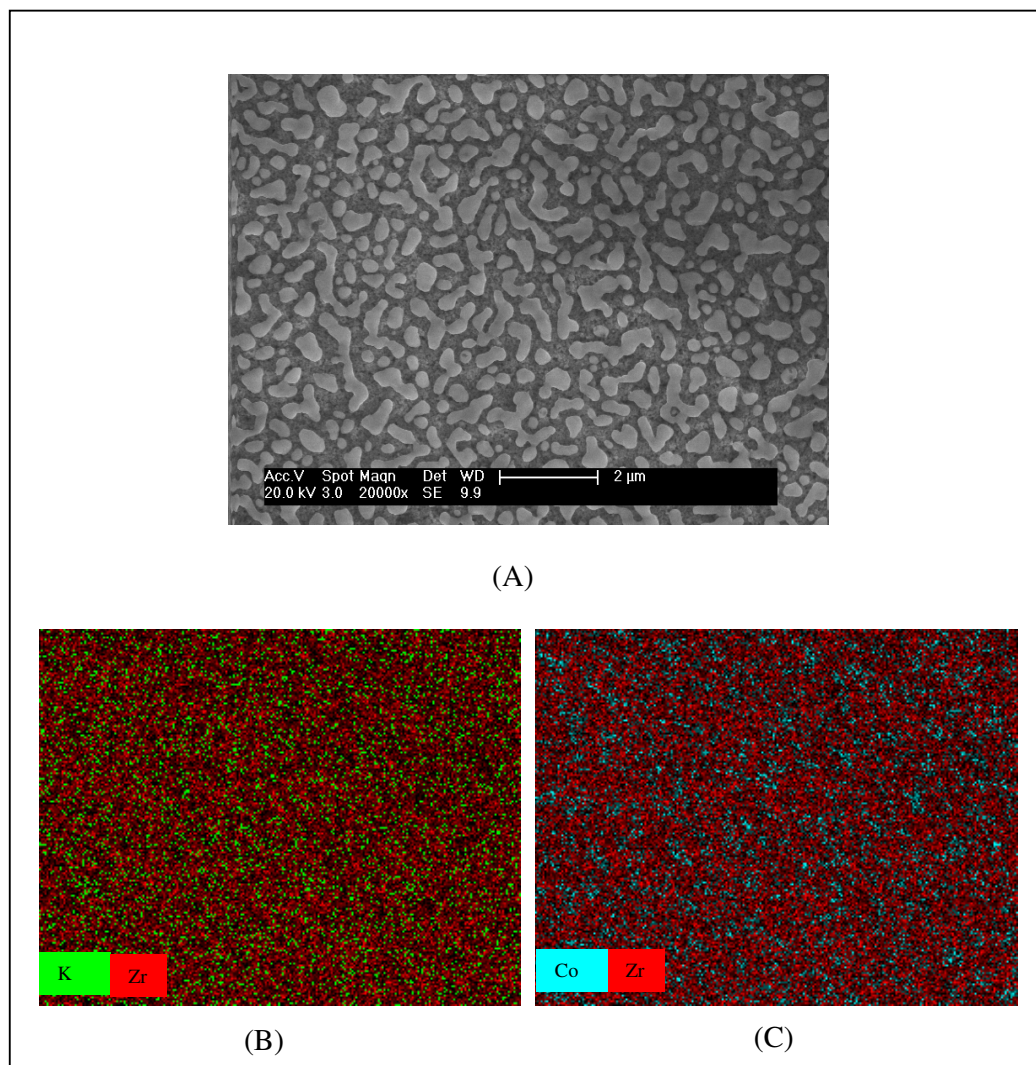


Figure 4.39. 5Co2K: A) SEM image, B) K + Zr mapping, C) Co + Zr mapping

In 5Co2K sample, on the other hand, the images (Figure 4.39) showed formation of metal phase on the support as larger particle sizes. The dispersion is not homogeneous and Co is in the form of agglomerates over the ZrO_2 support, which is confirmed both by the SEM image and the Co+Zr mapping. The addition of potassium resulted in the formation of Co agglomerates and low dispersion properties. The results clearly showed that K addition did not lead to stabilization of Co centers on the support and did not prevent metal sintering.

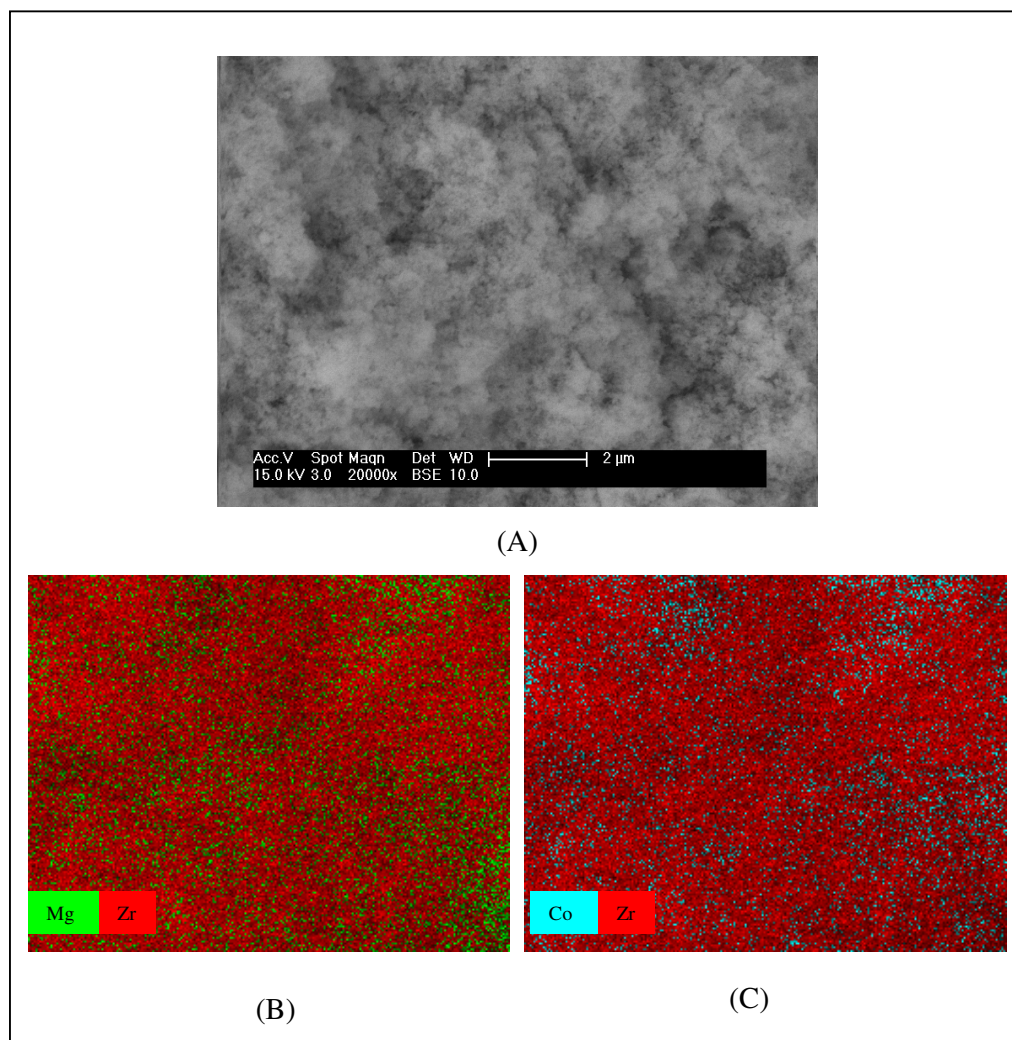


Figure 4.40. 5Co2Mg: A) SEM image, B) Mg + Zr mapping, C) Co + Zr mapping

Parallel micro-characterization of 5Co2Mg sample revealed that, both Mg and Co centers were formed as metal islands over the surface and the active metal phase was not distributed evenly (Figure 4.40). However, the morphology of distributed metal components and the clusters formed significantly differs from that of the 5Co2K sample. Based on those results, it can be proposed that the type of the metal additive also affects the microstructure and morphology of the Co clusters that form on the surface during the high temperature calcination and reduction pretreatments.

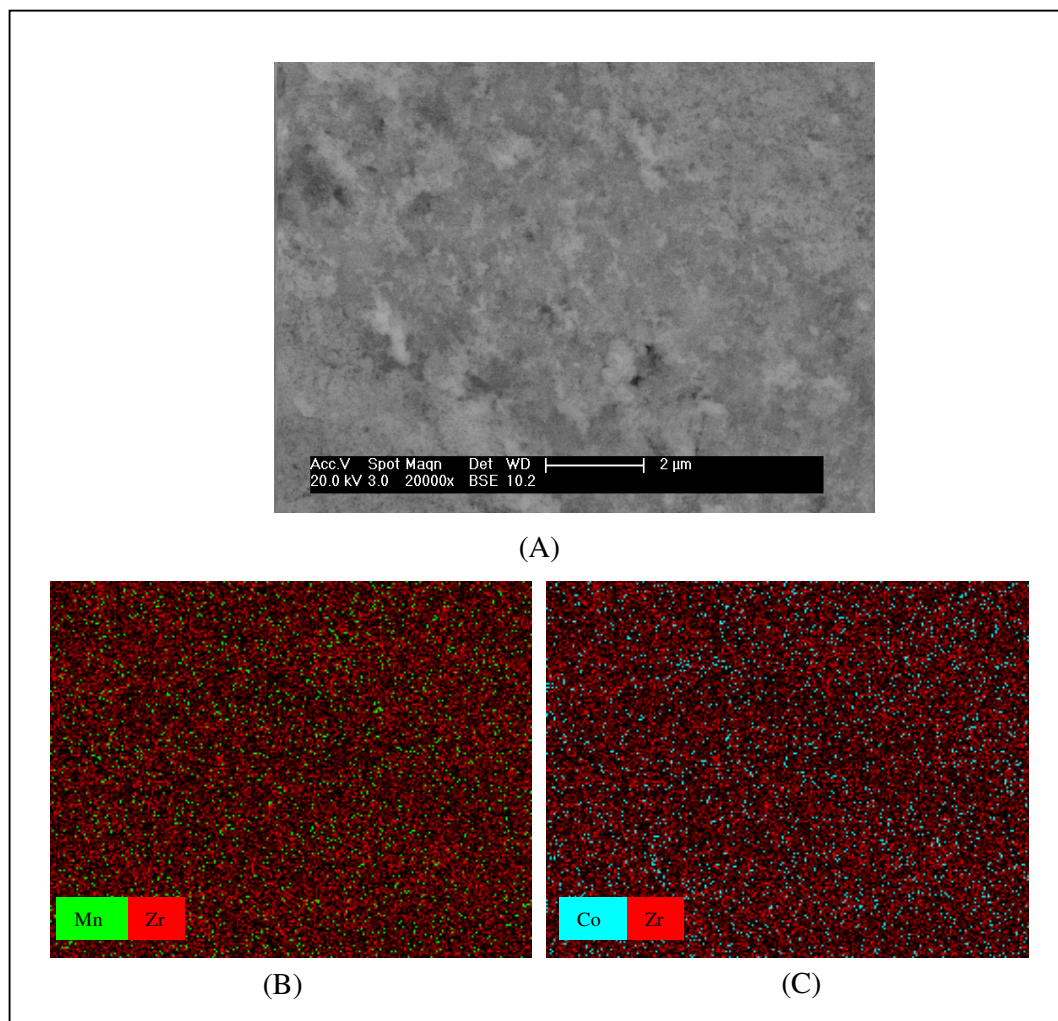


Figure 4.41. 5Co2Mn: A) SEM image, B) Mn + Zr mapping, C) Co + Zr mapping

The SEM-EDX characterization of the 5Co2Mn sample indicates that the effects of Mn and La additives on Co dispersion are very similar (Figure 4.41). It is observed that both Mn and Co are homogeneously dispersed over the surface of the catalyst as small particles.

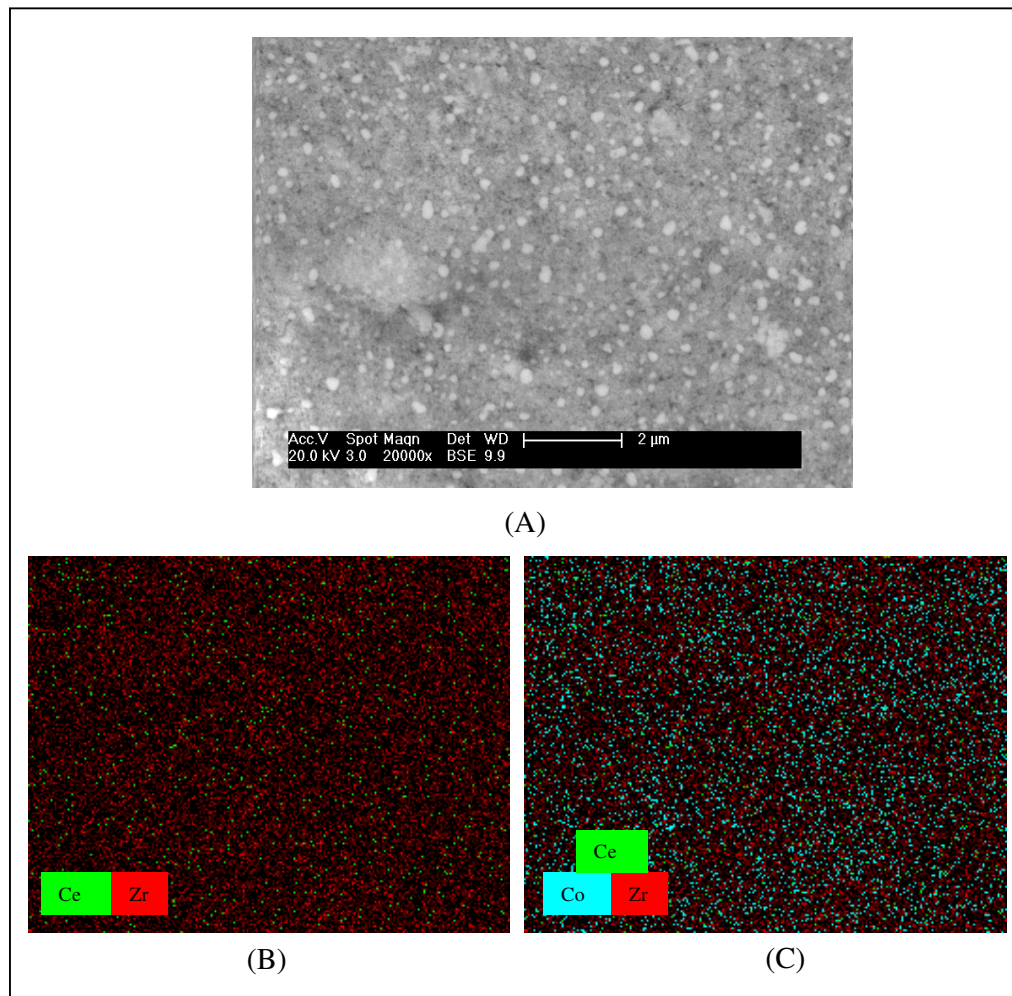


Figure 4.42. 5Co₂Ce: A) SEM image, B) Ce + Zr mapping, C) Co + Zr mapping

The micro-structural analysis of the last bimetallic sample, Ce-promoted Co/ZrO₂, revealed that densely populated Co centers, which are shown in BSE as well as EDX mapping, cover almost the whole support and partially cover the Ce centers (Figure 4.42).

Moreover; weight percentages of the surface metallic species from SEM-EDX data are given in Table 4.21 and show that the surface Co content of Co-Ce and Co-K samples are very high, indicating coverage of surface with Co, and surface Ce and K contents of Co-Ce and Co-K samples, respectively, are relatively low, indicating partial coverage of promoter centers by Co.

Table 4.21. Weight percentages of the surface metallic species from SEM-EDX data

Catalyst #	Co wt. %	Promoter wt.%
5Co2La	3.94	2.08
5Co2K	21.44	1.04
5Co2Mn	3.66	1.45
5Co2Mg	6.41	2.74
5Co2Ce	15.64	0.98

4.4.1.2. X-Ray Diffraction. Co-containing species present in the freshly reduced catalysts at 773 K were identified by XRD. According to the XRD spectra, Co was detected in its metallic phase for all the catalysts prepared except for the 5Co2Mg sample for which Co was in the form of CoO crystallites.

4.4.1.3. Temperature Programmed Oxidation. Figure 4.43 shows the TGA curves of the all spent catalysts, which were used to determine the amount of carbon formation after 6 h of time on stream reaction tests at 923 K for the reaction with a space velocity of 60,000 ml/h.g-cat. In the TPO profiles, an increase in weight of the catalysts were observed within the range of 350-500°C depending on the type of the catalyst, which corresponds to the oxidation of metallic cobalt species, except for the 5CoMg2 case, for which the cobalt species is in oxide form in the original catalyst. This result is also confirmed by the XRD test results. TGA tests showed a maximum weight loss of ca. 4 % for the unpromoted Co/ZrO₂, indicating a significant amount of carbon deposition on that sample during the course of 6 h on-stream reaction. The high amount of deposited carbon on Co/ZrO₂ is a clear indication that monometallic sample suffers from activity loss led by covering of its active sites by coke. Mn- and La-doped samples showed a slight decrease in the weight of catalysts, specifying that negligible amount of carbon was formed on these samples during reaction. The other remaining catalysts lost about 2 per cent of their weights, pointing out to a moderate amount of carbon deposition at the end of 6h on-stream reaction.

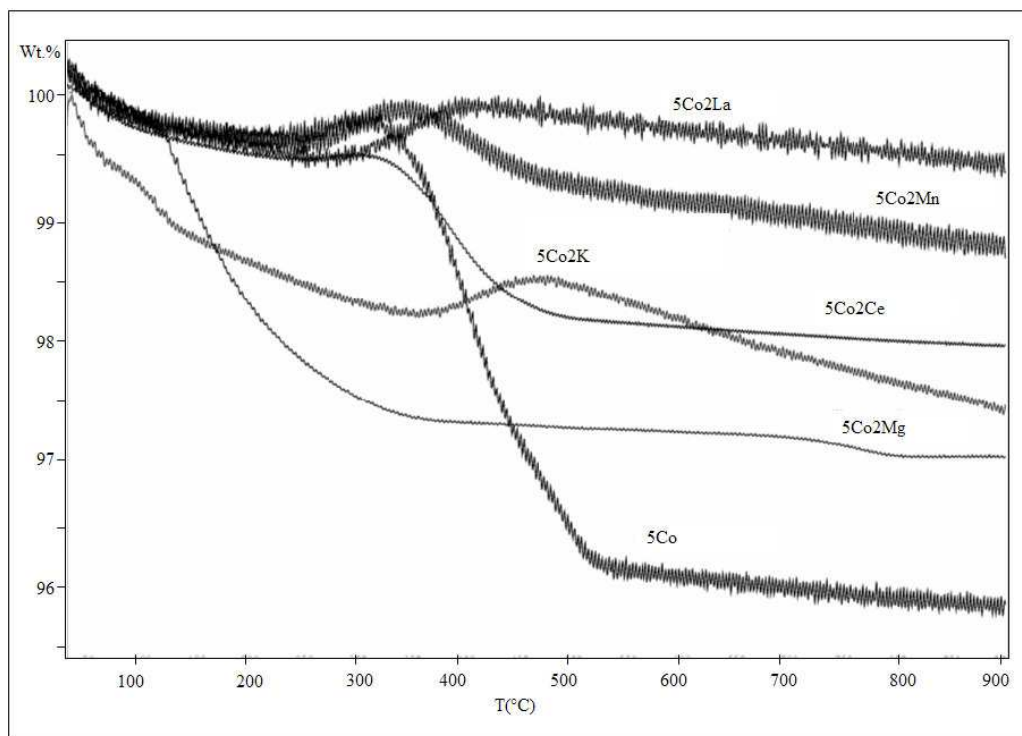


Figure 4.43. Temperature programmed oxidation (TPO) profiles of spent catalysts after 6 h of time on stream reaction tests at 923 K with SV = 60,000 ml/h.g-cat

4.4.2. CO₂ Reforming of Methane over Co-X/ZrO₂ (X=La, K, Mn, Mg, Ce)

Co catalysts with different metal additives were tested in CO₂ reforming of methane at 923 K with CH₄: CO₂ ratio of 1:1 for 6h of times-on-stream (TOS) at atmospheric pressure with a space velocity of 60,000 mL/h.g-cat. Figures 4.44 - 4.46 show the CH₄ and CO₂ conversions and the H₂/CO molar ratio in the product stream as a function of reaction time on stream, respectively, for all catalyst samples. Table 4.22 summarizes the catalytic performance of the bimetallic Co-X/ZrO₂ samples, expressed as CH₄ conversion, H₂/CO ratio, and amount of coke deposition at 923 K.

The different activity levels of the catalysts clearly show that the catalytic performances of promoted-Co/ZrO₂ samples strongly depends on the type of the metal additive used. The observed order of methane conversions over doped cobalt catalysts is Ce > none > La ≈ Mn > Mo > K > Mg for the reaction performed 6h TOS.

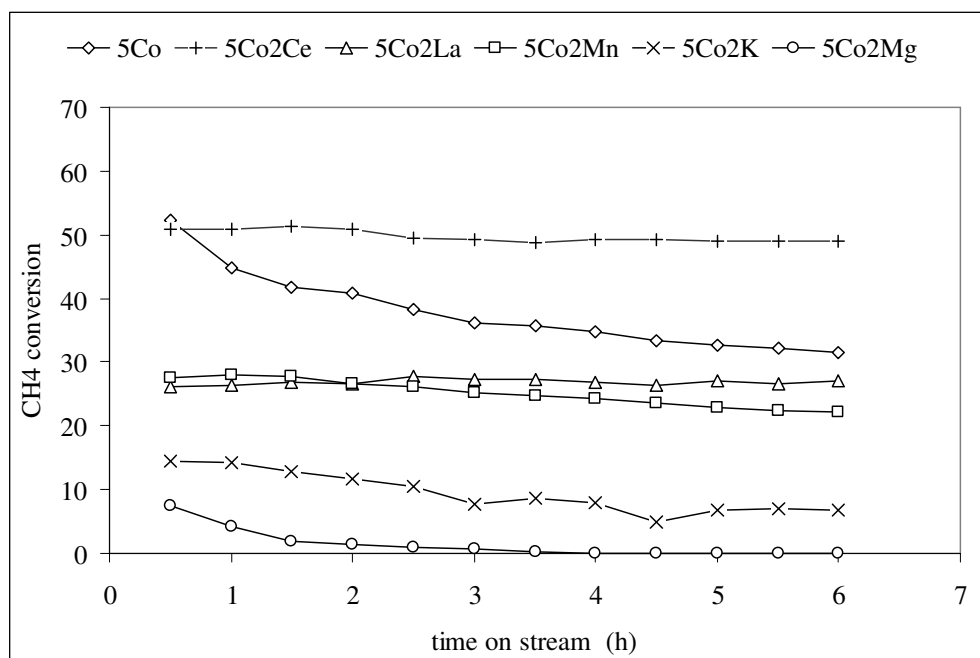


Figure 4.44. Effect of modifier on CH₄ conversion as a function of reaction time. Reaction Temperature = 923 K. CH₄ / CO₂ = 1/1. Space velocity = 60,000 mL/h.g-cat

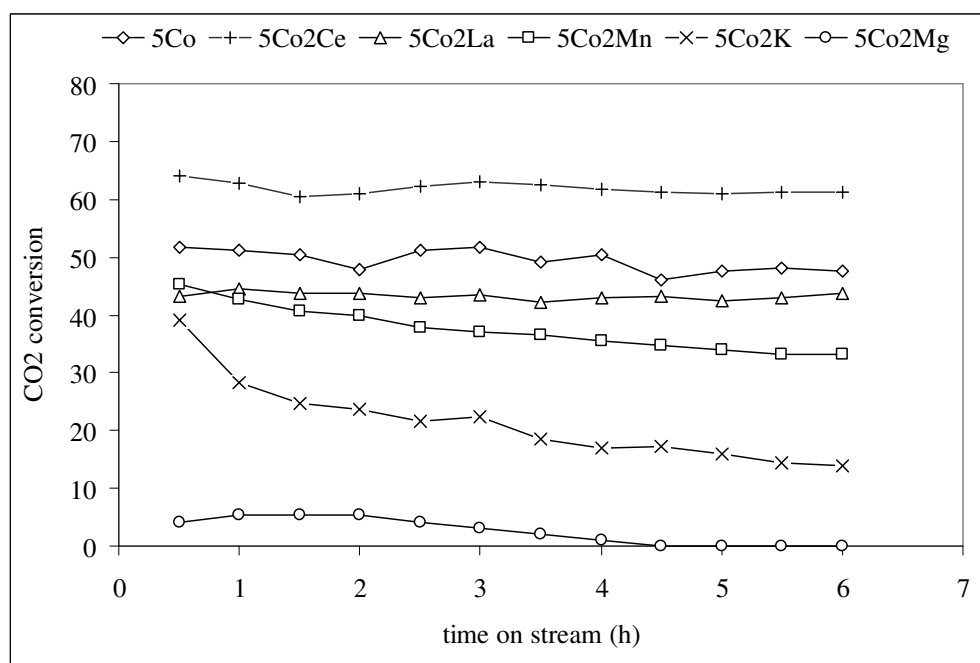


Figure 4.45. Effect of modifier on CO₂ conversion as a function of reaction time. Reaction Temperature = 923 K. CH₄ / CO₂ = 1/1. Space velocity = 60,000 mL/h.g-cat

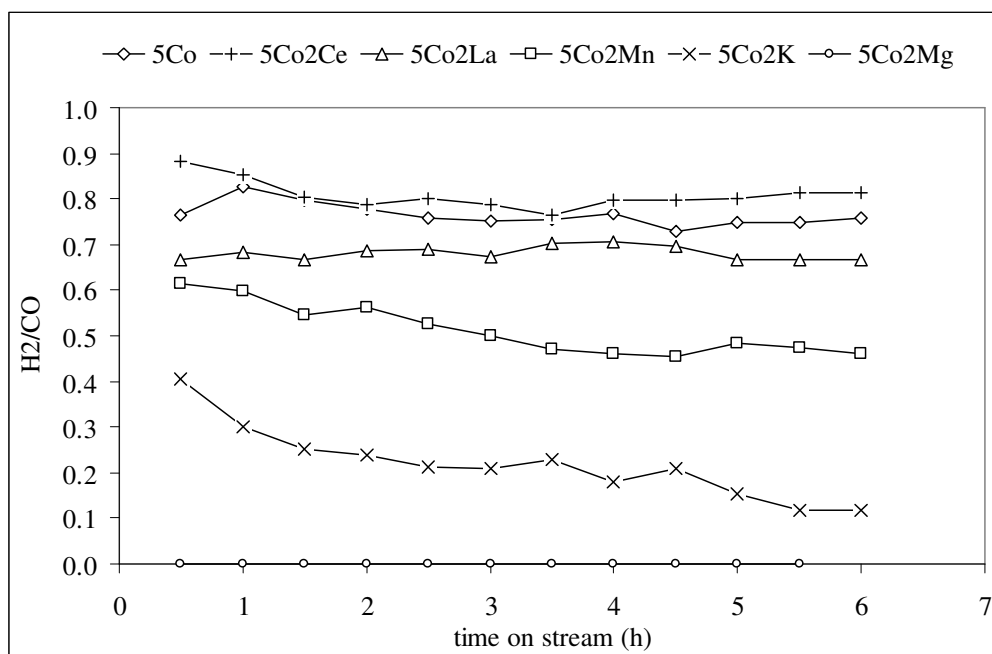


Figure 4.46. Effect of modifier on H₂/CO ratio as a function of reaction time.

Reaction Temperature = 923 K. CH₄ / CO₂ = 1/1. Space velocity = 60,000 mL/h.g-cat

Table 4.22. The effect of modification of cobalt catalyst for CO₂ reforming of methane

Catalyst	CH ₄ Conversion (%)			H ₂ /CO			Coke (wt. %) at the end of 6 h reaction
	0.5 h	3 h	6 h	0.5 h	3 h	6 h	
5Co	52.4	36.1	31.5	0.77	0.75	0.76	4.0
5Co2La	26.2	27.1	27.2	0.67	0.67	0.67	0.2
5Co2K	14.5	7.6	6.8	0.40	0.21	0.12	2.0
5Co2Mn	27.6	25.2	22.3	0.61	0.50	0.46	0.8
5Co2Mg	7.4	0.8	0.0	0.09	-	-	2.6
5Co2Ce	50.8	49.3	48.9	0.88	0.79	0.81	2.0

It is evident from the results that unpromoted Co catalyst was one of the samples having high activity at the beginning of the reaction, but since its resistance to coke deposition is poor, it lost 40 per cent of its initial CH₄ activity. Though the activity level of Co/ZrO₂ is the same as the activity of 5Co2La sample at the end of the 6th hour, La promoted sample did not suffer from any activity loss during the TOS reaction tests. When

the unpromoted sample was characterized by SEM after 6 h of reaction, the formation of filamentous type carbon was also observed over the zirconia surface (Figure 4.47). According to the EDX results on different spots of the SEM image area, the amount of coke deposited over the surface of 5Co catalyst was determined as ca. 50 per cent. This result is parallel to the findings reported by Ji *et al.* (2001), which showed that CDRM over Co catalysts can lead to the formation of the filamentous carbons and the carbon grows in a whiskerlike structure associated with cobalt particles.

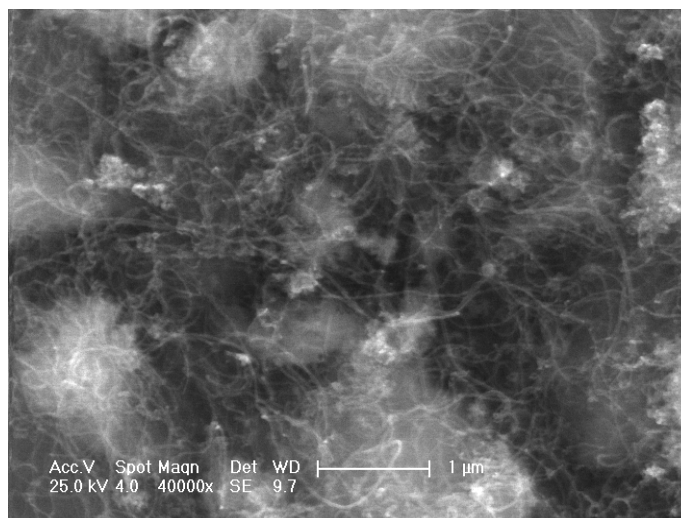


Figure 4.47. Morphology of carbon deposit on the 5Co catalyst after 6h of CDRM reaction

It is noteworthy from Figures 4.44 - 4.46 that introduction of small amount of Ce to the Co/ZrO₂ catalyst led to a superior catalytic performance with the highest CH₄ and CO₂ conversions as well as the highest H₂/CO molar ratios over the whole temperature range. This may be related with (i) the increased amount of surface cobalt (Table 4.21) covering almost the whole ZrO₂ surface and partially covering Ce centers (Figure 4.42), (ii) though partially covered by Co, the enhancement of coke gasification ability of catalyst led by oxygen utilization character of Ce through redox cycle. Ceria is known to be a material with high oxygen storage capacity, which can be combined with other solid materials such as ZrO₂ to make a material that promotes the formation of oxygen vacancies and increases the mobility of oxygen through the lattice (Stagg-Williams *et al.*, 2000; Yao *et al.*, 1997). As explained previously in Section 4.1 for Pt-Ce system, the presence of Ce on the surface creates an additional storage capacity for oxygen coming from ZrO₂ support, it goes

through continuous reduction/oxidation cycle during the reaction producing mobile surface oxygen, and enhance the oxygen transfer; this makes the metal more resistant to carbon deposition.

5Co2Ce sample lost only 3 per cent of its initial activity: the CH₄ conversion decreased from 50.8% at the 0.5th hour of TOS to 48.9% at the end 6th hour of TOS. However; H₂/CO ratio decreased from 0.88 to 0.81 over the whole time-on-stream data. The carbon deposited over the catalyst surface was about 2 per cent. From the SEM images and EDX mappings; it is observed that Co is densely populated on the zirconia support almost covering the entire zirconia support surface and partially hindering the access of reactants to Ce sites, which create additional oxygen to clean the surface from the carbon deposited.

On the other hand; La- promoted catalysts displayed the most stable catalytic profile at a fixed conversion level of ca. 27 per cent and retained the majority of its catalytic activity during the 6h of reaction time. It exhibited a strong resistance for carbon deposition; no carbon deposition was detected over this catalyst both from TGA and SEM-EDX analyses. The main reason for the high and stable activity of 5Co2La sample may be the high and homogeneous dispersion of small-sized metal particles. Previous studies have shown that the addition of promoters to the ZrO₂ support results in increased activity and stability for the reforming reaction (Stagg *et al.*, 1998; Stagg-Williams *et al.*, 2000). It is well established that the addition of La oxides enhances the surface area and the thermal stability of ZrO₂ by stabilizing the tetragonal phase of zirconia (Stagg-Williams *et al.*, 2000; Blom *et al.*, 1994). This stabilization results in an increase in the density of CO₂ adsorption sites near the metal particle due to the basicity of the support (Stagg-Williams *et al.*, 2000). The BET surface areas of freshly reduced Co5 and Co5La2 were measured in order to determine the effect of addition of La on the surface area in this study; BET measurements showed that the total surface area of the Co5La2 sample is 27 m²/g, which is significantly higher than that of Co5 having TSA as 22 m²/g. This increase in BET surface area with La addition results from enhancement of thermal stability of ZrO₂ support by La. The temperature-programmed oxidation studies also show that the La-promoted catalyst had less amount of deposited carbon than either the Ce-promoted or the unpromoted ZrO₂

catalyst after TOS tests. Clearly, lanthanum has promotional effects through improving the stability of the dry reforming catalysts.

The addition of manganese onto zirconia-supported cobalt catalyst also had a stabilizing effect on the CDRM activity through suppressing the formation of coke in some extent; for the Mn-promoted sample, 80 per cent of its activity was maintained after 6 h of reaction. It is observed that addition of Mn also enhances the metal dispersion properties on the surface (Figure 4.41). Yet, its stabilizing effect is not as good as that of the 5Co2La. The deactivation observed for Co-Mn sample as well as the change in H₂/CO production ratio during TOS tests was limited.

K-promoted Co/ZrO₂ started from relatively lower activity levels (ca. 14 per cent) and lost about 50 per cent of its initial CH₄ activity at the end of 6 hour due to coke deposition. H₂/CO ratio decreased drastically from 0.40 to 0.12 over the whole TOS data. Its high coking capacity and the low conversion profile can be attributed to the formation of Co clusters over the surface with large particle size and low metal dispersion properties.

The initial activity of Mg-promoted Co/ZrO₂ was about 7.4 per cent at 0.5 h of TOS and lost all its activity at the end of 3 hour due to coke deposition. Its low activity profile and rapid deactivation can be caused by large Mg and Co metal islands formed over the surface.

4.4.3. Effect of Space Velocity on CDRM Activity

Considering their high activity levels and insignificant activity losses due to their strong coke resistance properties, Co-La and Co-Ce systems were tested further. In order to improve the activity and selectivity (H₂/CO ratio), the effect of space velocity on the catalytic activity and stability of both catalysts was studied (Figures 4.48 & 4.49).

As expected; CH₄ and CO₂ conversions increased with the decrease in space velocity and attained 50% and 61% CH₄ and CO₂ conversion levels, respectively, for La-promoted cobalt catalyst. This sample did not show any significant deactivation with time on stream for ca. 6 h for each space velocity values studied. The coke formation, which was

measured upon reaction tests in each case, was less than 0.3 wt%. In a parallel study over 5Co2Ce sample, both the CH₄ and CO₂ conversions increased with the decrease in space velocity, and leveled off to 63% and 72%, respectively.

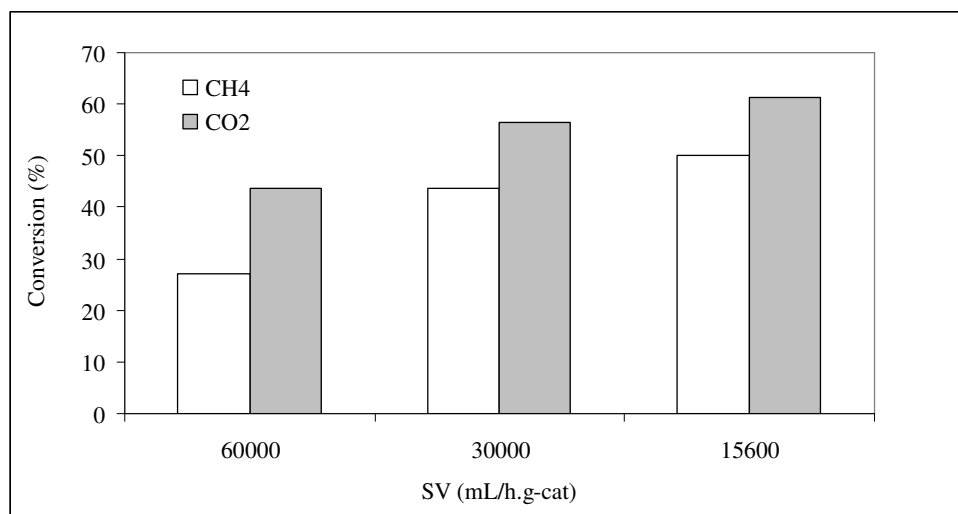


Figure 4.48. Effect of space velocity (SV) on CH₄ and CO₂ conversions. Conversion values measured at the end of 6 h on stream Catalyst: 5Co2La
Reaction Temperature = 923 K. CH₄ / CO₂ = 1/1.

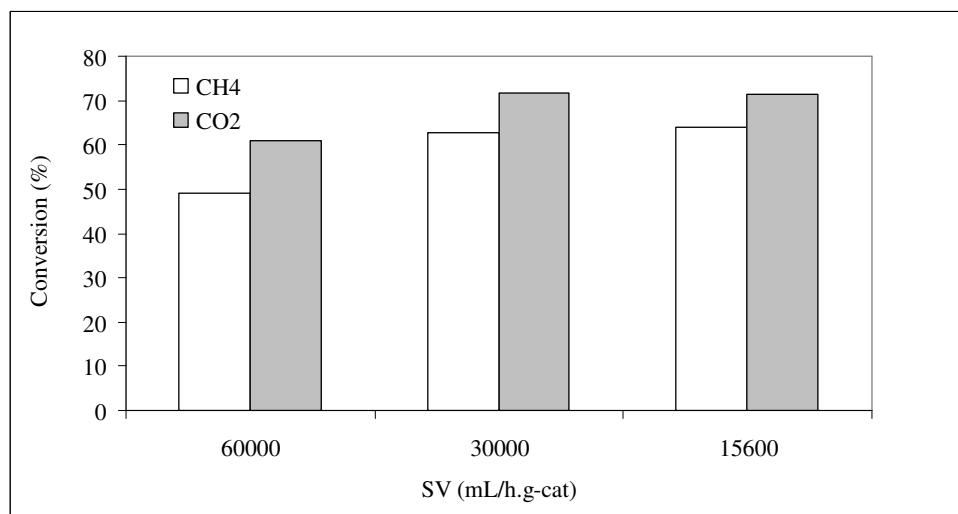


Figure 4.49. Effect of space velocity (SV) on CH₄ and CO₂ conversions. Conversion values measured at the end of 6 h on stream Catalyst: 5Co2Ce
Reaction Temperature = 923 K. CH₄ / CO₂ = 1/1.

4.4.4. Summary

CO₂ reforming of methane was studied over modified Co/ZrO₂ catalysts. The metal modifiers were La, Ce, Mn, Mg and K. The following conclusions can be drawn from the SEM-EDX, TGA and activity data:

- The type of the promoter used significantly affects the metal dispersion properties of the Co/ZrO₂ catalyst.
- Monometallic Co/ZrO₂ has high initial activity but it suffers from severe carbon deposition.
- The different activity levels of the catalysts clearly show that the catalytic performances of promoted-Co/ZrO₂ samples strongly depends on the type of the metal additive used.
- La-modified catalyst exhibited high stability, but moderate activity. It showed no severe coke deposition.
- Ce-doped Co/ZrO₂ displayed the highest activity among all the catalysts prepared and had a very limited activity loss in time-on-stream tests.

5. CONCLUSIONS AND RECOMMENDATIONS

5.1. Conclusions

The overall purpose of this research study was to investigate new catalysts to produce syngas via CO₂ reforming of methane under optimized reaction conditions. The thesis consists of four parts. In the first part of the study; the purpose was to design and develop effective Pt-based bimetallic CDRM catalysts supported on zirconia. Aiming to have bimetallic catalysts with enhanced performance properties, Ce was used as a promoter in order to increase the oxygen storage capacity of the catalysts via controlling the electronic structure of the metals over the support. The major conclusions that can be drawn from the first part of this study can be given as follows:

- Use of cerium was found to be potentially beneficial for CO₂ reforming of methane activity of Pt/ZrO₂. The effects of the Ce on catalyst activity depended on the cerium loading used and impregnation strategy.
- Introduction of 1 wt.% Ce to the Pt/ZrO₂ catalyst via coimpregnation method led to superior catalytic activities and stabilities. The catalyst displayed a significant improvement in the H₂/CO ratio.
- Coimpregnation of Pt and Ce together onto ZrO₂ surface and subsequent high temperature thermal treatment (calcination and reduction at 773 K) have led to strong and extensive Pt-Ce surface interaction, which produced the formation of Ce⁺³ sites and that the presence of Ce⁺³ sites enhanced the dispersion of Pt.
- The existence of Ce⁺³ sites resulted in increased number of oxygen vacancies, which acted as oxygen buffer when going through Ce⁺⁴/Ce⁺³ redox cycle and this led to cleaning of surface from deposited carbon.

In the second part of the thesis, a set of Pt-Ni bimetallic catalysts supported on δ -Al₂O₃ were designed and developed for carbon dioxide reforming of methane as the main reaction in order to determine an effective catalyst with optimum Pt/Ni metal composition assuring both high activity and stability. By changing the Pt/Ni ratios of the catalysts and with the addition of small amounts of either oxygen or water to the feed stream, the

catalysts' resistance to coking reactions were tried to elucidate. The following conclusions can be drawn on the basis of the characterization and catalytic activity data:

- The different activity levels of the catalysts clearly show that the catalytic performances of bimetallic Pt-Ni samples strongly depended on the metal loading and Ni/Pt ratio. Among all the catalysts, 0.3Pt-10Ni catalyst with the lowest Ni/Pt ratio (ca. 110) exhibited the highest catalytic activity and stability over the whole TOS tests in CDRM reaction.
- The carbon formation on the surface of the catalysts depends on the size of nickel metal particles; the higher coke resistance is observed on smaller nickel particles due to the "dilution" effect of Pt that leads to a higher nickel dispersion.
- Easy reduction of nickel oxide species and a better dispersion of nickel metal particles favor the formation of a more reactive intermediate carbonaceous species, thus limiting the deactivation rate.
- 0.3Pt-10Ni catalyst is capable of operating under a variety of feed conditions without significant deactivation and this suggests that 0.3Pt-10Ni catalyst is very promising for synthesis gas production for GTL technology.

Based on the different performance and stability profiles of the Pt-Ni catalysts in part two in response to the changes in their Pt:Ni ratio as well as the reaction conditions, a kinetic and mechanistic study was performed in the third part of the study, which aims to investigate the relation between Pt-Ni loading ratio and kinetics of dry reforming reaction. The conclusions and detailed information provided by the characterization results from the previous section were combined with the present results to propose a plausible mechanistic scheme and a kinetic model of the reaction catalysts with different Pt:Ni ratios. The following conclusions are given as follows:

- The kinetics of CO₂ reforming of methane within the parameter range investigated over 0.3Pt-10Ni and 0.2Pt-15Ni can be expressed by a simple power-law rate equation, with reaction orders of 1 and 1.09 for CH₄ and 0.87 and 1.40 for CO₂, respectively.
- CH₄ consumption rates were found to decrease with increasing CO content. The reaction order with respect to CO in the power-function rate expression is calculated

as -0.26 and -0.41 for 0.3Pt-10Ni and 0.2Pt-15Ni samples, respectively.

- The rate of consumption of methane for 0.2Pt-15Ni sample was found more sensitive to the increase in partial pressure of CO as the reaction order with respect to CO for this sample is 1.6 times the value of that of the 0.3Pt-10Ni catalyst.
- Upon the addition of hydrogen to the feed, the rate of conversion of methane is initially declined for 0.2Pt-15Ni sample whereas it is slightly promoted for 0.3Pt-10Ni sample. However; increasing H₂ partial pressure further had essentially no effect on the CH₄ reforming activity of the both Ni catalysts, as evidenced by the invariance of the rate of methane consumption with increasing H₂ partial pressure.

In the final part of the research, the effect of addition of metal additives to Co/ZrO₂ on both surface micro-structural properties and catalytic performance was investigated. The most promising catalysts with desired micro-structural and catalytic characteristics were chosen for further investigation aimed to optimize the reaction conditions and surface properties. The metal modifiers were La, Ce, Mn, Mg and K. The major conclusions that can be drawn from this section can be given as follows:

- The type of the promoter used significantly affects the metal dispersion properties of the Co/ZrO₂ catalyst.
- Monometallic Co/ZrO₂ has high initial activity but it suffers from severe carbon deposition.
- The different activity levels of the catalysts clearly show that the catalytic performances of promoted-Co/ZrO₂ samples strongly depends on the type of the metal additive used.
- La-modified catalyst exhibited high stability, but moderate activity. It showed no severe coke deposition.
- Ce-doped Co/ZrO₂ displayed the highest activity among all the catalysts prepared and had a very limited activity loss in time-on-stream tests.

5.2. Recommendations

According to the results of the present study, the following points are thought to be beneficial for the future studies on catalytic carbon dioxide reforming of methane:

- The kinetic studies can be performed over a wider range of partial pressures of both methane and carbon dioxide in order to observe the effects of high pressures of each reactant on the reforming activity.
- Ce- and La-promoted Co/ZrO₂ catalysts can also be prepared by coimpregnation method to estimate the effect of impregnation strategy on the reforming performance. By this way, catalytic activity and stability of these catalysts can be further enhanced by the interaction between the metal precursors during the coimpregnation process as in the case of Pt-Ce/ZrO₂ samples.
- Different Co and Ce loadings can be studied to find an optimum Co/Ce ratio, which will prevent the partial coverage of Ce sites by the presence of Co centers. Hence, the stability of Ce-Co/ZrO₂ catalyst can be improved by enabling the access of reactants to the Ce sites, which create additional oxygen to clean the surface from the carbon deposited.
- The effect of heat treatment conditions (calcination temperature and time) on the reforming activity and structural characteristics of Co-X/ZrO₂ can also be investigated.

APPENDIX A: CALIBRATION CURVES OF THE MASS FLOW CONTROLLERS

Calibration curves of the mass flow controllers used in the experiments are given below.

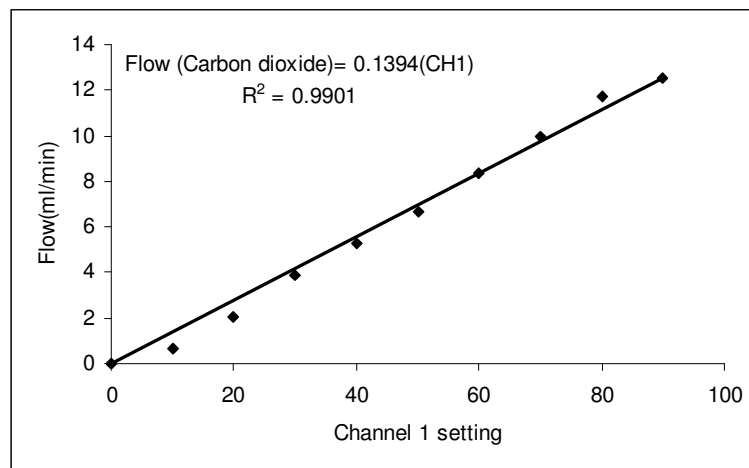


Figure A.1. Calibration curve of the carbon dioxide mass flow controller

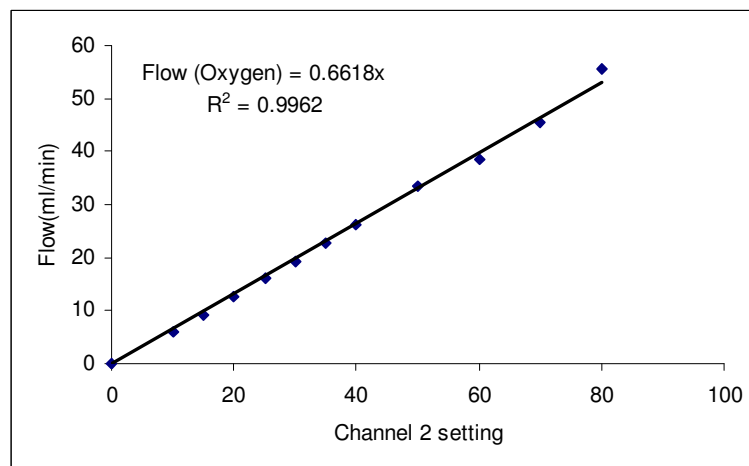


Figure A.2. Calibration curve of the oxygen mass flow controller

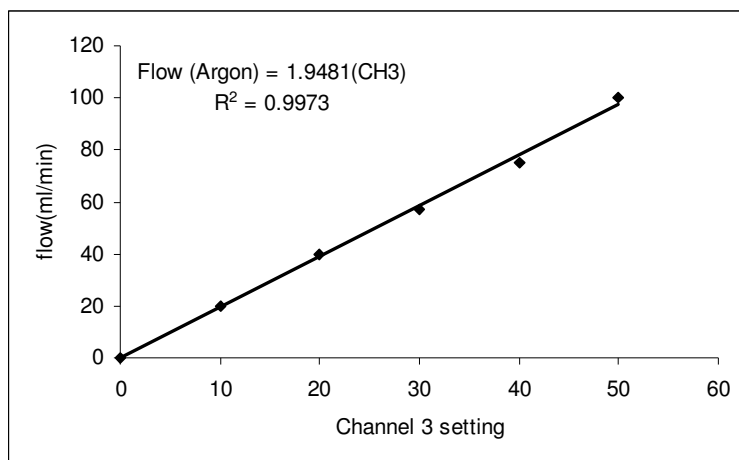


Figure A.3. Calibration curve of the argon mass flow controller

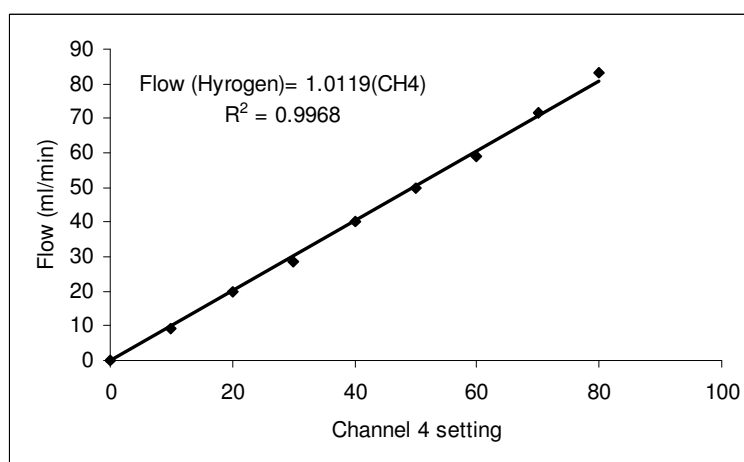


Figure A.4. Calibration curve of the hydrogen mass flow controller

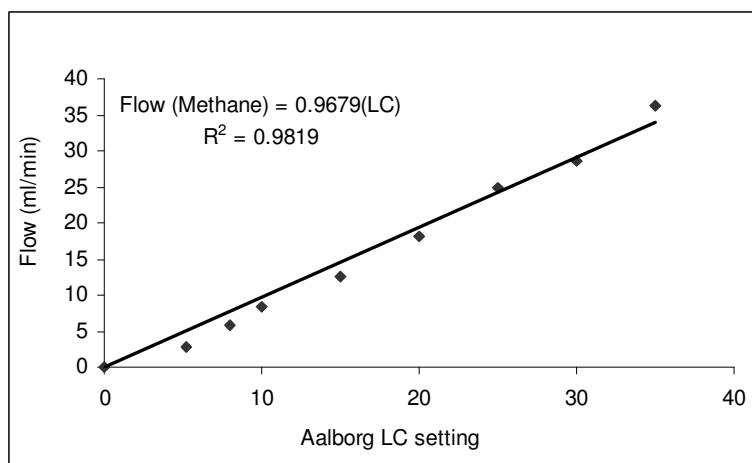


Figure A.5. Calibration curve of the methane mass flow controller

APPENDIX B: CALIBRATION CURVES OF THE GAS CHROMATOGRAPH

Calibration curves of the gas chromatograph used in the experiments are given below.

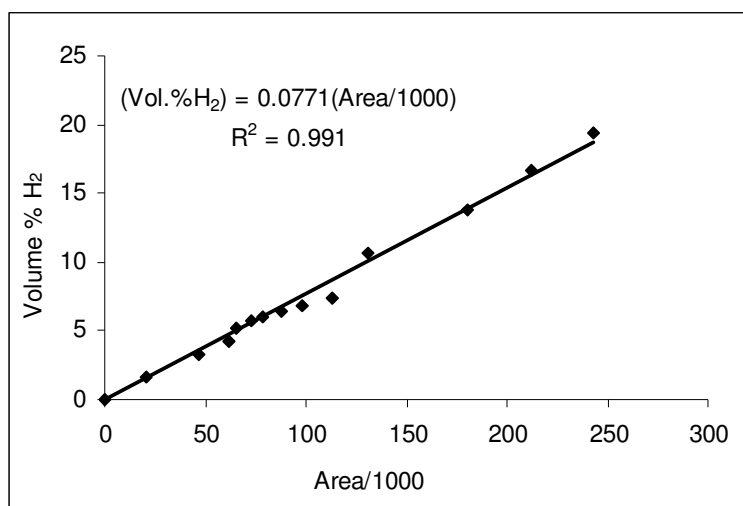


Figure B.1. Calibration curve of hydrogen

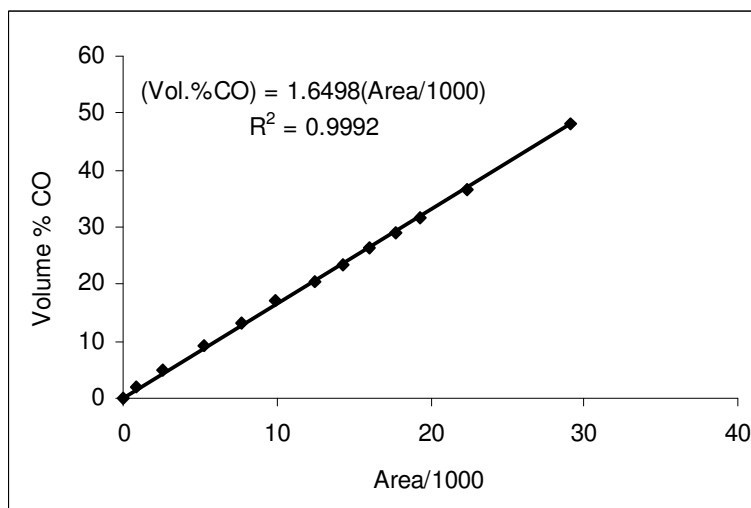


Figure B.2. Calibration curve of carbon monoxide

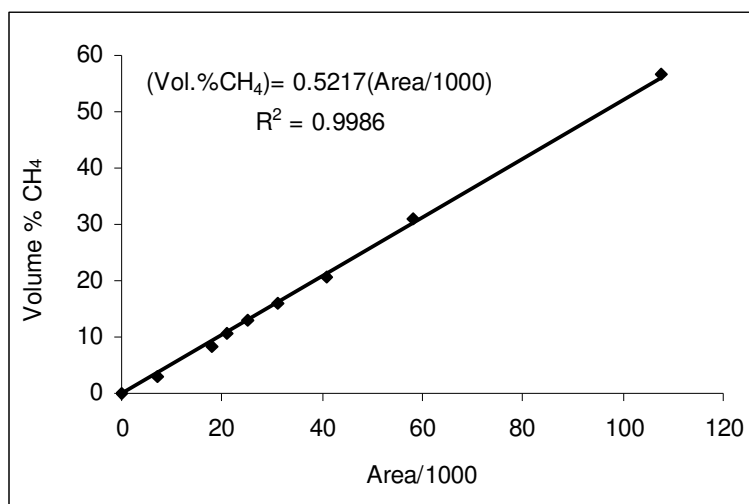


Figure B.3. Calibration curve of methane

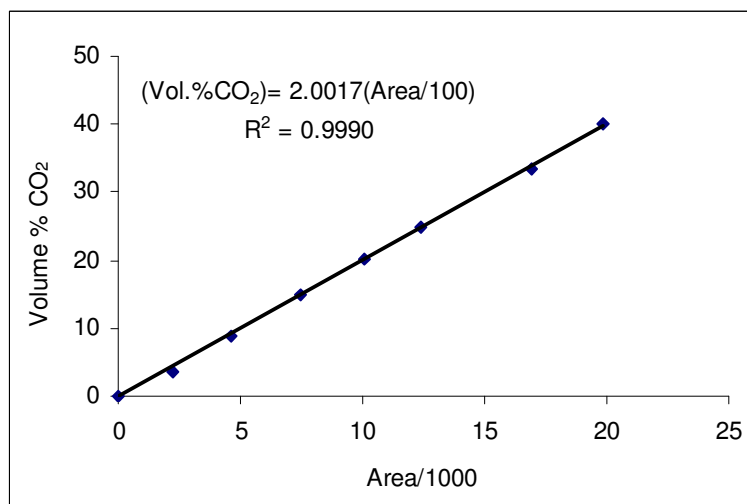


Figure B.4. Calibration curve of carbon dioxide

APPENDIX C: CONVERSION VERSUS RESIDENCE TIME GRAPHS

Methane conversion versus residence time graphs for carbon dioxide reforming of methane are given below.

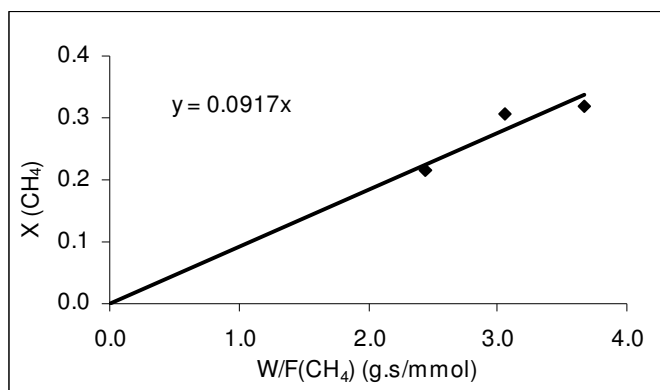


Figure C.1. Fractional CH₄ conversion vs. residence time graph of experiments 1-3.

Catalyst: 0.2Pt-15Ni

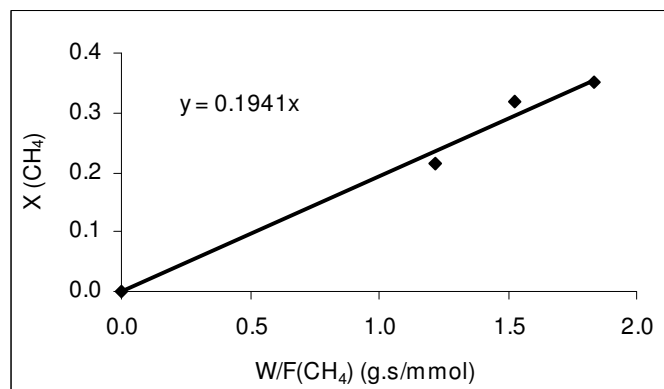


Figure C.2. Fractional CH₄ conversion vs. residence time graph of experiments 4-6.

Catalyst: 0.2Pt-15Ni

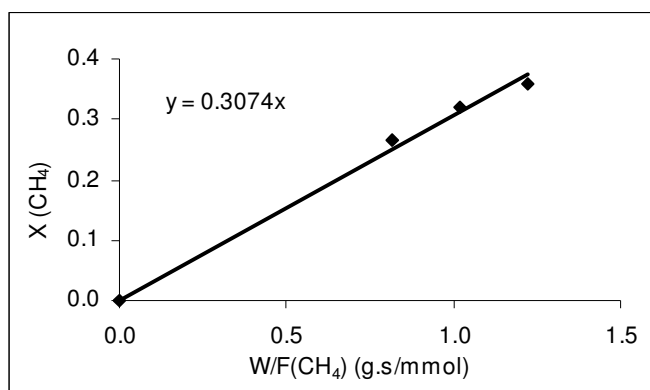


Figure C.3. Fractional CH_4 conversion vs. residence time graph of experiments 7-9.
Catalyst: 0.2Pt-15Ni

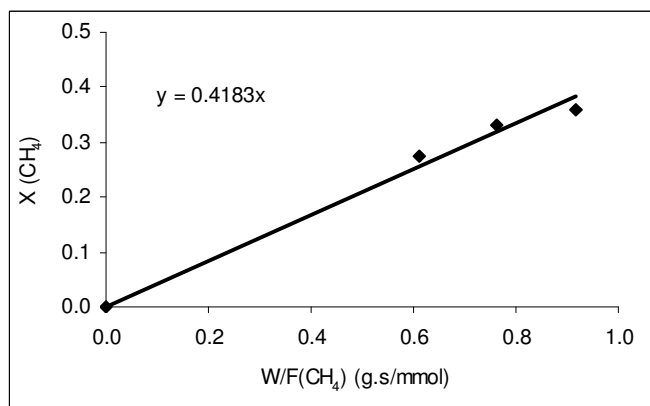


Figure C.4. Fractional CH_4 conversion vs. residence time graph of experiments 10-12.
Catalyst: 0.2Pt-15Ni

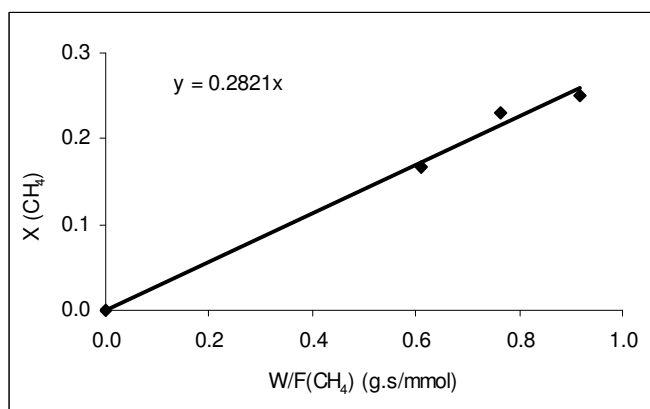


Figure C.5. Fractional CH_4 conversion vs. residence time graph of experiments 13-15.
Catalyst: 0.2Pt-15Ni

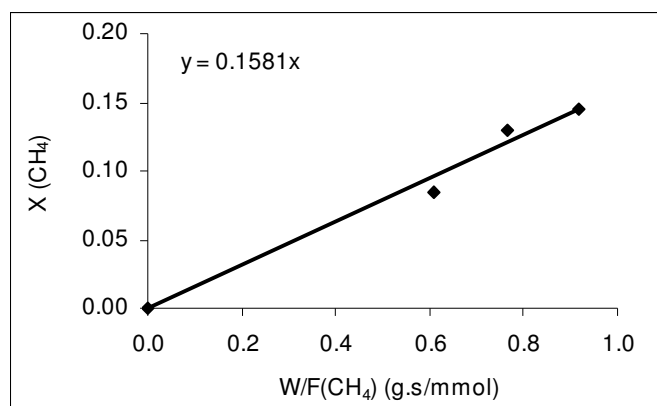


Figure C.6. Fractional CH_4 conversion vs. residence time graph of experiments 16-18.
Catalyst: 0.2Pt-15Ni

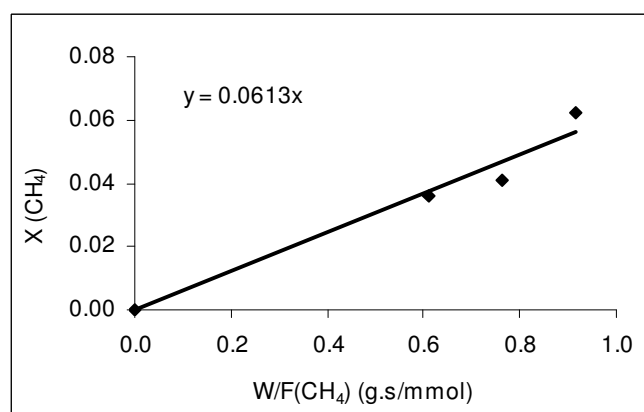


Figure C.7. Fractional CH_4 conversion vs. residence time graph of experiments 19-21.
Catalyst: 0.2Pt-15Ni

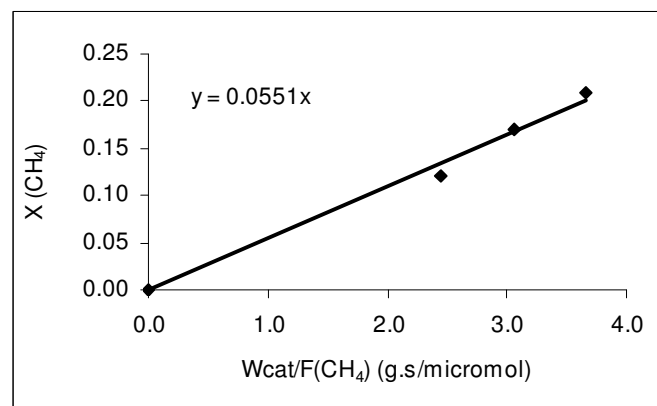


Figure C.8. Fractional CH_4 conversion vs. residence time graph of experiments 1-3.
Catalyst: 0.3Pt-10Ni

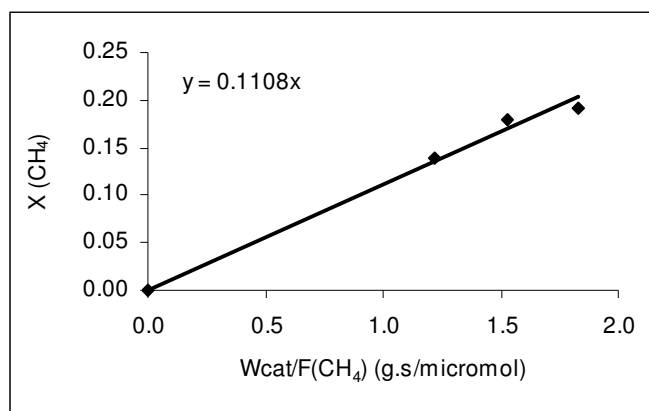


Figure C.9. Fractional CH_4 conversion vs. residence time graph of experiments 4-6.

Catalyst: 0.3Pt-10Ni

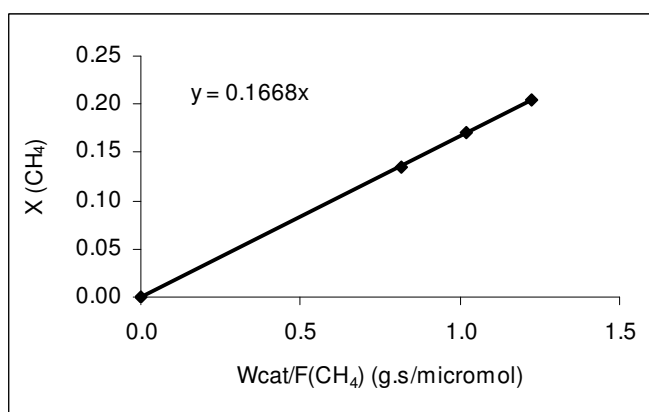


Figure C.10. Fractional CH_4 conversion vs. residence time graph of experiments 7-9.

Catalyst: 0.3Pt-10Ni

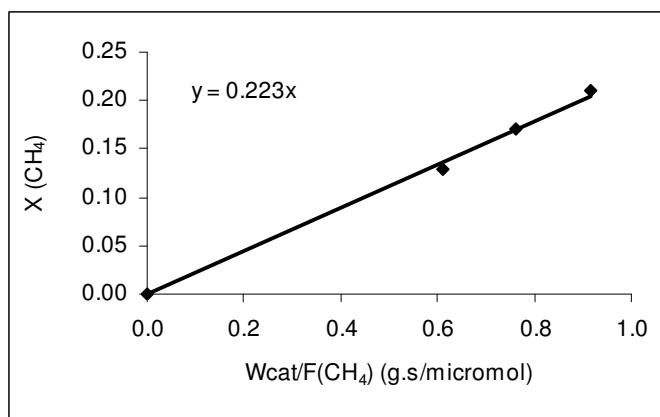


Figure C.11. Fractional CH_4 conversion vs. residence time graph of experiments 10-12.

Catalyst: 0.3Pt-10Ni

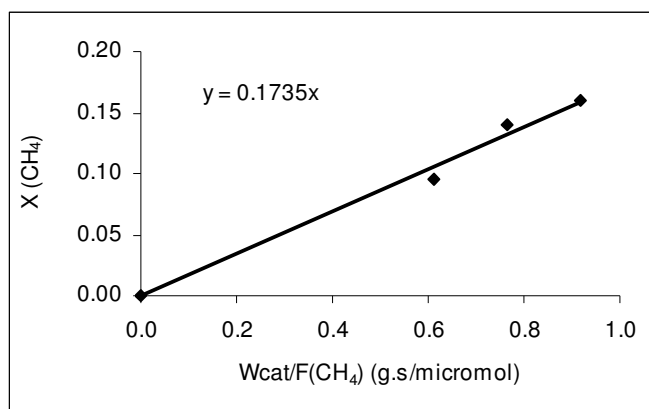


Figure C.12. Fractional CH₄ conversion vs. residence time graph of experiments 13-15.

Catalyst: 0.3Pt-10Ni

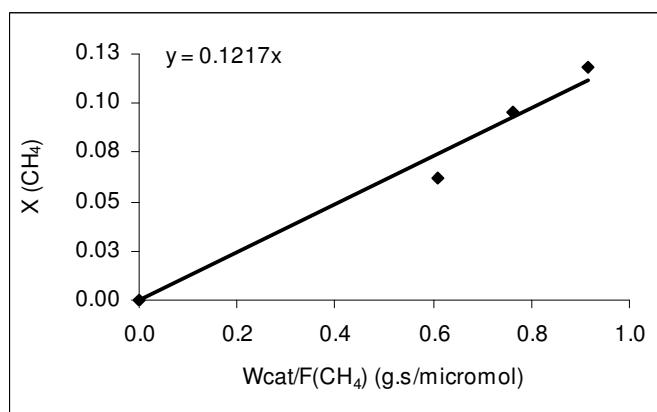


Figure C.13. Fractional CH₄ conversion vs. residence time graph of experiments 16-18.

Catalyst: 0.3Pt-10Ni

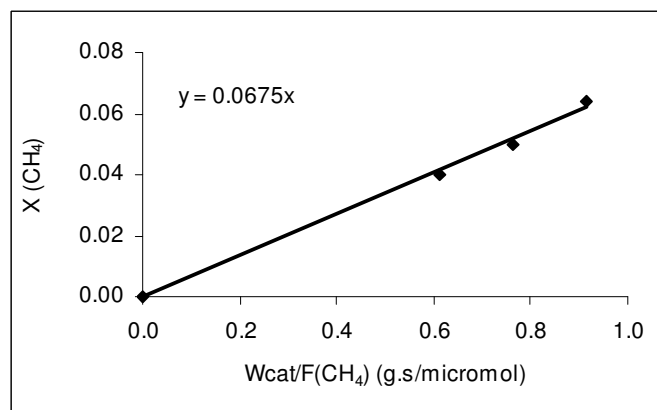


Figure C.14. Fractional CH₄ conversion vs. residence time graph of experiments 19-21.

Catalyst: 0.3Pt-10Ni

REFERENCES

- Akın, A. N., 1996, *Development of Coprecipitated Cobalt-Alumina Catalysts for the Production of C₁-C₄ Hydrocarbons by Carbon Monoxide Hydrogenation*, Ph. D. Dissertation, Boğaziçi University.
- Akpan, E., Y. Sun, P. Kumar, H. Ibrahim, A. Aboudheir and R. Idem, 2006, “Kinetics, Experimental and Reactor Modeling Studies of the Carbon Dioxide Reforming of Methane (CDRM) over a New Ni/CeO₂-ZrO₂ Catalyst in a Packed Bed Tubular Reactor”, *Chemical Engineering Science*, Vol. 62, pp. 4012-4024.
- Aparicio, L.M., 1997, “Transient Isotopic Studies and Microkinetic Modeling of Methane Reforming over Nickel Catalysts”, *Journal of Catalysis*, Vol. 165, pp. 262-274.
- Arai, H. and M. Machida, 1996, “Thermal Stabilization of Catalyst Supports and Their Application to High-Temperature Catalytic combustion”, *Applied Catalysis A: General*, Vol. 138, pp. 161-176.
- Arena, F., F. Frusteri and A. Parmaliana, 1999, “Alkali Promotion of Ni/MgO Catalysts”, *Applied Catalysis A: General*, Vol. 187, pp. 127-140.
- Asami, K., X. Li, K. Fujimoto, Y. Koyama, A. Sakurama, N. Kometani and Y. Yonezawa, 2003, “CO₂ Reforming of CH₄ over Ceria-Supported Metal Catalysts”, *Catalysis Today*, Vol. 84, pp. 27-31.
- Ballarini, A. D., S. R. de Miguel, E. L. Jablonski, O. A. Scelza and A. A. Castro, 2005, “Reforming of CH₄ with CO₂ on Pt-supported Catalysts Effect of the Support on the Catalytic Behaviour”, *Catalysis Today*, Vol. 107-108, pp. 481-486.
- Bartholomew, C. H., 2001, “Mechanisms of Catalyst Deactivation”, *Applied Catalysis A: General*, Vol. 212, pp. 17-60.

- Bitter, J. H., K. Seshan and J. A. Lercher, 1997, "The State of Zirconia Supported Platinum Catalysts for CO₂/CH₄ Reforming", *Journal of Catalysis*, Vol. 171, pp. 279-286.
- Blom, R., I. M. Dahl, A. Slagtern, B. Sortland, A. Spjelkavik and E. Tangstad, 1994, "Carbon Dioxide Reforming of Methane over Lanthanum-modified Catalysts in a Fluidized-bed Reactor", *Catalysis Today*, Vol. 21, pp. 535- 543.
- Bozo, C., N. Guilhaume, E. Garbowski and M. Primet, 2000, "Combustion of Methane on CeO₂-ZrO₂ Based Catalysts", *Catalysis Today*, Vol. 59, pp. 33-45.
- Bradford, M. C. J. and M. A. Vannice, 1996, "Catalytic Reforming of Methane with Carbon Dioxide over Nickel Catalysts II. Reaction Kinetics" *Applied Catalysis A: General*, Vol. 142, pp. 97-122.
- Bradford, M. C. J. and M. A. Vannice, 1998, "CO₂ Reforming of CH₄ over Supported Pt Catalysts", *Journal of Catalysis*, Vol. 173, pp. 157-171.
- Bradford, M. C. J. and M. A. Vannice, 1999, "CO₂ Reforming of CH₄", *Catalysis Reviews-Science and Engineering*, Vol. 41, pp. 1-42.
- Burroughs, P., A. Hammett, A. F. Orchard and G. Thornton, 1976, "Satellite Structure in X-Ray Photoelectron-Spectra of Some Binary and Mixed Oxides of Lanthanum and Cerium", *Journal of the Chemical Society-Dalton Transactions*, Vol. 17, pp. 1686-1698.
- Chang, J.S., S.E. Park, K.W. Lee and M.J. Choi, "Catalytic Reforming of Methane with Carbon-Dioxide over Pentasil Zeolite-Supported Nickel-Catalyst", *Studies in Surface Science and Catalysis*, Vol. 84, pp. 1587-1594.
- Chang, J. S., S. E. Park, J. W. Yoo and J. N. Park, 2000, "Catalytic Behavior of Supported KNiCa Catalyst and Mechanistic Consideration for Carbon Dioxide Reforming of Methane", *Journal of Catalysis*, Vol. 195, pp. 1-11.

- Chen, Y. G. and J. Ren, 1994, "Conversion of Methane and Carbon-Dioxide into Synthesis Gas over Alumina-Supported Nickel-Catalysts: Effect of Ni-Al₂O₃ Interactions", *Catalysis Letters*, Vol. 29, pp. 39-48.
- Chen, H. W., C. Y. Wang, C. H. Yu, L. T. Tseng and P. H. Liao, 2004, "Carbon Dioxide Reforming of Methane Reaction Catalyzed by Stable Nickel Copper Catalysts", *Catalysis Today*, Vol. 97, pp. 173-180.
- Cheng, Z., Q. Wu, J. Li and Q. Zhu, 1996, "Effects of Promoters and Preparation Procedures on Reforming of Methane with Carbon Dioxide over Ni/Al₂O₃ Catalyst", *Catalysis Today*, Vol. 30, pp. 147-155.
- Cheng, Z.X., X.G. Zhao, J.L. Li and Q.M. Zhu, 2001, "Role of Support in CO₂ Reforming of CH₄ over a Ni/ γ -Al₂O₃ Catalyst", *Applied Catalysis A: General*, Vol. 205, pp. 31-36.
- Choi, J.S., K.I. Moon, Y.G. Kim, J.S. Lee, C.H. Kim and D.L. Trimm, 1998, "Stable Carbon Dioxide Reforming of Methane over Modified Ni/Al₂O₃ Catalysts", *Catalysis Letters*, Vol.52, pp. 43-47.
- Choudhary, V. R., A. M. Rajput and B. Prabhakar, 1995, "Energy-Efficient Methane-to-Syngas Conversion with Low H₂/CO Ratio by Simultaneous Catalytic Reactions of Methane with Carbon-Dioxide and Oxygen", *Catalysis Letters*, Vol. 32, pp. 391-396.
- Choudhary, V. R., V. H. Rane and A. M. Rajput, 1997, "Beneficial Effects of Cobalt Addition to Ni-Catalysts for Oxidative Conversion of Methane to Syngas", *Applied Catalysis A: General*, Vol. 162, pp. 235-238.
- Choudhary, V.R. and A.S. Mamman, 1998, "Simultaneous Oxidative Conversion and CO₂ or Steam Reforming of Methane to Syngas over CoO-NiO-MgO Catalyst", *Journal of Chemical Technology and Biotechnology*, Vol. 73, pp. 345-350.

- Choudhary, V. R. and K. C. Mondal, 2006, "CO₂ Reforming of Methane Combined with Steam Reforming or Partial Oxidation of Methane to Syngas over NdCoO₃ Perovskite-type Mixed Metal-Oxide Catalyst", *Applied Energy*, Vol. 83, pp. 1024-1032.
- Claridge, J. B., A. P. E. York, A.J. Brungs, C. Marquez-Alvarez, J. Sloan, S. C. Tsang and M. L. H. Green, 1998, "New Catalysts for the Conversion of Methane to Synthesis Gas: Molybdenum and Tungsten Carbide", *Journal of Catalysis*, Vol. 180, pp. 85-100.
- Crisafulli, C., S. Scire, R. Maggiore, S. Minico and S. Galvagno, 1999, "CO₂ Reforming of Methane over Ni–Ru and Ni–Pd Bimetallic Catalysts", *Catalysis Letters*, Vol. 59, pp. 21-26.
- Crisafulli, C., S. Scire, S. Minico and L. Solarina, 2002, "Ni–Ru Bimetallic Catalysts for the CO₂ Reforming of Methane", *Applied Catalysis A: General*, Vol. 225, pp. 1-9.
- Cui, Y., H. Xu, Q. Ge, Y. Wang, S. Hou and W. Li, 2006, "Structure Sensitive Dissociation of CH₄ on Ni/ α -Al₂O₃: Ni Nano-Scale Particles Linearly Compensate the E_a and $\ln A$ for the CH₄ Pulse Kinetics", *Journal of Molecular Catalysis A: Chemical*, Vol. 249, pp. 53-59.
- Cui, Y., H. Zhang, H. Xu and W. Li, 2007, "Kinetic Study of the Catalytic Reforming of CH₄ with CO₂ to Syngas over Ni/ α -Al₂O₃ Catalyst: The Effect of Temperature on the Reforming Mechanism", *Applied Catalysis A: General*, Vol. 318, pp. 79–88.
- Çağlayan, B. S., A. K. Avcı, Z. İ. Önsan and A. E. Aksoylu, 2005, "Production of Hydrogen over Bimetallic Pt–Ni/ δ -Al₂O₃ I. Indirect Partial Oxidation of Propane", *Applied Catalysis A: General*, Vol. 280, pp. 181-188.
- Damyanova, S. and J. M. C. Bueno, 2003, "Effect of CeO₂ Loading on the Surface and Catalytic Behaviors of CeO₂-Al₂O₃-Supported Pt Catalysts", *Applied Catalysis A: General*, Vol. 253, pp. 135-150.

- Damyanova, S., B. Pawelec, K. Arishtirova, M.V. Martinez Huerta and J.L.G. Fierro, 2008, "Study of the Surface and Redox Properties of Ceria-Zirconia Oxides", *Applied Catalysis A: General*, Vol. 337, pp. 86-96.
- Dias, J. A. C. and J. M. Assaf, 2004, "Autothermal Reforming of Methane over Ni/ γ -Al₂O₃ Catalysts: The Enhancement Effect of Small Quantities of Noble Metals", *Journal of Power Sources*, Vol. 130, pp. 106-110.
- Dias, J. A. C. and J. M. Assaf, 2005, "Autoreduction of Promoted Ni/ γ -Al₂O₃ during Autothermal Reforming of Methane", *Journal of Power Sources*, Vol. 139, pp. 176-181.
- Djaidja, A., S. Libs, A. Kiennemann and A. Barama, 2006, "Characterization and Activity in Dry Reforming of Methane on NiMg/Al and Ni/MgO Catalysts", *Catalysis Today*, Vol. 113, pp. 194-200.
- Efstathiou, A. M., A. Kladi, V. A. Tsipouriari and X. E. Verykios, 1996, "Reforming of Methane with Carbon Dioxide to Synthesis Gas over Supported Rhodium Catalysts: II. A Steady-State Tracing Analysis: Mechanistic Aspects of the Carbon and Oxygen Reaction Pathways to Form CO", *Journal of Catalysis*, Vol. 158, pp.64-75.
- Erdöhelyi, A., J. Cserenyi, E. Papp and F. Solymosi, 1994, "Catalytic Reaction of Methane with Carbon-Dioxide over Supported Palladium", *Applied Catalysis A: General*, Vol. 108, pp. 205-219.
- Ernst, B., L. Hilaire and A. Kiennemann, 1999, "Effects of Highly Dispersed Ceria Addition on Reducibility, Activity and Hydrocarbon Chain Growth of a Co/SiO₂ Fischer-Tropsch Catalyst", *Catalysis Today*, Vol. 50, pp. 413-427.
- Farrauto, R. J. and R. M. Heck, 1999, "Catalytic Converters: State of the Art and Perspectives", *Catalysis Today*, Vol. 51, pp. 351-360.

- Fischer, F. and H. Tropsch, 1928, "Conversion of Methane into Hydrogen and Carbon Monoxide", *Brennst.-Chem.*, Vol. 9, pp.39-46.
- Ferreira-Aparicio, P., A. Guerrero-Ruiz and I. Rodríguez-Ramos, 1998, "Comparative Study at Low and Medium Reaction Temperatures of Syngas Production by Methane Reforming with Carbon Dioxide over Silica and Alumina Supported Catalysts", *Applied Catalysis A: General*, Vol. 170, pp. 177-187.
- Ferreira-Aparicio, P., I. Rodríguez-Ramos, J. A. Anderson and A. Guerrero-Ruiz, 2000, "Mechanistic Aspects of the Dry Reforming of Methane over Ruthenium Catalysts", *Applied Catalysis A: General*, Vol. 202, pp. 183-196.
- Forzatti, P. and L. Lietti, 1999, "Catalyst Deactivation", *Catalysis Today*, Vol. 52, pp. 165-181.
- Goodman, D. W., R. D. Kelley, T. E. Madey and J. T. Yates, 1980, "Kinetics of the Hydrogenation of CO over a Single Crystal Nickel Catalyst", *Journal of Catalysis*, Vol. 63, pp. 226-234.
- Gronchi, P., D. Fumagalli, R. DelRosso and P. Centola, 1996, "Carbon Deposition in Methane Reforming with Carbon Dioxide - Dry Reforming", *Journal of Thermal Analysis*, Vol. 47, pp. 227-234.
- Guerrero-Ruiz, A., A. Sepúlveda-Escribano and I. Rodríguez-Ramos, 1994, "Cooperative Action of Cobalt and MgO for the Catalysed Reforming of CH₄ with CO₂", *Catalysis Today*, Vol. 21, pp. 545-550.
- Gulyuz, B, 2007, *Kinetics of Low Temperature CO Oxidation over Activated Carbon Supported Pt-CeO_x Catalyst*, M.S. Thesis, Boğaziçi University.
- Guo, J., H. Lou, H. Zhao, D. Chai and X. Zheng, 2004, "Dry Reforming of Methane over Nickel Catalysts Supported on Magnesium Aluminate Spinels", *Applied Catalysis A: General*, Vol. 273, pp. 75-82.

- Hashimoto, K., S. Watase and N. Toukai, 2002, "Reforming of Methane with Carbon Dioxide over a Catalyst Consisting of Ruthenium Metal and Cerium Oxide Supported on Mordenite", *Catalysis Letters*, Vol. 80, pp. 147-152.
- Hegarty, M. E. S., A. M. O'Connor and J. R. H. Ross, 1998, "Syngas Production from Natural Gas Using ZrO₂-supported Metals", *Catalysis Today*, Vol. 42, pp. 225-232.
- Holmgren, A. and B. Andersson, 1998, "Oxygen Storage Dynamics in Pt/CeO₂/Al₂O₃ Catalysts", *Journal of Catalysis*, Vol. 178, pp. 14-25.
- Hou, Z., O. Yokota, T. Tanaka and T. Yashima, 2003a, "A Novel KCaNi/ α -Al₂O₃ Catalyst for CH₄ Reforming with CO₂", *Catalysis Letters*, Vol. 87, pp. 37-42.
- Hou, Z., and T. Yashima, 2003b, "Small Amounts of Rh-Promoted Ni Catalysts for Methane Reforming with CO₂", *Catalysis Letters*, Vol. 89, pp. 193-197.
- Hou, Z., O. Yokota, T. Tanaka and T. Yashima, 2004a, "Surface Properties of a Coke-Free Sn Doped Nickel Catalyst for the CO₂ Reforming of Methane", *Applied Surface Science*, Vol. 233, pp. 58-68.
- Hou, Z. and T. Yashima, 2004b, "Meso-porous Ni/Mg/Al Catalysts for Methane Reforming with CO₂", *Applied Catalysis A: General*, Vol.261, pp. 205-209.
- Hou, Z., P. Chen, H. Fang, X. Zheng, and T. Yashima, 2006, "Production of Synthesis Gas via Methane Reforming with CO₂ on Noble Metals and Small Amount of Noble-(Rh) Promoted Ni Catalysts", *International Journal of Hydrogen Energy*, Vol. 31, pp. 555-561.
- Horiuchi, T., K. Sakuma, T. Fukui, Y. Kubo, T. Osaki and T. Mori, 1996, "Suppression of Carbon Deposition in the CO₂-reforming of CH₄ by Adding Basic Metal Oxides to a Ni/Al₂O₃ Catalyst", *Applied Catalysis A: General*, Vol. 144, pp. 111-120.

- Hu, Y.H. and E. Ruckenstein, 1996, "Temperature-Programmed Desorption of CO Adsorbed on NiO/MgO", *Journal of Catalysis*, Vol. 163, pp. 306-311.
- Hwang, K. S., H.Y. Zhu and G.Q. Lu, 2001, "New Nickel Catalysts Supported on Highly Porous Alumina Intercalated Laponite for Methane Reforming with CO₂", *Catalysis Today*, Vol. 68, pp. 183-190.
- Inui, T., K. Saigo, Y. Fujii and K. Fujioka, 1995, "Catalytic Combustion of Natural Gas as the Role of on-site Heat Supply in Rapid Catalytic CO₂-H₂O Reforming of Methane", *Catalysis Today*, Vol. 26, pp. 295-302.
- Irusta, S., L. M. Cornaglia and E.A. Lombardo, 2002, "Hydrogen Production using Ni-Rh on La₂O₃ as Potential Low-Temperature Catalysts for Membrane Reactors", *Journal of Catalysis*, Vol. 210, pp. 7-16.
- Iyer, M. V., 2001, *New Catalysts for Syngas Production from Carbon Dioxide and Methane*, Ph. D. Dissertation, West Virginia University..
- Ji, L., S. Tang, H. C. Zeng, J. Lin and K. L. Tan, 2001, "CO₂ Reforming of Methane to Synthesis Gas over Sol-Gel Made Co/ γ -Al₂O₃ Catalysts from Organometallic Precursors", *Applied Catalysis A: General*, Vol. 207, pp. 247-255.
- Józwiak, W.K., M. Nowosielska and J. Rynkowski, 2005, "Reforming of Methane with Carbon Dioxide over Supported Bimetallic Catalysts Containing Ni and Noble Metal I. Characterization and Activity of SiO₂ Supported Ni-Rh Catalysts", *Applied Catalysis A: General*, Vol. 280, pp. 233-244.
- Juan-Juan, J., M.C. Román-Martinez and M.J. Illán-Gómez, 2004, "Catalytic Activity and Characterization of Ni/Al₂O₃ and NiK/Al₂O₃ Catalysts for CO₂ Methane Reforming", *Applied Catalysis A: General*, Vol. 264, pp. 169-174.

- Juan-Juan, J., M.C. Román-Martinez and M.J. Illán-Gómez, 2006, "Effect of Potassium Content in the Activity of K-Promoted Ni/Al₂O₃ Catalysts for the Dry Reforming of Methane", *Applied Catalysis A: General*, Vol. 301, pp. 9-15.
- Jung, K. T. and A. T. Bell, 2000, "The Effects of Synthesis and Pretreatment Conditions on the Bulk Structure and Surface Properties of Zirconia", *Journal of Molecular Catalysis A: Chemical*, Vol. 163, pp. 27-42.
- Kašpar, J., P. Fornasiero and M. Graziani, 1999, "Use of CeO₂-based Oxides in the Three-Way Catalysis", *Catalysis Today*, Vol. 50, pp.285-298.
- Kozlov, A. I., D. H. Kim, A. Yezerets and P. Anderson, H. H. Kung and M. C. Kung, 2002, "Effect of Preparation Method and Redox Treatment on the Reducibility and Structure of Supported Ceria-Zirconia Mixed Oxide", *Journal of Catalysis*, Vol. 209, pp. 417-426.
- Kroll, V.C.H., H.M. Swaan and C. Mirodatos, 1996a, "Methane Reforming Reaction with Carbon Dioxide over Ni/SiO₂ Catalyst: I. Deactivation Studies", *Journal of Catalysis*, Vol. 161, pp. 409-422.
- Kroll, V. C. H., H. M. Swaan, S. Lacombe and C. Mirodatos, 1996b, "Methane Reforming Reaction with Carbon Dioxide over Ni/SiO₂Catalyst II. A Mechanistic Study", *Journal of Catalysis*, Vol. 164, pp. 387-398.
- Laachir, A., V. Perrichon, A. Badri, J. Lamotte, E. Catherine, J.C. Lavalley, J. El Fallah, L. Hilaire, F. le Normand, E. Quemere, N.S. Sauvion and O. Touret, 1991, "Reduction of CeO₂ by Hydrogen - Magnetic-Susceptibility and Fourier-Transform Infrared, Ultraviolet and X-Ray Photoelectron-Spectroscopy Measurements", *Journal of the Chemical Society-Faraday Transactions*, Vol. 87, pp. 1601-1609.
- Lassi, U., 2003, "Deactivation Correlations of Pd/Rh Three-way Catalysts Designed for Euro IV Emission Limits. Effect of Ageing Atmosphere, Temperature and Time", Ph.D. Dissertation, University of Oulu.

- Lee, J. H., E. G. Lee, O. S. Joo and K. D. Jung, 2004, "Stabilization of Ni/Al₂O₃ Catalyst by Cu Addition for CO₂ Reforming of Methane", *Applied Catalysis A: General*, Vol. 269, pp. 1-6.
- Lemonidou, A. A. and I. A. Vasalos, 2002, "Carbon Dioxide Reforming of Methane over 5 wt.% Ni/CaO-Al₂O₃ Catalyst", *Applied Catalysis A: General*, Vol. 228, pp. 227-235.
- Luo, J. Z., Z. L. Yu, C. F. Ng and C. T. Au, 2000, "CO₂/CH₄ Reforming over Ni-La₂O₃/5A: An Investigation on Carbon Deposition and Reaction Steps", *Journal of Catalysis*, Vol. 194, pp. 198-210.
- Mark, F. M., F. Mark and W. F. Maier, 1997, "Reaction Kinetics of the CO₂ Reforming of Methane", *Chemical Engineering & Technology*, Vol. 20, pp. 361-370.
- Martinez, R., E. Romero, C. Guimon and R. Bilboa, 2004, "CO₂ Reforming of Methane over Coprecipitated Ni-Al Catalysts Modified with Lanthanum", *Applied Catalysis A: General*, Vol. 274, pp. 139-149.
- Matsukata, M., T. Matsushita and K. Ueyama, 1995, "A Circulating Fluidized-Bed CH₄ Reformer - Performance of Supported Ni Catalysts", *Energy and Fuels*, Vol. 9, pp. 822 – 828.
- Matsukata, M., T. Matsushita and K. Ueyama, 1996, "A Novel Hydrogen/Syngas Production Process: Catalytic Activity and Stability of Ni/SiO₂", *Chemical Engineering Science*, Vol. 51, pp. 2769- 2774.
- Mattos, L. V., E. Rodino, D.E. Resasco, F. B. Passos and F.B. Noronha, 2003, "Partial Oxidation and CO₂ Reforming of Methane on Pt/Al₂O₃, Pt/ZrO₂, and Pt/Ce-ZrO₂ Catalysts", *Fuel Processing Technology*, Vol. 83, pp.147-161.

- Menad, S., P. Ferreira-Aparaicio, O. Cherifi, A. Guerrero-Ruiz and I. Rodriguez-Ramos, 2003, "Designing New High Oxygen Mobility Supports to Improve the Stability of Ru Catalysts under Dry Reforming of Methane", *Catalysis Letters*, Vol. 89, pp. 63-67.
- Monteiro, R. S., L. C. Dieguez and M. Schmal, 2001, "The Role of Pd Precursors in the Oxidation of Carbon Monoxide over Pd/Al₂O₃ and Pd/CeO₂/Al₂O₃ Catalysts", *Catalysis Today*, Vol. 65, pp. 77-89.
- Montoya, J.A., E. Romero-Pascual, C. Gimón, P. Del Angel and A. Monzón, 2000, "Methane Reforming with CO₂ over Ni/ZrO₂-CeO₂ Catalysts Prepared by Sol-Gel", *Catalysis Today*, Vol. 63, pp. 71-85.
- Nagaoka, K., K. Seshan, K. Aika and J. A. Lercher, 2001a, "Carbon Deposition during Carbon Dioxide Reforming of Methane-Comparison between Pt/Al₂O₃ and Pt/ZrO₂", *Journal of Catalysis*, Vol. 197, pp. 34-42.
- Nagaoka, K., M. Okamura and K. Aika, 2001b, "Titania Supported Ruthenium as a Coking-Resistant Catalyst for High Pressure Dry Reforming of Methane", *Catalysis Communications*, Vol. 2, pp. 255-260.
- Nagaoka, K., K. Takanabe and K. Aika, 2004, "Modification of Co/TiO₂ for Dry Reforming of Methane at 2MPa by Pt, Ru or Ni", *Applied Catalysis A: General*, Vol. 268, pp. 151-158.
- Nandini, A., K.K. Pant and S.C. Dhingra, 2005, "K-, CeO₂-, and Mn-Promoted Ni/Al₂O₃ Catalysts for Stable CO₂ Reforming of Methane", *Applied Catalysis A: General*, Vol. 290, pp. 166-174.
- Nandini, A., K.K. Pant and S.C. Dhingra, 2006, "Kinetic Study of the Catalytic Carbon Dioxide Reforming of Methane to Synthesis Gas over Ni-K/CeO₂-Al₂O₃ Catalyst", *Applied Catalysis A: General*, Vol.308, pp. 119-127.

- Noronha, F. B., A. Shamsi, C. Taylor, E. C. Fendley, S. Stagg-Williams and D. E. Resasco, 2003, "Catalytic Performance of Pt/ZrO₂ And Pt/Ce-ZrO₂ Catalysts on CO₂ Reforming of CH₄ Coupled with Steam Reforming or under High Pressure", *Catalysis Letters*, Vol. 90, pp. 13-21.
- Noronha, F. B., E. C. Fendley, R. R. Soares, W. E. Alvarez and D. E. Resasco, 2001, "Correlation between Catalytic Activity and Support Reducibility in the CO₂ Reforming of Methane over Pt/Ce_xZr_{1-x}O₂ Catalysts", *Chemical Engineering Journal*, Vol. 82, pp. 21-31.
- O'Connor, A. M. and J. R. H. Ross, 1998, "The Effect of O₂ Addition on the Carbon Dioxide Reforming of Methane over Pt/ZrO₂ Catalysts", *Catalysis Today*, Vol. 46, pp. 203-210.
- Olsbye, U., T. Wurzel and L. Mleczko, 1997, "Kinetic and Reaction Engineering Studies of Dry Reforming of Methane over a Ni/La/Al₂O₃ Catalyst", *Industrial & Engineering Chemistry Research*, Vol. 36, pp. 5180-5188.
- Osaki, T., H. Fukaya, T. Horiuchi, K. Suzuki and T. Mori, 1998, "Isotope Effect and Rate-Determining Step of the CO₂-Reforming of Methane over Supported Ni Catalyst", *Journal of Catalysis*, Vol. 180, pp. 106-109.
- Osaki, T. and T. Mori, 2001, "Role of Potassium in Carbon-Free CO₂ Reforming of Methane on K-Promoted Ni/Al₂O₃ Catalysts", *Journal of Catalysis*, Vol. 204, pp. 89-97.
- Paparazzo, E., 1990, "XPS Studies Of Damage Induced By X-Ray-Irradiation On CeO₂ Surfaces", *Surface Science*, Vol. 234, pp. L253-L258.
- Passos, F. B., E. R. Oliveira, L. V. Mattos and F. B. Noronha, 2005, "Partial Oxidation of Methane to Synthesis Gas on Pt/Ce_xZr_{1-x}O₂ Catalysts: The Effect of the Support Reducibility and of the Metal Dispersion on the Stability of the Catalysts", *Catalysis Today*, Vol. 101, pp. 23-30.

- Pawelec, B., S. Damyanova, K. Arishtirova, J.L.G. Fierro and L. Petrov, 2007, "Structural and Surface Features of PtNi Catalysts for Reforming of Methane with CO₂", *Applied Catalysis A: General*, Vol.323, pp. 188-201.
- Pompeo, F., N. N. Nichio, M. G.González and M. Montes, 2005, "Characterization of Ni/SiO₂ and Ni/Li-SiO₂ Catalysts for Methane Dry Reforming", *Catalysis Today*, Vol.107-108, pp. 856-862.
- Pompeo, F., N. N. Nichio, M. M.V.M. Souza, D. V. Cesar, O. A. Ferretti and M. Schmal, 2007, "Study of Ni and Pt Catalysts Supported on α -Al₂O₃ and ZrO₂ Applied in Methane Reforming with CO₂", *Applied Catalysis A: General*, Vol. 316, pp. 175.183.
- Querino, P. S., J. R. C. Bispo and M. C. Rangel, 2005, "The effect of Cerium on the Properties of Pt/ZrO₂ Catalysts in the WGS", *Catalysis Today*, Vol.107-108, pp. 920-925.
- Richardson, J. T. and S. A. Paripatyadar, 1990, "Carbon Dioxide Reforming of Methane with Supported Rhodium", *Applied Catalysis*, Vol. 61, pp. 293-309.
- Rodriguez-Reinoso, F., 1998, "The Role of Carbon Materials in Heterogeneous Catalysis", *Carbon*, Vol. 36, pp. 159-175.
- Roh, H. S., H. S. Potdar and K. W. Jun, 2004, "Carbon Dioxide Reforming of Methane over Co-precipitated Ni-CeO₂, Ni-ZrO₂ and Ni-Ce-ZrO₂ Catalysts", *Catalysis Today*, Vol. 93-95, pp. 39-44.
- Romeo, M., K. Bak, J. El Fallah and F. Le Normond, 1993, "XPS Study of the Reduction of Cerium Dioxide", *Surface and Interface Analysis*, Vol. 20, pp. 508-512.
- Ross J. R. H., A. N. J. van Keulen, M. E. S. Hegarty and K. Seshan, 1996, "The Catalytic Conversion of Natural Gas to Useful Products", *Catalysis Today*, Vol. 30, pp. 193-199.

- Rostrup-Nielsen, J. R., 1984, "Catalytic Steam Reforming", in J. R. Anderson and M. Boudart (Eds.), *Catalysis, Science & Technology*, Vol. 5, pp. 1-117, Springer-Verlag, Berlin.
- Rostrup-Nielsen, J.R., L. J. Christiansen and J. H. B. Hansen, 1988, "Activity of Steam Reforming Catalysts: Role and Assessment", *Applied Catalysis A: General*, Vol. 43, pp. 287-303.
- Rostrup-Nielsen, J. R. and J. H. B. Hansen, 1993, "CO₂-Reforming of Methane over Transition Metals", *Journal of Catalysis*, Vol. 144, pp. 38-49.
- Rostrup-Nielsen, J. R., 1997, "Industrial Relevance of Coking", *Catalysis Today*, Vol. 37, pp. 225-232.
- Rostrup-Nielsen, J. R., 2000, "New Aspects of Syngas Production and Use", *Catalysis Today*, Vol. 63, pp. 159-164.
- Ruckenstein, E. and Y. H. Hu, 1996, "Interactions between Ni and La₂O₃ in Ni/La₂O₃ Catalysts Prepared using Different Ni Precursors", *Journal of Catalysis*, Vol. 161, pp.55-61.
- Ruckenstein, E. and H. Y. Wang, 2000, "Carbon Dioxide Reforming of Methane to Synthesis Gas over Supported Cobalt Catalysts", *Applied Catalysis A: General*, Vol. 204, pp. 257-263.
- Ruckenstein, E. and H. Y. Wang, 2002, "Carbon Deposition and Catalytic Deactivation during CO₂ Reforming of CH₄ over Co/ γ -Al₂O₃ Catalysts", *Journal of Catalysis*, Vol. 205, pp.289-293.
- Satterfield, C., N., 1991, *Heterogeneous Catalysis in Industrial Practice*, McGraw-Hill, USA.

- Schuurman, Y. C. Marquez-Alvarez, V. C. H. Kroll and C. Mirodatos, 1998, "Unraveling Mechanistic Features for the Methane Reforming by Carbon Dioxide over Different Metals and Supports by TAP Experiments", *Catalysis Today*, Vol. 46, pp. 185-192.
- Schuurman, Y. C. Mirodatos, P. Ferreira-Aparicio, I. Rodriguez-Ramos and A. Guerrero-Ruiz, 2000, "Bifunctional Pathways in the Carbon Dioxide Reforming of Methane over MgO-Promoted Ru/C Catalysts", *Catalysis Letters*, Vol. 66, pp. 33-37.
- Seok, S., S. H. Choi, E. D. Park, S. H. Han and J. S. Lee, 2002, "Mn-Promoted Ni/Al₂O₃ Catalysts for Stable Carbon Dioxide Reforming of Methane", *Journal of Catalysis*, Vol. 209, pp.6-15.
- Serrano-Ruiz, J. C., J. Luetlich, A. Sepúlveda-Escribano and F. Rodríguez-Reinoso, 2006, "Effect of the Support Composition on the Vapor-phase Hydrogenation of Crotonaldehyde over Pt/Ce_xZr_{1-x}O₂ Catalysts", *Journal of Catalysis*, Vol. 241, pp.45-55.
- Serre, C., F. Garin, G. Belot and G. Maire, 1993, "Reactivity of Pt/Al₂O₃ and Pt-CeO₂/Al₂O₃ Catalysts for the Oxidation of Carbon Monoxide by Oxygen : I. Catalyst Characterization by TPR Using CO as Reducing Agent", *Journal of Catalysis*, Vol. 101, pp.1-8.
- Shi, J. L., J. Y. Zhang and Z. Liu, 1995, "Study of Stepwise Syngas Production from Methane and Carbon Dioxide on Supported Nickel Catalyst", *Natural Gas Chemical Engineering*, Vol. 20, pp. 14-18.
- Shyu, J. Z. and K. Otto, 1988, "Identification of Platinum Phases on γ -alumina by XPS", *Applied Surface Science*, Vol. 32, pp. 246-252.
- Shyu, J. Z., K. Otto, W. L. H. Watkins, G. W. Graham, R. K. Belitz and H. S. Gandhi, 1988, "Characterization of Pd/ γ -alumina Catalysts Containing Ceria", *Journal of Catalysis*, Vol. 114, pp. 23-33.

- Silvestre-Albero, J., F. Rodríguez-Reinoso and A. Sepúlveda-Escribano, 2002, "Improved Metal-Support Interaction in Pt/CeO₂/SiO₂ Catalysts after Zinc Addition", *Journal of Catalysis*, Vol. 210, pp.127-136.
- Slagtern, A., Y. Schwarman, C. Leclercq, X. Verykios and C. Mirodatos, 1997, "Specific Features Concerning the Mechanism of Methane Reforming by Carbon Dioxide over Ni/La₂O₃Catalyst", *Journal of Catalysis*, Vol.172, pp.118-126.
- Sohier, M. P., G. Wrobel, J. P. Bonnelle and J. P. Marcq, 1992, "Hydrogenation Catalysts Based on Nickel and Rare Earths Oxides: I. Relation between Cations Nature, Preparation Route, Hydrogen Content and Catalytic Activity", *Applied Catalysis A: General*, Vol. 84, pp. 169-186.
- Solh, T.E., K. Jarosch and H. Lasa, 2003, "Catalytic Dry Reforming of Methane in a CREC Riser Simulator Kinetic Modeling and Model Discrimination", *Industrial & Engineering Chemistry Research*, Vol. 42, pp. 2507 - 2515.
- Solymosi, F., G. Kutsan and A. Erdohelyi, 1991, "Catalytic Reaction of CH₄ with CO₂ over Alumina-Supported Pt Metals", *Catalysis Letters*, Vol. 11, pp. 149-156.
- Solymosi, F., J. Cserenyi J and L. Ovari, 1997, "A Comparative Study of the Complete Oxidation of Dimethyl Ether on Supported Group VIII Metals", *Catalysis Letters*, Vol. 44, pp. 89-93.
- Son, I.H. and A. M. Lane, 2001, "Promotion of Pt/ γ -Al₂O₃ by Ce for Preferential Oxidation of CO in H₂", *Catalysis Letters*, Vol. 76, No. 3-4, pp. 151-154.
- Souza, M. M. V. M., D. A. G. Aranda and M. Schmal, 2001, "Reforming of Methane with Carbon Dioxide over Pt/ZrO₂/Al₂O₃ Catalysts", *Journal of Catalysis*, Vol. 204, pp. 498-511.

- Souza, M. M. V. M. and M. Schmal, 2003, "Combination of Carbon Dioxide Reforming and Partial Oxidation of Methane over Supported Platinum Catalysts", *Applied Catalysis A: General*, Vol. 255, pp. 83-92.
- Stagg, S. M., E. Romeo, C. Padro and D. E. Resasco, 1998, "Effect of Promotion with Sn on Supported Pt Catalysts for CO₂ Reforming of CH₄", *Journal of Catalysis*, Vol. 178, pp. 137-145.
- Stagg-Williams, S. M., F. B. Noronha, G. Fendley and D. E. Resasco, 2000, "CO₂ Reforming of CH₄ over Pt/ZrO₂ Catalysts Promoted with La and Ce Oxides", *Journal of Catalysis*, Vol. 194, pp. 240-249.
- Swaan, H. M., V. C. H. Kroll, G. A. Martin and C. Mirodatos, 1994, "Deactivation of Supported Nickel Catalysts during the Reforming of Methane by Carbon Dioxide", *Catalysis Today*, Vol. 21, pp. 571-578.
- Takanabe, K., K. Nagaoka, K. Nariai and K. Aika, 2005, "Titania-Supported Cobalt and Nickel Bimetallic Catalysts for Carbon Dioxide Reforming of Methane", *Journal of Catalysis*, Vol. 232, pp. 268-275.
- Tang, S. B., F. L. Qiu and S. J. Lu, 1995, "Effect of Supports on the Carbon Deposition of Nickel Catalysts for Methane Reforming with CO₂", *Catalysis Today*, Vol. 24, pp. 253-255.
- Tang, S., L. Ji, J. Lin, H. C. Zeng, K. L. Tan and K. Li, 2000, "CO₂ Reforming of Methane to Synthesis Gas over Sol-Gel-made Ni/ γ -Al₂O₃ Catalysts from Organometallic Precursors", *Journal of Catalysis*, Vol. 194, pp. 424-430.
- Thevenin, P. O., A. G. Ersson, H. M. J. Kusar, P. G. Menon and S. G. Jaras, 2001, "Deactivation of High Temperature Combustion Catalysts", *Applied Catalysis A: General*, Vol. 212, pp. 189-197.

- Tieman, M. J. and O. E. Finlayson, 1998, "Effects of Ceria on the Combustion Activity and Surface Properties of Pt/Al₂O₃ Catalysts", *Applied Catalysis B: Environmental*, Vol. 19, pp. 23-35.
- Tomishige, K., Y. G. Chen and K. Fujimoto, 1999, "Studies on Carbon Deposition in CO₂ Reforming of CH₄ over Nickel–Magnesia Solid Solution Catalysts", *Journal of Catalysis*, Vol. 181, pp. 91-103.
- Tomishige, K., S. Kanazawa, M. Sato and K. Kunimori, 2002a, "Catalyst Design of Pt Modified Ni/Al₂O₃ Catalyst with Flat Temperature Profile in Methane Reforming with CO₂ and O₂", *Catalysis Letters*, Vol. 84, pp. 69-74.
- Tomishige, K., S. Kanazawa, K. Suzuki, M. Asadullah, M. Sato, K. Ikushima and K. Kunimori, 2002b, "Effective Heat Supply from Combustion to Reforming in Methane Reforming with CO₂ and O₂: Comparison between Ni and Pt Catalysts", *Applied Catalysis A: General*, Vol. 233, pp. 35-44.
- Tomishige, K., S. Kanazawa, S. Ito and K. Kunimori, 2003, "Catalyst Development for Direct Heat Supply from Combustion to Reforming in Methane Reforming with CO₂ and O₂", *Applied Catalysis A: General*, Vol. 244, pp. 71-82.
- Trimm, D. L., 1999, "Catalysts for the Control of Coking during Steam Reforming", *Catalysis Today*, Vol. 49, pp. 3-10.
- Trimm, D. L., 2001, "The Regeneration or Disposal of Deactivated Heterogeneous Catalysts", *Applied Catalysis A: General*, Vol. 212, pp. 153-160.
- Trovarelli, A., 1996, "Catalytic Properties of Ceria and CeO₂ Containing Materials", *Catalysis Reviews-Science and Engineering*, Vol. 38, pp. 439-520.
- Tsipouriari, V. A., A. M. Efstathiou, Z. L. Zhang and X. E. Verykios, 1994, "Reforming of methane with carbon dioxide to synthesis gas over supported Rh catalysts", *Catalysis Today*, Vol. 21, pp. 579-587.

- Tsipouriari, V. A. and X. E. Verykios, 2001, "Kinetic Study of the Catalytic Reforming of Methane with Carbon Dioxide to Synthesis Gas over Ni/La₂O₃ Catalyst", *Catalysis Today*, Vol. 64, pp. 83-90.
- van Keulen, A. N. J., K. Seshan, J. H. B. J. Hoebink and J. R. H. Ross, 1997, "TAP Investigations of the CO₂ Reforming of CH₄ over Pt/ZrO₂", *Journal of Catalysis*, Vol. 166, pp. 306-314.
- Vernon, P. D. F., M. L. H. Green, A. K. Cheetham and A. T. Ashcroft, 1992, "Partial Oxidation of Methane to Synthesis Gas, and Carbon-Dioxide as an Oxidizing-Agent for Methane Conversion", *Catalysis Today*, Vol. 13, pp. 417-426.
- Walter, K., O. V. Buyevskaya, D. Wolf and M. Baerns, 1994, "Rhodium-Catalyzed Partial Oxidation of Methane to CO and H₂ - In-Situ Drifts Studies on Surface Intermediates", *Catalysis Letters*, Vol.29, pp. 261-270
- Wang, H.Y. and C.T. Au, 1992, "CH₄/CD₄ Isotope Effects in the Carbon Dioxide Reforming of Methane to Syngas over SiO₂-supported Nickel Catalysts", *Catalysis Letters*, Vol.38, pp. 77-79.
- Wang, S., G. Q. Lu and G. J. Millar, 1996, "Carbon Dioxide Reforming of Methane to Produce Synthesis Gas over Metal-Supported Catalysts: State of the Art", *Energy & Fuels*, Vol. 10, pp. 896-904.
- Wang, S. and G. Q. Lu, 1998, "Role of CeO₂ in Ni/CeO₂-Al₂O₃ Catalysts for Carbon Dioxide Reforming of Methane", *Applied Catalysis B: Environmental*, Vol. 19, pp. 267-277.
- Wang, S. and G. Q. Lu, 1999, "A Comprehensive Study on Carbon Dioxide Reforming of Methane over Ni/γ-Al₂O₃ Catalysts", *Industrial & Engineering Chemistry Research*, Vol. 38, pp. 2615 – 2625.

- Wang, H. Y. and E. Ruckenstein, 2000, "Carbon Dioxide Reforming of Methane to Synthesis Gas over Supported Rhodium Catalysts: The Effect of Support", *Applied Catalysis A: General*, Vol. 204, pp. 143-152.
- Wang, H. Y. and E. Ruckenstein, 2001, "CO₂ Reforming of CH₄ over Co/MgO Solid Solution Catalysts — Effect of Calcination Temperature and Co Loading", *Applied Catalysis A: General*, Vol. 209, pp. 207-215.
- Wang, J. B., L. E. Kuo and T. J. Huang, 2003, "Study of Carbon Dioxide Reforming of Methane over Bimetallic Ni-Cr/Yttria-Doped Ceria Catalysts", *Applied Catalysis A: General*, Vol. 249, pp. 93-105.
- Wang, W., S. M. Stagg-Williams, F. B. Noronha, L. V. Mattos and F. B. Passos, 2004, "Partial Oxidation and Combined Reforming of Methane on Ce-promoted Catalysts", *Catalysis Today*, Vol. 98, pp. 553-563.
- Watwe, R. M., H. S. Bengaard, J. R. Rostrup-Nielsen, J. A. Dumesic, J. K. Nørskov, 2000, "Theoretical Studies of Stability and Reactivity of CH_x Species on Ni(111)", *Journal of Catalysis*, Vol. 189, pp. 16-30.
- Wei, J.M. and E. Iglesia, 2004, "Isotopic and Kinetic Assessment of the Mechanism of Reactions of CH₄ with CO₂ or H₂O to Form Synthesis Gas and Carbon on Nickel Catalysts", *Journal of Catalysis*, Vol. 224, pp. 370-383.
- Xu, G., K. Shi, Y. Gao, H. Xu and Y. Wei, 1999, "Studies of Reforming Natural Gas with Carbon Dioxide to Produce Synthesis Gas X. The Role of CeO and MgO Promoters", *Journal of Molecular Catalysis*, Vol. 147, pp. 47-54.
- Yan, Q. G., W. Z. Weng, H. L. Wan, H. Toghiani, R. K. Toghiani and C. U. Pittman, 2003, "Activation of Methane to Syngas over a Ni/TiO₂ Catalyst", *Applied Catalysis A: General*, Vol. 239, pp. 43-58.

- Yang, M. and H. Papp, 2006, "CO₂ Reforming of Methane to Syngas over Highly Active and Stable Pt/MgO Catalysts", *Catalysis Today*, Vol. 115, pp. 199-204.
- Yao, M. H., R. J. Baird, F.W. Kunz and T. E. Hoost, 1997, "An XRD and TEM Investigation of the Structure of Alumina-Supported Ceria-Zirconia", *Journal of Catalysis*, Vol. 166, pp. 67-74.
- Zhang, Z. L. and X. E. Verykios, 1994, "Carbon Dioxide Reforming of Methane to Synthesis Gas over Supported Ni Catalysts", *Catalysis Today*, Vol. 21, pp. 589-595.
- Zhang, Z. L. and X. E. Verykios, 1996a, "Carbon Dioxide Reforming of Methane to Synthesis Gas over Ni/La₂O₃ Catalysts", *Applied Catalysis A: General*, Vol. 138, pp. 109-133.
- Zhang, Z. L., V. A. Tsipouriari, A. M. Efstathiou and X. E. Verykios, 1996b, "Reforming of Methane with Carbon Dioxide to Synthesis Gas over Supported Rhodium Catalysts 1. Effects of Support and Metal Crystallite Size on Reaction Activity and Deactivation Characteristics", *Journal of Catalysis*, Vol. 158, pp. 51-63.
- Zhang, J., H. Wang, A. K. Dalai, 2007, "Development of Stable Bimetallic Catalysts for Carbon Dioxide Reforming of Methane", *Journal of Catalysis*, Vol. 249, pp. 300-310.